

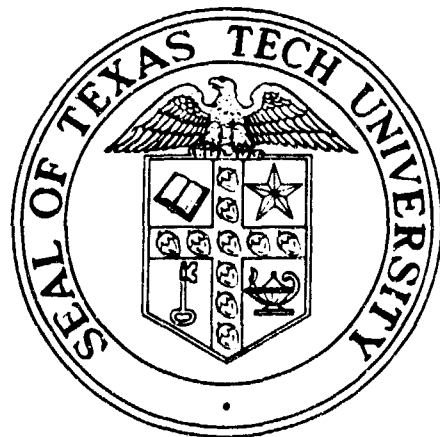
1

WORKSHOP
ON
SOLID STATE SWITCHES FOR PULSED POWER

(January 12-14, 1983)

W. M Portnoy and M. Kristiansen
Workshop Co-Chairmen

A/32684



Sponsored by
Battelle Columbus Laboratories

May 31, 1983

SD 100
S
SEP 21 1983

This document has been approved
for public release and sale; its
distribution is unlimited

FILE COPY

Department of Electrical Engineering
TEXAS TECH UNIVERSITY

Lubbock, Texas 79409

83 09 20 174

Unclassified

SECURITY CLASSIFICATION OF THIS PAGE (When Data Entered)

| REPORT DOCUMENTATION PAGE | | READ INSTRUCTIONS BEFORE COMPLETING FORM |
|--|---|---|
| 1. REPORT NUMBER | 4. GOVT ACCESSION NO. | RECIPIENT'S CATALOG NUMBER |
| 4. TITLE (and Subtitle) Workshop on Solid State Switches for Pulsed Power | | 5. TYPE OF REPORT & PERIOD COVERED Final |
| 7. AUTHOR(s) Workshop Co-Chairmen: W. M. Portnoy M. Kristiansen | 8. CONTRACT OR GRANT NUMBER(s) DAAG29 81 D 0100 | |
| 9. PERFORMING ORGANIZATION NAME AND ADDRESS Texas Tech University Lubbock, TX 79409 | 10. PROGRAM ELEMENT, PROJECT, TASK AREA & WORK UNIT NUMBERS | |
| 11. CONTROLLING OFFICE NAME AND ADDRESS U. S. Army Research Office Post Office Box 12211 Research Triangle Park, NC 27709 | 12. REPORT DATE May 31, 1983 | |
| 14. MONITORING AGENCY NAME & ADDRESS (if different from Controlling Office) | 13. NUMBER OF PAGES 367 | |
| 15. SECURITY CLASS. (of this report) Unclassified | | |
| 16. DISTRIBUTION STATEMENT (of this Report) Approved for public release; distribution unlimited. | | |
| 17. DISTRIBUTION STATEMENT (of the abstract entered in Block 20, if different from Report) S DTIC ELECTED SEP 21 1983 A | | |
| 18. SUPPLEMENTARY NOTES The view, opinions, and/or findings contained in this report are those of the author(s) and should not be construed as an official Department of the Army position, policy, or decision, unless so designated by other documentation | | |
| 19. KEY WORDS (Continue on reverse side if necessary and identify by block number) | | |
| 20. ABSTRACT (Continue on reverse side if necessary and identify by block number) A Workshop on Solid State Pulsed Power Switching was conducted by Texas Tech U at Tamarron, Colorado, in January, 1983 for the US Army Research Office. The Workshop addressed the state-of-the-art in solid state switching, particularly semiconductor switches, and new solid state related switching concepts for pulsed power applications. An important objective of the Workshop was to establish research priorities. Group discussions were augmented by invited presentations. The principal topics included opening switches, high power closing switches, extremely fast risetime closing switches and state transition switches; devices of particular | | |

UNCLASSIFIED

SECURITY CLASSIFICATION OF THIS PAGE (When Data Entered)

ABSTRACT (cont.)

interest were thyristors, avalanche switches and the optically triggered intrinsic switch. The invited papers, along with summaries of the Working Group discussions and recommendations, are presented in this report. A general summary, including suggested research topics, is included.

2

Scientific Services Program
U.S. Army Research Office

Final Report
on
WORKSHOP ON SOLID STATE SWITCHES FOR PULSED POWER
Sponsored by
Battelle Columbus Laboratories
200 Park Drive
Research Triangle Park, NC 27709
under
Contract DAAG29-81-D-0100
Delivery Order 0424

Conducted by
Solid State Electronics Laboratory
Department of Electrical Engineering
Texas Tech University
Lubbock, Texas 79409

at
Tamarron, Colorado
on
January 12-14, 1983

Submitted by
W. M. Portnoy
Workshop Co-Chairman
and
M. Kristiansen
Workshop Co-Chairman

May 31, 1983

The views, opinions, and/or findings contained in this report are those of the authors, and should not be construed as an official Department of the Army position, policy, or decision, unless so designated by other documentation.

| | |
|--------------------|-------------------------------------|
| Accession For | |
| NTIS GRATI | <input checked="" type="checkbox"/> |
| DTIC TAB | <input type="checkbox"/> |
| Unannounced | <input type="checkbox"/> |
| Justification | |
| By | |
| Distribution/ | |
| Availability Codes | |
| Avail and/or | |
| Dist | Special |

A

This document has been approved
for public release and its
distribution is unlimited

TABLE OF CONTENTS

| | | |
|------|--|-----|
| I. | Workshop Advisory Committee | iii |
| II. | Abstract | 1 |
| III. | Working Groups | 2 |
| IV. | Introduction | 4 |
| V. | Workshop Summary | 9 |
| VI. | Invited Overview Papers | |
| 1. | Pulsed Power Technology (P. J. Turchi) | 15 |
| 2. | Survey of Solid State Switch Applications (J. P. O'Loughlin) | 26 |
| 3. | Light Triggered Thyristors (V. A. K. Temple) | 48 |
| 4. | Avalanche Devices: State-of-the-Art (M. D. Pocha) | 79 |
| 5. | Gallium Arsenide Power Transistors (M. S. Adler) | 89 |
| 6. | Failure in High Power Semiconductor Switches (D. C. Wunsch) | 97 |
| 7. | Optically Induced High Power Switching (G. Mourou) | 114 |
| 8. | Picosecond Photoconductivity and its Applications (C. H. Lee) | 160 |
| VII. | Group Reports | |
| 1. | Solid State Opening Switches (M. Weiner, Chairman) | 189 |
| 2. | High Power Closing Switches (L. R. Lowry, Chairman) | 202 |
| 3. | Extremely Fast Risetime Switches (R. B. Hammond, Chairman) | 222 |
| 4. | State Transition Switches (I. M. Vitkovitsky, Chairman) | 258 |
| 5. | Applications Related Issues (J. P. O'Loughlin, Chairman) | 272 |

VIII. Appendices

| | |
|--|-----|
| A. Deep Impurity Trapping Concepts (G. R. Sundberg and H. T. Henderson) | 289 |
| B. Nonlinear Resistive Switches (R. D. Ford and I. M. Vitkovitsky) | 309 |
| C. Photoconductive Power Switches (W. C. Nunnally) | 327 |
| D. High Power Superconducting Switches (D. U. Gubser) | 361 |
| E. List of Participants | 363 |

WORKSHOP ADVISORY COMMITTEE

W. M. Portnoy (Co-Chairman) Texas Tech University

M. Kristiansen (Co-Chairman) Texas Tech University

M. S. Adler General Electric Company

D. W. Borst International Rectifier

A. H. Guenther Air Force Weapons Laboratory

L. M. Levinson General Electric Company

L. R. Lowry Westinghouse Electric Corp.

P. F. Pittman Westinghouse Electric Corp.

M. Weiner U.S. Army ERADCOM

EX-OFFICIO MEMBERS

B. D. Guenther Army Research Office

H. R. Wittman Army Research Office

ABSTRACT

A Workshop on Solid State Pulsed Power Switching was conducted by Texas Tech University at Tamarron, Colorado, in January, 1983 for the U.S. Army Research Office. The Workshop addressed the state-of-the-art in solid state switching, particularly semiconductor switches, and new solid state related switching concepts for pulsed power applications. An important objective of the Workshop was to establish research priorities. Group discussions were augmented by invited presentations. The principal topics included opening switches, high power closing switches, extremely fast risetime closing switches and state transition switches; devices of particular interest were thyristors, avalanche switches and the optically triggered intrinsic switch. The invited papers, along with summaries of the Working Group discussions and recommendations, are presented in this report. A general summary, including suggested research topics, is included.

WORKING GROUPS

1. Solid State Opening Switches

| | |
|---------------------|------------------------------|
| M. Weiner, Chairman | U.S. Army ERADCOM |
| D. L. Blackburn | National Bureau of Standards |
| J. B. Brewster | Westinghouse Electric Corp. |
| Y. Kao | Westinghouse Electric Corp. |
| M. Kristiansen | Texas Tech University |
| K. Schoenbach | Texas Tech University |
| P. J. Turchi | R & D Associates |
| G. R. Sundberg | NASA Lewis Research Center |
| D. Wolley | General Electric Company |

2. High Power Closing Switches

| | |
|-----------------------|-----------------------------|
| L. R. Lowry, Chairman | Westinghouse Electric Corp. |
| B. L. Ballard | Foreign Technology Division |
| | U.S. Air Force |
| T. R. Burkes | T. R. Burkes, Inc. |
| B. Gray | Rome Air Development Center |
| J. L. Hudgins | Texas Tech University |
| P. F. Pittman | Westinghouse Electric Corp. |
| W. M. Portnoy | Texas Tech University |
| V. A. K. Temple | General Electric Company |
| P. F. Williams | Texas Tech University |
| W. C. Nunnally | Los Alamos National Lab. |

3. Extremely Fast Risetime Switches

| | |
|-------------------------|--------------------------|
| R. B. Hammond, Chairman | Los Alamos National Lab. |
| M. S. Adler | General Electric Company |
| P. Haugsjaa | GTE Laboratories |

| | |
|-----------------|------------------------------|
| H. T. Henderson | University of Cincinnati |
| E. E. Kunhardt | Texas Tech University |
| M. D. Pocha | Lawrence Livermore |
| | National Laboratory |
| M. E. Snyder | Air Force Weapons Laboratory |

4. State Transition Switches

| | |
|--------------------------|---------------------------|
| I. M. Vitkovitsky, Chmn. | Naval Research Laboratory |
| R. D. Ford | Naval Research Laboratory |
| B. Lalevic | Rutgers University |
| C. H. Lee | University of Maryland |
| L. M. Levinson | General Electric Company |
| G. Mourou | University of Rochester |
| R. W. Rice | Naval Research Laboratory |
| H. R. Wittman | Army Research Office |

5. Applications Related Issues

| | |
|-------------------------|---|
| J. P. O'Loughlin, Chmn. | Air Force Weapons Laboratory |
| D. W. Borst | International Rectifier |
| A. H. Guenther | Air Force Weapons Lab. |
| E. Honig | Los Alamos National Lab. |
| M. Mando | U.S. Army MERADCOM |
| D. L. Pruitt | RCA |
| L. R. Turner | Foreign Science and Technology Centers, U.S. Army |
| D. C. Wunsch | The BDM Corporation |

INTRODUCTION

A Workshop on Solid State Switching for Pulsed Power was conducted by Texas Tech University at Tamarron, Colorado, on January 12-14, 1983, under the sponsorship of the Army Research Office. The general objectives of the Workshop were to determine the state-of-the-art in high power, repetitive, solid state switching, and to identify critical research issues which should be addressed in order to improve their performance.

Pulsed power switching has been largely accomplished using spark gaps for very high peak powers, and thyratrons for intermediate powers. However, the limited life, and to some extent, the custom design required for some applications, have stimulated considerable interest in solid state switches because of their recognized reliability, lifetime, and reproducibility. Despite that interest, there has been no coherent examination of the possibility of using such switches for pulsed power, nor any regular exchange of information between solid state device physicists and manufacturers and the pulsed power user community. This workshop represented an initial attempt to establish a meaningful interaction.

The goals of the Workshop were:

1. to promote the exchange of information between scientists and engineers working in research areas related to solid state pulsed power switching;
2. to identify the limitations of high power, repetitive solid state switches with respect to their possible applications;

3. to identify unresolved problems and suggest research that should be conducted to resolve those problems; and
4. to establish research objectives.

In order to achieve these goals, it is imperative to understand the complicated and interrelated physical and electrical processes occurring during switching. These issues require a considerable range of knowledge: device physics and modeling, materials, packaging and thermal management, and so on.

Individual laboratories have been concerned with these separate problems, and it was considered appropriate and timely to assemble specialists from the various research groups and workers from relevant subdisciplines to consider the issues from a pulsed power switching point of view. Representatives from federal government agencies with potential interest in pulsed power repetitive switching were also invited to suggest realistic background scenarios and requirements.

An Advisory Committee was formed to help establish the content of the Workshop, its goals, and the type of expert knowledge required to meet its objectives, and to identify suitable personnel with the requisite knowledge for contributing to the success of the Workshop. The Advisory Committee met for two days at Texas Tech University at the end of September, in 1982. An extensive list of possible names were proposed, from which a total of forty-two were invited. These represented universities, industrial laboratories and manufacturers, national laboratories, and government agencies.

Overview papers were presented the first day. Two were presented after submission to the Workshop participants, who

agreed that the submitted material was important and relevant as background information. This event was not anticipated by the Workshop Co-Chairmen, but strongly approved, inasmuch as it indicated that a good and desirable exchange of information was, in fact, beginning to take place. These papers (Sundberg and Henderson, and Ford and Vitkovsky) have been included in the Appendices to the report. (Two additional papers (Nunnally and Gubser) have also been included; these were not presented, but are clearly so relevant that their inclusion was considered appropriate.) The working groups then met, coordinated by selected chairmen who led the discussions, to consider their individual charges. It is interesting to note that one of the working groups, on state transition switches, was not one of the groups originally established, but was formed at the Workshop by members of other groups who had identified a switching phenomenon and issue which had not been recognized by the Advisory Committee. The conclusions and recommendations of the individual groups were presented at a general meeting on the last day of the formal Workshop. The Advisory Committee met the next day to consider the results and make their own recommendations.

We (the Workshop Co-Chairmen) believe that the Workshop successfully met its goals. The success of the first, the exchange of information and the stimulation of interest, can certainly be demonstrated by the participants' request for additional presentations and the formation of a new, additional, working group. Also, members of the various working groups circulated, not only to convey information back to their own groups, but also because of their own interest.

Although the other three goals were also met successfully, the results were not quite as dramatic as for the first. This Workshop represents the first time that users and device and material scientists have been brought together to consider solid state switching for pulsed power. Language and objectives were unfamiliar to each other, and a productive exchange of information could not occur until the participants became comfortable with the new ideas. That process of familiarization is evident in the success of the first goal. Nevertheless, the reports of the working groups clearly demonstrate that the issue of the limitations of solid state devices, as discrete elements and in arrays, has been substantially addressed. For example, conventional junction devices, and arrays of these, have been identified as doubtful for pulsed power switching applications. Furthermore, unresolved problems in the basic physics and mechanisms of operation of candidate devices have been identified; these are discussed in the sections of the reports which consider those devices. Finally, specific research objectives and approaches have been tabulated in the reports.

The problems which have been identified and the proposed research objectives are similar in the working group reports. This is not a surprising result, inasmuch as a significant number of participants were semiconductor specialists, and much of the discussion involved semiconductor devices and device concepts. In one respect, this was unfortunate, because there was not much time devoted to other solid state switches, such as Hall or superconducting switches; however, semiconductor device technology is the most advanced solid state switch technology, and it is

reasonable to consider these switches as most important (but not necessarily from a long range research standpoint). Moreover, state transition switches were considered. It is interesting to note that rectifiers are mentioned only briefly; these have special and important applications in switching, but are different because they have no gain. Thermal management was identified as a very important issue, but was not considered in detail, an unfortunate omission. Packaging studies are not very common, possibly because they are closely applications related. This problem, the applied research character of much semiconductor device work, was discussed during the final Advisory Committee meeting. The distinction between basic and applied work becomes quite critical when research funding is involved, and the nature of device research is still ambiguous.

The research objectives tabulated in the summary were drafted by the Workshop Co-Chairmen, with some input from the Advisory Committee. Most of the suggested topics were extracted from the various group reports. There was not enough time to distribute copies to the members of the Advisory Committee for their comments; however, each received a copy before the Report was printed, with a request for comment in case of strong disagreement.

WORKSHOP SUMMARY AND RESEARCH RECOMMENDATIONS

The conclusions and research recommendations contained in the reports are related, which is to be expected because of the related physical basis of operation of different semiconductor switches. It was generally agreed that the optically triggered bulk semiconductor switch was probably the most important new switch technology, largely because of its anticipated scalability. However, the projected performance of other types of discrete switches made their continued exploration and assessment desirable.

State transition switches were discussed as possible replacements for metallic fuses in inductive storage because of their large off-to-on resistivity ratios and the possibility of scaling and reusability. These switches are not, however, as well-understood as semiconductor devices, nor is their technology as well-developed.

The working group on applications related issues pointed out that the limited present ratings of discrete switches requires their assembly into arrays to meet the demands of medium and high power applications. Using the conventional silicon thyristor as a typical element, voltage overstress, without compensation, on one element mismatched in switching speed and delay relative to the other matched elements was considered in detail. The need for compensation, with the resultant degradation of the array performance from single element characteristics, was the basis for the recommendations for better matching of components to enhance array performance and reliability.

The working groups on opening and closing switches considered basically the same semiconductor devices, but from different application points of view. Both applications require high blocking voltages and peak current densities, low forward voltage drop to minimize power dissipation, high repetition rates, good timing control, good thermal management, and matched characteristics. One important difference between them is that performance in a closing switch is limited by turn-on dI/dt , and in an opening switch, by turn-off dV/dt . An important common recommendation was the pulse mode electrical characterization of a discrete device, and the relationship of its electrical behavior to basic device physics. Both the working groups and the group on applications related issues recommended studying light activated turn-on phenomena in p-n junction devices.

The group on fast risetime switching considered several types of semiconductor switches which are essentially in the development stage; these are photoconductors, avalanche transistors, gallium arsenide JFETs and double injection, deep impurity [(DI)²] devices. The later three devices incorporate junctions (although the (DI)² device blocking voltage is limited by the breakdown field in bulk silicon, and the JFET is a majority carrier device). The operation of avalanche transistors is not well-understood, and appears to be limited by current filamentation. JFETs are fast, with low on resistance, and potentially scalable to high currents and voltages. The possible scalability of (DI)² switches to high voltages make them interesting, but filamentation may limit their maximum current handling capability.

Bulk photoconductors were considered by the three switch working groups to be of most immediate possible use, with suitable research and development support. Their potential value lies in their scalability up to very high voltages and currents, replacing arrays of junction type devices. Their principal limitation, however, is the light source and its interaction with the switching material. There are also the problems of low gain and efficiency, although avalanche photoconduction, in which a photoconductive switch latches on after being optically triggered, may increase efficiency considerably. Avalanche photoconduction has been reported only once.

The major research recommendations made by the working groups are summarized in Table 1. There is no priority implied in their order. One important recommendation was that of thermal management. Although the principles of heat conduction are known, their detailed relationship to package structures (particularly when other constraints, such as low inductance design, are present) has not been adequately developed. The problems of thermal properties of materials and alloys, thermal conduction across interfaces, and the thermal impedance of structures must be addressed.

Table 1. Summary of research recommendations.

1. Solid State Opening Switches
 - a. Pulse mode characterization and physics of junction devices
 - b. Interaction of light and p-n junctions
 - c. Bulk switching
 - i. New materials: candidates and characterization
 - ii. Surface breakdown
2. High Power Closing Switches
 - a. Pulse mode characterization and physics of switching devices
 - i. Maximum current density, filamentation
 - ii. Forward voltage drop, ohmic contacts
 - iii. Failure modes and mechanisms
 - b. Scalability
 - c. Thermal management
 - d. Photoconductive gain
 - e. Fast switching rectifiers
3. Extremely Fast Risetime Switches
 - a. Photoconductors
 - i. Light sources
 - ii. Contact technology
 - iii. Surface breakdown
 - IV. Thermal management
 - V. Scaling
 - b. Avalanche Photoconductors
 - i. Fundamental mechanism
 - ii. Steady-state forward voltage drop

- iii. Material characterization and relation to performance
- iv. Aging: performance as a function of switching history
- c. Avalanche Transistors
 - i. Filamentation: phenomenology, dynamics
 - ii. Forward voltage drop
- d. GaAs JFETs
 - i. Analysis and design of fast scaled devices
- e. (DI)²
 - i. Scaling
 - ii. Switching efficiency for light gating

4. State Transition Switches

- a. Properties of and relationships between single and polycrystals.
- b. Filling materials
- c. Mechanical properties: fatigue and fracture
- d. Switching kinetics
- e. New materials

5. Applications Related Issues

- a. Relationship between discrete element and array performance
- b. Element matching
- c. Improved compensation
- d. Element-circuit interfacial problems
- e. Thermal management
- f. Optical triggering

INVITED OVERVIEW PAPERS

PULSED POWER TECHNOLOGY

P. J. Turchi
R and D Associates

INTRODUCTION

The following viewgraphs are intended to summarize some of the most important aspects of pulsed power technology, since many of the Workshop participants did not have a pulsed power background. Some of the parameter ranges which are outlined set the background for the switch requirements of interest. The summary, although brief, covers the most important concerns and targets for pulsed power development.

PULSED POWER TECHNOLOGY

Q. What is "Pulsed Power Technology"?

A. By exception

1. Not CW power engineering

By arithmetic

2. FWHM of power pulse << time between pulses

By history

3. Technology that derives from single pulse devices

By intention

4. Technology that tries to achieve the benefits of high power without the burdens of high average power

PULSED POWER TECHNOLOGY

STEADY POWER ELEMENTS

Sources

- batteries
- fuel cells
- alternators
- thermoelectric, -ionic
- steady MHD generators
- photovoltaic

PULSED POWER ELEMENTS

Sources

- explosives, propellants, flywheels acting to provide an impulse to conducting material
- temporary storage in capacitors, inductors, electromagnetic waves, particle beams, moving conductors

Power Conditioning

Static, linear components

- fixed capacitors, resistors, and inductors

Power Conditioning

static components
dynamic components

- active and/or nonlinear components
 - switches
 - electrical properties functions of internal conditions and external influences

nonlinear loads

Pulsed Power Technology (Continued)

STEADY POWER ELEMENTS

Engineering Concerns

- steady heat transfer
- steady mechanical stress levels
- stability against perturbations (electrical, mechanical, thermal)

PULSED POWER ELEMENTS

Engineering Concerns (additional)

- peak stress, temperature, heat flux
- design of large scale perturbation

Pulsed Power Technology
Applications of Pulsed Power

TASK

COMMENT

Flash x-ray photography

single pulse, ~ 40 nsec, 20 kV-20 MV,
1-2 kA

Nuclear weapons effects simulation

- electromagnetic pulse (EMP) single pulse
- hard x-rays (bremsstrahlung sources) very high powers
- soft x-rays (plasma radiators) $0.2 - 10 \text{ MV}, 10^{-2} - 10^2 \text{ MA},$
 $< 0.1 - 1 \text{ usec}$

Particle accelerators

- high energy physics research
- exotic beam weapons
- repetitive pulses, bursts, bolts, etc.
higher particle energies, but
volts/stage modest.

Pulsed Power Technology
Applications of Pulsed Power (continued)

TASK

Electrically driven lasers

- flashlamp - excitation
- electrical discharge - excitation
- electron beam - pumped

modest voltages
10 - 1000 kV

long pulses (flashlamp) > 100 μ sec
short pulses (e-beam) \leq 1 μ sec
repetitive and single-shot

Pulsed Power Technology

Applications of Pulsed Power (continued)

| <u>TASK</u> | <u>COMMENT</u> |
|----------------------|---|
| Microwave generators | closely related to particle accelerator technology |
| Electromagnetic guns | typically high currents, - rail guns - other variants - launchers |
| Electric thrusters | modest average power - pulsed plasma thruster - quasi-steady MPD arcjet |

Pulsed Power Technology

A Sampling of Pulsed Power Requirements*

| <u>Task</u> | <u>Pulse Width</u> | <u>Voltage</u> | <u>Current</u> | <u>Pulse Rate</u> |
|-----------------|--------------------|----------------|----------------|-------------------|
| FXR | 80 nsec | 20MV | 2 KA | (1/3 Hz) |
| NWE | < 100 nsec | ~ 1 MV | ~ 1 MA | 0 |
| ATA | 50 nsec | 50 MV | 10 KA | 1 KHz |
| <hr/> | | | | |
| Lasers | | | | |
| flashlamp | 1-500 μ sec | 20 KV | 10-1000 KA | 0 |
| discharge | 40 nsec (rise) | 50 KV | - | 100 Hz |
| LiS | 60 nsec | 60 KV | 10-1000 KA | < 1250 Hz |
| CO ₂ | 200 nsec | 25 KV | 1-2 KA | 1 Hz |
| EM guns | 1-5 msec | 3 KV | 2 MA | 0-100 Hz |
| PPT | 20 μ sec | 3 KV | 40 KA | 1 Hz |
| HPD arc et | 1 msec | 2 KV | 20 KA | 10 Hz |

* Not necessarily consistent values

FXR - Flash X-ray
 NWE - Nuclear Weapons Effects
 ATA - Advanced Test Accelerator
 EM Guns - Electro-Magnetic Guns
 PPT - Pulsed Plasma Thruster
 MHD - Magneto-Hydro-Dynamic

Pulsed Power Technology

Some Figures of Merit

| | | |
|------------------|------------------------|--------------------------|
| current density | > 1 KA/cm ² | > 1 MW/cm ³ |
| electric field | > 1 KV/cm | |
| turn-on/off time | < 100 nsec, | for high voltage pulsers |
| | < 10 μ sec, | for electric thrusters |
| | < 1 msec, | for EM guns |

relative voltage drops, resistances, > order of magnitude better than current conduction

e.g., opening switch: $\frac{\text{hold-off voltage}}{\text{closed voltage}} > 10 \times \frac{\text{conduction time}}{\text{opening time}}$

duty cycle (for repetitive systems)

Pulsed Power Technology

Some Physics Concerns for High Power Circuits

1. Low allowable power density implies larger volume of material so transit time effects may limit risetime. For example, if $P_D = 0.1 \text{ MW/cm}^3$ and $P = (10 \text{ kA}) (1 \text{ MV}) = 10^{10} \text{ W}$, then volume = 10^5 cm^3 , so the characteristic distance may be $x = 46 \text{ cm}$, corresponding to a vacuum transit time of 1.5 nsec. Dielectric material and magnetic diffusion will slow portions of the electromagnetic wave.
2. Magnetic diffusion will affect the local magnetic fields during switch operation, changing electric potentials and, for magnetically-controlled switches, altering switch operation. A hollow cylinder of copper with diameter 46 cm and thickness of 1 mm has a diffusion time:

$$L/R \approx \frac{\mu}{2\eta} r \Delta r = 8 \text{ msec}$$

Pulsed Power Technology

Some Physics Concerns for High Power Circuits (continued)

3. Pulsed heat addition may occur too quickly for conduction out of the switch itself. Heat transport away from surfaces may not be able to react fast enough to the change in surface temperature. Heat sink and cooling flow design can provide limits more severe than intrinsic physics of switch.

SURVEY OF SOLID STATE SWITCH APPLICATIONS

James P. O'Loughlin
Air Force Weapons Laboratory

INTRODUCTION

At the power generation and control end of the spectrum, solid state switching is, and has for many years been, heavily applied to motor controls, rectification, power factor correction and, most spectacularly, to extremely high power switching inverters. Low power pulse switching applications, such as air-borne navigation and weather radar, are also dominated by solid state devices. However, even though the satisfactory performance of several solid state pulse switches suitable for most high power radar, linear accelerators and similar applications have been demonstrated in the past ten years, their utilization remains almost non-existent. There is no simple explanation as to why solid state switching has become stagnant with respect to medium and high power pulse applications.

At the present time, there are many pulse power switching applications with technical requirements orders of magnitude more demanding than the most advanced state-of-the art discrete solid state switches. There are a few extremely high power fast switching applications where large bulk semiconductor switches driven by photons and electrons or both may be the ultimate answer. Because individual solid state devices are limited in voltage, current, and switching speed, it is necessary to use arrays of devices, sometimes thousands, to attempt to accomplish the higher power switching functions. The utilization of solid

state switching in these applications depends as strongly upon the design, characteristics and behavior of the arrays as it does upon the individual elements.

RANGE OF APPLICATION

To completely characterize any particular switching application requires at least five to ten parameters. Obviously, any two parameter representation has many shortcomings, but plotting the domain in terms of pulse width and peak power provides a worthwhile overview. Figure 1 displays a range of 10^2 to 10^{14} peak watts and 10^{-9} to 10^{-3} seconds of pulse width. The approximate boundary of the state-of-the-art capability of solid state switches is indicated in addition to the approximate boundary of present conceivable applications. In addition, certain areas are designated as typical of specific applications. It is significant to note that the solid state switching limit boundary has not changed appreciably in the last five years, probably because that the boundary represents switch arrays and "improvements"⁽¹⁾ in devices do not affect the improvement in the arrays as much as one might hope.

Even more significant is the fact that there has been, over the past five year period, no application of solid state switches to high power radars and accelerators, in spite of the fact that there are no technical performance barriers. There is no single clear reason for this non-utilization of solid state pulse switches. Figure 2 shows an overlay of the approximate area where solid state switches are being utilized to a significant degree and indicates the region where applications are stagnant.

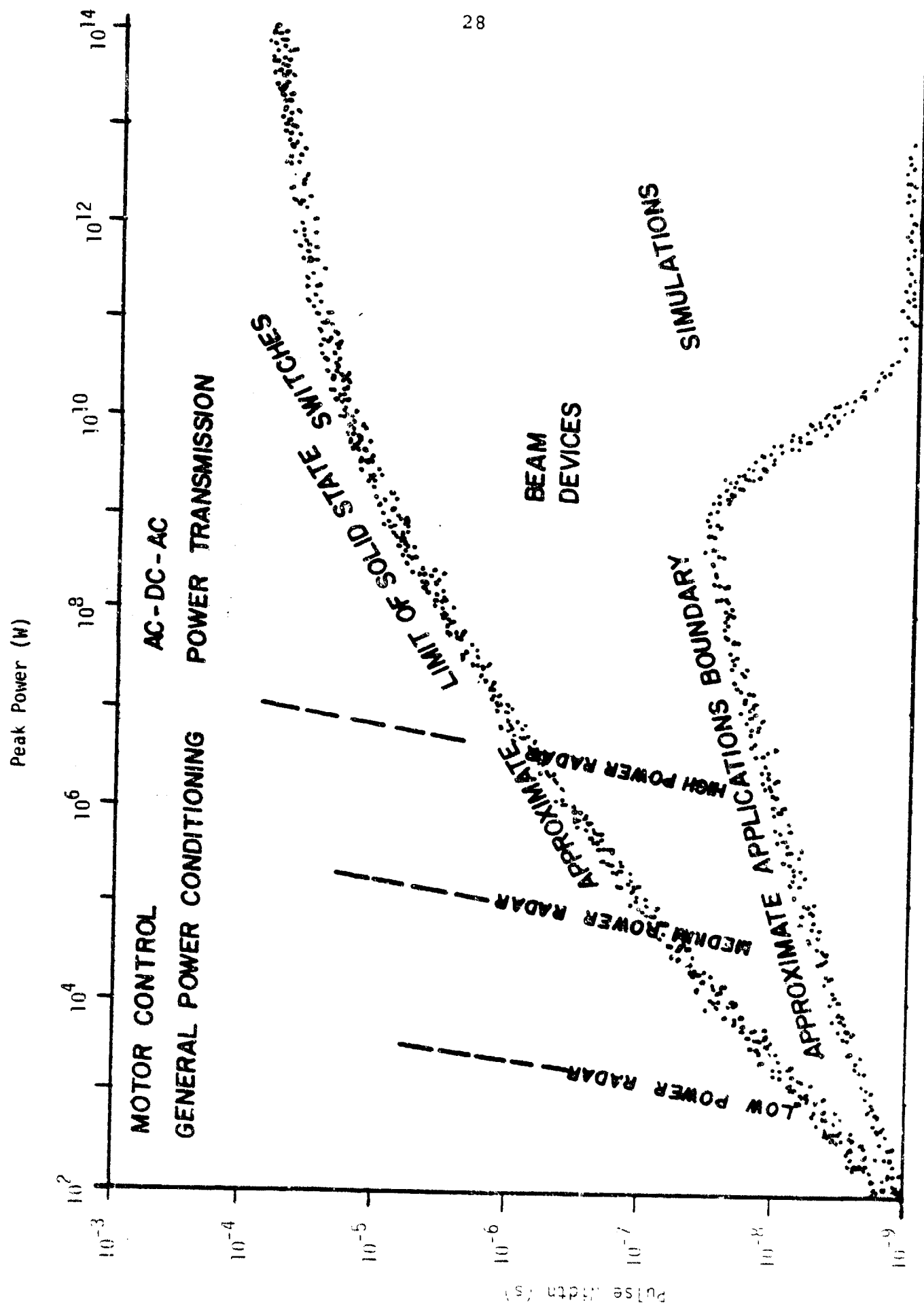


Figure 1. Ranges of switching applications.

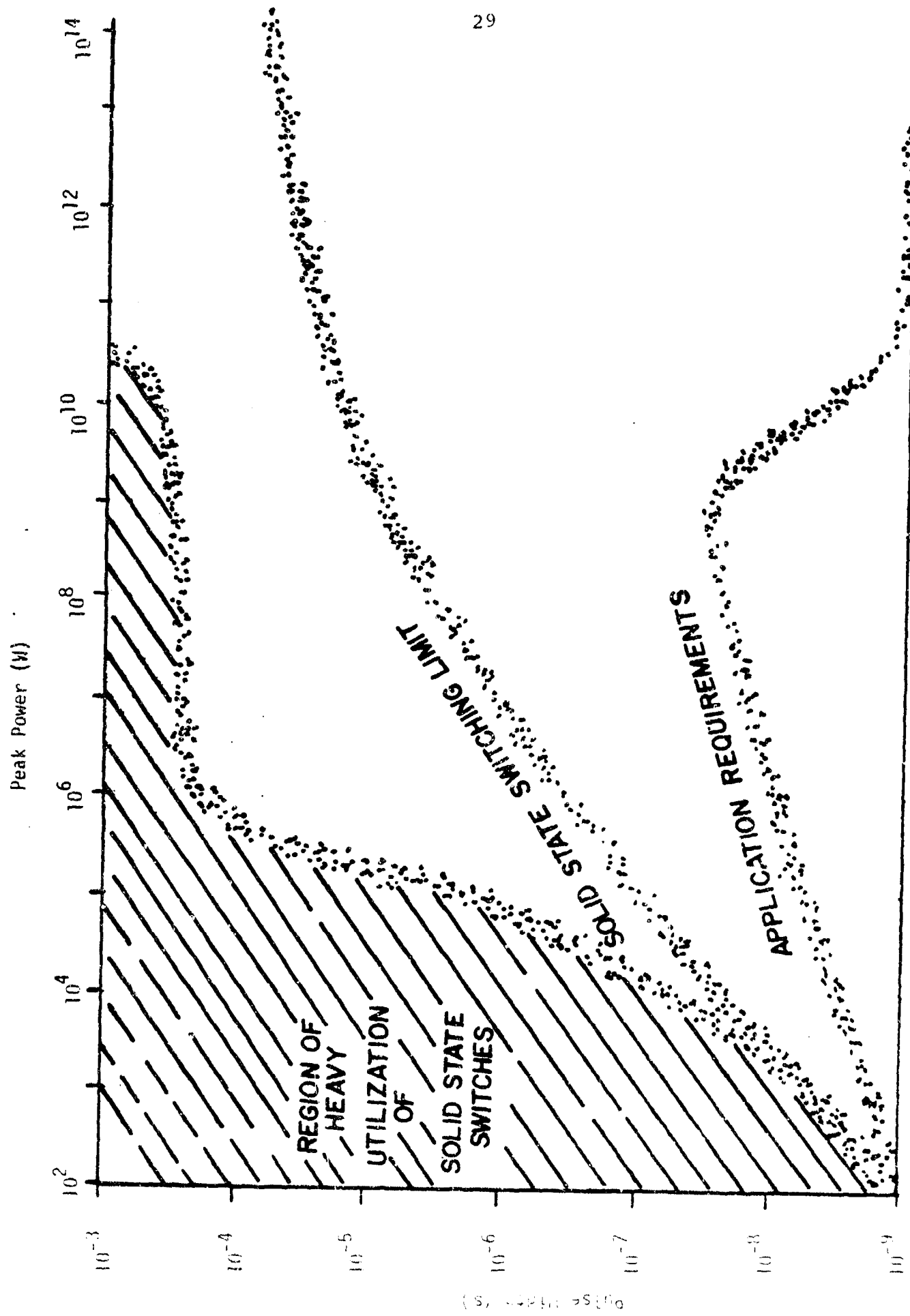


Figure 2. Utilization of solid state switches.

As of 1975, both RCA^(2,3) and Westinghouse⁽⁴⁾ had clearly demonstrated the technical performance capabilities of solid state pulsed power switching suitable for high power radar type applications. The RCA approach was based on a series-parallel array of 200 type 2N3873 SCRs. Westinghouse used a series string of 6 type T60R RSRs (Reverse Switching Rectifier) devices (which has been since renamed the RBDT (Reverse Breakdown Diode Thyristor)). The performance data for both demonstrations are summarized in Table 1A. To date, a survey to find applications of this solid state switching technology has turned up only three equipments, shown in Table 1B. All three are RBDT applications. No SCR pulse switch arrays were found in medium to high power radar, linear accelerators or similar applications.

Areas where applications are heavy and continuing to expand are in low power radars, typically fusing, weather and navigation, motor controls at all power levels, and the entire field of power conditioning, such as regulated power supplies, rectifiers, invertors, lighting controls, etc. The area where the most impressive gains are being made both in growth rate and power rating is the commercial power industry application of high voltage inverters to DC power transmission and the linking of asynchronous AC power grids. Some present installations and projected increases are shown in Table 2.

A new commercial power application which is just emerging is the use of forced commutation inverters for fully electronic VAR management.⁽⁵⁾ These inverters will replace capacitors and

Table 1A. Performance data of solid state pulser switches (2,3,4)
(Circa 1975)

| | WESTINGHOUSE | RCA |
|------------------|-----------------------|-----------------------|
| Contract | AFWL F29601-74-C-0021 | RADC F30602-74-C-0195 |
| Hold-off Voltage | 5000 V | 100000 V |
| Peak Current | 5000 A | 7000 A |
| Pulse Width | 20 μ s | 20 μ s |
| Rise Time | 22 μ s | 1.7 μ s |
| PRF | 250 | 250 |
| Peak Power | 12.5 MW | 32 MW |
| Average Power | 62.5 KW | 160 KW |
| Device | RBDT (RSR) T60R | SCR 2N3873 |
| Array | 6 Series | 10 Parallel-20 Series |

Table 1B. Applications of solid state pulse switches (1983)

| APPLICATIONS | DEVICE | NUMBER |
|------------------------------|--------|--------|
| ARSR-3 FAA Radar | RBDT | 25 |
| AN/TPS-43 TAC, Surface RADAR | RBDT | 50 |
| TRACS FAA (Canadian) RADAR | RBDT | 14 |

Table 2. Worldwide thyristor inverter systems for asynchronous A.C. interconnections and HVDC transmission⁽⁵⁾.

| <u>COUNTRY</u> | <u>VENDOR</u> | <u>PRESENT MW</u> | <u>MW BY YEAR</u> | <u>VOLTAGE KV</u> |
|--------------------|-----------------|-------------------|-------------------|----------------------|
| Austria | S-B-A | - | 550 1983 | 150 |
| Brazil | ASEA | - | 6300 1985 | \pm 600 |
| Canada | GE/CGE | 800 | - - | 140, 160 |
| | S-B-A | 900 | 1900 1985 | \pm 500 |
| Japan | Hitachi/Toshiba | 600 | - - | 125, 250 |
| Mozambique | S-B-A | 1920 | - - | \pm 533 |
| Norway | ASEA | 500 | - - | \pm 250 |
| Paraguay | S-B-A | 50 | | 26 |
| Sweden | ASEA | 10 | 130 1983 | 150 |
| England/ France | Aisthom | 80 | | \pm 100 |
| | Aisthom-GEC | | 2000 1986 | \pm 270 |
| USA | ASEA | 1000 | 3600 1986 | \pm 100, \pm 500 |
| | GE | 600 | 1220 1986 | \pm 200, \pm 400 |
| USSR | USSR | 670 | 330 1983 | \pm 500 |
| Zaire | ASEA | 560 | | \pm 500 |
| | | 7690 | 16030 | |

S-B-A, joint Siemens, Brown Boveri, AEG Telefunken;
 ASEA (Sweden); GE, General Electric; CGE, Canadian General
 Electric

synchronous capacitors used for power factor correction, and in more unusual cases, power factor correction inductors.

The application of solid state switches to circuit breaker applications is restricted to lower power levels and will most likely remain so. Although solid state switch assemblies, such as used in inverters, are technically capable of handling the circuit breaker interruption type service, there are decisive factors which rule them out. Specifically, the cost of the megawatt-multikilovolt class solid state breaker is considerably more than the conventional breaker and, in addition, utility companies now assign a present value to power losses at \$3000 per kilowatt.⁽⁵⁾ This loss penalty can easily amount to tens of thousands of dollars for a solid state breaker compared to almost nothing for a conventional metal-to-metal unit.

The applications which are the most remote from the array type solid state switches are the extremely high peak power beam devices and simulators. In fact, it is safe to conclude that these applications are in the never-never land for array type solid state switches. However, a bulk type solid state switch now being investigated at LANL could have both opening and closing applications in beam devices and simulators.⁽⁶⁾ The device is a bulk semiconductor, such as silicon, with conductivity controlled by incident photon radiation which determines the conduction electron number density. Hold-off voltage stresses of up to 100 KV/cm and peak current densities of tens of KA/cm² are projected.

TYPICAL APPLICATION CIRCUITS

The most impressive application of solid state switching in terms of voltage and power is the switching inverter used in power transmission for the past ten years or so. These circuits are used both for HVDC transmission and for linking asynchronous AC power grids. A simplified schematic diagram of a so-called 12 pulse inverter is shown in figure 3. The sequencing of the switch elements is shown with the corresponding waveforms which are combined in a summing transformer to approximate an AC sine wave. The actual inverter is far more complicated than that shown but the principle of operation is the same. The harmonic components are filtered from the output before it is distributed on an AC power grid. Each of the numbered switch elements represents hundreds of SCRs in a series array with typical ratings of hundreds of kilovolts and hundreds of megawatts.

The most common pulse switch application is the line type modulator, such as used in a radar transmitter or linear accelerator RF source. The simplified diagram of a line modulator including a command charging switch is shown in figure 4a. The performance requirements for the charging switch is typically at least an order of magnitude less in terms of switching speed, and peak and RMS current, than the pulse discharge switch. Magnetic energy storage require both a closing switch to charge the store and a pulse opening switch to transfer the energy from the store to the pulse load. A simplified schematic diagram of such a system is shown in figure 4b.

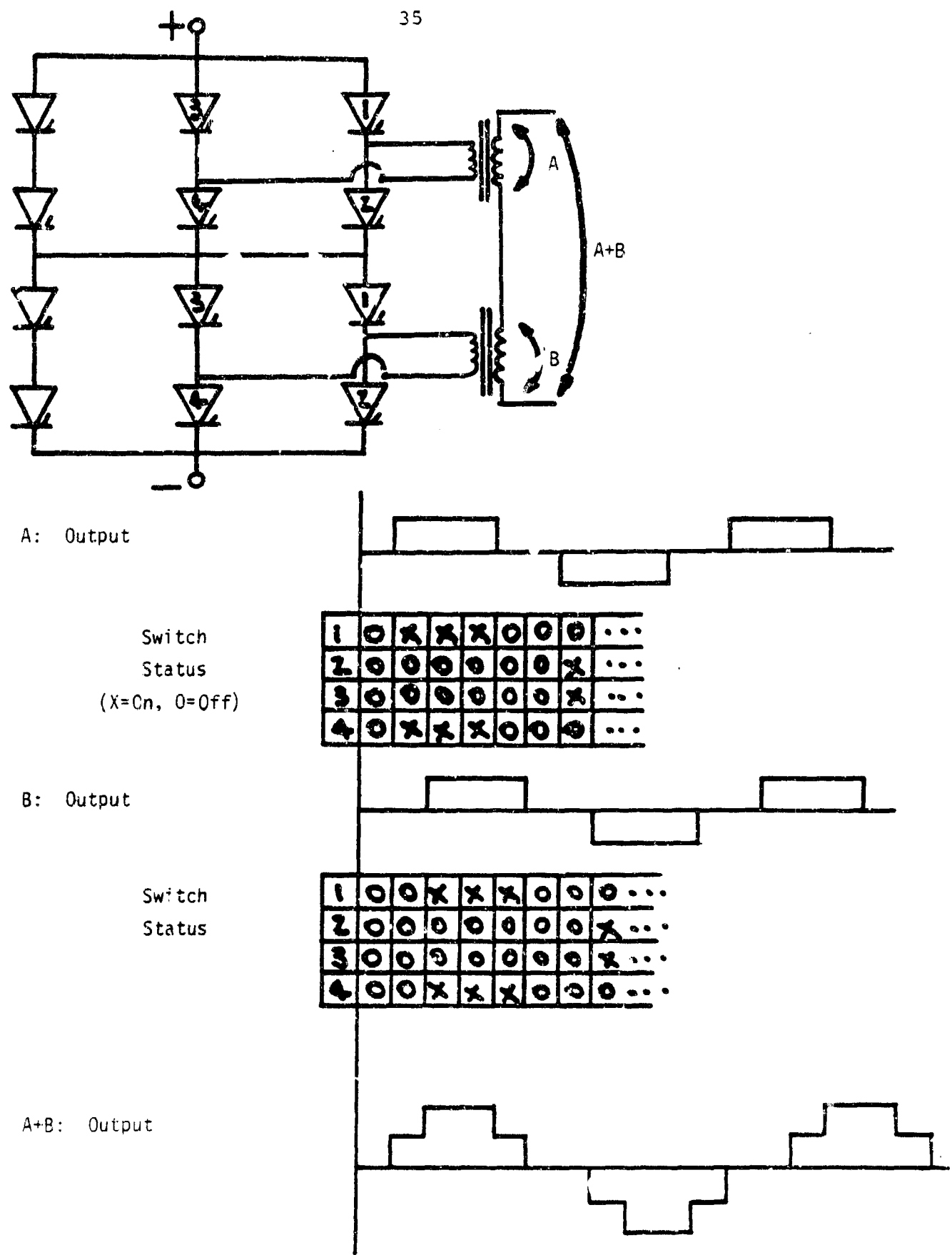


Figure 3. Simplified circuit of a 12-channel inverter.

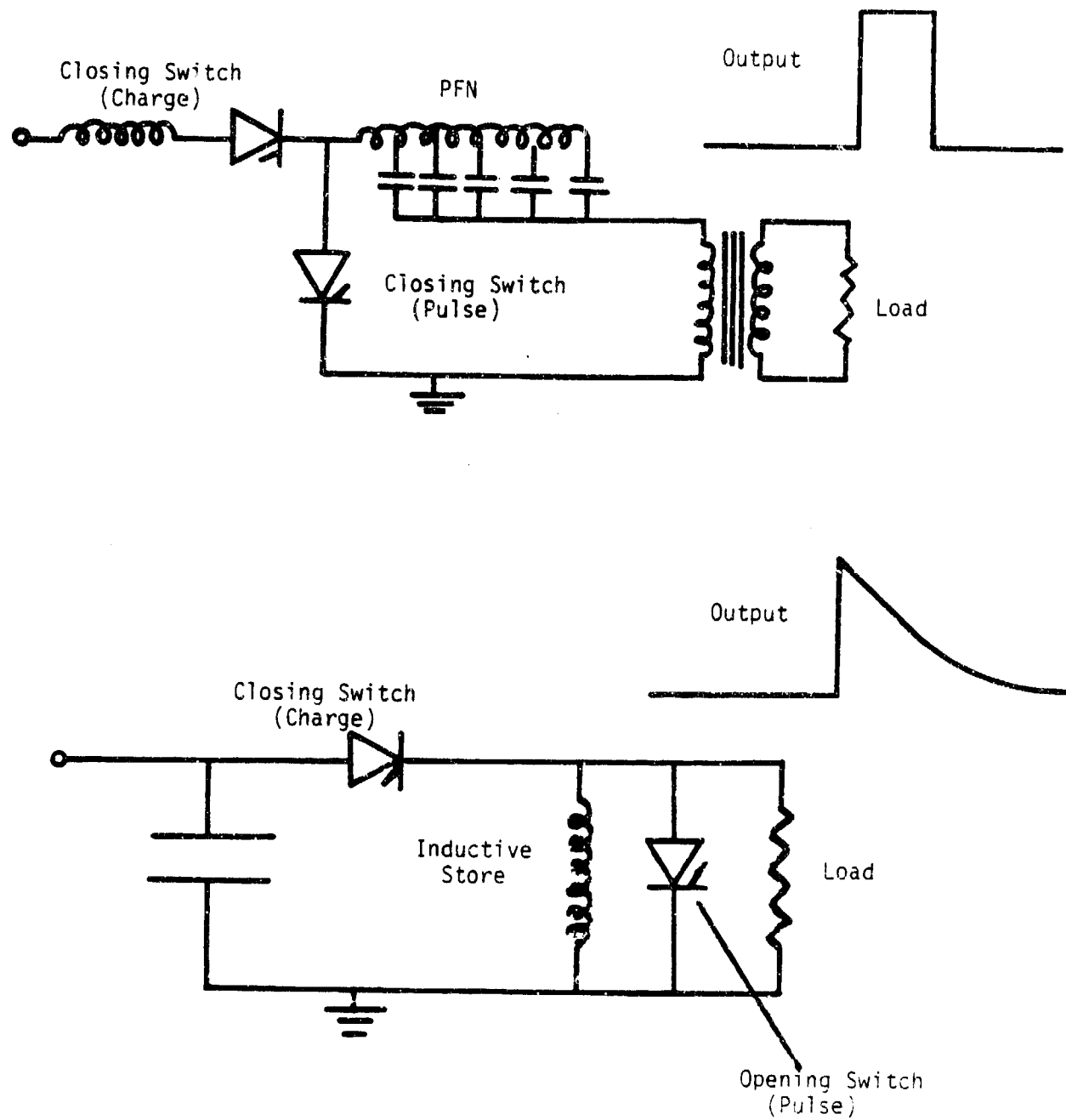


Figure 4. Typical pulse switch applications: a - closing switch
b - opening switch

In general, except for fuses, all switches must be capable of traversing to and from both states of open and close. Switches are usually designated opening or closing switches according to the state which corresponds to the transfer of pulse energy to the load. However, there is a type of pulse switch which has the capability of interrupting the flow of energy to the load as well as initiating it; that is, the pulse of energy transferred to the load is measured from the energy store by the switch. In the simple opening and closing switch circuit, all of the energy in the store is transferred to the load when the switch activates. Solid state switches capable of turning on and also interrupting power flow are transistors, gate turn-off thyristors and commutated SCRs. Examples are shown in figure 5. The conventional analog of this type switch is the hard vacuum tube. Since this switch must perform both closing and opening functions and is distinct from simple closing and opening switches, it seems appropriate to give it a separate designation such as a clopening switch.

SOLID STATE SWITCH ARRAYS

All discrete solid state switching devices have limited voltage, current, power and speed limitations, due to the physical laws governing semiconductor junctions and the practical limitations governing the size and perfection with which they can be fabricated. Consequently, all switching applications of even modest power and speed require arrays of these devices. When large numbers of devices are arrayed, consideration must be provided for the mismatch of the individual elements; this compen-

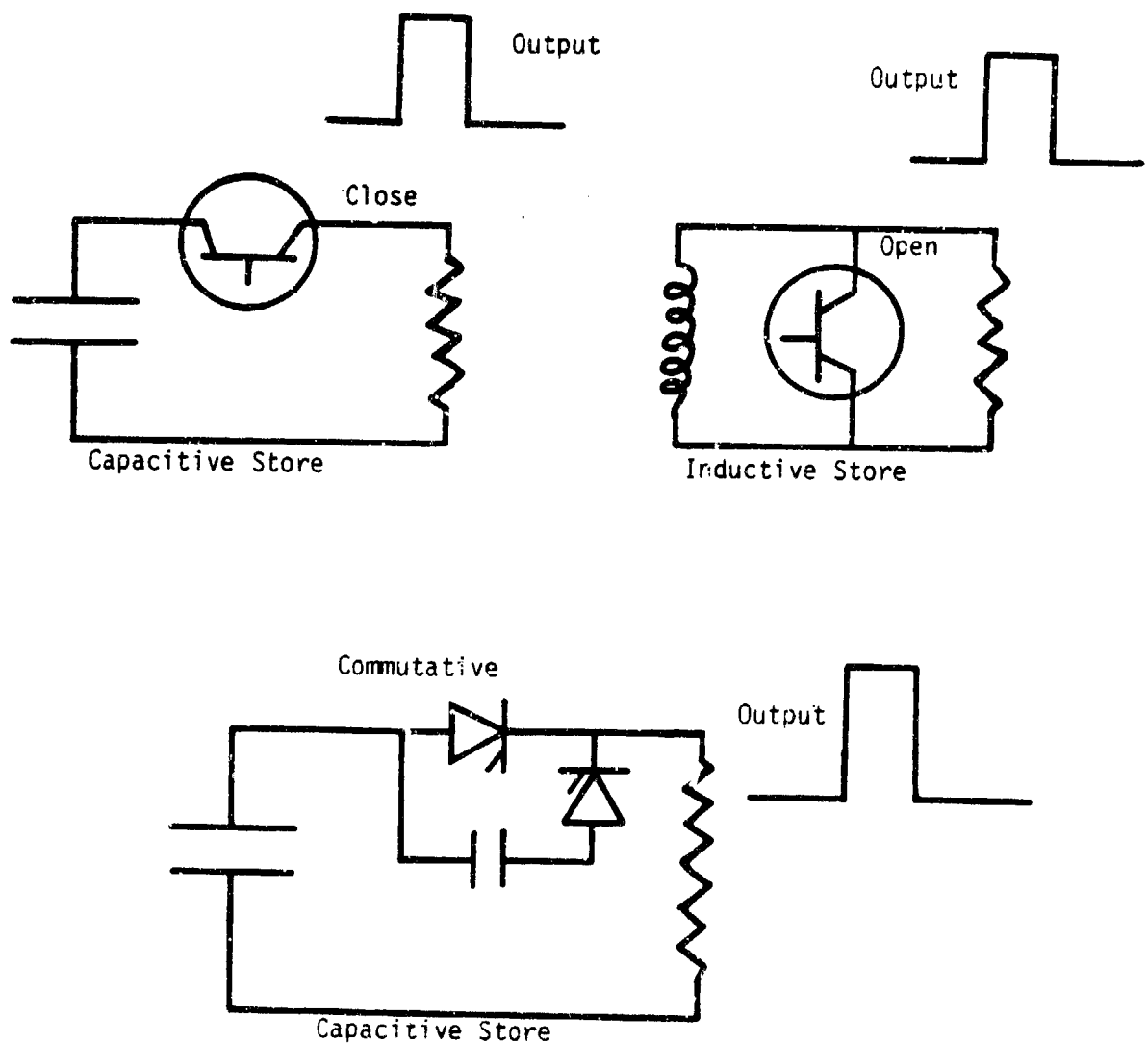
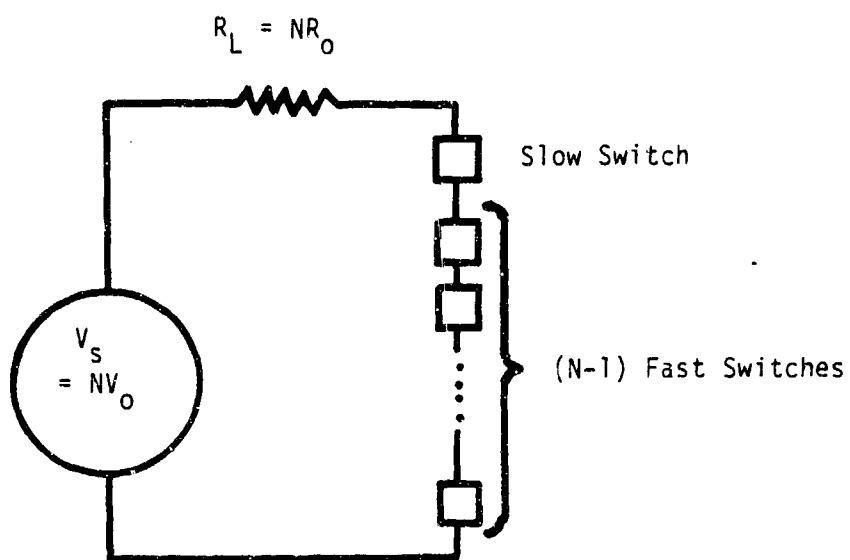


Figure 5. Closing and opening switch applications.

sation leads to degradations in performance, utilization, economics, size, weight, efficiency, and reliability. The larger the number of elements, the greater the degradations: therein lie most of the reasons for not using solid state switches for the more demanding high power pulse applications.

The best array in terms of degradation is simply a parallel combination of N elements to achieve a peak power level; however, as more elements are added, the most serious problem is the impedance level of the circuit. This decreases as $1/N$, and an impractically low level of impedance is soon reached, and the array can no longer be extended unless series elements are added.

To illustrate the matching problem of series arrays, the simplified model of figure 6 is used. Both the switching speed and switching delay are accounted for. Each element is modeled as a closing switch with an exponential resistance. The extreme case is taken where $N-1$ elements are identical and one additional element is slower and has a longer delay. (A more realistic analysis would use statistical distributions of speeds and delays but this simplified case illustrates the general conditions as well.) A parametric analysis of the overstress of the slow element as a function of the mismatch of speed and delay and the total number of elements is shown in figures 7 and 8. The results show that, to hold the overstress factor below 2, the match must be in the order of 5%, which is far from achievable even with the most carefully controlled and selected raw elements. The alternative is to swamp out the real differences in elements with compensation networks, which in turn degrade the



Slow Switch: $R_s(t) = R_x \exp[-\alpha_s(t-\delta/\alpha_f)]$;

Fast Switch: $R_f(t) = R_x \exp(-\alpha_f t)$;

Array Switching Time: $t_A = (1/\alpha_f) \ln \left[\frac{R_0/R_x}{e-1} \right]$;

The voltage (normalized) across the Slow Switch is

$$V_{sn} = \frac{N \exp(-\alpha_s t + \eta \delta)}{N(R_0/R_x) + \exp(-\alpha_s t + \eta \delta) + (N-1) \exp(-\alpha_f t)} ;$$

This voltage is a maximum when

$$t_m = (1/\alpha_f) \ln \left[\frac{(1-\eta)(N-1)}{\eta N(R_0/R_x)} \right] ;$$

where η = mismatch in switching speeds = α_s/α_f ,

δ = fractional delay mismatch = $\alpha_f \Delta t$.

Figure 6. Series array switching model.

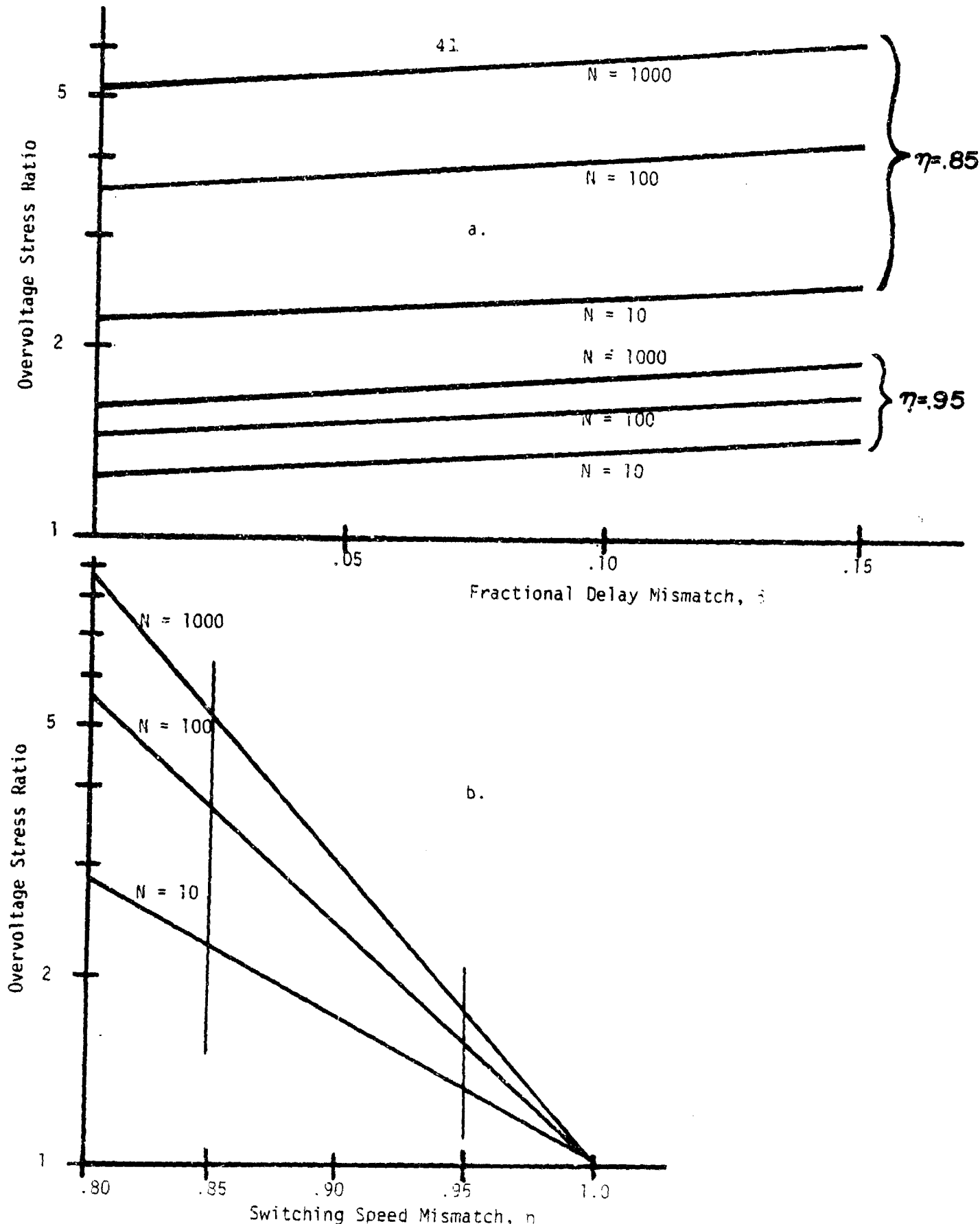
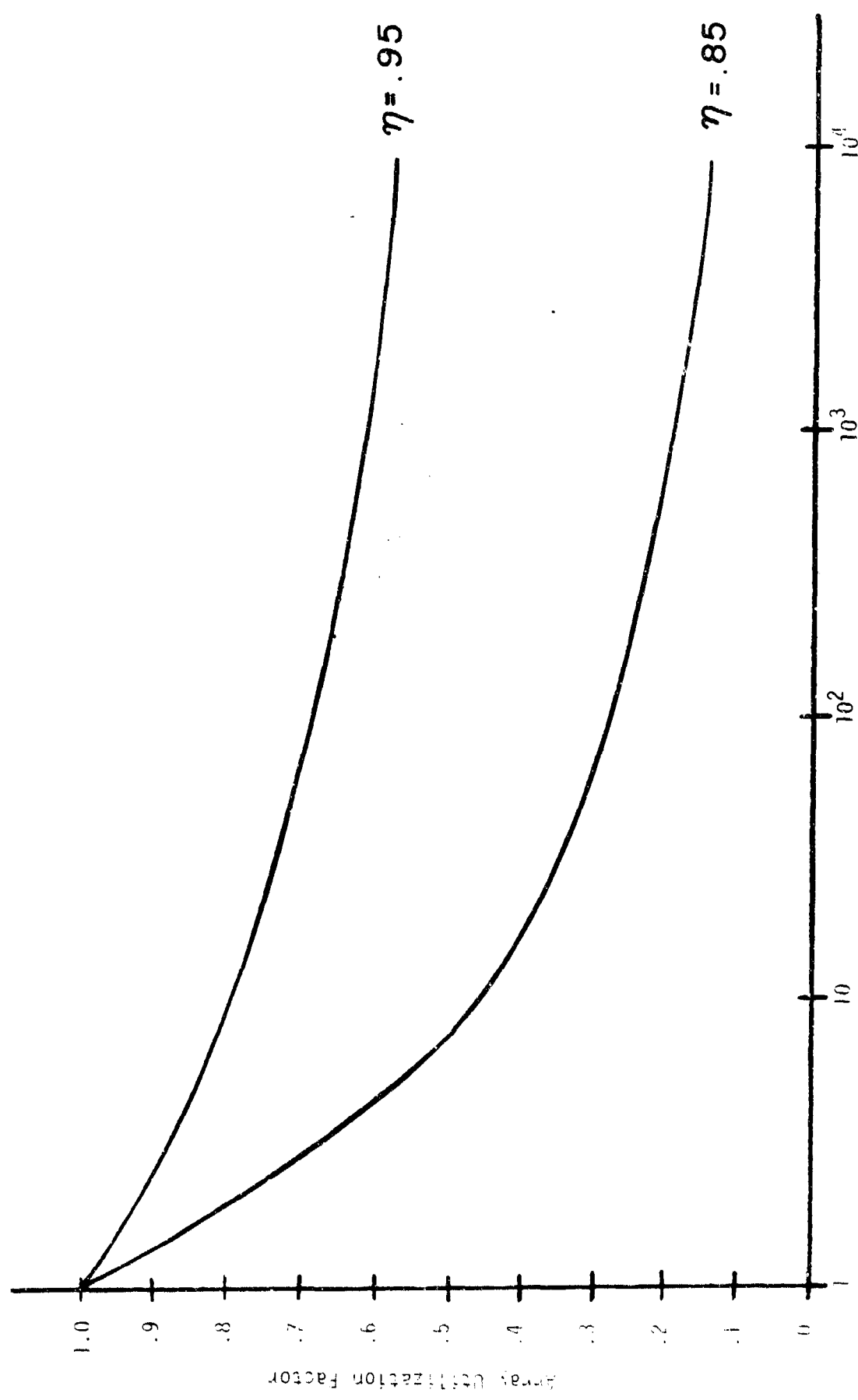


Figure 7. Overvoltage stress ratio for a slow element in an N -element array: a) dependence on relay mismatch; b) dependence on speed mismatch.



switching speed, typically by an order of magnitude or more; the degradation increases still further with larger arrays due to the larger number of elements. In the case of power inverter arrays the degradation is acceptable; 2 to 3 microsecond elements are degraded to 20 to 30, or even to 100 microseconds, in arrays which are perfectly useful for power frequency applications. However, such degradation is by no means even close to acceptable for most pulse switching application.

Another lesser problem with arrays is providing trigger signals to all the elements. However, several methods have been perfected which have solved this problem completely. They include current transformer type coupling, optical triggers coupled to floating trigger amplifiers, and direct optically triggered devices. Simplified diagrams of these triggering methods are shown in figure 9.

SUPER SWITCHES

There are a few applications for extremely exotic switches. One such is shown diagrammatically in figure 10. At the present time there is no switch, even of the fuse type, which can meet these requirements. In view of the limitations of array type solid state switches, there is no possibility that such applications would ever be feasible using semiconductor junction devices. However, it is conceivable that bulk semiconductor elements, driven by photons, electrons or X-rays, might be a good approach. LANL has already demonstrated⁽⁶⁾ switching of 3 KA at 120 KV in 200 ns with a bulk silicon switch, 0.5 x 0.5 x 2.4 cm, using a laser to modulate photoconductivity. These voltage

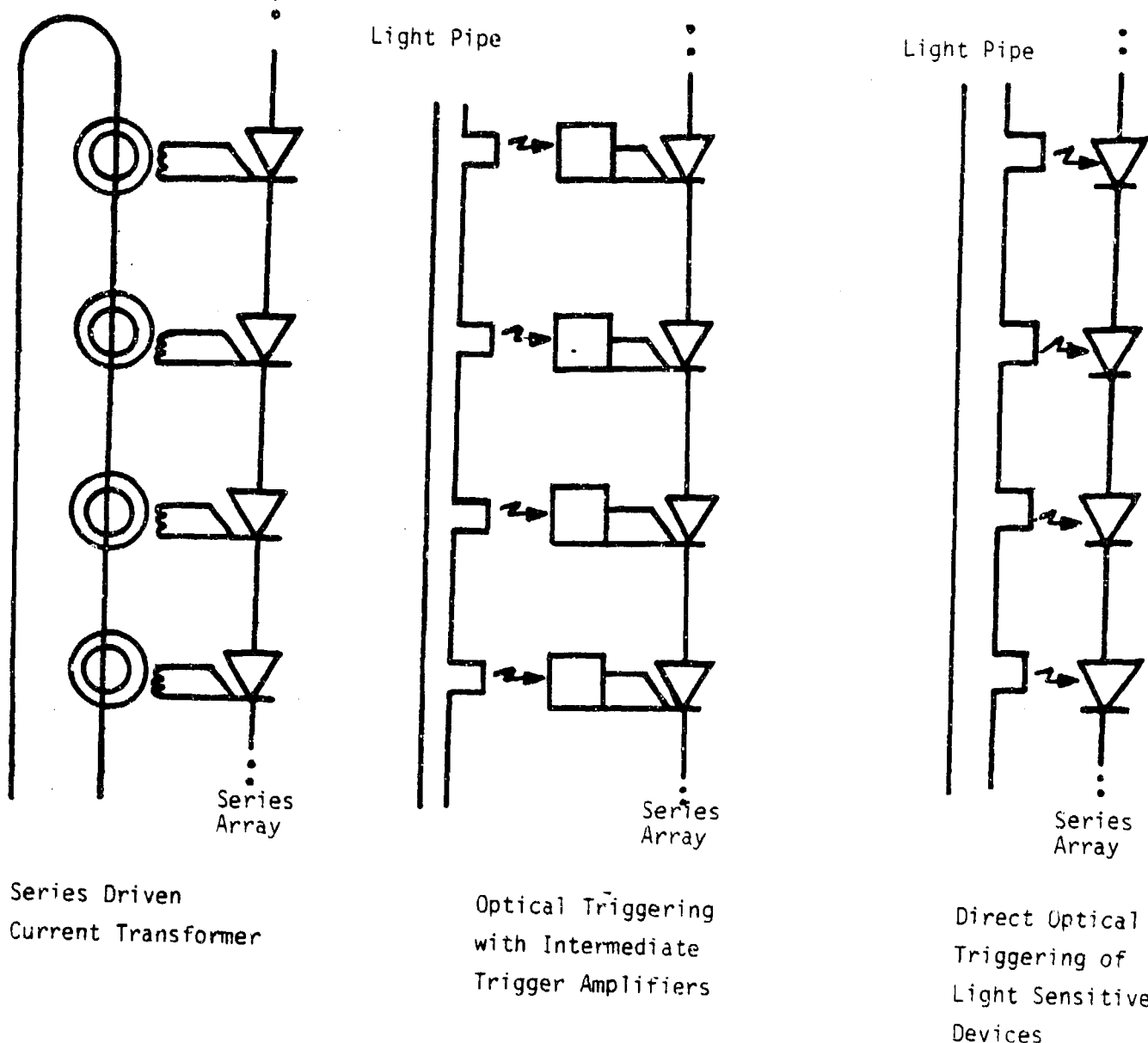
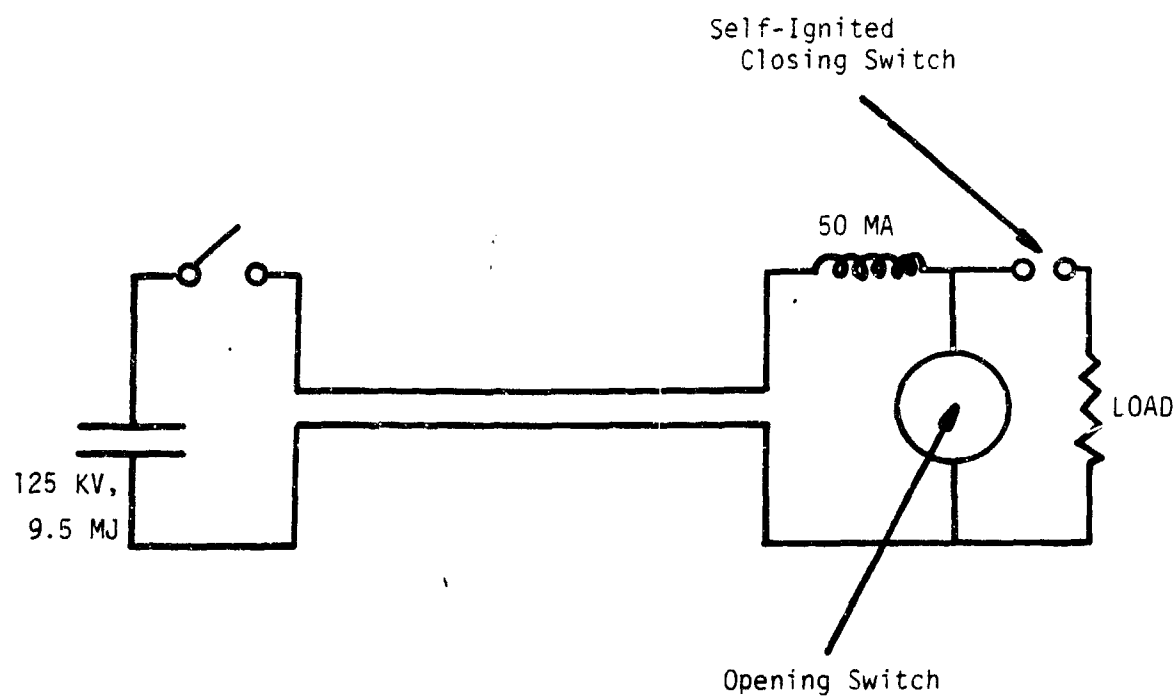


Figure 9. Trigger procedures for switch arrays.



Switch Requirements:

| | |
|---------------------------|--------|
| Interrupted current | 50 MA |
| Interrupt time | 200 ns |
| Voltage to load | 1 MV |
| Maximum switch inductance | 1 nH |
| Peak power | 50 TW |

Figure 10. Schematic of the switch circuit.

gradients, current densities and switching speeds provide a reasonable basis for projecting the eventual development of terawatt class switches as described in figure 10.

CONCLUSIONS

The utilization of solid state devices in switching applications is governed by a number of factors which differ somewhat with each application. As one would expect, the most prolific growth is in areas which have actually come into being as a result of the capabilities of the devices. The slowest rate of utilization is in applications where competitive switches are already well-established or where other disadvantages exist, primarily associated with the use of large arrays of solid state devices.

Although bulk semiconductor switches have a promising and unique potential for very high power fast pulse applications, future utilization of solid state switches in high power fast pulse applications will continue to progress rather slowly for the following reasons. Large arrays of switch elements have several disadvantages, the most important being the total number of elements. The second is the degradation in switch speed caused by compensation of the mismatches between the elements. The number can be decreased by using higher voltage elements, but higher voltage elements inherently have slower switching speeds. However, if the uniformity of the speed and delay characteristics of the elements can be improved, so as to permit a smaller penalty in array switching speed resulting from less compensation, then a net overall performance advantage might be gained.

It is not expected that an improvement of more than about a two-to-one in element count per array will occur in the next two to five years.

REFERENCES

1. "Power semiconductors," B. J. Baliga, IEEE Spectrum, December, 1981.
2. Multi-Megawatt Solid State Switch, RCA Kirtland/RADC Presentation, November 1, 1974.
3. Multiple Chip SCR, R. Casolano and D. Pruitt, Final Technical Report, RADC-TR-77-264.
4. Advanced Reverse Switching Rectifier Modulator, E. H. Hooper and D. L. Jordan, Technical Report, AFWL-TR-75-100.
5. "Thyristors: future workhorses in power transmission," Godi Kaplan, IEEE Spectrum, December, 1982.
6. Private communication, W. C. Nunnally, Los Alamos National Laboratory, 1982.

LIGHT TRIGGERED THYRISTORS*

V. A. K. Temple
Corporate Research and Development Center
General Electric Company

High voltage DC applications have stimulated GE's work in advanced thyristor development. Much of its recent work has been related to light triggering, with high intensity light drives, rather than to conventional electrical gating, where a relatively weak gate signal turns on a small portion of the device, followed by a gradual increase in stored base charge and anode current. Electrical triggering is device limited, whereas turn-on in light triggered devices is limited primarily by the gate energy input rate. Figure 1 contains a list of the advantages (and some disadvantages) of light triggering vs. electrical triggering.

Light triggered devices have their greatest impact in series strings that need to be triggered as a unit. Gate isolation leads to simple, less costly systems. Other important systems, such as high power drives, depend on the noise immunity of the light triggered system. However, a practical system has very low available gate photoenergy, leading to both noise (dv/dt) and turn-on (di/dt) problems (figure 2). Only recently have we been able to make light triggered devices which function as well as their electrically gated counterparts. Figure 3 illustrates an

*Much of this work has been supported by EPRI.

ADVANTAGES OF LIGHT TRIGGERING

- GATE ISOLATION
- NOISE IMMUNITY
- REDUCED DELAY TIME
- SYSTEM SIMPLICITY
- HIGHER GATE EFFICIENCY
- OVERALL RELIABILITY
- LOWER SYSTEM COST

DISADVANTAGES

- HIGHER DEVICE COST (<5%)
- INCREASED PACKAGE COST

Figure 1. Advantages and disadvantages of light triggering.

SPECIAL PROBLEMS OF LIGHT-FIRED DEVICE DESIGN

- In Practice, Photo-Gate Energy Is Small
- Result; a Critical Gate Sensitivity — dv/dt Sensitivity Trade-Off
- Small Gate Size a Practical Solution But Leads to di/dt Problems
- di/dt Capability Improved by
 - Amplifying Stages
 - Controlled Turn-On Line Dissipation
 - Controlled Inter-Stage Transients
 - Large Final Stage Turn-On Line

Figure 2. Problems of light triggered devices.

example of turn-on failure; the external current increases faster than the turned-on region can spread. Here, a 0.010 in. diameter cylinder has melted through a 0.024 in. thick silicon wafer. Our fast successful light triggered thyristor (LTT) is shown in figure 4. This is a 1200 V, 200 A converter thyristor which, although less rugged in di/dt than its electrically gated counterpart, still met the specification for 60 KVA aircraft inverter systems.

In 1978 our first successful 3 KV, 1000 A LTT was delivered under contract to EPRI. Each doubling of voltage rating means about a 7-fold increase in turn-on thermal stress. This jump from 1200 to 3000 volts was made by optimizing a two-stage amplifying gate structure, illustrated in figure 5. To obtain 5 KV, we had to remove the light triggered function from the device and dissipate some of the turn-on losses in an external resistor (figure 6). The gate device is a 5 KV, 40 A (pulse) device with a 4 KV/ μ s dv/dt and an infinite di/dt rating, providing the resistor is greater than 125 ohms. Gate sensitivity is about 1-3 nanojoules. The front and back of the separate LTT are shown in figure 7. Figure 8 illustrates the turn-on characteristics of the configuration of figure 7 with two different values of the resistor. (The top two current scales in the two photographs should be interchanged.) Finally, figure 9 illustrates a 5 KV, 53 mm LTT, made with EPRI support, which attempts to integrate the configuration of figure 6.

The center of figure 9 is shown enlarged in figure 10. It includes resistor and current collector areas between its first

CA 133 # 28 - Main Div/DT

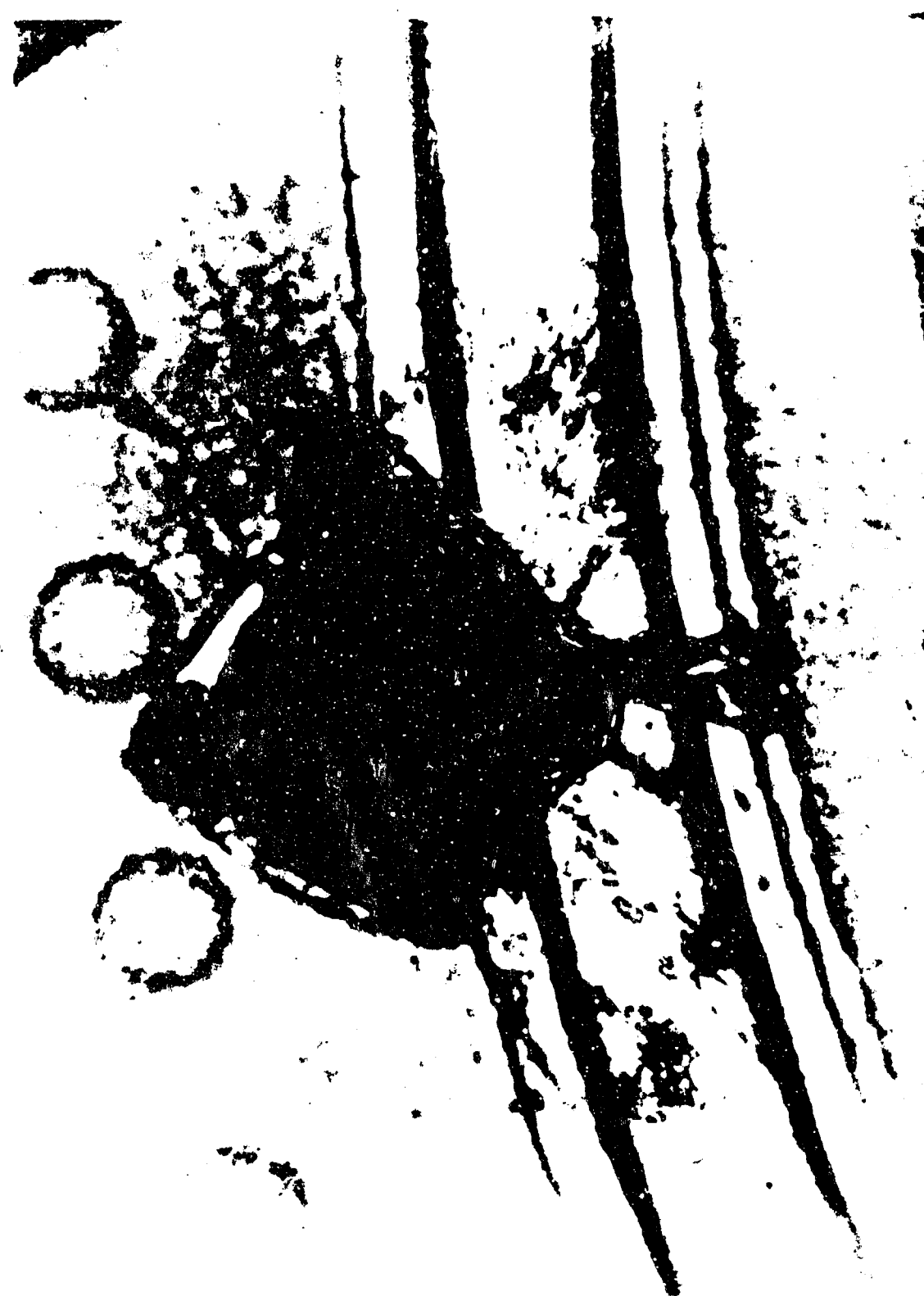


Figure 3. Example of turn-on failure.

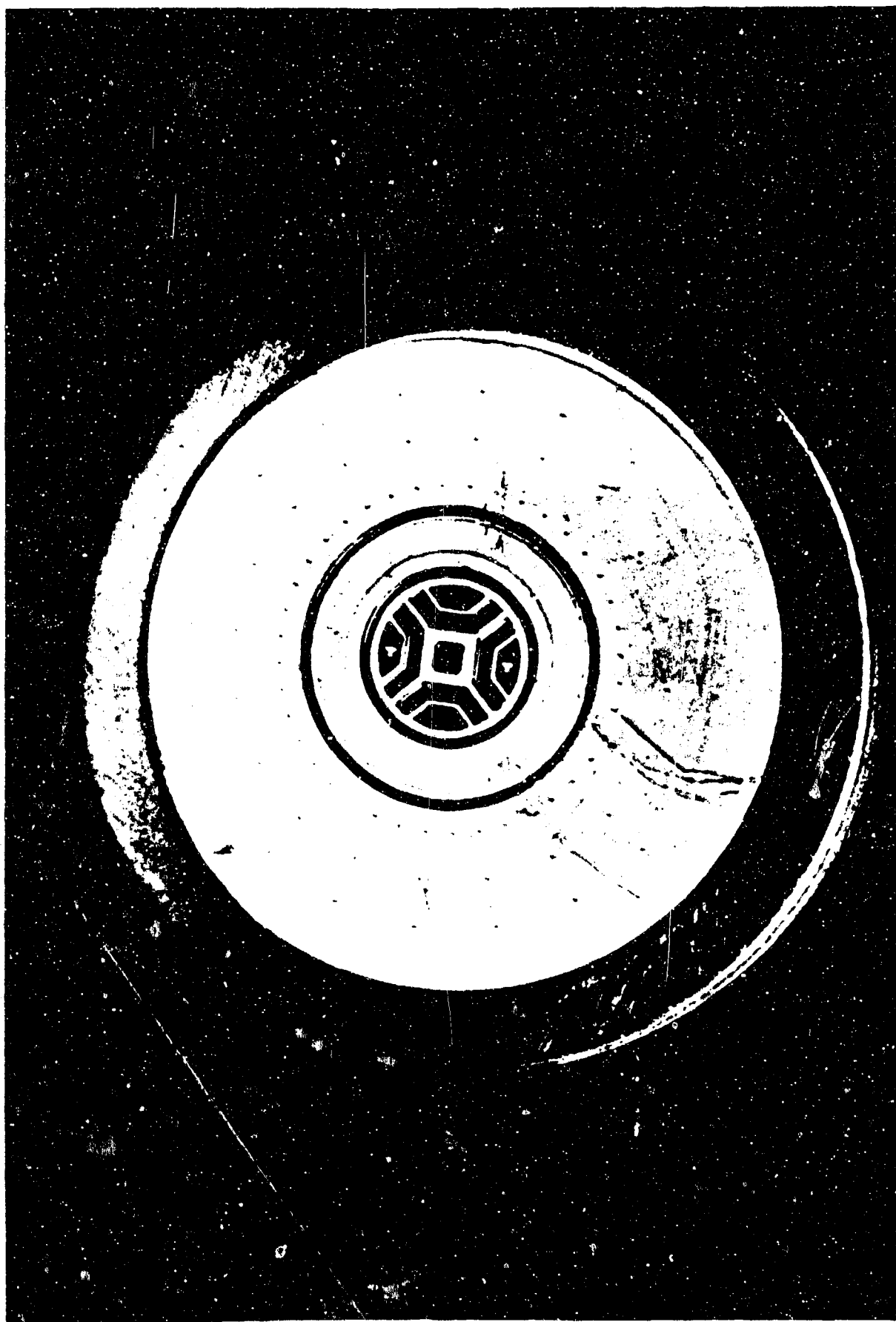


Figure 4. Light triggered thyristor.



Figure 5. Two-stage amplifying gate.

SEPARATE GATE TRIGGER SYSTEM

- **ADVANTAGES**

- Wider Range of Application

- Better Performance

- **DISADVANTAGES**

- 20V Minimum Firing Voltage

- Extra Device

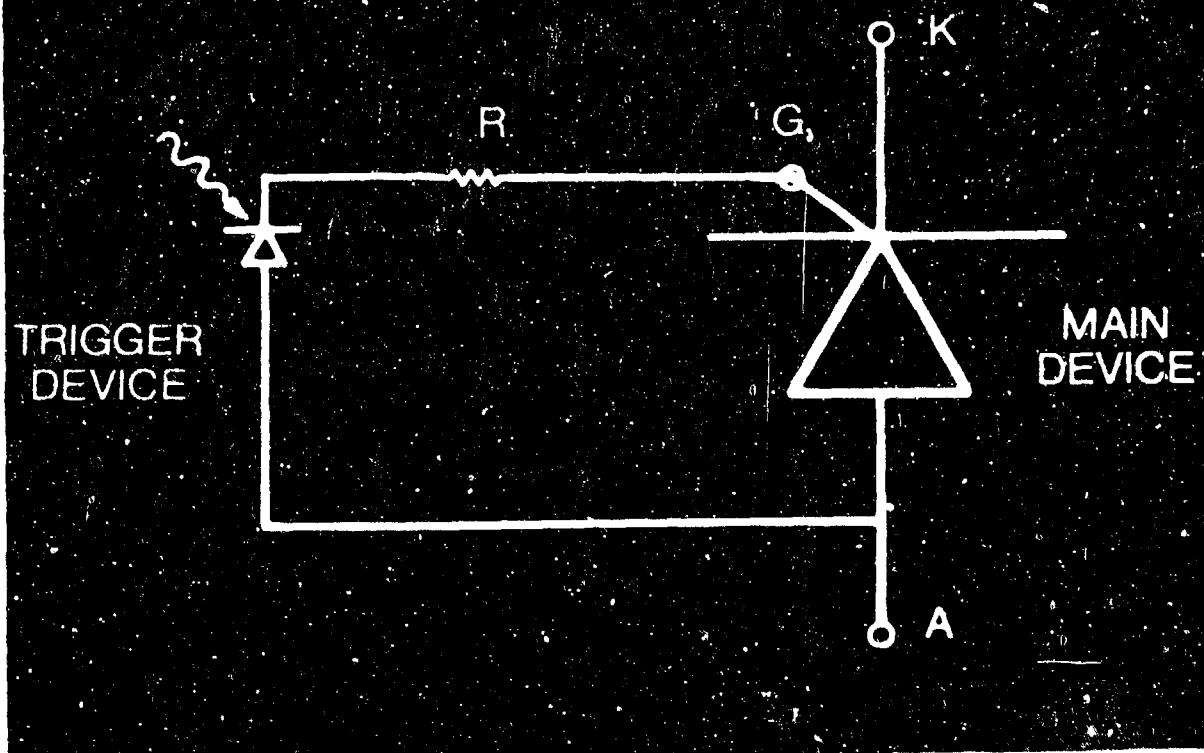


Figure 6. Separate gate trigger configuration.

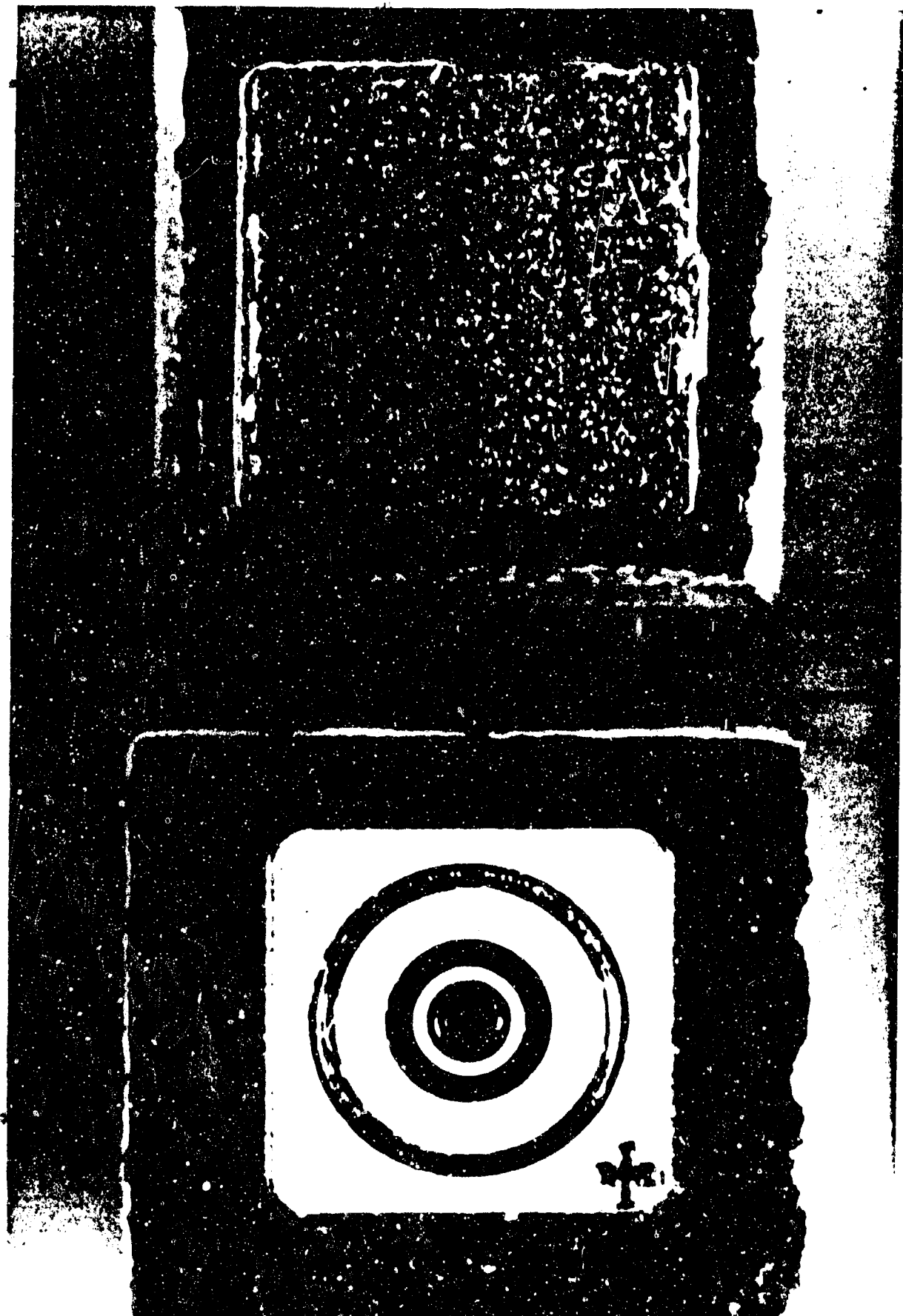


Figure 7. Front and back views of an LTI chip. The upper photograph is the back side.

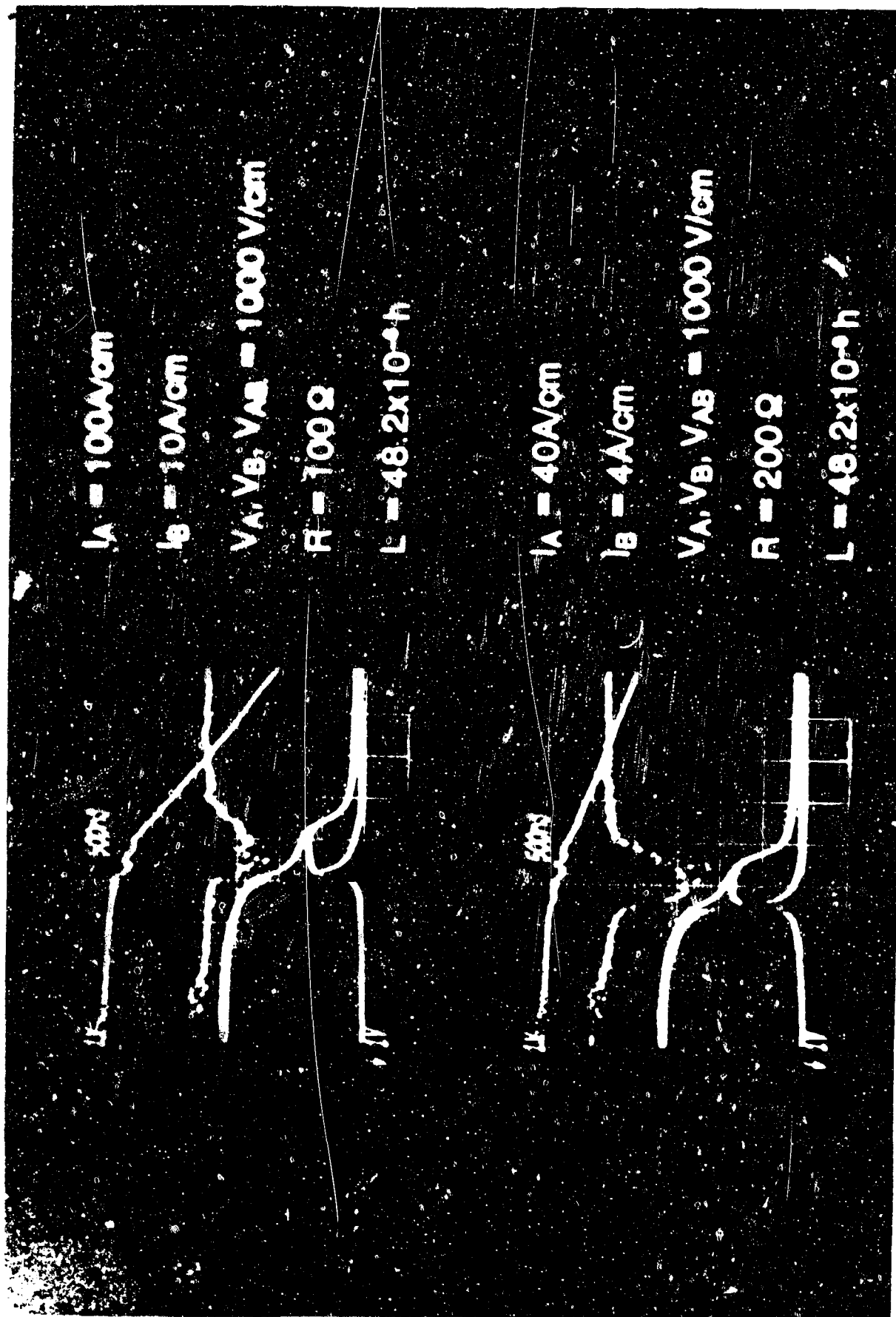


Figure 8. Turn-on characteristics of an LTI.



Figure 9. Structure of a 5 KV LTI.

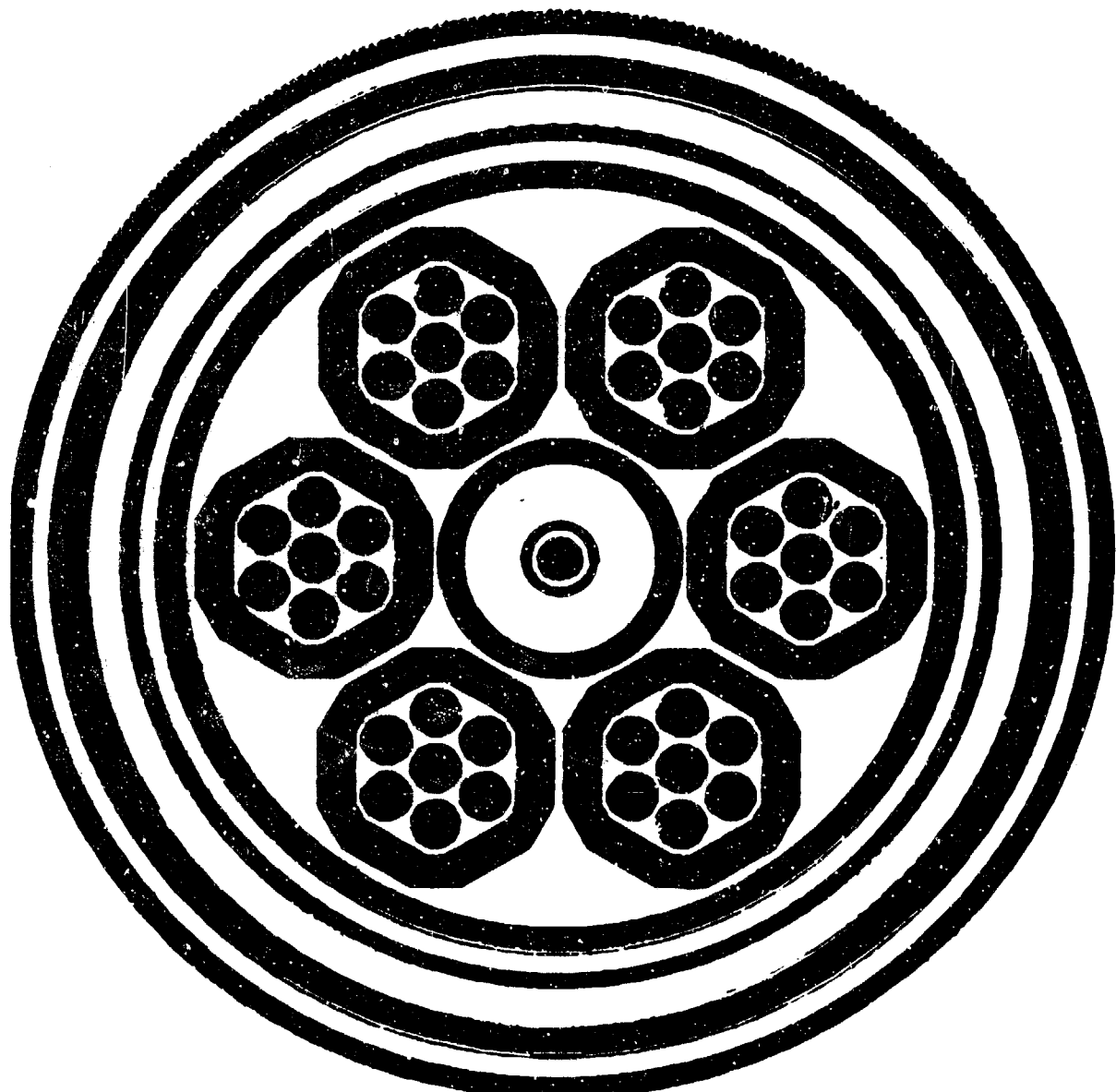


Figure 10. Center region (enlarged) of a 5 KV LTI.

(photo) stage and its second (pilot) stages, and also between the pilot and ministages. A later version of this device has the following characteristics:

1. 4800 volts forward blocking and 6000 volts reverse blocking;
2. 900 A current;
3. 5000 V dv/dt with safe dv/dt turn-on if exceeded;
4. greater than 500 A/ μ sec di/dt at 4 KV;
5. typically 1.2 nanojoules gate incident photoenergy to trigger at 25 volts forward blocking.

The secret ingredient appears to be the controlled turn-on introduced by the built-in resistor. Figure 11 summarizes the characteristics of the 5 KV LTT. Higher di/dt could be achieved by increasing the main stage turn-on line (gate-cathode periphery).

Figure 12 depicts the factors involved in the auto-generation of the gate photocurrent. It assumes that electron hole pairs created in the light active volume will appear as gate current. Figure 13 illustrates the effect of wavelength and device blocking voltage on the collected current. The response is more complex than figure 12 suggests, because the device first appears as a phototransistor with voltage dependent gain and then, at higher voltage, as an avalanche or near avalanche phototransistor. Figure 14 depicts a charge control model of a one-dimensional thyristor. Terms A are required to model turn-on delay time; Term B models the gate current source resulting from the electron part of the photocurrent. The solutions for this model are shown in figure 15, which illustrates the current

5 KV LTT SUMMARY

• TURN ON SPEED & RELIABILITY IMPROVED BY

- LONG TURN-ON LINE
- HIGH GATE ENERGY
- AMPLIFYING STAGES
(FOR LOW GATE ENERGY)
- LIGHT TRIGGERING
- CONTROLLED TURN-ON

Figure 11. Summary of properties of the 5 KV LTT.

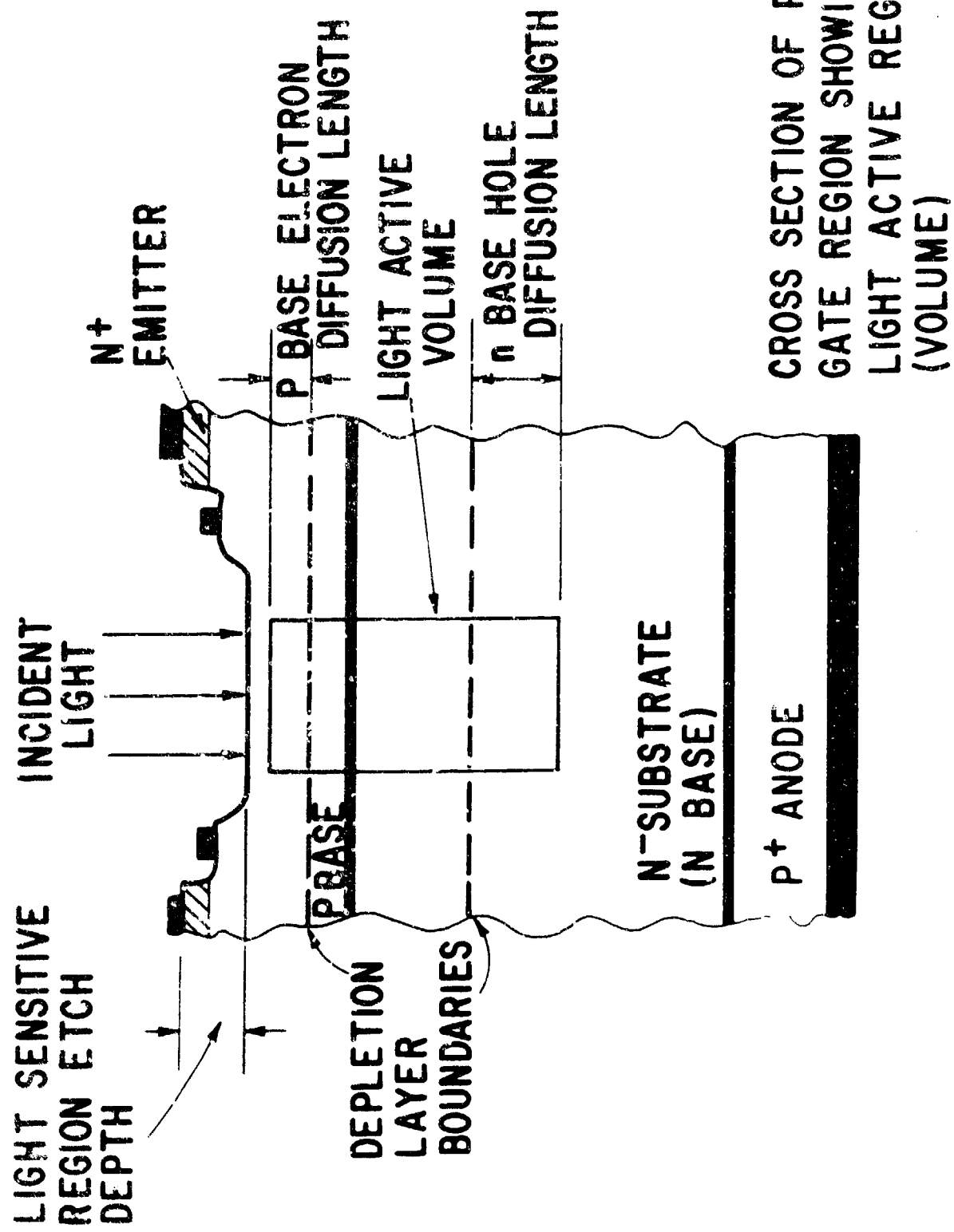
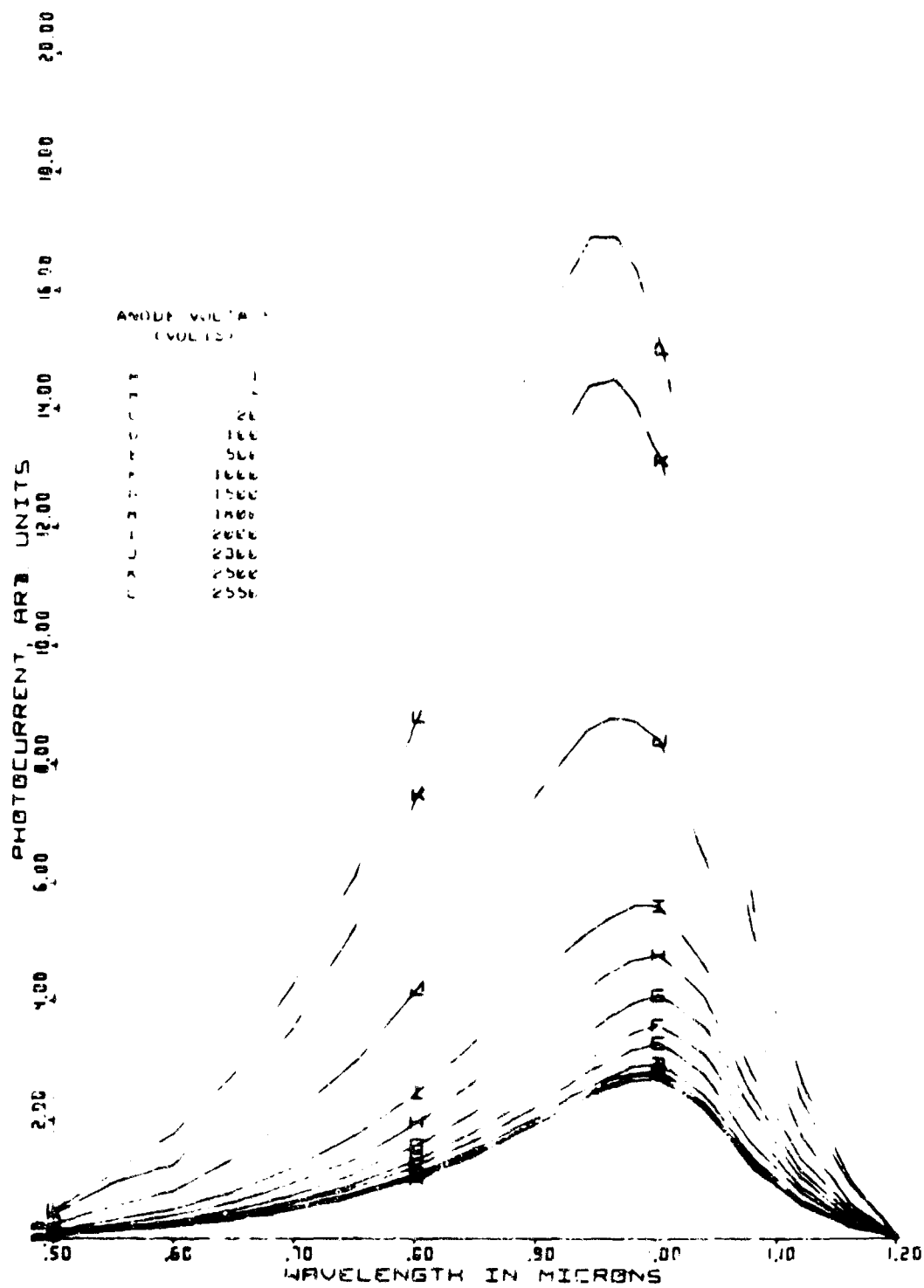


Figure 12. Autogeneration of gate current.



TYPICAL THYRISTOR PHOTORESPONSE

Figure 13. Wavelength and blocking voltage dependence of collected current.

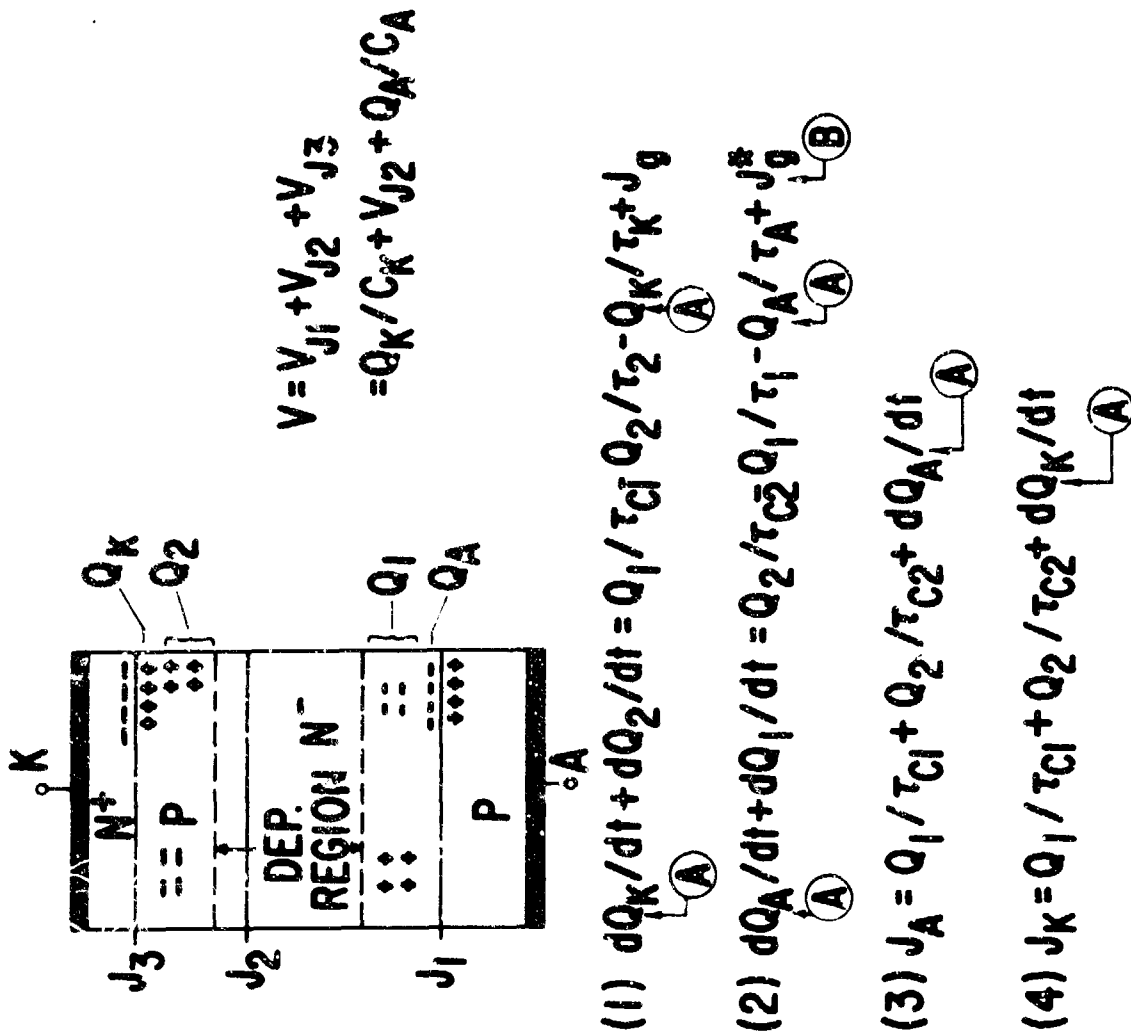


Figure 14. Charge control model for a one-dimensional thyristor.

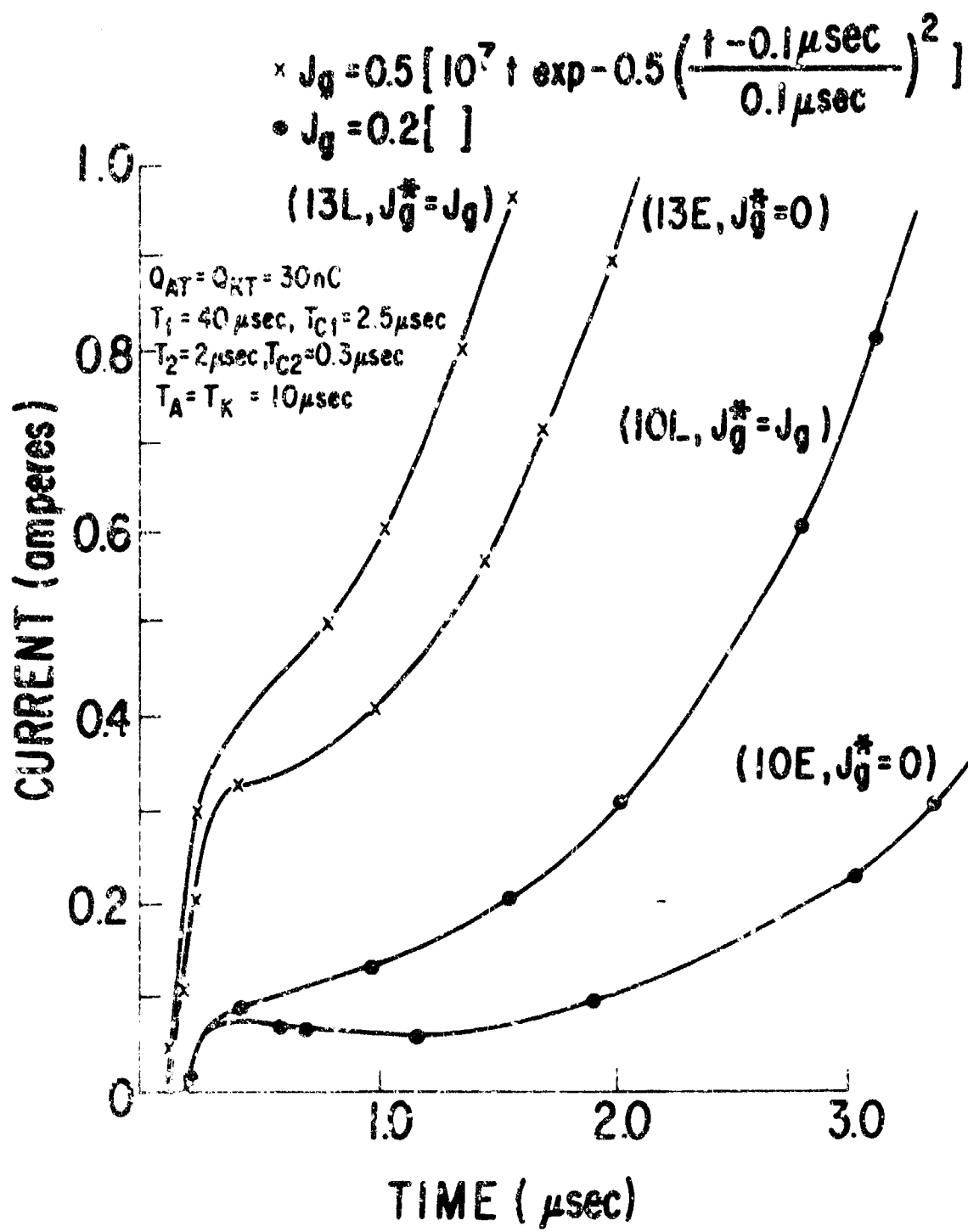


Figure 15. Solutions for the charge control model.

(and charge) built up during turn-on for two different levels of gate drive, for both an electrically gated and a light gated device. Note that, after the initial turn-on phase, the electrically gated and the light gated devices have the same rate of current rise. In the limit, one would expect to have the light triggered device to have a one base transport time advantage. Figure 16 summarizes the information of the last several illustrations. Note that there is an unsupported (here) conclusion that a two-dimensional effect (spreading velocity) will depend on the charge build-up speed considered in figures 14, and 15.

Figure 17 illustrates the doping profiles of three high voltage thyristors. Note that the 20 KV device is 0.335 cm thick! Figure 18 contains the impurity profile of an asymmetric thyristor whose reverse blocking has been sacrificed for a 20 KV device 0.15 cm thinner than its symmetric counterpart.

The minority carrier lifetime must be high to obtain a low forward drop in very high voltage devices, so that slow turn-off is the cost of a reasonable forward voltage. Figure 19 illustrates this trade-off. Several temperatures are shown because the trade-off is not quite immutable and can be affected by temperature. One reason for improved low temperature behavior is increased minority carrier diffusion coefficient (figure 20, for holes), which means a longer diffusion length, more conductivity modulation, and less forward drop for the same device thickness and carrier lifetime. Another reason is the lower resistivity because of the higher low temperature mobility (figure 21).

Figure 22 is a summary of the previous discussion. It should be

ET VS LT SUMMARY

- LT GATES BOTH BASES
- CHARGE BUILD UP IS FASTER
 - AT HIGHER TURN-ON VOLTAGE
 - IN THINNER DEVICES
- SPREADING VELOCITY AFTER TURN-ON VARIES LIKE CHARGE BUILD UP

Figure 16. Physical events in an LTI.

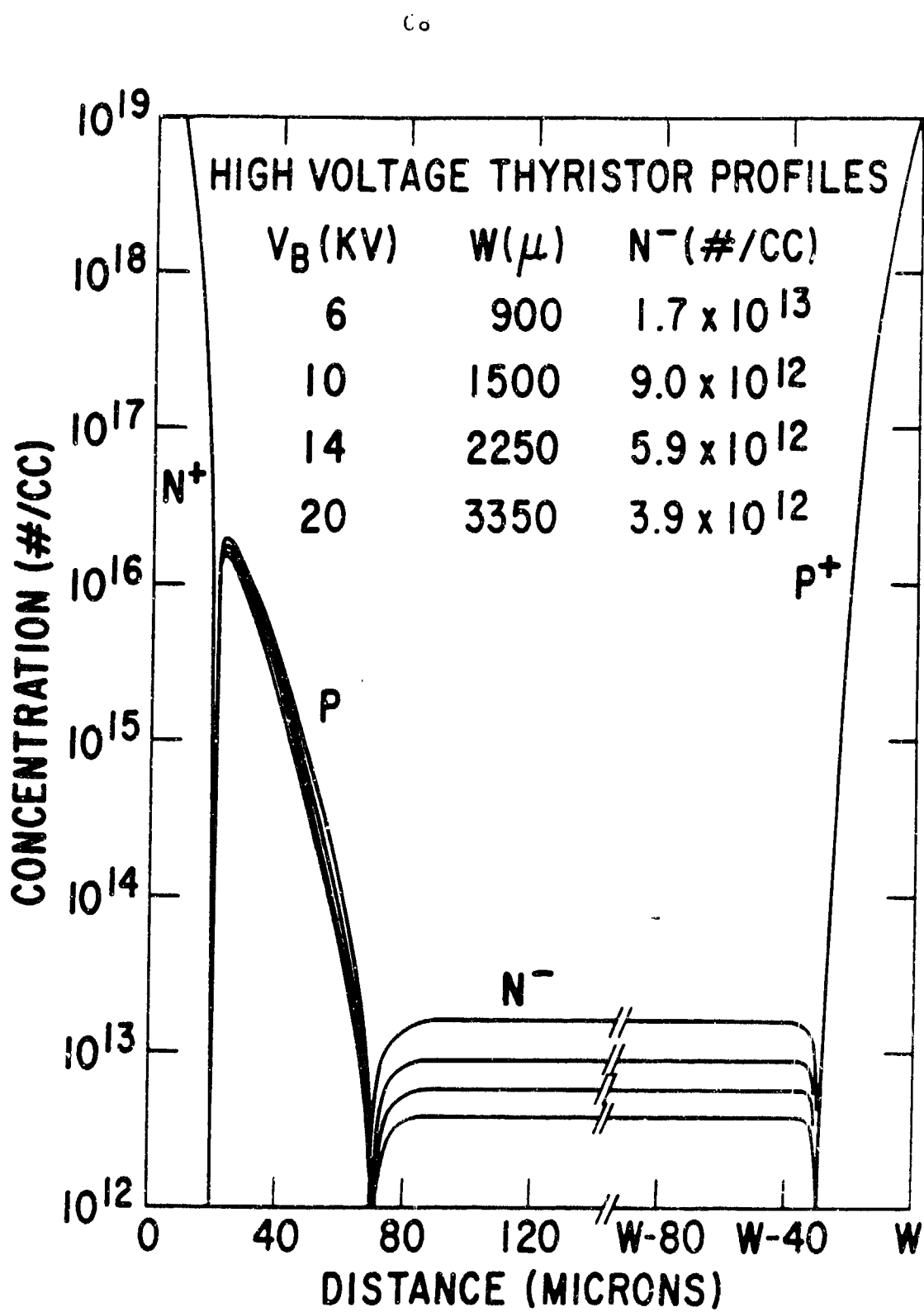


Figure 17. Impurity profiles for high voltage thyristors.

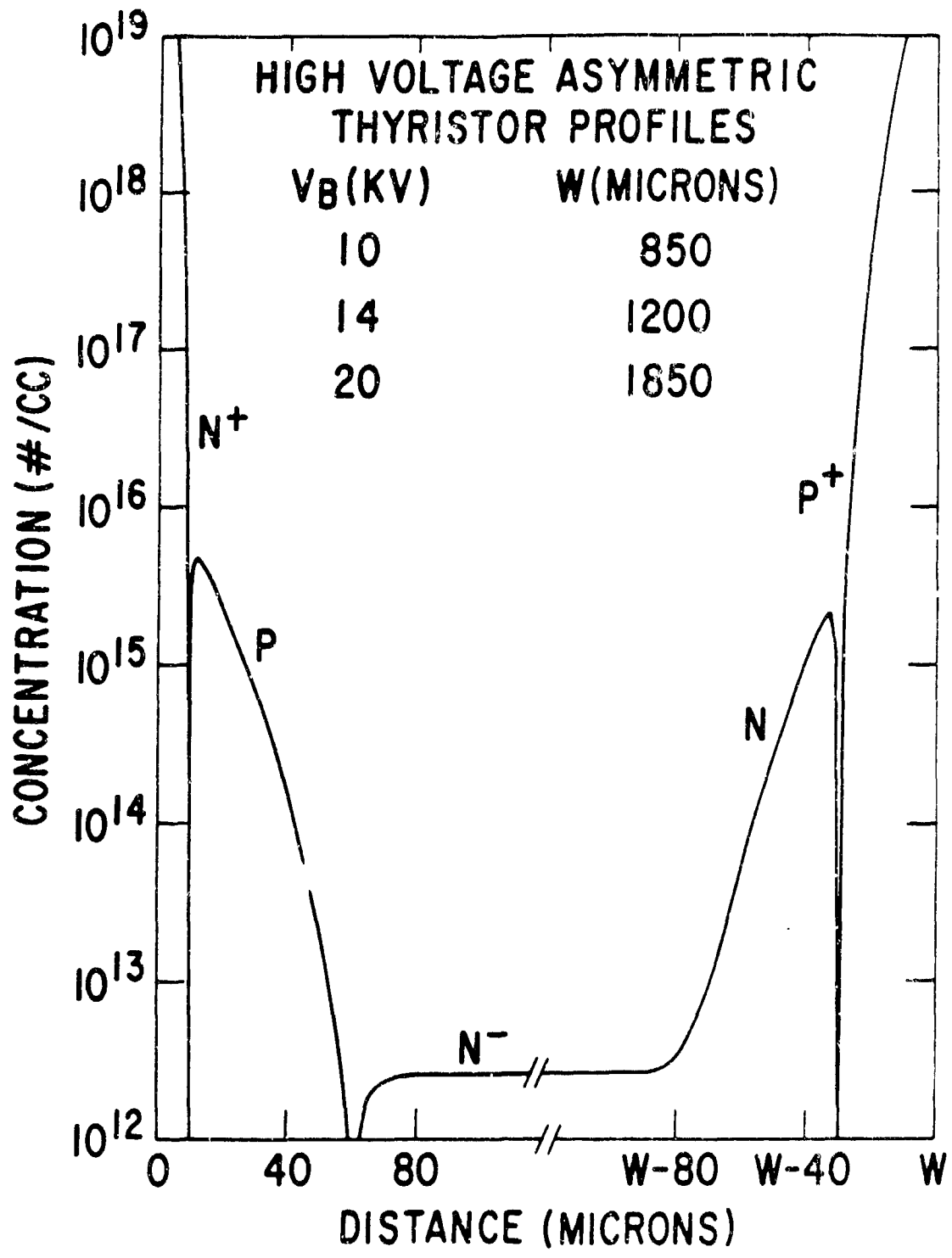


Figure 18. Impurity profile in an asymmetric thyristor.

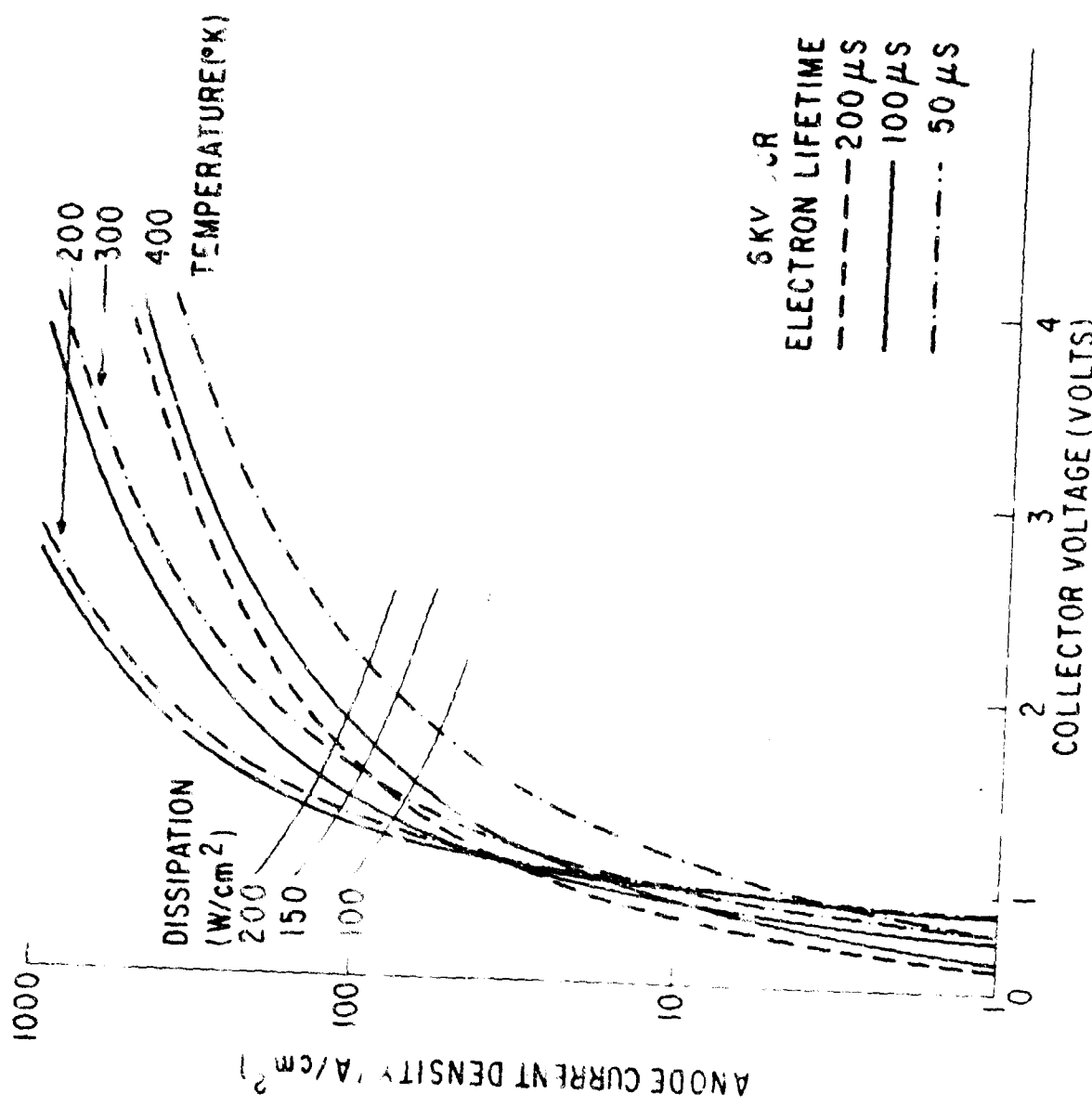


Figure 19. Trade-off between turn-off time and forward voltage drop.

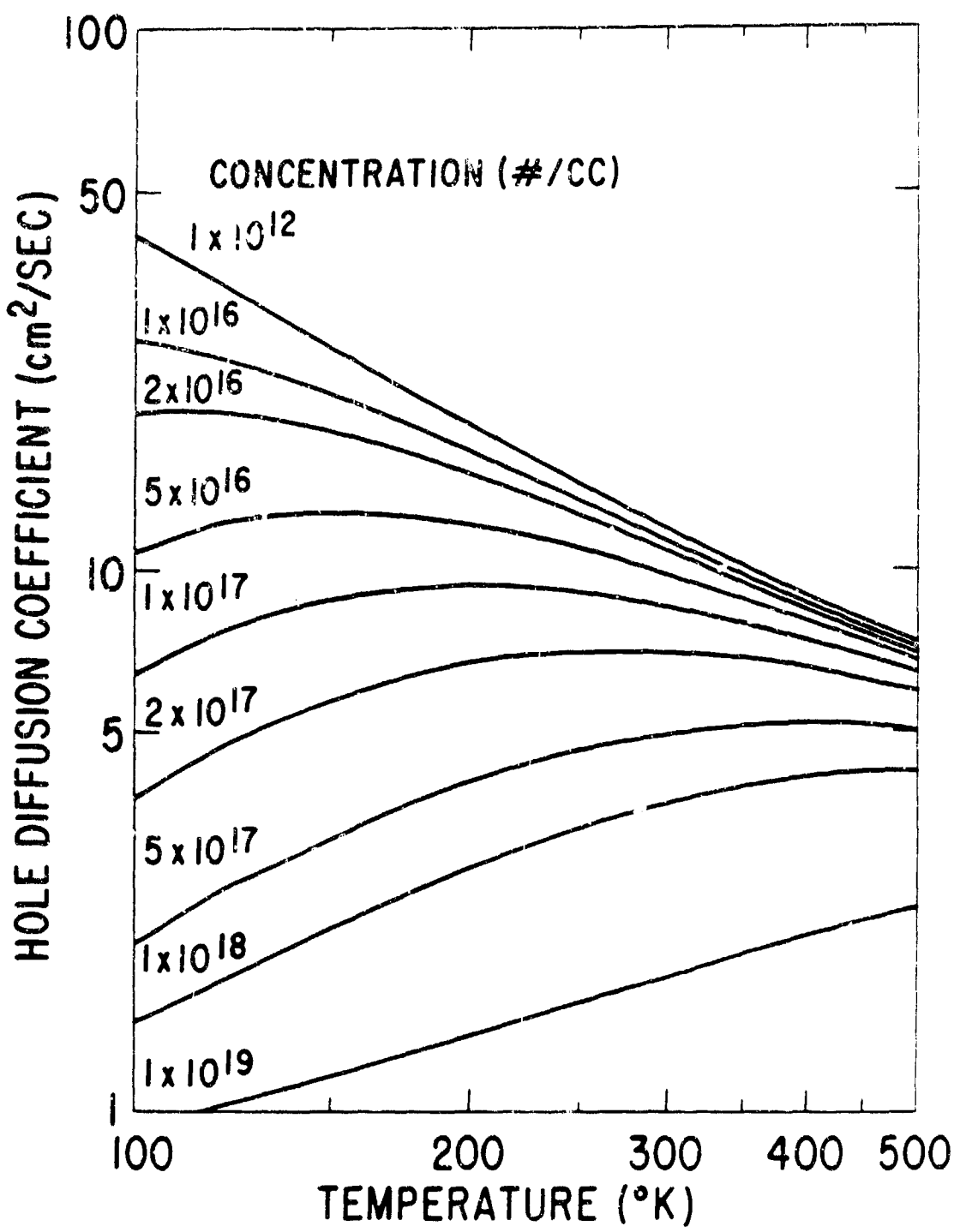


Figure 20. Hole diffusion coefficient vs. temperature.

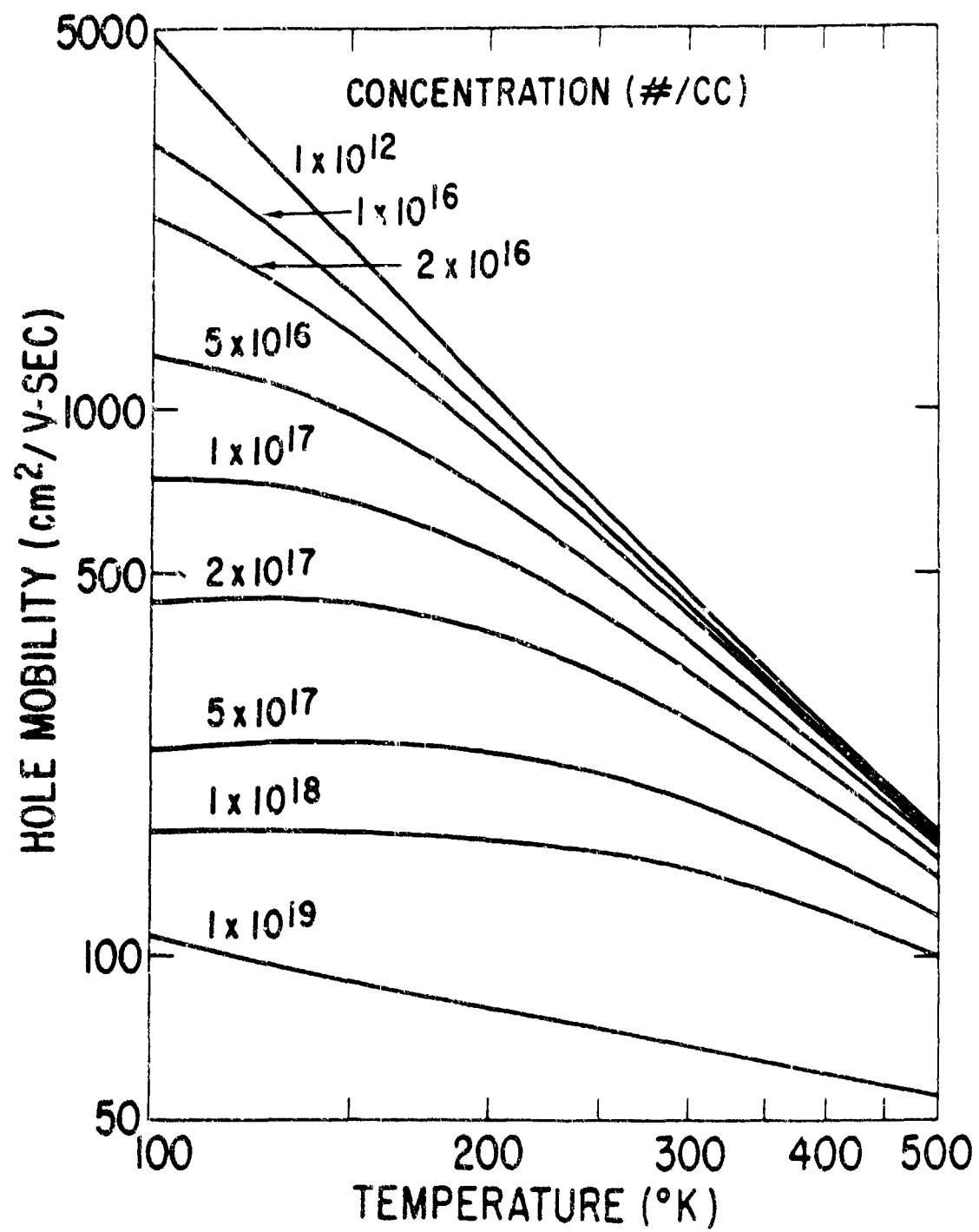


Figure 21. Hole mobility vs. temperature

BREAKDOWN VOLTAGE SUMMARY

- % OF IDEAL VOLTAGE ACHIEVED VARIES INVERSELY WITH VOLTAGE
- ASYMMETRIC THYRISTORS ARE THINNER, FASTER FOR THE SAME VOLTAGE RATING
- FOR 60 HZ APPLICATION, THYRISTORS MAY HAVE TO BE OPERATED AT LOWER TEMPERATURE

Figure 22. Breakdown voltage summary.

noted that, in the last few figures, we have been dealing with the ideal, or absolute, maximum breakdown voltage that can be obtained with a given doping profile. In practice, only about 90% of that value can be obtained for voltages up to 3 KV, about 80% at 6 KV, and much less at higher voltages. This effect results in greater thickness and resistivity needed to obtain a given rated voltage.

Figure 23 illustrates calculated turn-off based on an exact one-dimensional model. The reverse current tail and the stored charge decay are largely carrier recombination lifetime dependent; their integrated values also depend on turn-off di/dt and former-on-state current. Figure 24 depicts carrier concentration at different times during turn-off. Figure 25 shows the actual reverse recovery current density as a function of time for a 14 KV thyristor operated at different temperatures and with different carrier lifetimes. The on-state and circuit are virtually identical (equal on-state power dissipation and identical circuit) for each case. The dominant effect of recombination lifetime is clearly demonstrated. Finally, figure 26 summarizes the turn-off data.

BIBLIOGRAPHY

1. V. A. K. Temple, IEEE Trans. El. Dev. ED-27, 583 (1980).
2. V. A. K. Temple, F. W. Holroy, M. S. Adler and P. V. Gray, pp. 155-163, Proc. PEJC, June, 1980, CH1529-7/80/000-0155.
3. V. A. K. Temple, IEEE Trans. El. Dev. ED-28, 801 (1981).
4. V. A. K. Temple, IEEE Trans. El. Dev. ED-28, 860 (1981).
5. V. A. K. Temple, pp. 406-409, IEDM Technical Digest, December, 981, CH1708-7/81/0000-0406.

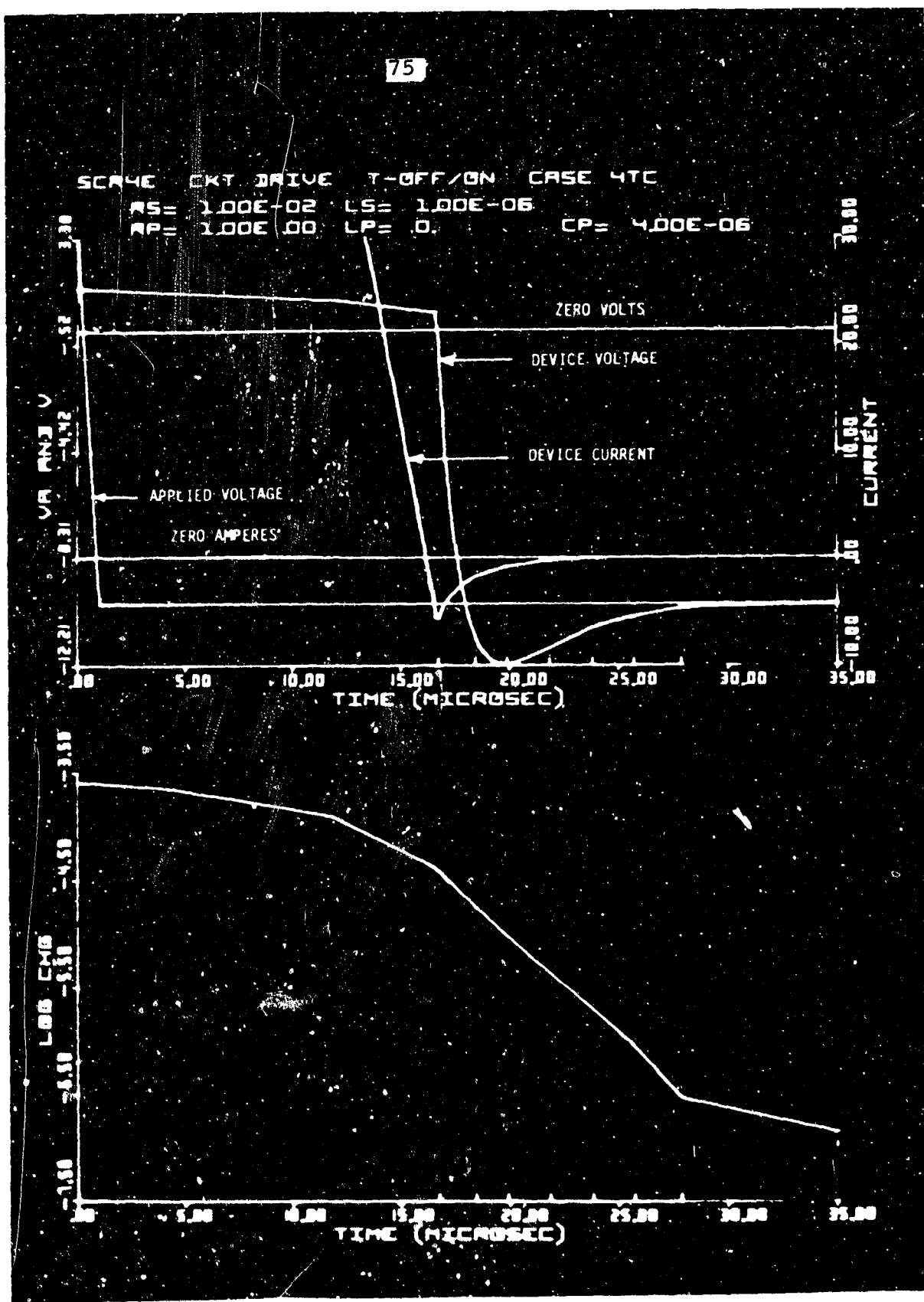


Figure 23. One-dimensional turn-off data.

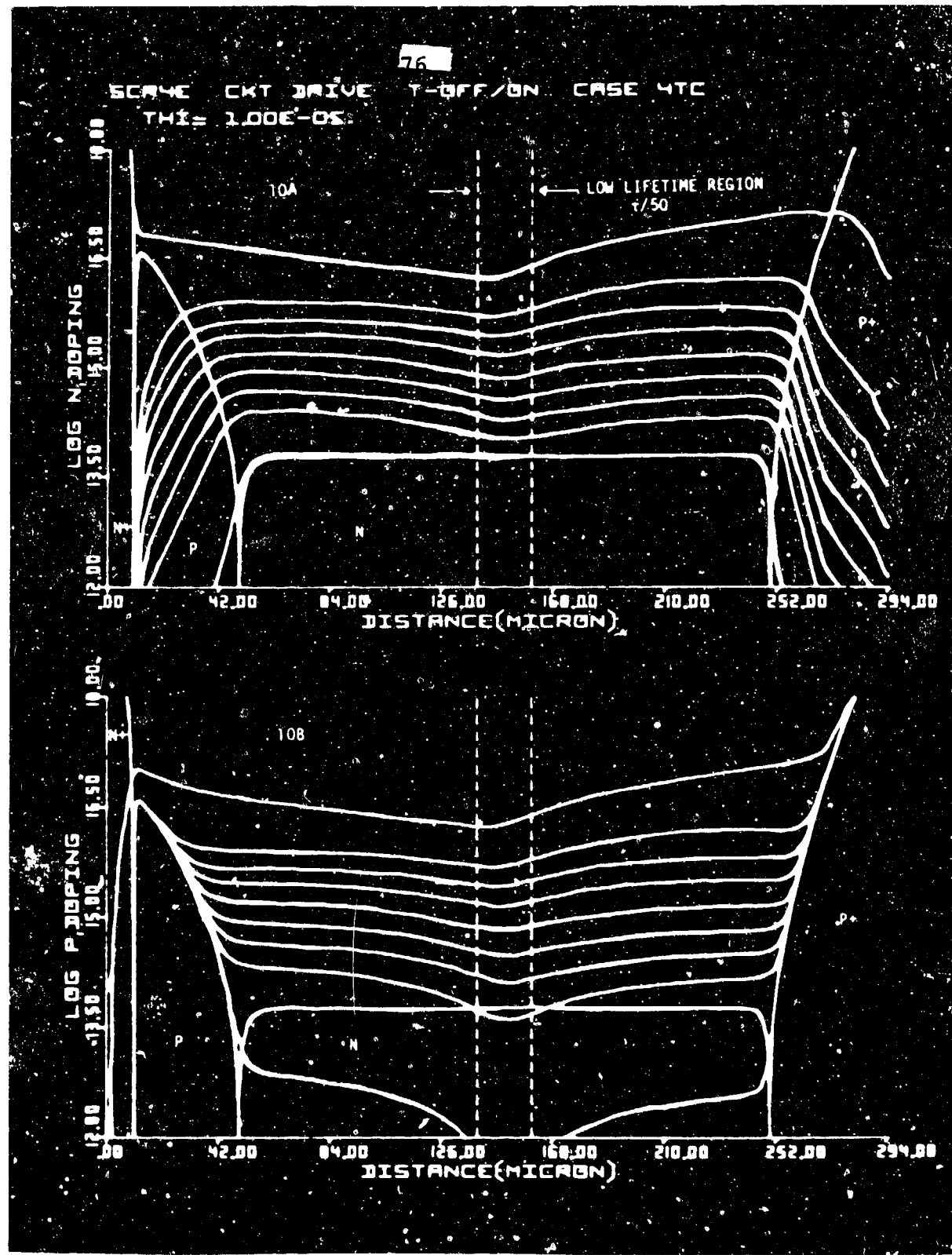


Figure 24. Carrier concentration vs. time.

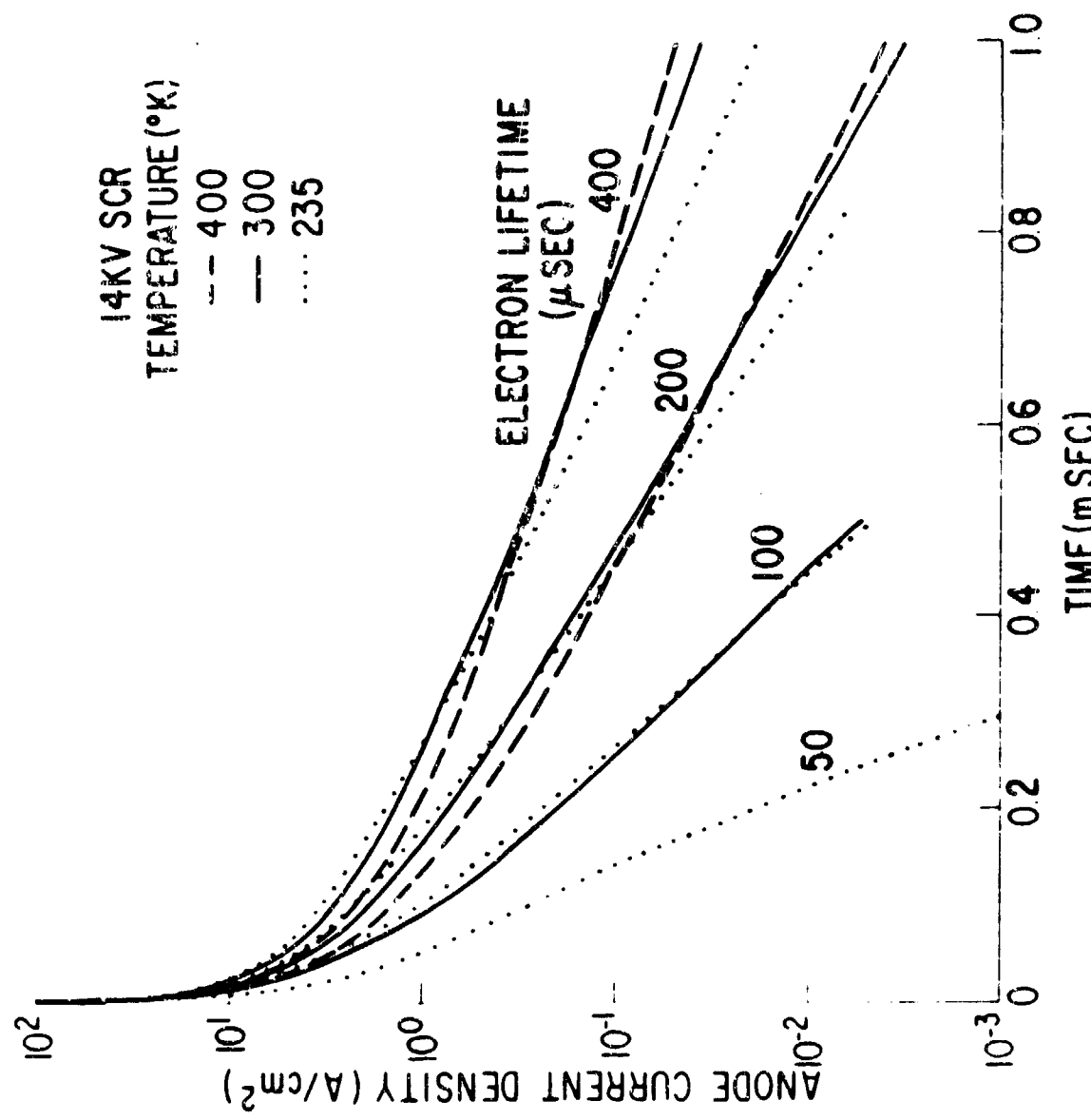


Figure 25. Anode current density vs. time.

TURN-OFF SUMMARY

- TURN-OFF TIME CONTROLLED PRIMARILY BY CARRIER RECOMBINATION LIFETIME
- SECONDARY EFFECTS ARE ON STATE CURRENT DENSITY
 - TURN-OFF di/dt
 - DEVICE THICKNESS

Figure 26. Summary of turn-off characteristics.

AVALANCHE DEVICES: STATE-OF-THE-ART*

Michael D. Pocha
Lawrence Livermore National Laboratory

There are a number of applications in instrumentation for observing high speed phenomena which require fast, electrically triggered, low-jitter electronic switches. Some examples of instrumentation needing fast rise time pulses are streak cameras, micro-channel plates, Pockel cell injection lasers, and general pulse and timing circuits. The range of desired characteristics for these applications are:

| | |
|-----------|---------------|
| Rise time | 0.1 ns - 5 ns |
| Voltage | 200 V - 10 KV |
| Current | 20 A - 1000 A |
| Jitter | <10 ps |

The key to the choice of avalanche transistors for these applications is low jitter and electrical triggering. At this time, the available devices are near the low end of the desired current and voltage range. However, this range of characteristics appears to be feasible using avalanche devices.

The primary problem is the unreliable availability of commercial devices. Since the market for these devices is small, there is not a great deal of incentive among semiconductor manufacturers to design for avalanche operation. We are aware of only one device which is sold for avalanche operation, the Raytheon RS3500. In general, devices for these applications must

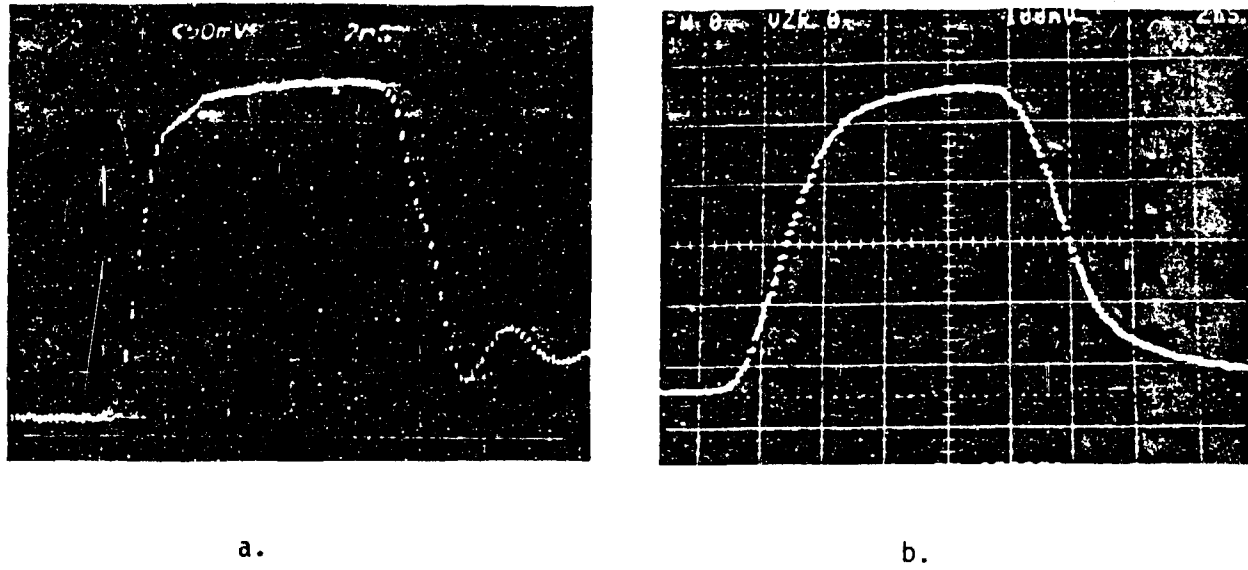
*Supported by the US Department of Energy.

be selected from transistors made for other purposes. Often, as semiconductor manufacturers change their processing, devices which used to function as avalanche transistors (and sometimes have been designed into equipment) no longer work in that application. The state-of-the-art among commercial devices is represented by the RS3500, which has a breakdown voltage of 200 to 300 volts and a pulse rise time of approximately 0.7 -1.0 ns in a typical charge line pulse generator circuit.

We began studying avalanche transistors approximately one and one-half years ago. Our goals were to determine how to design devices which would reliably operate in this mode without the need for selection, and to attempt to fabricate devices with improved characteristics. We have succeeded in the first goal and have fabricated devices with breakdown voltages greater than 800 volts, but at the sacrifice of switching speed as discussed below. Figure 1 shows typical pulse waveforms generated using our devices. Figure 2 shows two different mask sets used to fabricate our structures.

The key to operation at higher voltage is to prevent premature surface breakdown. We feel that surface breakdown is limiting our ability to go to even higher operating voltages and need to improve our surface field limiting techniques. Some interesting observations we have made are:

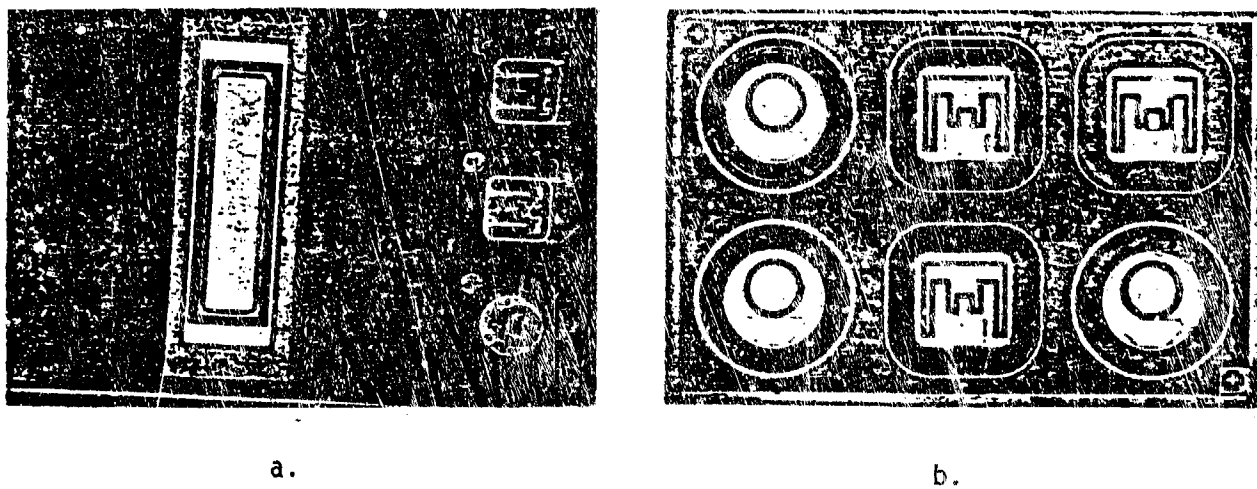
- 1) Surface topology does not seem to affect the rise time. We have tried several different types of layout, from interdigitated structures to concentric rectangles and concentric circles for base and emitter diffusions, and with emitter



a.

b.

Figure 1. Typical pulse waveforms for a) 200 V and b) 800 V avalanche transistors in a charged line pulse generation circuit.



a.

b.

Figure 2. Two sets of masks for fabricating transistors with different topologies.

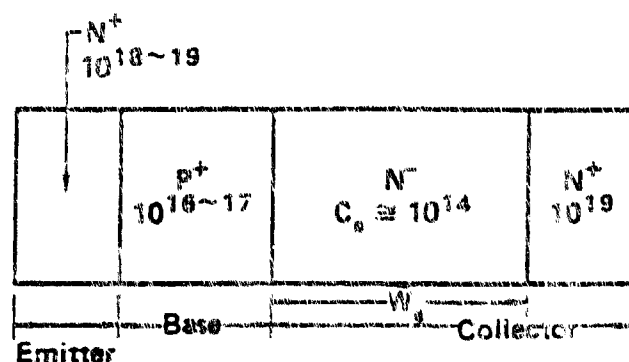


Figure 3. Schematic sketch of the one-dimensional structure of an avalanche transistor.

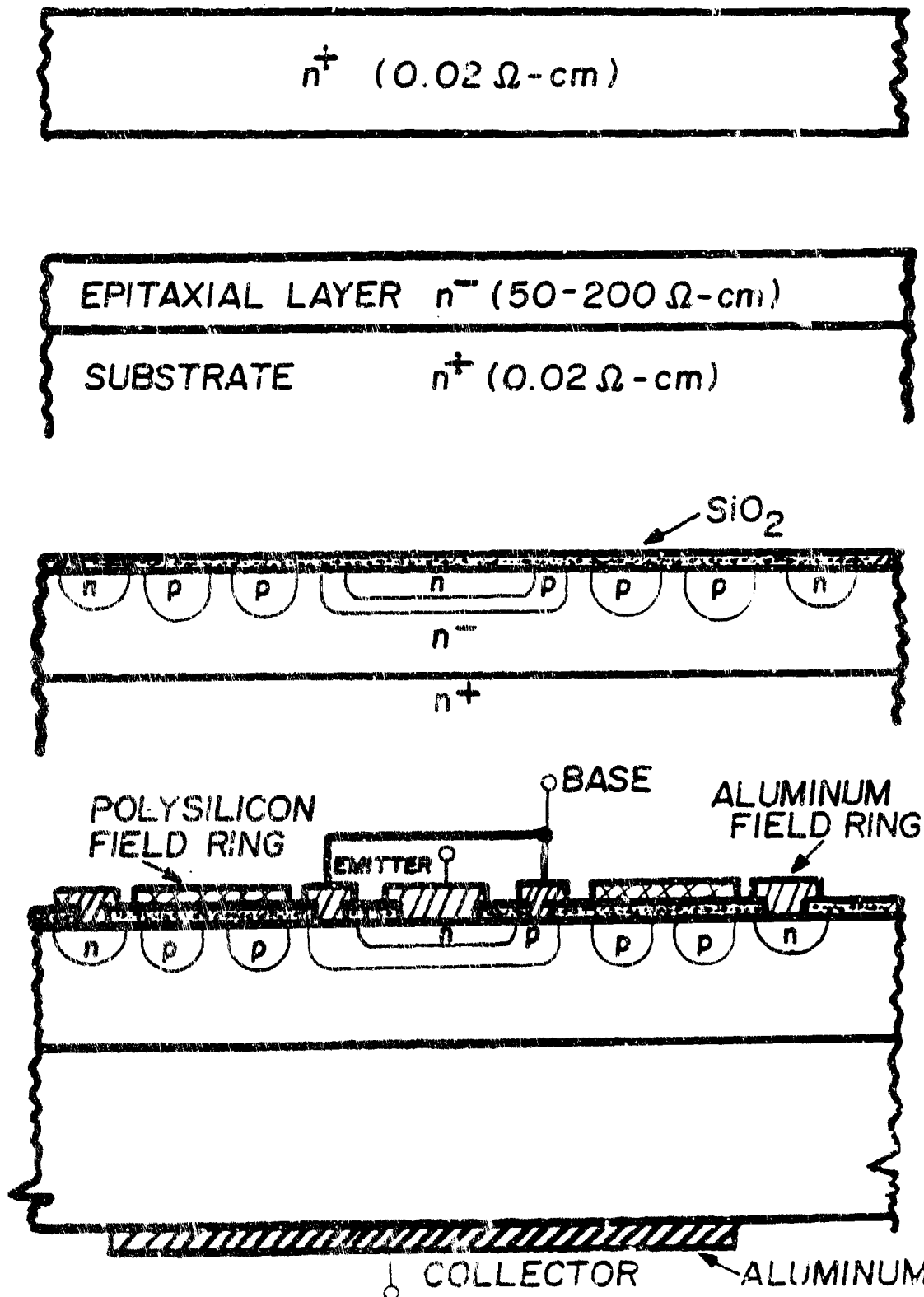


Fig. 1.2.2. The cross-sectional structure of an NPN transistor with a polysilicon field ring. The top contact is insulated with a layer of SiO_2 . The middle contact is labeled "n⁻". The bottom contact is labeled "n⁺". The bottom-most contact is labeled "COLLECTOR". The bottom-most layer is labeled "ALUMINUM".

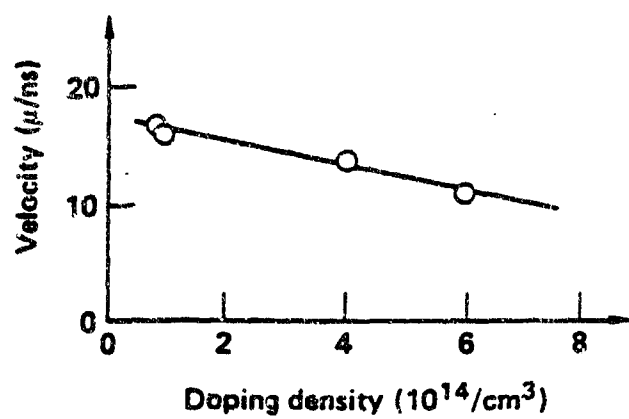


Figure 5. Velocity of the plasma wavefront vs. impurity concentration in the epitaxial layer.

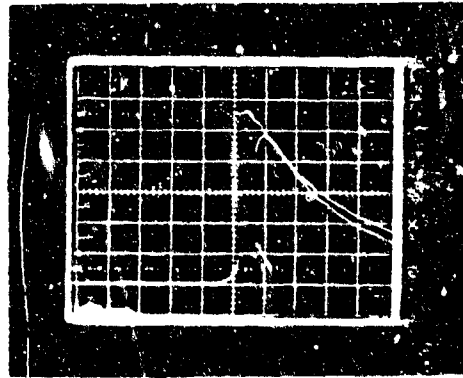


Figure 6. Comparison of pulse waveforms for a single 900 V avalanche transistor (lower curve) and two 500 V avalanche transistors in series (faster rising upper curve).

areas varying by a factor of six. Rise time appears to be determined strictly by epitaxial layer resistivity and thickness. Figure 3 shows a simplified cross-section of a device. More detail is presented in Figure 4, along with major fabrication steps.

- 2) Increasing the area of the diffusions does not affect the current handling capability. This result supports the generally accepted concept that breakdown occurs at localized hot spots where the current pinches down into small channels.
- 3) The breakdown voltage divided by the rise time is an almost constant value, approximately 200 to 300 V/ns, as shown by the values in Table 1. This result implies a constant velocity of the breakdown wave. Figure 5 shows a plot of this velocity vs. doping concentration. Therefore, as a thicker epitaxial layer is used to obtain a higher voltage, a longer time is needed to breakdown.
- 4) Series connection of transistors does not degrade rise time. Figure 6 shows that two 500 volt transistors connected in series will generate a faster pulse of approximately the same voltage as a single 800 volt transistor, even though only one of the lower voltage devices is triggered to initiate the breakdown.

The latter two results appear to be contradictory and lead us to consider the possibility that the 200 to 300 V/ns number may be determined by the particular circuit configuration used for testing rather than being a fundamental limitation of the semiconductor material.

Table 1. Results of measurements made on several different avalanche transistor structures.

| Sample | Epi Thickness (μm) | Epi Resistance (Ω cm) | Measured Breakdown Voltage (V) | Calculated Breakdown Voltage (V) | Sustained Voltage (V) | τ | dv/dt (V/ns) | Wave Velocity (μm/ns) |
|--------|--------------------|-----------------------|--------------------------------|----------------------------------|-----------------------|------|--------------|-----------------------|
| 1 | 46 | 50 | 900 | 780 | 80 | 2.9 | 248 | 16 |
| 2 | 29 | 70 | 550 | 528 | 50 | 1.5 | 333 | 19 |
| 3 | 32 | 15 | 450 | 452 | 66 | 2.25 | 171 | 14 |
| 4 | 7 | 10 | 186 | 184 | 14 | 0.63 | 273 | 11 |

There is some evidence that this switching phenomenon is faster than indicated by the 200 to 300 V/ns ratio. A group of researchers in the Soviet Union have reported pulse sharpening using silicon diodes which result in rise times as fast as 0.2 ns for pulses over 1600 volts.⁽¹⁾ We have begun some experiments with diodes and see qualitatively the behavior they describe, but have not been able to duplicate their results yet (see Figure 7 and Figure 8).

Our plans for future work are to explore the pulse sharpening effect described by the Russians and attempt to incorporate it into our avalanche structure; to continue development of higher voltage structures; and to explore ballasting techniques for improvements in current handling capability.

I would like to acknowledge the substantial contributions made to this project by Dr. Jackson C. Koo and Mr. Wayne E. Tindall of Lawrence Livermore National Laboratory.

This work has performed under the auspices of the U.S. Department of Energy by the Lawrence Livermore National Laboratory under contract number W-7405-ENG-48.

REFERENCES

1. I. V. Grekov, A. F. Kardo-Sysoev, and S. V. Shenderei, "High-Power subnanosecond semiconductor pulse peakers," Instruments and Experimental Techniques (Pribori I Teknika Experimenta), Number 4, p. 135, July-August 1981.

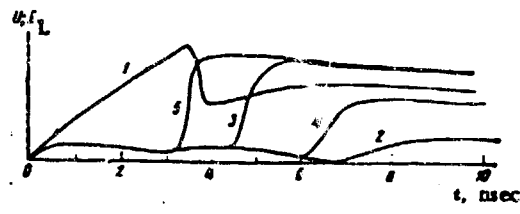


Figure 7. Pulse peaking diode waveforms: 1) incident wave; 2) to 5) voltage across load for different DC bias conditions: 2) 200 V; 3) 400 V; 4) 700 V; 5) 1000 V (from reference 1).

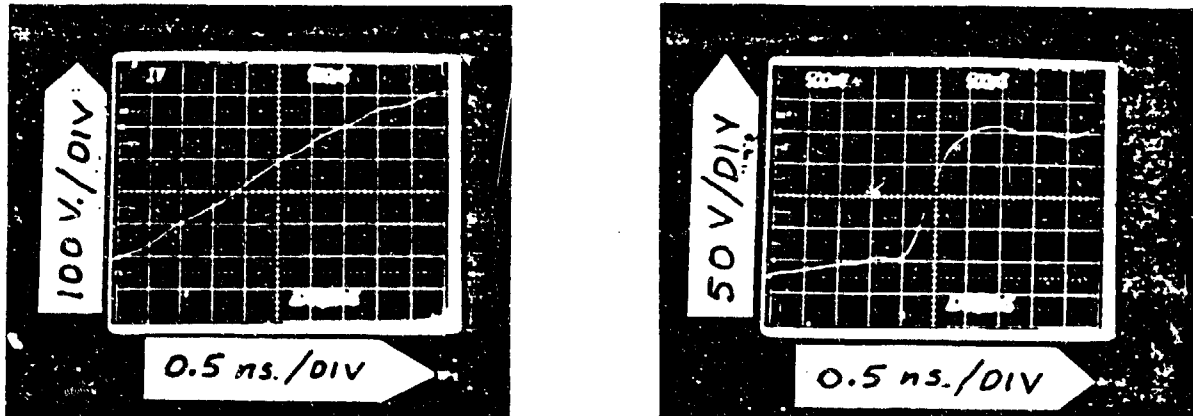


Figure 8. Results of LLNL experiments with pulse peaking diodes: left trace, incident waveform; right trace, output across load with diode biased at 600 V DC.

GALLIUM ARSENIDE POWER TRANSISTORS*

Michael S. Adler
Corporate Research and Development Center
General Electric Company

INTRODUCTION

Silicon high voltage power MOSFETs are attractive for power switching applications because of their high input impedance and fast switching speeds. Their major limitation is their high on-resistance per unit area, compared with bipolar transistors. It has been theoretically demonstrated that devices made from gallium arsenide have superior switching properties, compared with silicon high voltage vertical channel power FETs; for example, GaAs FETs will have at least 10 times lower on-resistance per unit area while also having faster switching speeds.(1) Table I compares several parameters in GaAs and Si. There is clearly a strong motivation for the development of high voltage GaAs power MOSFETs. However, the development of these devices requires highly advanced technology, such as very high purity n-type epitaxial layers with doping levels below $10^{10}/\text{cm}^3$ and good electron mobilities; the fabrication of high voltage p-n junctions; and the ability to invert the surface of p-type GaAs to obtain n-channel MOSFETs. It has been recently shown that high purity GaAs can be grown by using liquid phase epitaxy to obtain high breakdown voltages Schottky diodes;(2) however, the

*Most of this material was presented at the 1982 IEDM by P. M. Campbell and others.

Table 1. Comparison between gallium arsenide and silicon field effect devices.

| <u>Material</u> | Breakdown Voltage(V) | Steady current at 2V(Acm ⁻²) | Pulse current at 20V(Acm ⁻²) |
|------------------|-------------------------|---|---|
| Gallium arsenide | 500 | 14 | 140 |
| Silicon | 500 | 170 | 1700 |
| Gallium arsenide | 1000 | 3 | 30 |
| Silicon | 1000 | 36 | 360 |

Parasitics are a factor of ten lower in gallium arsenide, leading to ten times faster switching in the limit of zero source impedance.

development of MIS structures on GaAs which allow inversion of its surface is a problem that remains unsolved. Under these circumstances, an alternative to the MOSFET is a junction gate FET. High voltage vertical channel JFETs fabricated using silicon technology have been already reported using either buried gate regions⁽³⁾ or surface gate regions.⁽⁴⁾ The buried gate regions have the advantage of exhibiting higher blocking gain because the gate fingers can be placed closer together to obtain superior channel pinch-off characteristics. A GaAs buried junction gate FET structure is described here in which the gate regions are formed by ion implantation. Devices with gate-drain breakdown voltages of up to 150 volts have been fabricated.

DEVICE STRUCTURE AND FABRICATION

To fabricate the vertical channel high voltage GaAs FET, an n-type drift layer was first grown on an n⁺-substrate by liquid phase epitaxy; a 200 V device requires a 12 micron thick epitaxial layer with a doping of $2 \times 10^{15}/\text{cm}^3$. The epitaxial surface was then coated with a 2500 Å thick layer of SiO₂, which was then patterned with positive photoresist thick enough (2 microns) to act as a mask for the p⁺-ion implant (200 KeV beryllium at a fluence of $5 \times 10^{13}/\text{cm}^2$), as shown in figure 1a.

After the implant, the photoresist was removed and a second 2500 Å SiO₂ layer was deposited. As shown in Figure 1b, windows were opened in this film, and a second n-type epitaxial layer was grown selectively in these opened windows. This second epitaxial layer had the same doping level as the first, but was only a few microns thick, because the gate-source voltage is much smaller

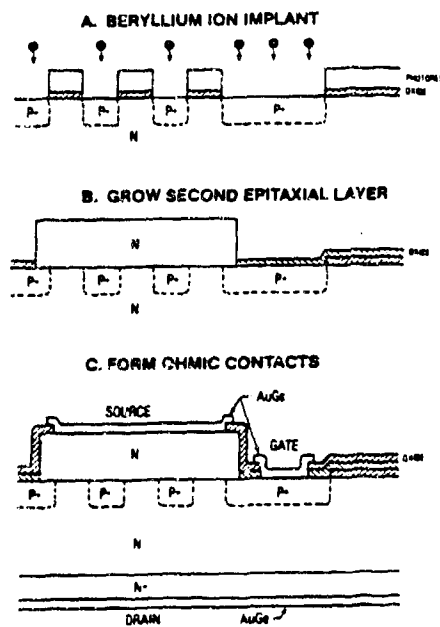


Figure 1. Fabrication of the buried gate JFET.

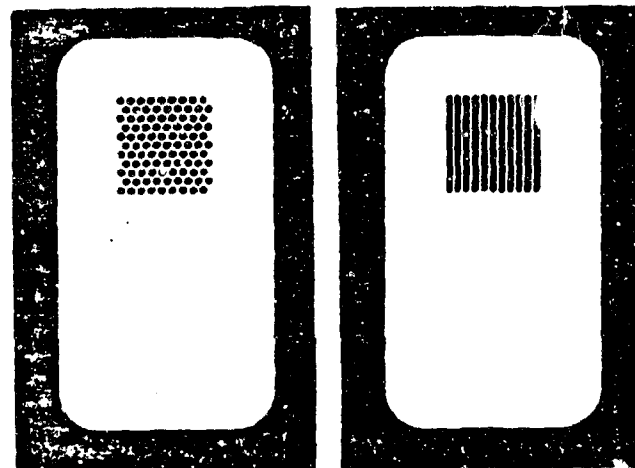


Figure 2. Circular and longitudinal channel geometries. The clear areas are the p+ implanted gate regions, surrounding the dark n-channels.

than the gate-drain voltage. The second epitaxial layer growth was performed at a high enough temperature (800°C for 30 minutes) that the beryllium implant was activated during the process. This procedure eliminates the need for a separate annealing step and avoids the problems of surface degradation associated with the high temperature annealing of GaAs.

After the second epitaxial growth, another layer of SiO₂ was deposited and patterned. A 2000 Å thick film of AuGe was then deposited by liftoff to form ohmic contacts to the source and gate, as shown in Figure 1c. AuGe was also deposited on the back side of the wafer to form the drain contact. Sintering the AuGe contact layers at 330°C for 1 hour enhanced the ohmic behavior of the contacts⁽⁵⁾ and completed the fabrication of the device.

The buried gate structure fabricated using the above process has the advantage of placing the source and gate regions on two different levels, thus allowing a large area source contact to be made. In addition, the gate regions do not have to be interdigitated with the source. This allows closer spacing between the gate regions which gives higher blocking gains. Finally, the avoidance of fine-line interdigititation produces higher yields.

DEVICE CHARACTERISTICS

Two basic device geometries were fabricated, incorporating either circular or longitudinal n-channels, as shown in Figure 2.

The dark areas are the n-regions, while the clear areas are the p⁺-implanted gate region. The circular channels have diameters, and the longitudinal channels have widths, of 4 μm, 6 μm, 8 μm, and 10 μm, respectively. The n-channels are confined to an area

of $125 \mu\text{m} \times 125 \mu\text{m}$, but the variation in channel size and number gives different channel areas for each of the eight device configurations. The second epitaxial layer, of area $170 \mu\text{m} \times 170 \mu\text{m}$, was grown directly over the n-channel regions, while the gate contact was made in the large open p⁺-region.

Working devices were obtained for all four channel sizes of both the circular and longitudinal devices. Figure 3 shows the I-V characteristics of a 4 μm longitudinal channel device. The left-most curve is the source-to-drain characteristic for a gate bias of zero volts. Successive curves to the right are for increasingly negative gate biases in two volt steps. The operation of a normally-on FET is clearly demonstrated. The onset of breakdown in this device can be seen to occur at about 140 V, close to the highest value we have obtained (150 V).

Figure 4 shows a plot of drain blocking capability vs. gate bias for a complete set of four longitudinal channel devices. As expected, the blocking gain (voltage blocked/gate bias) increases with decreasing channel width, with a maximum blocking gain of approximately 10 observed in the 4 μm channel width device. A similar plot for the circular channel devices shows the same trend, although the circular devices tend to have slightly higher blocking gains. This is due to the greater ease of constricting a circular channel, which squeezes from all directions, compared with a longitudinal channel that pinches from only two directions.

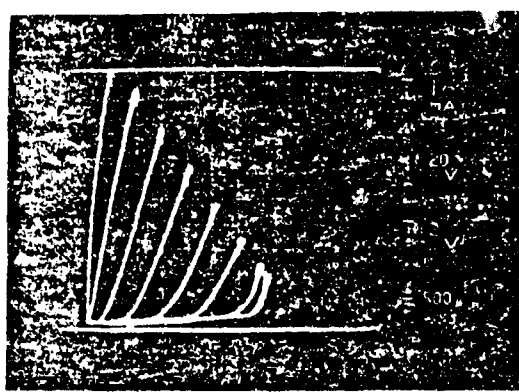


Figure 3. Characteristic curves for a longitudinal channel device (channel width, 4 μm).

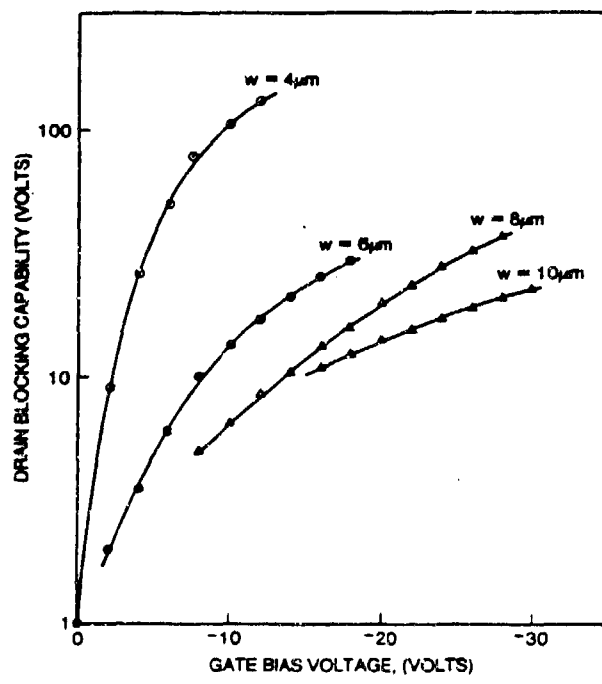


Figure 4. Drain blocking capability vs. gate bias for longitudinal channel devices with various channel widths.

These devices are expected to have fast switching speeds because of the absence of minority carrier injection. Measurements with both turn-on and turn-off pulses have shown that the switching occurs in both cases in less than 5 nanoseconds.

REFERENCES

1. B. J. Baliga, "Semiconductors for high voltage vertical channel FETs," *J. Appl. Phys.* 53, 1759-1764 (1982).
2. B. J. Baliga, R. Ehle, J. R. Shealy, and W. Garwacki, "Breakdown characteristics of gallium arsenide," *IEEE Electron Device Letters* ED-2, 301-304 (1981).
3. J. I. Nishizawa, T. Terasaki, and J. Shibata, "Field effect transistor versus analog transistor (static induction transistor)" *IEEE Trans. Electron Devices*, ED-22, 185-197 (1975).
4. B. J. Baliga, "A power junction gate FET structure with high blocking gain," *IEEE Trans. Electron Devices*, ED-27, 368-373 (1980).
5. O. Aina, W. Katz, B. J. Baliga, and K. Rose, "Low-temperature sintered AuGe/GaAs ohmic contact," *J. Appl. Phys.* 53, 777-780 (1982).

FAILURE IN HIGH POWER SEMICONDUCTOR SWITCHES

Donald C. Wunsch
The BDM Corporation

This material is organized to consider failure in high power semiconductor switches, and to identify important mechanisms of semiconductor switch failure. Understanding some of these failure mechanisms will aid the design of new devices that will withstand higher power, voltage, current, dv/dt, and di/dt switching levels. The material can be divided into three broad areas of concern: 1) inherent limits in device performance; 2) device reliability; and 3) failure due to unique problems associated with particular device switching applications.

The first topic for consideration is the inherent limits in device performance arising from the basic physical properties of the device and the physics of device operation. Such limitations are important in establishing maximum switching capabilities as well as failure threshold limits. Examples of such limitations are the maximum continuous junction operating temperature of approximately 250°C, eutectic temperature in the range of 600° to 650°C, the melting temperature of silicon at 1415°C, bulk voltage breakdown levels of 10^5 volts per centimeter, and present manufacturing limitations in terms of doping uniformity over standard wafer sizes and bulk silicon single crystal sizes. Other issues such as surface voltage breakdown also become important in devices for light activated switching.

The second topic to be considered is device reliability. This issue may not seem important in determining maximum switching capability, but it becomes a critical matter in terms of making high capability switches through construction of large parallel and series arrays of smaller switching devices. Thousands of individual components may be involved in single-switch arrays. This fact makes device reliability and uniformity extremely important. There is still a considerable need for research to improve device uniformity and to establish methods of screening to improve device reliability.

The third topic of concern is device failure due to unique problems associated with the particular device switching application. One such application, that of large parallel and series arrays has already been mentioned. Other application issues include switching of large inductive loads, opening and closing switches, extremely high initial di/dt rates as opposed to high di/dt rates after the device has been uniformly turned on, the switching of sources to highly nonlinear loads, and situations where the source and load are badly impedance mismatched. Other application issues such as duty cycle, environmental conditions, and geometry are also important.

Table 1 lists a number of elements associated with device failure mechanisms. The first grouping has to do primarily with reliability problems already present in the device at the time of acquisition. The second grouping deals with overstress of a specific limiting physical parameter of the device. Finally, there are long-term wearout issues such as metal migration of

Table 1. Elements of device failure.

Reliability/Infant Mortality Failure

| | |
|--|------------------------------------|
| Encapsulation Defects | Oxide/Passivation Defects |
| Macrochip Cracks | Aluminum to Silicon Ohmic Contacts |
| Imperfect Chip Attachment to Substrate | Diffusion Faults |
| Wire Bonds | Wafer Faults |
| Aluminum/Gold Conductors | Mask Misalignments |
| | |
| <u>Overstress Failure</u> | <u>Lifetime Failure</u> |
| Thermal Overstress | Wearout |
| Electrical Overstress | Aluminum Migration |
| Mechanical Overstress | Impurity Ion Migration |
| | Material Stress Fatigue |

aluminum stripes; mechanical fatigue and the resulting failure of electrical bonds; and long-term humidity and chemical interactions which cause device failure.

Of the previously mentioned failure issues, the one of most concern here is probably the issue involving conditions for both continuous operation and for transient switching; this results in an overstress that causes current crowding and filamentary conduction, which eventually causes thermal failure of the device. Although the final failure mechanism may be of a thermal nature due to filamentary current conduction, the initiation of filamentary conduction can be caused by several entirely different physical mechanisms resulting from current, voltage, energy, or thermal overstress. A very high transient carrier injection can initiate filamentary current conduction. Voltage overstress can cause several different physical events. In some devices, voltage overstress can cause the depletion region to spread completely across the lightly doped junction region and filamentary conduction may follow. In other cases, junction defects such as diffusion spikes along grain boundaries may result in filamentary conduction when a high voltage transient initiates localized avalanching. Voltage overstress can also cause surface breakdown or dielectric failure. Filamentary conduction may also be initiated by transient thermal overstress caused by energy overstress, or similarly by longer term thermal heating following operation above rated average-power dissipation.

Four of the major factors involved in semiconductor failure are: 1) the basic silicon properties, 2) junction area, 3) dop-

ing levels, particularly on the lightly doped side of the junction, and 4) the basic geometry of the device. Figure 1 illustrates the resistivity of silicon versus temperature for various doping levels. Several important parameters should be noted. At room temperature, there is a positive gradient of resistivity versus temperature, thereby providing a ballasting action against filamentary conduction and local thermal runaway. However, at increasing temperature, there is a region where the resistivity is negative with respect to increasing temperature. In these regions, thermal runaway and filamentary conduction can occur if the total current is not limited or other ballasting action is not provided within the semiconductor device. Note that the temperature of turnover into negative resistivity is lowest for high purity bulk silicon and increases to higher values as the doping increases. Also, there is a much higher positive resistivity versus temperature gradient for lighter doping levels. This causes greater current spreading and greater temperature variation within lightly doped regions. It should be cautioned, however, that these curves do not accurately apply for regions with high carrier injection or high electric field because the mobilities are extremely nonlinear and the carrier velocity will saturate at high electric field strengths. Junction area effects are quite straightforward. Obviously, if the device is carrying current uniformly over a junction cross-section, a larger area device can carry more total current. As might be expected, however, the maximum current density before failure is higher for smaller area devices because nonhomogeneities in larger area

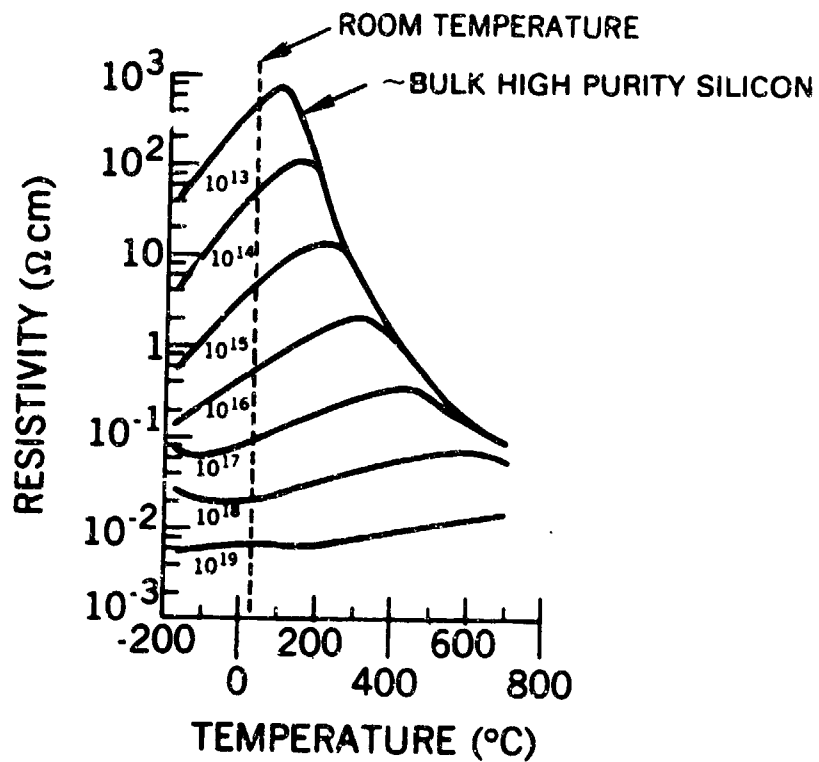


Figure 1. Resistivity of silicon as a function of temperature.

devices cause filamentary conduction at lower current densities. Figure 2 illustrates some of the many geometrical and physical properties of the device that determine both operational and maximum stress conditions for semiconductor devices. The lateral and vertical geometrical features of the device determine electrical field gradients and current flow. Diffusion depths, doping levels, and junction areas are very critical parameters. Reliability problems can result from thin metallization stripes, diffusion defects, and metallization spikes. All of these parameters which effect device operation and reliability are what make the modeling of device failure so difficult, even though many of the specific physical phenomena are well-understood.

Because of the many failure parameters previously mentioned, it is extremely important that experimental and theoretical conditions are exactly understood. Table 2 identifies some of these conditions. In many switching devices such as thyristors and SCRs there will be as few as three and as many as eight or more junctions within the device. Current filamentation and localized thermal runaway is not dependent on junction action and can occur in bulk silicon. Therefore, when one is discussing failure conditions, one must adequately describe all of the conditions including whether the device is under forward or reverse stress, whether it is single or multiple junction action, and whether the device is continuously biased or merely undergoing a transient stress across two terminals.

The next few figures illustrate the formation of micro-plasmas within silicon devices and provide a better understanding

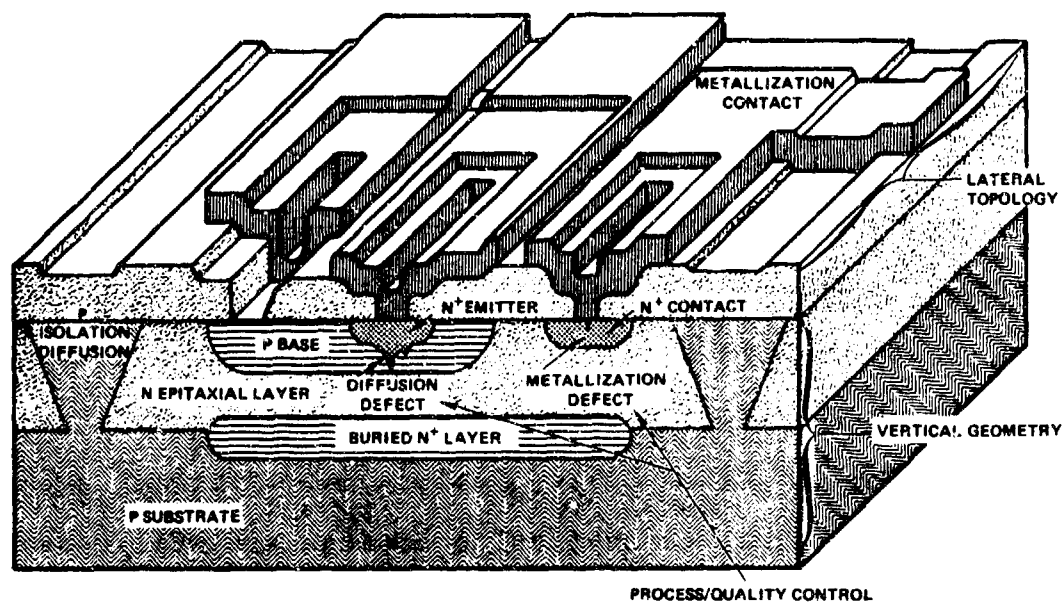


Figure 2. Structure of a typical semiconductor device.

Table 2. Operational conditions.

| Thyristor/SCRs | Transistors | Diodes | Bulk Silicon |
|---------------------------|---------------------------|---------------------|--------------|
| 3 Junction | 2 Junction | 1 Junction | 0 Junction |
| A-K | B-E | | |
| A-G | B-C | A-C | -- |
| K-G | C-E | | |
| Forward/ Reverse | Forward/ Reverse | Forward/ Reverse | Forward |
| Single/Multi- Junction | Single/Multi- Junction | -- | -- |
| Biased/ Unbiased | Biased/ Unbiased | -- | -- |

of the complexity of semiconductor device operation under high stress conditions such as may occur during high power switching. These particular experiments were performed using a very simple diode geometry, as illustrated in figure 3. A one-micron n^+ - n - p^+ silicon diode is fabricated on a sapphire substrate. Because both the silicon and sapphire are very thin, light can be transmitted through the device and observed through a microscope, as illustrated in figure 4. By using a very short light pulse of 20 ns, the device operation can be probed anytime during an electrical overstress pulse. Because the opacity of the silicon changes dramatically as a function of temperature, the thermal patterns within the device can be observed. Figures 5, 6 and 7 present the resulting thermal patterns and microplasma development within these types of silicon-on-sapphire diodes. (The photographs are from the work of P. Budenstein and others at Auburn University.) In figure 5, a constant current pulse was applied, and the device was observed at various times after the pulse was initiated. The thermal pattern along the lightly doped n - p^+ junction, and the development of the microplasmas within the n -region, can be seen. When one of the microplasmas extends across the n -region and bridges the p^+ n^+ regions, extreme filamentary conduction will occur and the device will fail. In figure 6, various constant current levels are applied, and the pulse is terminated just before device failure occurs. The photographs are made at the end of each pulse. In such a uniform geometrical device, uniformly spaced microplasmas occur, and the number of microplasmas increases with increasing current density.

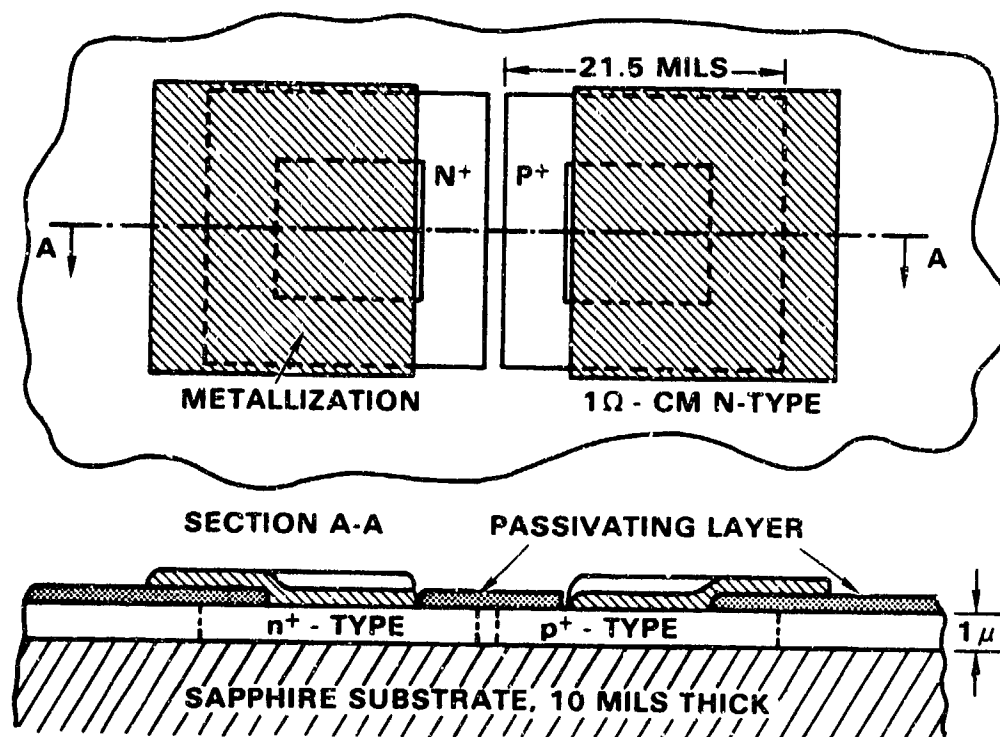


Figure 3. Geometry of a silicon-on-sapphire diode.

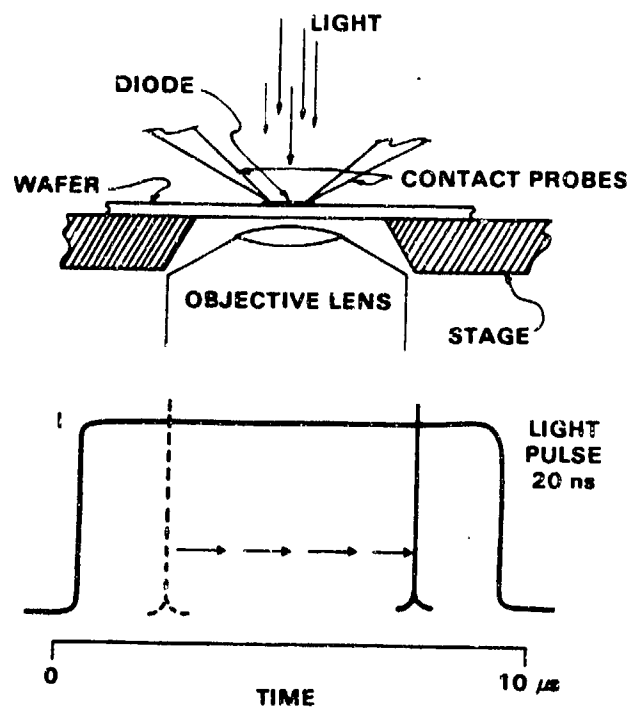


Figure 4. Experimental arrangement for SOS diode measurements.

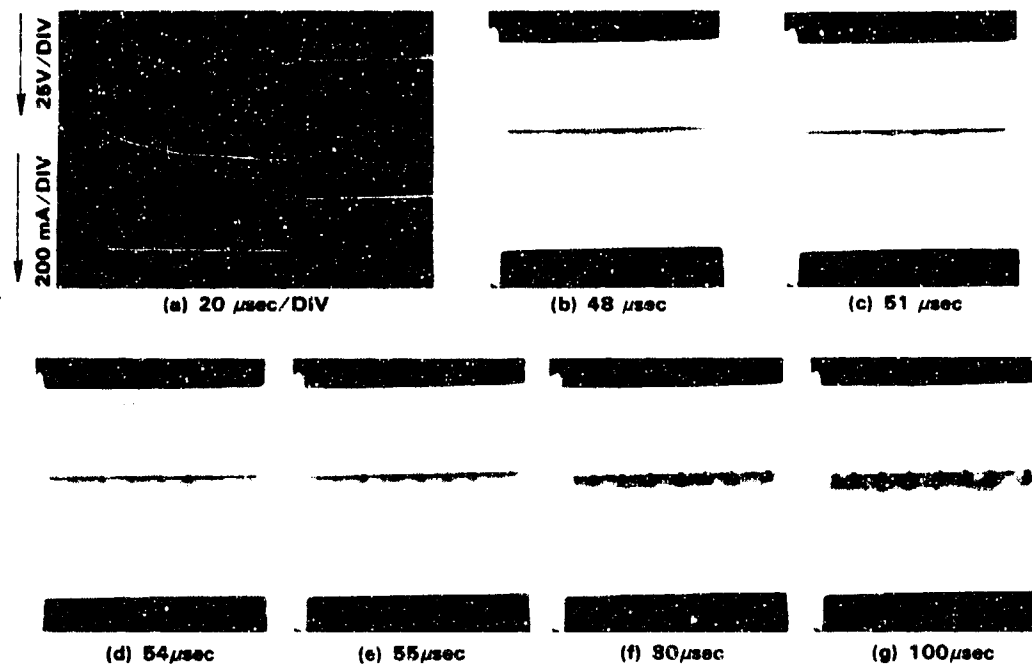
SOS DIODE — CONSTANT CURRENT

Figure 5. Development of hot spots in an SOS diode: constant current.

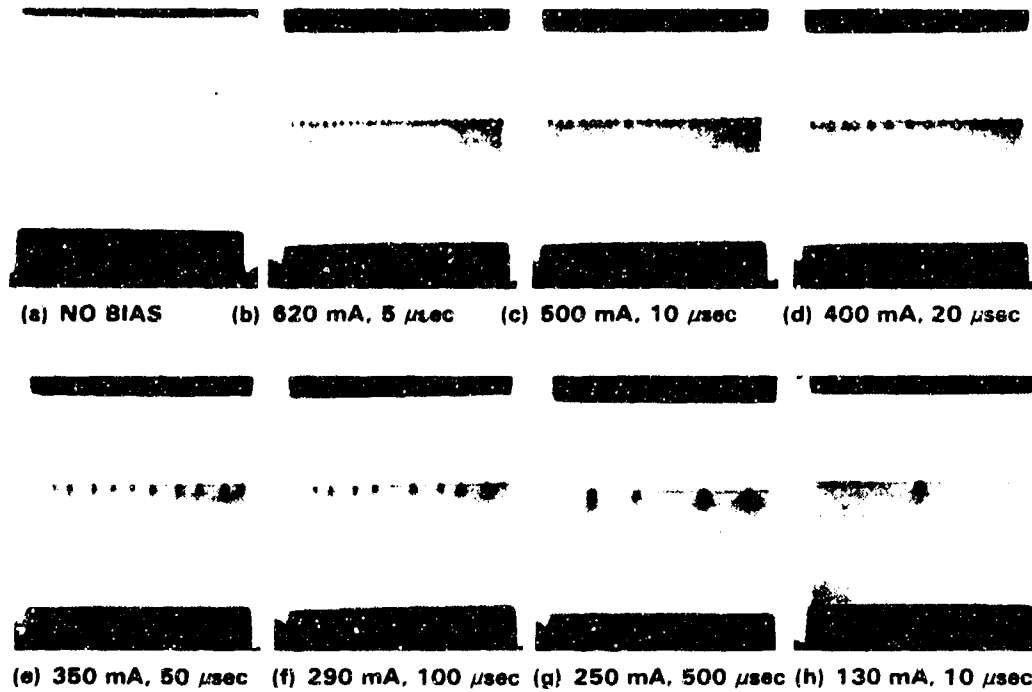
SOS DIODE — DECREASING CURRENT DENSITY

Figure 6. Development of hot spots in an SOS diode: decreasing currents.

Other device experiments have shown that avalanching is quenched on each side of the thermal microplasma and within the microplasma, and that the temperature on each side of the microplasma is very low compared to its interior or elsewhere along the junction. Geometrical considerations can dramatically effect the formation of the microplasmas, as illustrated in figure 7. In figure 7a, a curved junction has been produced, much like a cross-section through a three-dimensional device. The microplasma is located at the maximum point of curvature both at the n-p⁺ junction and at the n-n⁺ junction. Figure 7b illustrates the formation of microplasmas in bulk silicon. In such situations, the microplasma is controlled by the geometry of the contacts. In this particular photograph, the microplasmas form off the high stress regions at the corners of the contact metallization.

In conclusion, it is clear that an understanding of basic failure mechanisms in high power semiconductor switching devices paves the way for an understanding of how devices with larger pulsed power switching capabilities might be made; how device selection might be influenced by operational conditions; and what types of screening tests might be used to obtain high reliability matched performance for large switching arrays.

BIBLIOGRAPHY

1. Neudeck, G. and D. C. Wunsch. Bibliography of Breakdown Effects in Semiconductors, Defense Nuclear Agency Report 4285T, August 1977.
2. Alexander, D. and S. Jones, Bibliography for Electrical Overstress Review, Defense Nuclear Agency Report 4146T, October 1977.

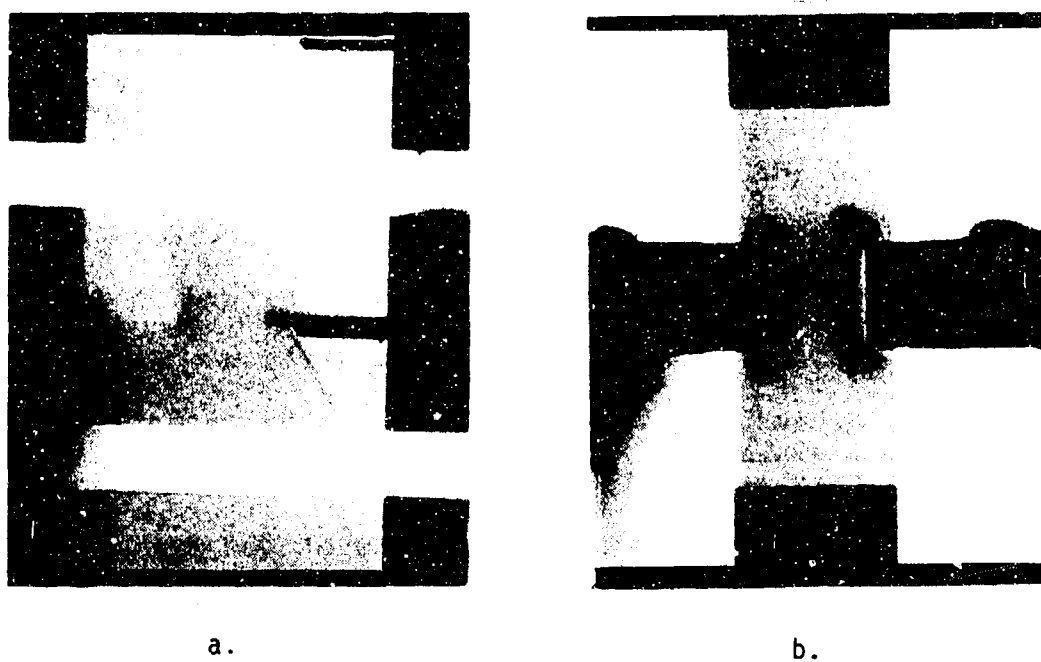


Figure 7. Geometry forced current flow; a) curved junction; b) bulk silicon.

3. Raburn, W. D. and W. H. Causey, Determination of Semiconductor Junction Vulnerability to Second Breakdown, University of Alabama Bureau of Research Report 200-93, July 1975.
4. Ward, A. L., "Studies of second breakdown in silicon diodes," IEEE Trans. PHP-13, 361-368 (1977).
5. Budenstein, P. P., et al., Second Breakdown and Damage in Semiconductor Junction Devices, Technical Report 72-15 (AD 740226), Army Missile Command, Redstone Arsenal, April 1972.
6. Pontius, D. H., et al., Second Breakdown in the Presence of Intense Ionizing Radiation, Report RG-75-24, Program AM CMS 691000.22.10799, Army Missile Research, Development and Engineering Laboratory, Redstone Arsenal, December 1974.
7. Wunsch, D. C. and R. R. Bell, "Determination of threshold failure levels of semiconductor diodes and transistors due to pulse voltages," IEEE Trans Nuclear Science NS-15, No. 6, December 1968.
8. Tasca, D., et al., Theoretical and Experimental Studies of Semiconductor Device Degradation Due to High Power Electrical Transients, General Electric Report 73 SD 4289, Contract DAAG 39-72-C-0066, Harry Diamond Laboratory, December 1973.
9. Schafft, H. A. and J. C. French, "A Survey of Second Breakdown," IEEE Trans Electron Devices, ED-13, 613-618 (1966).
10. Budenstein, P. P., A Survey of Second Breakdown Phenomena, Mechanisms, and Damage in Semiconductor Junction Devices, Report RG-TR-70-19, DA Project No. IM262303A204, Army Missile Command, Redstone Arsenal, December 1970.
11. Egelkrout, D. W. et. al., Metallization Failure and Thermo-mechanical Shock Studies (U). The Boeing Company, Defense Atomic Support Agency Report 2611 (SRD), November 1971.
12. Olwecard, A., et al., "Improvement of Transmission Capacity by Thyristor Controlled Reactive Power," IEEE Transactions on Power Apparatus and Systems, PAS-100, 3930-3939 (1981).
13. Blicher, A., Physics of Semiconductor Power Devices, Rep. Prog. Phys., Vol. 45, 1982. Printed in Great Britain.
14. Ward, A., Calculations of Second Breakdown in Silicon Diodes, U.S. Army Electronics Research and Development Command, Harry Diamond Laboratories, HDL-TR-1978, August 1982.

OPTICALLY INDUCED HIGH POWER
SWITCHING IN BULK SEMICONDUCTORS

Gerard Mourou
Laboratory for Laser Energetics
University of Rochester

HIGH POWER PHOTOCONDUCTIVE SWITCHING

Scaling and performance data of laser-activated Si and GaAs switches in the picosecond domain are discussed here. It is shown that, although nearly intrinsic silicon is prone to thermal runaway,⁽¹⁾ DC or quasi-DC bias⁽²⁾ operation is possible in a manner which relaxes synchronization requirements. Up to 10 KV was switched in 40 ps with a 35 ± 5 ps FWHM optical pulse. In addition, 8 KV DC was switched effectively with semi-insulating GaAs, and cryogenically cooled Au-doped silicon, yielding synchronized high-voltage subnano-second pulses.

Fast high-voltage switching has been demonstrated up to 1.5 KV by Auston et al.,⁽³⁾ and up to 10 KV by Mourou et al.,⁽⁴⁾ with nearly intrinsic silicon. Lee⁽⁵⁾ showed that 5 KV could be held off by semi-insulating GaAs but reported a switching efficiency of only 30%. Because nearly intrinsic silicon with a resistivity of $\sim 20 \times 10^3 \Omega \text{ cm}$ at room temperature is not an effective insulator, the thermal instability problem was avoided by biasing the Si with a 10 ns bias pulse. This method calls for nanosecond synchronization, which severely complicates the use of Si as a photoconductive element for fast high power switching. Since the dielectric relaxation time is ~ 20 ns in Si, the nanosecond bias pulse experiences a high capacitance depletion layer leading to

significant capacitance coupling and unanticipated dielectric breakdown.

a) Turn-on sensitivity⁽¹⁾

A piece of nearly intrinsic Si (highly boron doped) with a resistivity of $(20-30) \times 10^3 \Omega \text{ cm}$ replaces a section of the central conductor of an HN connector. The crystal is typically 10 mm long, 1 mm wide, and 0.5 mm thick. Two aluminum electrodes are applied by evaporation and the gap is protected by film of 1000 Å of SiO_2 and clear epoxy. The electrodes are spaced between 2 and 4 mm apart, depending on voltage hold-off and optical energy requirements. The gap is activated with a short optical pulse, $3.5 \pm 5 \text{ ps}$, centered at $1.064 \mu\text{m}$, generated by a passively mode-locked $\text{Nd}^{3+}:\text{YAG}$ laser. At this wavelength, the penetration depth is a few hundred microns, so that carriers can be implanted in situ throughout the bulk during the optical pulse. For fields $> 10^4 \text{ V/cm}$, the gap resistance is governed by the expression

$$r = \frac{h \nu l V_0}{2 v_s e E_\alpha} , \quad (1)$$

where E_α is the absorbed optical energy, ν is the optical frequency, l is the length between the electrodes, V_0 is the bias voltage, v_s is the carrier saturation velocity (10^7 cm/s), e is the charge of the electron, and h is Planck's constant. After optical activation, the gap resistance will return to the intrinsic level in the carrier recombination time of about 20 μs . For efficient switching, the gap resistance must be small compared to the cable impedance Z_0 . In practice, 95% switching,

that is, a pulse voltage of $0.95 V_0/2$, is achieved with a gap resistance $r = Z_0/10$. The corresponding optical energy requirement is expressed by

$$E_\alpha(95\%) = \frac{5V_0 l h\nu}{Z_0 V_s e} . \quad (2)$$

For example, for $l = 2 \text{ mm}$, $Z_0 = 50 \Omega$, and $V_0 = 8000 \text{ V}$, $30 \mu\text{J}$ of absorbed optical energy is sufficient to achieve efficient switching.

b) Power handling

Pulse bias mode ⁽¹⁾

The contacts are not purely ohmic, so the two electrodes behave as two back-to-back surface barrier diodes and application of a bias on either side of the gap will forward bias one contact and reverse bias the other. The I-V characteristic of the gap exhibits a linear behavior at low voltage and at about 100 V turns upward quickly, indicating a space charge saturated regime. At high voltage (3 KV), gap impedance measurements conducted with μs high-voltage pulses indicate a gap impedance limited by the gap bulk resistance, $\sim M\Omega$. This relatively low impedance allows significant heat dissipation, which contributes to local lower resistivity and leads ultimately to thermal runaway. Assuming that, at high voltage, the gap behaves in an ohmic manner, the gap temperature, T , at low repetition rate scales according to

$$dT = \frac{V_0^2}{dcl^2\rho} dt , \quad (3)$$

where dt is the temperature rise during the time interval dt , d is the mass density, c is the specific heat, E_g is the gap

energy, and ρ and ρ_0 are the resistivities at temperature T and T_0 , respectively, with T_0 here taken to be room temperature. The resistivity of the silicon, assumed to be intrinsic at room temperature, is

$$\rho = \rho_0 (T/T_0)^{3/2} \exp(-Eg/2K) \left(\frac{1}{T} - \frac{1}{T_0} \right), \quad (4)$$

The set of curves in figure 1 has been generated from Eqs. (3) and (4) for different voltage step functions applied to the gap. In particular, it is seen that a gap of 2 mm can hold off 8000 V for a period of 100 μ s, after which its resistivity will drop below $\rho_0/2$. It is important to note that, in this period of time, a Nd³⁺ laser with a typical jitter time of 5 μ s can be easily synchronized. From Eqs. (2), (3) and (4), we generated a set of curves (figure 2) showing the interdependence of the voltage hold-off, thermal runaway growth time, and turn-on energy for optimized switching.

A thyratron pulse generator used as a quasi-dc bias source puts out a 20 μ s pulse. This pulse biases, through a 10 K Ω current limiting resistor, a charge line attached to a laser-activated silicon switch with a gap length of 2 mm. The charge line length can be chosen from 100 ps to several hundred nanoseconds. About 30 μ J of absorbed optical energy is found to be sufficient in this case to bring the switch into the on state, in agreement with equation (2). Figure 3 displays a typical bias pulse and output pulse thus obtained. The charge line voltage is shown on the same figure, where we see the effective action of the laser pulse. The rise time of the square pulse is somewhat affected by

the oscilloscope bandwidth, a relatively long cable between the device and the oscilloscope, and the string of attenuators utilized to attenuate the signal. Figure 4 illustrates the relationship between the electrical pulse and the optical pulse.

DC bias mode⁽²⁾

At room temperature, a typical photoconductive device can hold off a multikilovolt bias voltage for only tens of microseconds, as seen in the previous paragraph, due to excessive thermal carrier generation. Reliable switching operation was achieved only with a pulsed bias. The duration of the bias pulse is set according to the thermal instability build up time, i.e., microseconds.

Electrooptic devices working in the picosecond domain often require picosecond switching synchronization and excellent voltage amplitude stability. Signal averaging with a streak camera is one example where amplitude fluctuations of less than 1% are required. This constraint precludes the use of pulse bias techniques in many cases because of the shot-to-shot voltage variation and the time fluctuation between the laser and the high voltage bias pulse. Here the photoconductive switching of a kilovolt DC bias by Au-doped Si held at liquid nitrogen temperature is demonstrated. In addition to the complete alleviation of bias timing and amplitude stability problems, DC photoconductive switching at cryogenic temperature should lead to KHz repetition rates. It should be noted that, while highly Cr-doped GaAs at room temperature exhibits similar voltage hold-off capability as the Au-doped Si used here at cryogenic temperature, the

inability to obtain pulse durations of more than a few hundred picoseconds restricts the room temperature use of such materials severely in electrooptic applications where square pulses that are several nanoseconds in duration are required. Also Si, with its band gap at 1.12 eV, as opposed to that of GaAs at 1.42 eV, can accommodate a near infrared excitation laser more efficiently.

The switching element is a piece of Au-doped Si (with dimensions 5mm x 1mm x 0.5mm) that is attached to a 1 mm thick sapphire plate with vacuum grease. The sapphire is mounted on a piece of brass that is fastened to a liquid nitrogen cold trap. The Si interrupts a 10 cm microstrip line that was made from shim stock. The 9 cm section of microstrip preceding the Si acts as a charge line and is biased through a 5 K Ω resistor. Connections to the microstrip are made with an HN connector and an SMA connector on the bias and high bandwidth ends respectively. The connections to the Si are silver painted. The whole assembly is mounted inside a vacuum chamber that is evacuated to about 10^{-3} Torr with a double stage mechanical pump. At this pressure, no corona or condensation was observed.

Nearly intrinsic Si ($3 \times 10^4 \Omega \text{ cm}$), as used in pulse bias, room temperature switching devices, was found to be an unacceptable switching element at liquid nitrogen temperature. At low voltage a ten-fold increase in resistivity was observed, followed by a premature bulk dielectric breakdown that was monitored on a nanosecond time scale for an electric field strength of ~ 100 V/cm. This behavior was consistently observed for 100 μm and 2

mm gaps. For the 100 μm gap sample, a Si disc with electrodes on opposite sides was used, eliminating the possibility of surface breakdown. An interpretation of these results that is well known from the early work on dielectric breakdown in insulating crystals;⁽⁶⁾ at low temperatures, the freezing out of phonons increases the mean free path of charged carriers, so that their kinetic energy can exceed the impact ionization energy even for small electric field strengths, leading to a collapse of the dielectric breakdown field.

To enhance the dielectric breakdown field at liquid nitrogen temperature, we used Si doped with deep lying Au impurities that were introduced to act as scattering centers to reduce the carrier mean free path. At room temperature, the sample resistivity, while greater than 3 $\text{K}\Omega\text{cm}$, is not sufficiently large to inhibit thermal instability for DC biases greater than 100 V applied to a 2 mm gap device. We estimated the Au concentration from the recovery time of the photoconductivity using the following formula:⁽⁷⁾

$$\tau \sim 1/\sigma_h v_h N_{\text{Au}} \quad . \quad (5)$$

With $\sigma_h v_h = 1.4 \times 10^{-8} \text{ cm}^3 \text{ s}^{-1}$ and $\tau = 100 \text{ ns}$, the Au concentration is estimated to be $10^{15}/\text{cm}^3$. The current voltage characteristics for a Au-doped Si switching element are displayed in figure 5 for both room and liquid nitrogen temperature. It is seen that thermal carrier generation in the KV bias range rather than the impact ionization of deep traps⁽⁸⁾ limits the voltage blocking capability of the switching device. The switching performance of

a 2 mm gap, Au-doped Si element at liquid nitrogen temperature was examined. A single pulse at $1.054 \mu\text{m}$, with an energy of $100 \pm 10 \mu\text{J}$ and a full width at half-maximum of about 35 ps, was selected from the mode-locked train of a $\text{Nd}^{3+}:\text{YLF}$ oscillator to activate the switching element. The output electrical pulse was monitored with a 5 GHz oscilloscope (Thomson CSF TSN 660). Figure 6 shows the electrical output when the Si is biased with 2 KV DC. The pulse duration is ~ 2 ns, corresponding to the charge line length. The 100 ns recovery time of the photoconduction establishes the maximum pulse duration. The rise time observed is cable and oscilloscope limited to 100 ps. The ringing sub-structure is caused by a string of attenuators and was not present at low voltage. A shoulder of 5% following the main pulse is due to a series contact resistance of 5Ω and is independent of the optical turn-on energy. Efficient switching was observed up to 4 KV biases with an optical turn-on energy of $\sim 50 \mu\text{J}$ for a 2 mm gap switching element.

Our switching arrangement is particularly well-suited for high repetition rate operation because the thermal load is only moderate, 0.1 W at 5 KV. The dissipation rate has been optimized by using a sapphire insulator which has an excellent low temperature thermal conductivity. In addition to the Joule heating due to the DC bias, the switching element experiences heating during the turn-on time because of series contact resistance of 5Ω and the incident optical energy. With the requirement that the additional turn-on heating does not exceed the bias Joule heating, and the assumptions of a 5 KV DC bias, 5Ω contact resistance, 5

ns electrical pulse duration, and 30 μ J of absorbed optical energy, a 1 KHz repetition rate is acceptable.

c) Rise time analysis

In the photoconductive mode, the switching speed is limited by a combination of four factors: the optical pulse width; the geometry bandwidth, defined as the bandwidth of the coaxial charge line and switch circuit; the dielectric relaxation time; and the RC time constant of the gap. The gap capacitance is $\sim 10^{-14}$ F, and at saturation, both the dielectric relaxation time and the RC time constant are of the order of 1 ps or smaller. Therefore, the turn-on time is dominated by the optical pulse width (35 ps) and the geometry bandwidth (~ 10 GHz).

The gap conductivity evolves in time linearly with the optical energy, so that the switching precision will depend, in principle, on the pulse energy and pulse shape variation. A numerical analysis carried out for a Gaussian pulse temporal profile and confirmed experimentally (see figure 4) indicates that, in the saturation range (gap resistance smaller than the cable impedance) a variation of one decade in laser energy offsets the switching time by less than one-half the laser pulse width. Therefore, a $\pm 20\%$ shot-to-shot variation in pulse width and in energy (typical for a Nd³⁺ laser) should not alter the switching precision by more than a few picoseconds.

To measure the pulse rise time⁽¹⁰⁾ and jitter, ⁽¹¹⁾ we produce a relatively long optical pulse (> 100 ps) synchronized to the short optical pulse. The long pulse is actively shaped by a fast Pockels cell and the short pulse drives the GaAs switch

which controls the Pockels cell. The pulse shaping system is diagrammed in figure 7. A passively mode locked Nd:YAG laser, including single-pulse switchout and YAG amplifier, produces single 2 mJ pulses with temporal widths in the range of 20 to 60 ps (no intracavity etalon is employed). The single pulses are then split into two optical beam lines. The first line sends the pulse through a pair of diffraction gratings which temporally stretch the pulse to 100 to 300 ps.⁽⁹⁾ The width of the stretched pulse is inversely proportional to the width of the pulse generated by the ND:YAG laser. The stretched pulse passes through a Laser-metrics Model 3048 Pockels cell which is placed between crossed Glan polarizers. The Pockels cell uses a 0° Z-cut cut highly deuterated KD*P crystal with cylindrical ring electrodes. It has a 7 KV half-wave voltage in the fast pulsed mode. The clear aperture is 2.5 mm and the length is 7 mm. Static contrast is measured to be > 400:1. In order to demonstrate the response characteristics of the Pockels cell, a half-wave plate is inserted after the first polarizer and adjusted so that a few percent of the stretched pulses passes through the modulator even when no voltage is applied to the cell. In this way, one can clearly see what part of the stretched pulse has been altered by the Pockels cell.

The stretched optical pulse which has been shaped by the Pockels cell is brought onto the slits of the Hadland Imacon 675 optical streak camera. Part of the stretched pulse is split off before the Pockels cell and brought to the streak camera as a reference. The reference pulse is delayed by several hundred

picoseconds with respect to the shaped pulse. A Princeton Applied Research optical multichannel analyzer optically coupled to the streak camera gives an instantaneous readout of pulse shape. The entire detector system is calibrated for both intensity response (found to be linear) and sweep speed, using a single oscillator pulse and a bounce etalon (pulse replicator) feeding a pulse train with 125 psec pulse (unstretched) to the GaAs switch. The arrival time of the pulse is controlled by an optical delay line. The Pockels cell is driven by a high voltage pulse formed by a charge line and the GaAs switch. The charge line is located between a 300 K Ω charging resistor and the GaAs crystal. It consists of a small section (~1 cm) of the coaxial barrel into which the GaAs has been mounted.

The GaAs switch⁽¹⁾ is made of a semi-insulating (resistivity $> 10^7 \Omega \text{ cm}$) GaAs bar which is highly doped with chromium. The bar is 10 mm long, 1 mm wide, and 0.5 mm thick, and is mounted in a coaxial geometry. Two electrodes are evaporated onto the GaAs bar, forming a 5 mm gap. The low voltage impedance is ~1 G Ω . The device can block up to 8 KV DC voltage. The entire gap is illuminated with the mode-locked pulse. In spite of the large bandgap energy of the GaAs ($E_g = 1.42 \text{ eV}$), the laser pulse is completely absorbed by intrinsic, extrinsic, and two-photon mechanisms throughout the crystal bulk (for the 1.06 μm photons, $h\nu$ is 1.17 eV). 50 μJ of absorbed light energy is sufficient to establish the coaxial transmission line conductivity. In the experiment, the switch is driven into saturation with a 200 μJ pulse. It is worth noting that the low electric field (2×10^4

V/cm) does not cause avalanche multiplication of the photoinduced carriers. Then the absorbed energy, E_α , required to achieve 95% electrical transmission efficiency is given by:

$$E_\alpha = 5V_0 \ell h\nu / Z_0 v_s e , \quad (6)$$

where V_0 is the bias voltage, v_s is the carrier saturation velocity, h is planck's constant, ν is the optical frequency, e is the charge of the electron, Z_0 is the line impedance, and ℓ is the gap length. The electrical rise time is limited essentially by the optical pulse width and the overall geometry band width (~10 GHz). The gap charge time is ~1 ps and the dielectric relaxation time ϵ/σ is < 1 ps, where ϵ is the dielectric permittivity and σ is the conductivity. The gap charge time and the dielectric relaxation time can be neglected for all practical purposes. Note that the temporal precision of switching is determined by the amplitude and shape of the optical driving pulse. The high resistivity of the crystal recovers in a few hundred picoseconds after the application of the optical field. The recovery is determined by the carrier recombination time in the crystal, which limits the maximum duration of the electrical pulse. Longer electrical pulses can be produced by reducing the concentration of the chromium impurity or by using near intrinsic silicon instead of the Cr-doped GaAs. (1)

d) Timing fluctuation analysis (11)

We found that the most sensitive way to estimate the jitter of photoconductive switch was to drive the deflection plate of a streak camera. (11) The jitter in this configuration will appear

as a timing fluctuation of the electron burst, generated by the laser pulse incident on the streak camera.

Figure 8 shows the experimental arrangement. A high voltage pulse is generated by a laser-activated silicon switch composed of one block (2 mm long by 1 mm wide by 0.5 mm thick) of high-resistivity silicon ($30 \text{ K}\Omega \text{ cm}$) which interrupts the central conductor of a type HN high voltage connector. The switch is illuminated with a single pulse of 40 ps duration from a $\text{ND}^{3+}:\text{YAG}$ mode-locked oscillator. At room temperature, the silicon is a poor insulator, and the thermal runaway buildup time for multi-kilovolt bias is in the order of tens of microseconds. In particular, a gap length of 2 mm, which requires $< 50 \mu\text{J}$ of optical energy can hold off a bias voltage of 8 KV for a period of 50 μs .⁽¹¹⁾ Bias is hence applied through a charge line to the switch in a pulse of duration 15 μs , and is easily synchronized with the laser mode-locked train output. Typically, the laser pulse timing with respect to the bias pulse varies by $\pm 3 \mu\text{s}$. Because the carrier recombination time is on the order of 10 μs in intrinsic silicon, under laser action, the duration of the generated voltage pulse corresponds to the charge-line length. The high voltage square pulse is applied to the deflection plate of an S-20 photocathode Photochron-II streak tube. The deflection plates form an R-C charging network in the transmission line, with an impedance of 50Ω and a capacitance of 9 pF. The rise time of the deflection voltage is then 450 ps. Slower streak ramp times can be obtained with the addition of an integrator. The streak image is recorded by an optical multichannel

analyzer (Princeton Applied Research, Inc.) optically coupled to a four-stage magnetically focused image intensifier.

Up to 4.5 KV can be applied to the plate, yielding a sweep speed of half the speed of light. The temporal and intensity calibration is provided by a leaky Fabry Perot etalon which splits the incoming pulse into a series of pulses. Figure 9 displays a typical streak record obtained with 1.5 KV on the charge line. For this sweep speed the temporal resolution is focusing limited to 5 ps.

In order to estimate the jitter which can be expected from this system, we recall that the high-voltage pulse generated by the silicon switch exhibits a temporal dependence governed by the relation

$$V(t) = V_0 Z_0 / \{2Z_0 + (G(t))^{-1}\} , \quad (7)$$

where V_0 is the bias voltage, Z_0 is the line impedance, and $G(t)$ is the gap conductance. The gap conductance, with the approximations of a long recombination time and bias field $> 10^4$ V/cm, is

$$G(t) = \frac{2 v_s e \alpha}{h v \ell V_0} \int_{-\infty}^t P(t') dt' , \quad (8)$$

where v_s is the carrier saturation velocity ($= 10^7$ cm/s), e is the electronic charge, α is the fraction of the light absorbed, h is Planck's constant, v is the optical frequency, ℓ is the gap length, and $P(t)$ is the incident laser power.

$V(t)$ has been numerically computed for $\alpha = 0.5$, $\ell = 2$ mm, and $V_0 = 2000$ V, with various optical energies, using a Gaussian laser pulse (figure 4), with the time axis normalized to the

pulse width. On the basis of the analysis, there are two distinct regions of operation.

(a) Nearly-saturated regime: $G(t)^{-1} \gg 2Z_0$. In this regime, the laser energy is not sufficient to reduce the gap resistance to a value much smaller than the line impedance. As a consequence, the switch output will scale according to the laser energy, leading to a shot-to-shot sweep speed variation. It is worth noting that, in this regime, the turn-on time, defined as the time between the optical pulse center and the half-rise point, will depend relatively little on the pulse width variation. This regime is illustrated in figure 9, where two different streaks are compared. Note the near coincidence early in the streak and the linear walkoff between corresponding peaks as time progresses, characteristics of an accurate turn-on time and a sweep-speed change. This sweep-speed change corresponds to a 2% change in high voltage.

(b) Saturated regime: $G(t)^{-1} \ll 2Z_0$. In this regime, the gap resistance becomes much smaller than the line impedance, and according to Eq. (8), the voltage amplitude becomes independent of the laser energy, so no sweep-speed fluctuations are expected. If, however, the device is strongly over-saturated in an attempt to minimize the sweep speed fluctuation further, as indicated in figure 4, a shift in the timing of the electrical pulse will appear. This shift is proportional to the laser pulse width and will lead to a zero-time offset fluctuation, scaling with laser pulse width fluctuation. This effect, which results in a translation of the streak as a whole by a fraction of the pulse width,

was not clearly observed but can be sizeable for longer laser pulses.

Of primary importance is the optical contrast of the laser pulse, which leads to both sweep-speed and zero-time offset variation. For optimum operation, it is desirable to have both an electrical contrast better than 10^3 and the switch driven slightly above saturation. This is obtained with a double Pockels cell switchout system (optical contrast $> 10^5$) and 100 J of laser energy.

With the present laser energy and pulse width fluctuations of $\pm 15\%$, we obtain a jitter of ± 1.7 ps; with laser stabilization, lower jitter is obtainable. This low jitter permits signal averaging over many shots without the need of fiducial markers to improve the statistics of the data. This capability is demonstrated in figure 10, which shows a streak of a fluorescent dye (Rose Bengal) in water, with 1 and 10 shots accumulated and 1 and 10 shots of the excitation pulse, which can be unfolded from the fluorescence trace with no zero-time reference shift.

Despite a jitter of 1.7 ps, we can measure time delays < 1.7 ps by signal averaging. This technique can be used to determine the duration of picosecond and subpicosecond events by measuring the time shift between the excitation and the signal maxima. This shift corresponds to the transient lifetime at $1/e$ for lifetimes much shorter than the excitation time. In the present experiment, averaging over only 100 shots could give access to a timing accuracy of 200 fs.

PICOSECOND SWITCHING USING PHOTOELECTRONS (12)

The photoconductive mode of operation leads to picosecond switching speeds, but requires a high level of optical excitation energy, inasmuch as all the carriers necessary to achieve complete switching are photogenerated. This relatively high energy requirement (equal to tens of microjoules) could prevent the use of this technique in a large number of applications in which only low energy optical pulses in the nanjoule range are available. Enhancing of switching sensitivity by three to four orders of magnitude was successfully accomplished using impact ionization in semiconductors but resulted in a loss of switching speed. There is, however, an alternative, leading to a potential picosecond switching sensitivity enhancement of 10^3 . This approach is based on electron-bombarded semiconductors,⁽⁴⁾ where the new feature is that a picosecond electron burst is generated by the front end of a streak camera, where a high-resistivity Si switching element replaces the standard phosphor screen (figure 11). The burst can be regarded as a replica in time and space of the input laser pulse, and is positioned on the silicon using the deflection plates. The interaction of each 15 KeV electron (typical for a streak camera) with the semiconductor results, on a picosecond time scale, in ionization producing a large number of electron-hole (e-h) pairs. For silicon, the average energy necessary to create one e-h pair is 3.6 eV, corresponding to a generation of about 5000 e-h pairs per absorbed electron.⁽¹³⁾ Upon penetration, the electrons lose their energy according to the relationship $(dE/dx) = -2.8 \text{ keV}/\mu\text{m}$,⁽¹³⁾ and a conductive

layer a few micrometers thick is formed in the electrode gap on the surface of the semiconductor, causing the switch to close. Thus, in this approach, the streak camera pulse is used as a high gain amplifier to trigger the switch (in effect reversing their previous roles), which can then be used for a variety of picosecond switching operations.

Electrical signals from the photoconductive and photoelectron conductivity modes of operations are shown in figure 12. In addition to enhancement of switching sensitivity, photoelectron switching offers other advantages over photoconductive switching:

- a) the possibility of deflecting the electron burst at a speed on the order of the speed of light, with picosecond accuracy, and potential application as a fast demultiplexing system with a bandwidth of over 20 GHz;
- b) the use of large bandgap materials with good holdoff characteristics;
- c) incorporation of fast response time switching elements, making this device useful as a fast and sensitive photodetector; and
- d) the possibility of further reduction of the switching rise time by deflecting the focused electron burst across the gap.

HIGH POWER SWITCHING WITH OPTICALLY-INDUCED AVALANCHE IN BULK SEMICONDUCTORS

Considerably less work has been done on high voltage switching via charge carrier avalanches in bulk semiconductors. The

process has been demonstrated for both p-n junctions⁽¹⁴⁾ and bulk⁽¹⁵⁾ (as in the cryosar) semiconductor devices. Both switching geometries turn on by way of impact ionization, though they differ in the mechanism by which they are triggered. Where the p-n junction relies on the electric field in order to break down (analogous to HV), the cryosar is based on differential negative resistance for its triggering.⁽¹⁶⁾ Laser-triggered thyristors (LASS)⁽¹⁷⁾ are the only devices we are aware of which specifically use laser-triggered avalanche switching in bulk semiconductors, hence combining some of the advantages of both categories mentioned above. Thyristors, however, are limited to ≤ 1.5 KV, and the laser trigger pulse employed was longer than 22 ns.

The mechanism governing avalanche multiplication of charge carriers is briefly as follows.⁽¹⁸⁻²¹⁾ Before the avalanche is triggered, the high field region of the junction exhibits a low residual current flow caused by thermal charge carriers. These thermal charge carriers (electrons and holes) are then accelerated in the applied field toward oppositely charged electrodes. An ionization energy of $E_i \sim 2.2$ eV at a bandgap energy of ~ 1.45 eV is required^(14,22) to generate additional charge carriers. The resulting drop in resistance across the electrodes due to saturation in the number of charge carriers can be seven orders of magnitude or more depending on the device.^(15,23)

In the switch we now describe, impact ionization is initiated by the creation of additional charge carriers in the bulk of a semi-insulating Cr-doped GaAs sample. The carriers were gener-

ated by injection of a 30 ps light pulse from a Q-switched mode-locked YAG laser into the high field region. Light energies as low as 35 nJ were sufficient to trigger the avalanche process. Control of both avalanche build-up time and build-up time jitter was maintained by controlling the energy of the light pulse.

a) Experiment

Figure 13 shows the experimental arrangement. To reduce the risk of thermal breakdown at high fields, the GaAs sample was cooled down, while under vacuum, to 195 and 77 K, respectively. The DC bias cable and transmission cable (both of semirigid coaxial type) passed through vacuum feedthroughs and were grounded within the chamber.

Spring leads soldered to the center lead of both coaxial cables were used as pressure contacts on opposite sides of the GaAs sample. The contacts were offset by ~500 μ m along the axis of the light pulse, in order that the high field region be accessible to the light pulse. A bead of conductive silver paint was placed on the end of each of the contacting pins and left to dry after contact was made. Such a contact was not purely ohmic, causing the two electrodes to behave to some extent as surface barrier diodes. At high fields, however, such a junction becomes unimportant, because the extent of these diode junctions is much smaller than the high field region across the entire gap.

A single pulse, switched out from the train of a mode-locked $\text{Nd}^{+3}:\text{YAG}$ laser, was used to photogenerate free carriers. The width of the HV pulse switched out through the GaAs was set by the cable length between the GaAs sample and the current limiting

resistor on the bias cable. The amplitude was load limited and independent of the trigger signal. The electrical pulse traveled out of the chamber and through a broadband attenuator into a 4 GHz oscilloscope. This system has a measured response time of 70 ps in the direct access mode.

b) Procedure

The chamber was first pumped down to 10^{-4} Torr, then the GaAs was brought to cryogenic temperature so that condensation of moisture on the GaAs was minimized. The field applied across the GaAs sample was 1% and 20% below self-breakdown (78 KV/cm at 77 K). The HV pulse generated by the avalanche was preceded by a small photoconductive signal with an amplitude as much as two orders of magnitude below that of the avalanche HV pulse, so that a 50 ps rise time photodiode receiving 10% of the laser pulse intensity could be used as a timing mark for the photoconductive signal. The build-up time of the avalanche was obtained from the time delay between the arrival of the injection light pulse, indicated by the 50 ps photodiode signal, and the 50% of full amplitude point of the avalanche HV pulse. Measurements were made of the build-up time as a function of the injected optical energy at 1% and 20% below self-breakdown, and at 77 and 195 K. As the energy of the injected light pulse increased, the build-up time became shorter, and at optical energies of ~ 10 nJ, the photoconductive rise due to the laser pulse made up the initial rise of the avalanche HV pulse. Measurements of the build-up time were made until the photoconductive contribution of the

incident light pulse to the leading edge of the avalanche HV pulse was ~20% of the amplitude of the avalanche HV pulse.

c) Results

The I-V curve for the Cr:GaAs sample at 77 K is shown in figure 14; at around ~3.8 KV (76 KV/cm), the crystal self-avalanched. As the temperature was increased to 195 K, the number of thermally generated carriers increased, resulting in a higher dark current flow of ~ 15 μ A. At 195 K the GaAs still self-avalanched at ~ 3.8 KV, but the avalanche threshold was less sharply defined than at 77 K. A typical HV pulse switched from this device is shown in figure 15. The photoconductive contribution of the optical signal triggering the avalanche can be seen to the left of the waveform near the baseline. The second smaller drop on the right of the waveform indicates less than 100% switching due to the circuit resistance (8 Ω) of the GaAs sample.

Figure 16 shows the observed build-up time, τ_B , versus incident optical energy for the two voltages and two temperatures mentioned above. The build-up time decreased with increased optical trigger energy. In all four plots, the slopes were similar and approximately 45 ps per decade. At constant injection light energy and constant voltage, there was a slight reduction in build-up time. At 3.7 KV, this reduction was from 1.42 ns at 195 K to 0.71 ns at 77 K. Also, we noted a reduction in the minimum energy required for initiating the avalanche, from 150 to 35 nJ. For constant temperature, no dependence of this minimum optical energy on the applied voltage was observed. For constant incident optical energy, the build-up time was seen to

vary only slightly with the applied field or temperature, i.e., ~3 ps per 10 V. With these results in mind, it is instructive to compare a semiconductor spark gap with other spark gap designs. Table 1 contains values which are largely taken from a review article on laser triggered HV switching⁽²³⁾ and represent the optimum performance for each row separately. It is evident that, at comparable build-up time and jitter, and at a somewhat increased rise time, a semiconductor spark gap is much more trigger sensitive.

In order to appreciate fully the validity of the results, one aspect of the trigger sensitivity of the device needs further discussion. A newly installed GaAs sample exhibited comparatively higher trigger sensitivity, faster rise time, and better switching efficiency, than after additional use. After roughly fifty to one hundred shots, however, these values settled down, and for thousands of shots thereafter, we observed no further change. Typically, the maximum trigger sensitivity increased from 35 to 50 nJ, the rise time slowed down from 500 to 700 ps, and the 85% switching efficiency changed by 5%. The build-up time jitter, however, remained within \pm 150 ps for 90% of all shots. We attribute this behavior to the creation of additional impurity sites,^(24,25) enabling fewer electrons to become energetic enough to ionize further impurity sites. This effect constitutes a drawback for some applications.

The sharp cutoff for the trigger energy required to initiate the avalanche makes the device potentially useful for discrimination between light pulses of various intensities. Figure 17

shows part of the train from a mode-locked laser, in which one pulse of a preselected intensity triggered the GaAs avalanche switch. Furthermore, the light from the laser diode, located very close to the GaAs sample, was also found sufficient to initiate avalanche switching. Both applications, however, do suffer in reproducibility.

In conclusion, we have demonstrated HV switching with sub-nanosecond rise times and ~ 150 ps timing jitter, using a light-initiated current avalanche in a sample of GaAs. We feel that, in comparison to conventional pressurized spark gaps, the particular usefulness of this device consists of its high trigger sensitivity, extending the possibility of efficient light-induced HV switching to hitherto unsuitable light sources.

REFERENCES

1. G. Mourou and W. Knox, *Appl. Phys. Lett.* 35, 492 (1979).
2. M. Stavola, M. Sceats and G. Mourou, *Opt. Comm.* 34, 409 (1980).
3. P. LeFur and D. Auston, *Appl. Phys. Lett.* 28, 21 (1976).
4. A. Antonetti, M. M. Malley, G. Mourou, and A. Orszag, *Opt. Commun.* 23, 435 (1977).
5. C. Lee, *Appl. Phys. Lett.* 30, 84 (1977).
6. N. F. Mott and R. W. Gurney, Electronic Processes in Ionic Crystals (Dover, New York, 1964) pp. 197-201.
7. W. M. Bullis, *Solid-State Electron.*, 9, 143 (1966).
8. A. G. Milnes, Deep Impurities in Semiconductors (Wiley, New York, 1973) p. 362.
9. J. Agostinelli, G. Harvey, T. Stone and C. Gabel, *Appl. Opt.* 18, 2500 (1979).
10. J. Agostinelli, G. Mourou and C. W. Gobel, *Appl. Phys. Lett.* 35, 731 (1979).

11. G. Mourou and W. Knox, *Appl. Phys. Lett.* 36, 624 (1980).
12. S. Williamson, S. Letzring, and G. Mourou, CLEO '81 paper WR5, Washington 1981.
13. P. Chevalier and J. Nussli *C R Acad. Sci., Paris*, 264, 462 (1967).
14. M. Sze, Physics of Semiconductor Devices (Wiley, New York, 1969).
15. A. L. McWhorter and R. H. Rediker, *Proc. IRE* 47, 1207 (1959).
16. B. K. Ridley, *Proc. Phys. Soc. London* 82, 954 (1963).
17. P. G. McMullin and L. R. Lowry, *IEEE Trans. Electron. Devices* 26, 1469 (1979).
18. S. L. Miller, *Phys. Rev.* 99, 1234 (1955).
19. C. A. Lee, R. A. Logan, R. L. Batdorf, J. J. Kleimack, and W. Wiegmann, *Phys. Rev.* 134, A761 (1964).
20. R. A. Logan and S. M. Sze, Proceedings of the International Conference on the Physics of Semiconductors (Kyoto) in *J. Phys. Soc. Jpn. Suppl.* 21, 1591 (1963).
21. A. Goetzberger, B. McDonald, R. H. Haitz, and R. M. Scarle, *J. Appl. Phys.* 34, 1591 (1963).
22. G. A. Baraff, *Phys. Rev.* 128, 2507 (1962).
23. A. H. Guenther and J. R. Bettis, *J. Phys. D.* 11, 1577 (1978).
24. A. S. Epstein and J. F. Caldwell, *J. Appl. Phys.* 35, 2481 (1964).
25. R. D. Gold and L. R. Weisberg, *Solid State Electron.*, 7, 881 (1964).

Table 1. Comparison of semiconductor spark gaps with other spark gaps.

| | Semiconductor spark gaps | Other spark gaps |
|---|---|---|
| Hold off | ~80 KV/cm | up to 500 KV/cm |
| Build-up time when switched close to self- breakdown | 0.5 to 1.5 ns, depending on field trigger energy, and material | > 1.5 ns, depend- ing on field, trigger energy, and pressure |
| Rise time | conservatively ~700 ps in a noncoaxial geometry | > 150 ps in well matched geo- metries |
| Build-up time jitter | $\leq \pm 150$ ps for 90% of all shots | > 150 ps average deviation |
| Trigger energy | $\gtrsim 1 \times 10^{-8}$ J | $\gtrsim 2 \times 10^{-5}$ J |

FIGURE CAPTIONS Mourou

Figure 1. Si resistivity as a function of time for different applied voltage step functions. Gap length: 2 mm.

Figure 2. Curves summarizing the bias voltage pulse width and the optical energy requirements as a function of the bias voltage for different gap lengths, to achieve 95% switching efficiency.

Figure 3. Optically synchronized electrical pulse generation (a) 8 KV bias pulse monitored between the current limiting resistor and the light-activated silicon switch (see figure 4). No light on the switch. (b) The optical pulse activates the switch 10 μ s after the bias pulse is applied on the switch. The charged line is quickly discharged. (c) A 4 KV, ~ 200 ns square pulse generated by discharging a ~ 20 m charge line. (d) A 4 KV, ~ 5 ns pulses generated with a ~ 50 cm charge line for two consecutive laser shots. The rounded pattern is due to the relatively long RG58 cable between the switch and the oscilloscope.

Figure 4. Generation of the electrical pulse for different optical energies. A:1 μ J, B:1 μ J, C:10 μ J, D:100 μ J. The pulse voltage varies with optical energy in A and B, giving rise to sweep speed fluctuations but with the zero time reference unchanged. In C and D the pulse voltage becomes constant and the zero time reference depends upon the laser pulse width variation. This effect is negligible for a 40 ps optical pulse for normal laser width fluctuations ($\pm 15\%$).

Figure 5. Current-voltage characteristics at room and liquid nitrogen temperatures demonstrate the improvement in DC hold-off for a 2 mm gap as the temperature is lowered. Joule heating and the resultant thermal generation of carriers gives these curves their shape.

Figure 6. A trace from a Thomson CSF TSN 660 oscilloscope. A DC bias voltage of 2 KV was used.

Figure 7. Block diagram of the experimental setup.

Figure 8. Experimental configuration. A single 40 ps pulse from a mode-locked Nd^{3+} :YAG laser is frequency doubled. A 15 μ s high-voltage bias pulse is applied to a charge line synchronous with the laser firing. A silicon block, which interrupts the continuity of a 50 Ω coaxial line, becomes conducting under the action of the IR laser pulse, and an electrical pulse is generated of length corresponding to the charge-line length; its rise time is limited by the optical pulse width. This pulse is applied to the deflection

plates of an image converter tube and the swept image is recorded by an intensified OMA. Time and intensity calibration data are provided by passing the green pulse through an etalon.

Figure 9. A: Streak obtained with 1.5 KV on charge line. B: Streak with 1% increase in voltage due to unsaturated switching. The shot-to-shot jitter in this mode increases linearly along the screen.

Figure 10. Fluorescence of Rose Bengal dye in water, showing the effect of signal averaging on signal-to-noise ratio. Note the coincidence of the excitation peak with the half-rise point of the fluorescence.

Figure 11. A Photochron II streak camera tube is used with a bulk high resistivity ($30 \text{ k}\Omega \text{ cm}$) Si switching element replacing the standard phosphor screen. E.M. is the extraction mesh, F.C. is the focus one, and A is the anode. The optical pulse produces photoelectrons from a 250 angstrom thick gold photocathode (PC).

Figure 12. Photoconductive and photoelectron switching. a) System response with the UV optical pulse incident on the silicon switch; no photoelectrons. The 10-90% risetime is 100 ps. (b) Illustration of the risetime with the photoelectron burst incident on the switch. The 10-90% risetime is 12L ps.

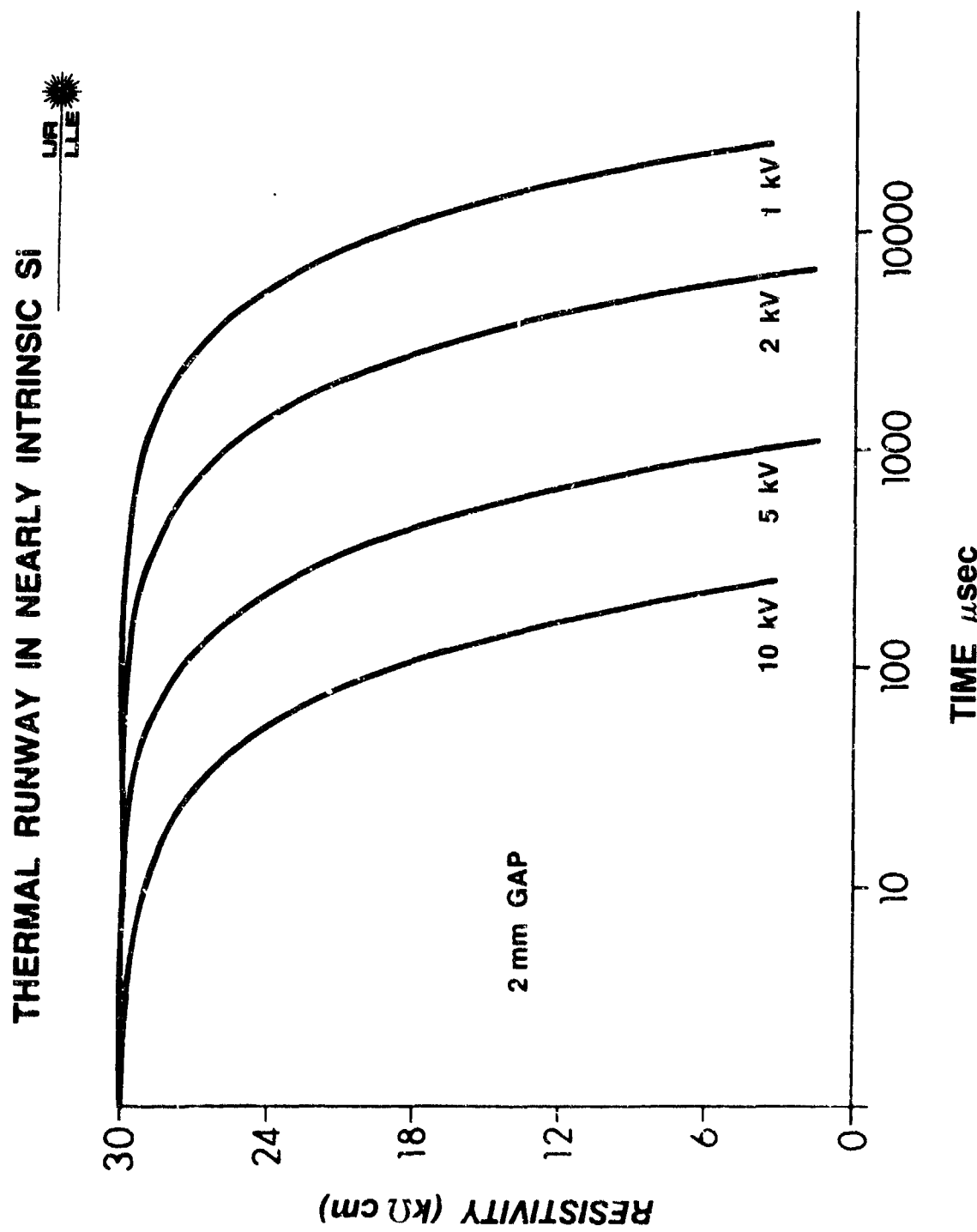
Figure 13. Schematic of the arrangement. A cable of length L, charged through R_{CH} , is discharged through the cooled GaAs sample, which is triggered by the $1.06 \mu\text{m}$ laser light. This produces a HV pulse of duration $\tau = 2L/C$.

Figure 14. I-V curve of the GaAs sample at 77 K. Self-breakdown is at 3.9 KV.

Figure 15. A typical HV pulse switched through the GaAs spark gap. The photoconductive contribution is the small wiggle $\sim 500 \text{ ps}$ before the foot of the main pulse.

Figure 16. Build-up time vs. trigger energy for an avalanche switched HV pulse at 195 K and at 77 K. The dots are measurements; the error bar indicates typical uncertainties in reading the oscilloscope traces; and the solid line is a least-squares fit. PCC > 20% means that, past the corresponding trigger energy, the photoconductive contribution to the main HV pulse exceeds 20% of the full amplitude. The insert illustrates how the buildup time, τ_B , was measured.

Figure 17. Three shots illustrating the discriminating capability of the avalanche switch. The spikes before the main pulse (off scale) are photoconductive signals due to individual pulses (10 ns apart) from the train of a mode-locked laser.



E513

Figure 1.

THERMAL RUNWAY IN NEARLY INTRINSIC Si

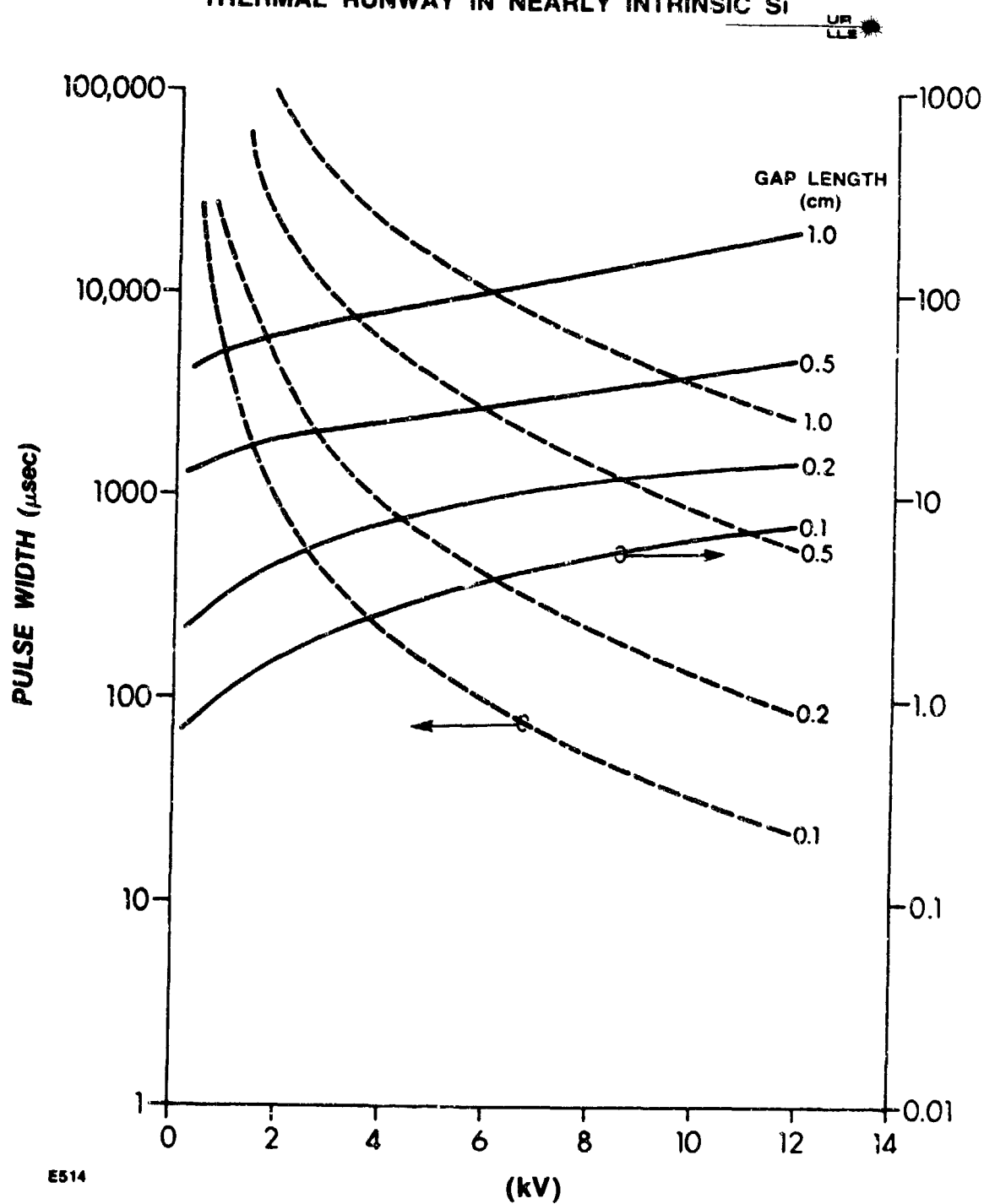


Figure 2.

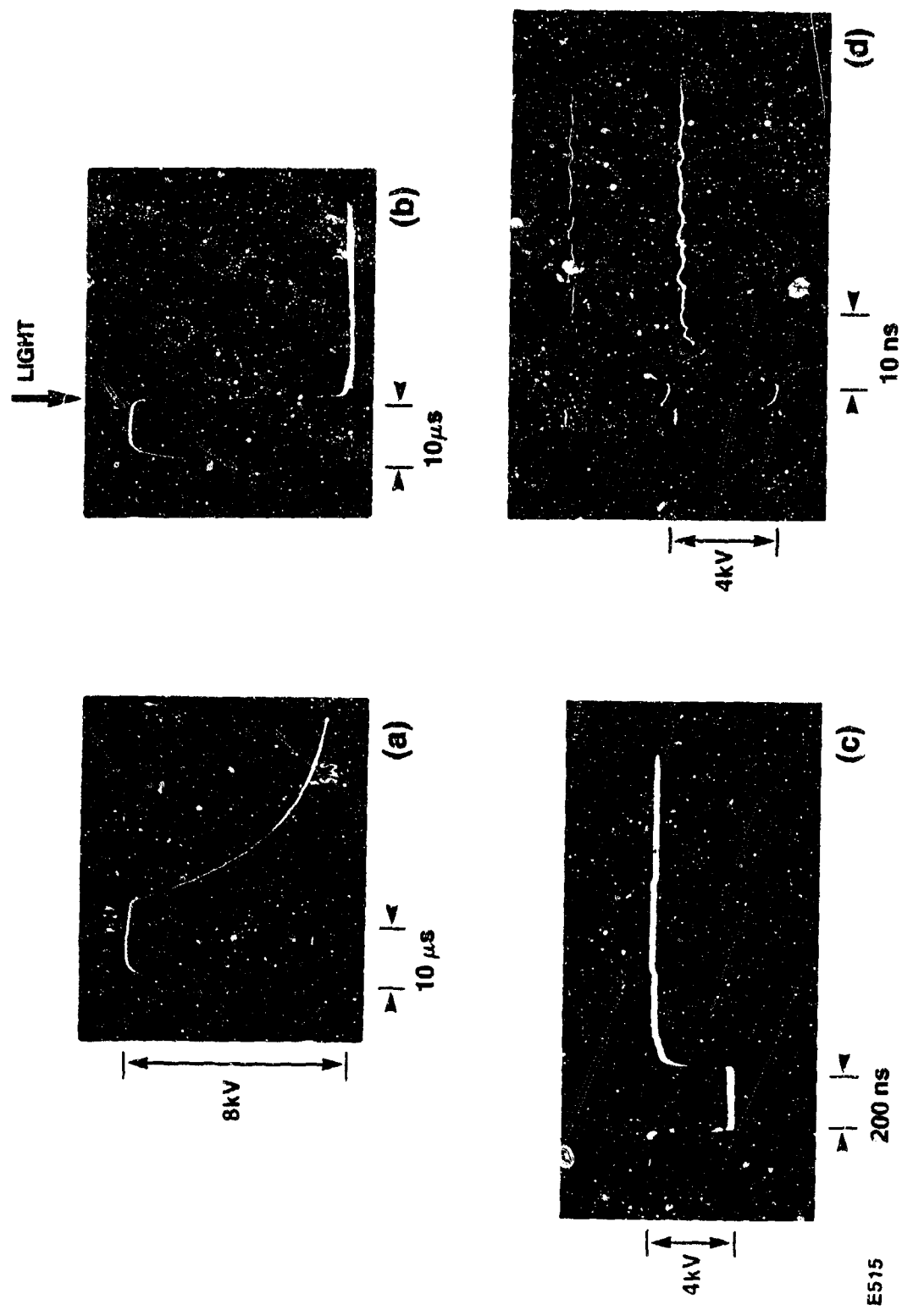


Figure 3.

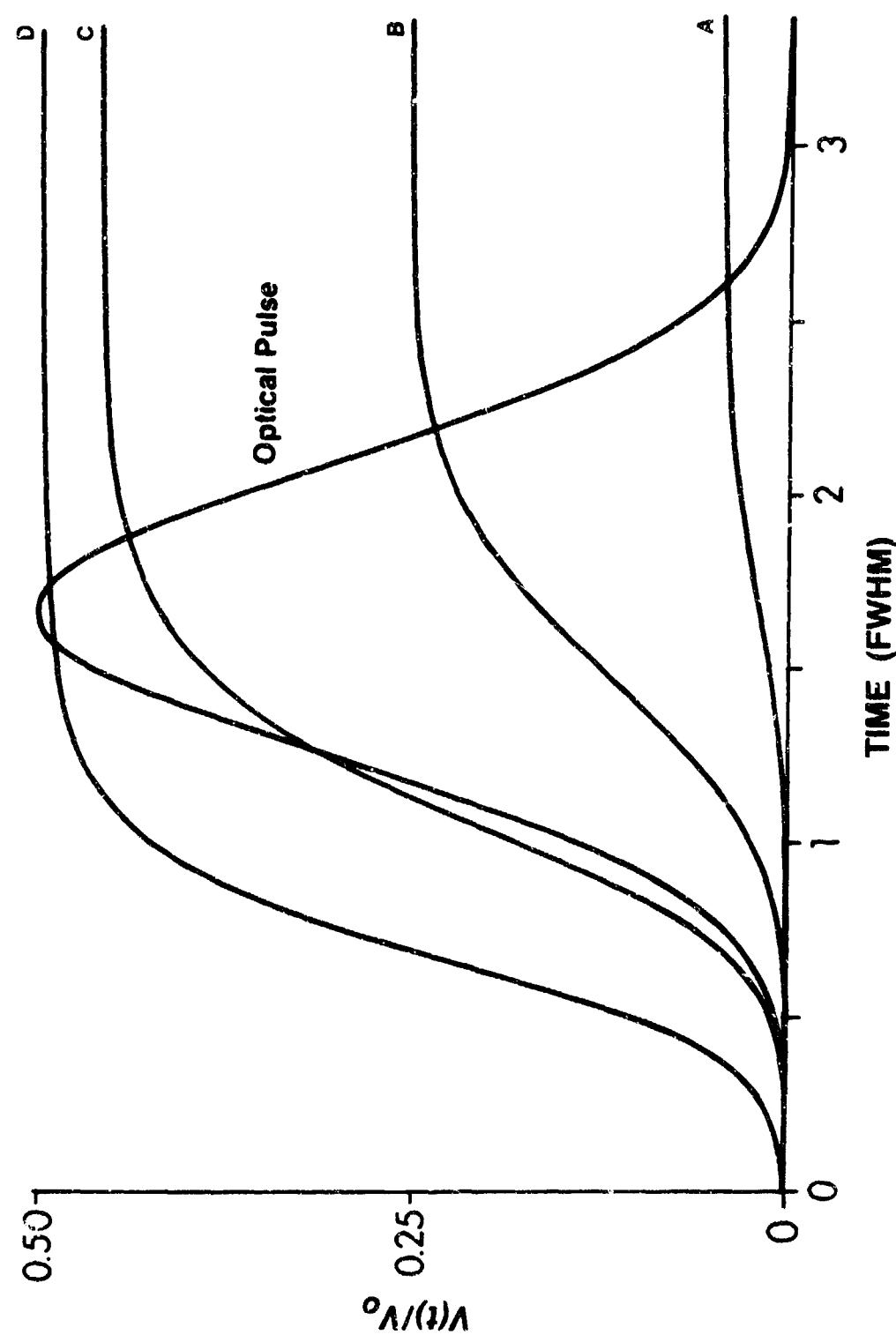


Figure 4.

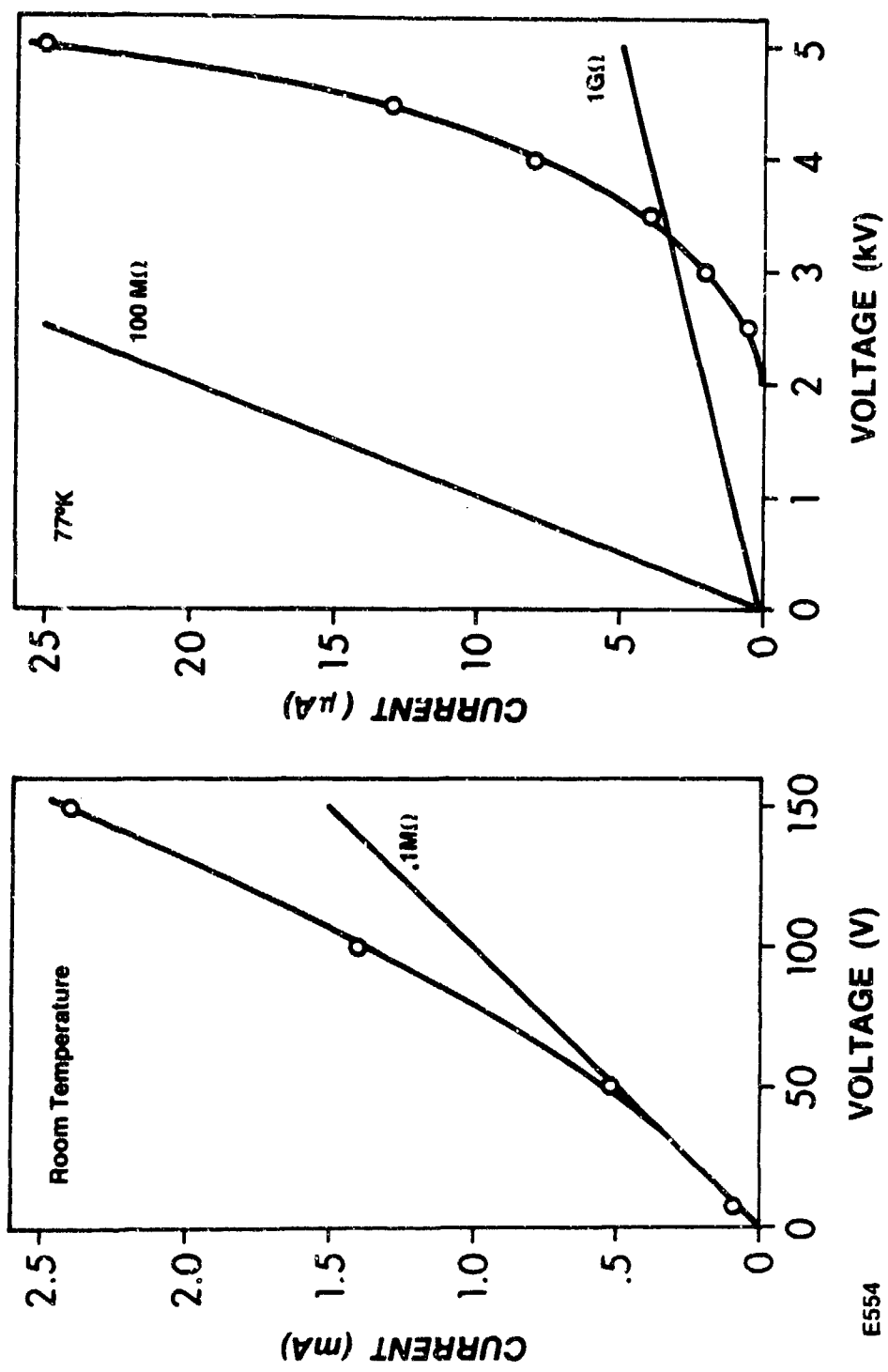
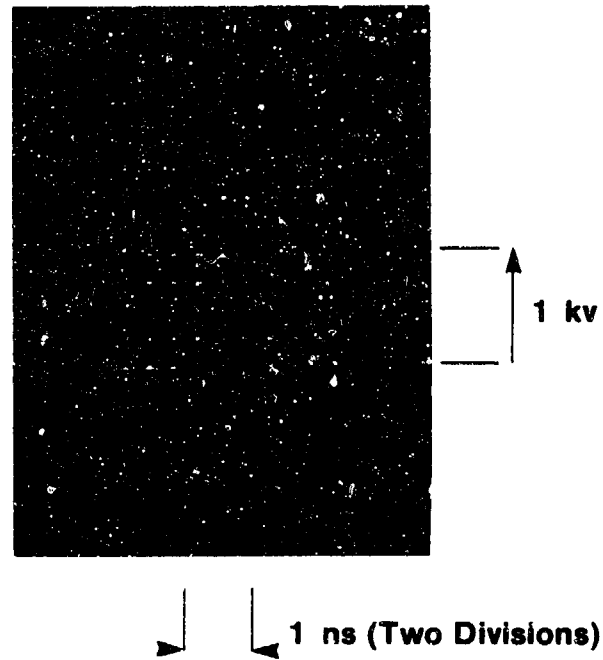


Figure 5.

E554

DC HIGH VOLTAGE SWITCHING AT CRYOGENIC TEMPERATURE



E741

Figure . . .

ACTIVE PULSE SHAPING 

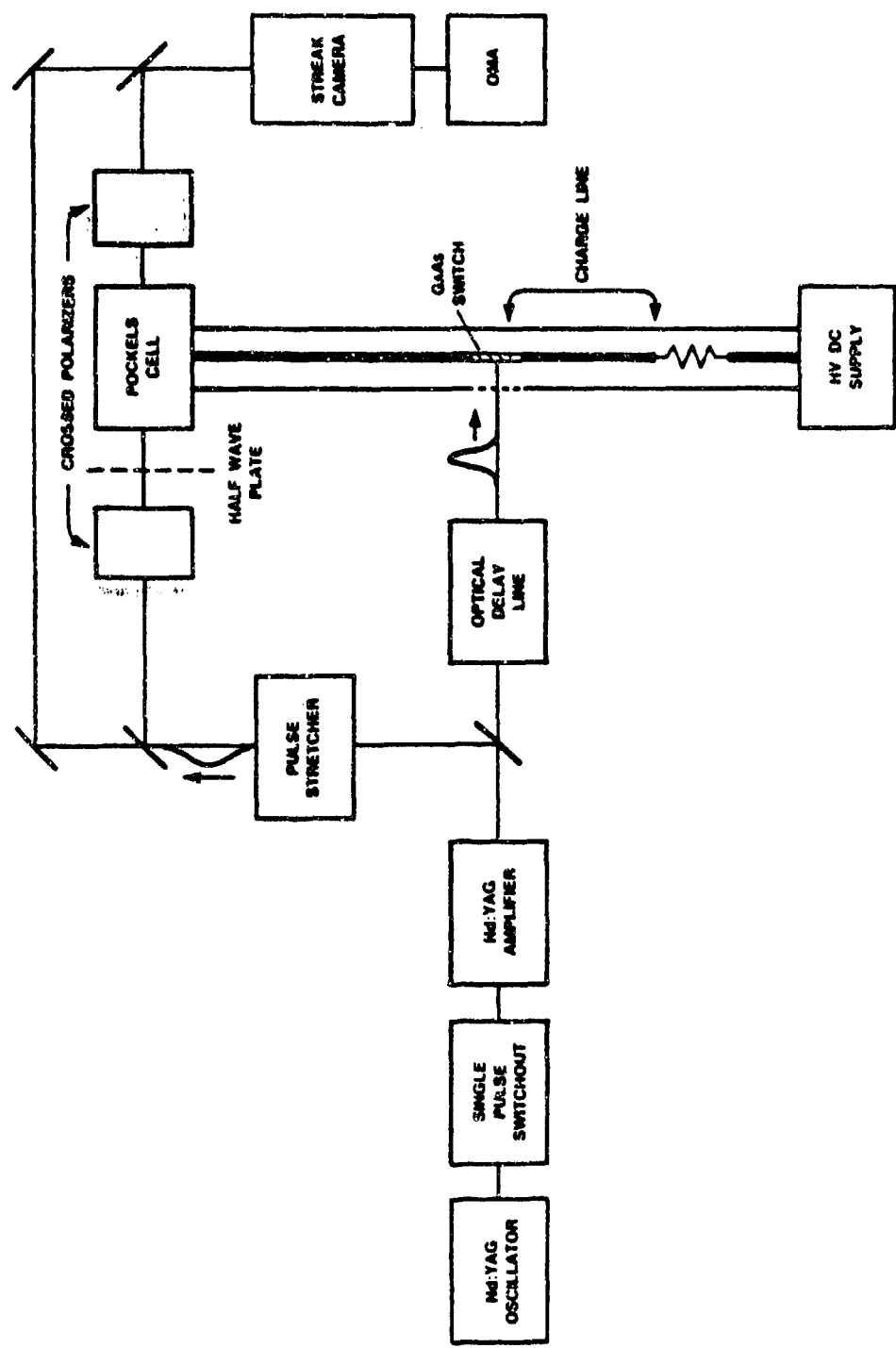
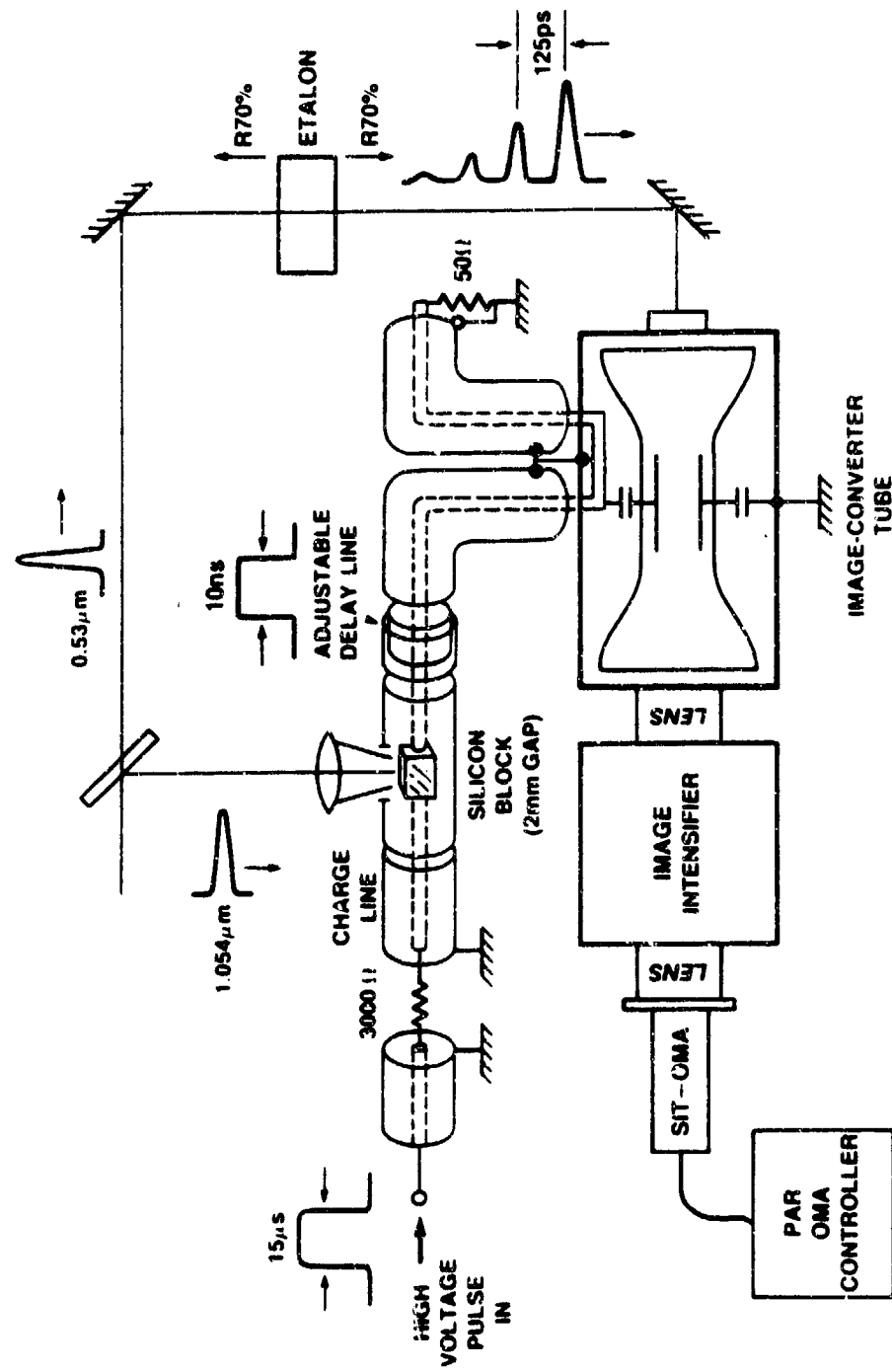
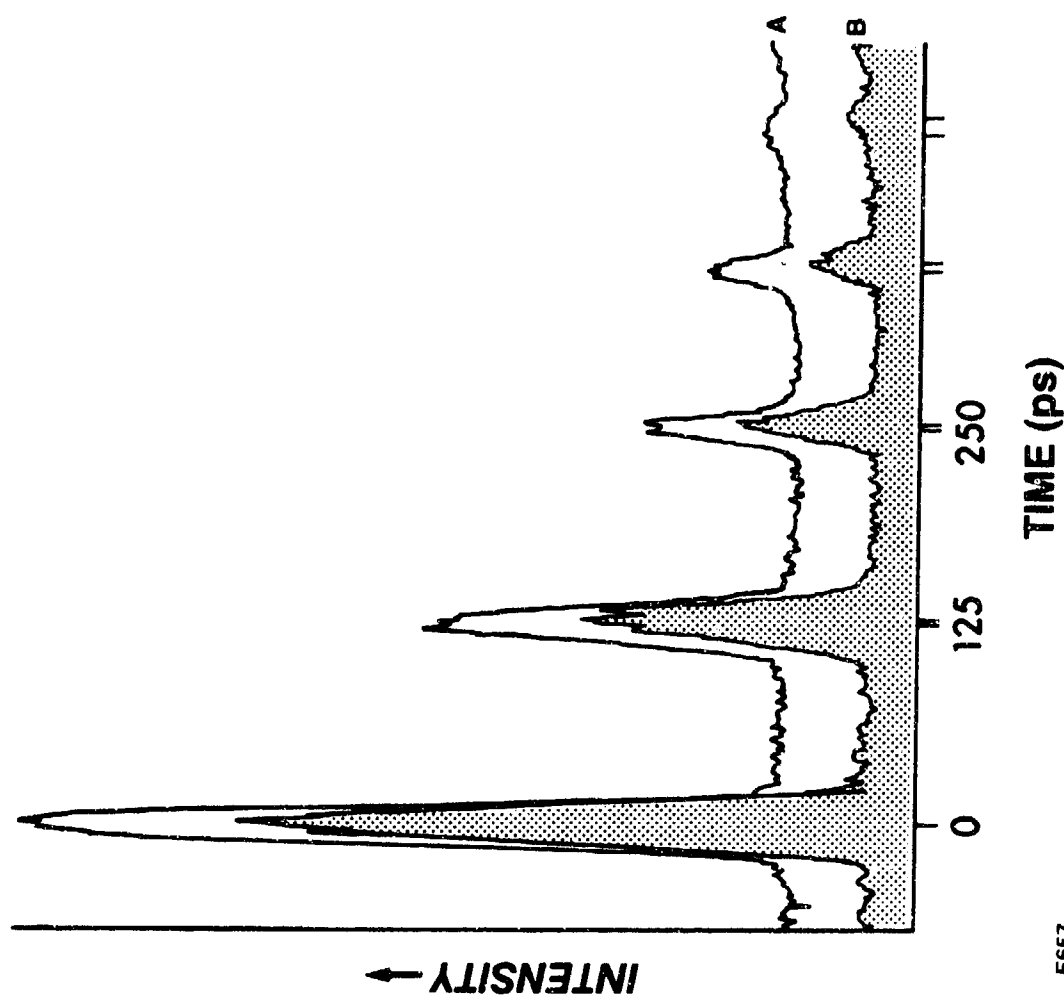


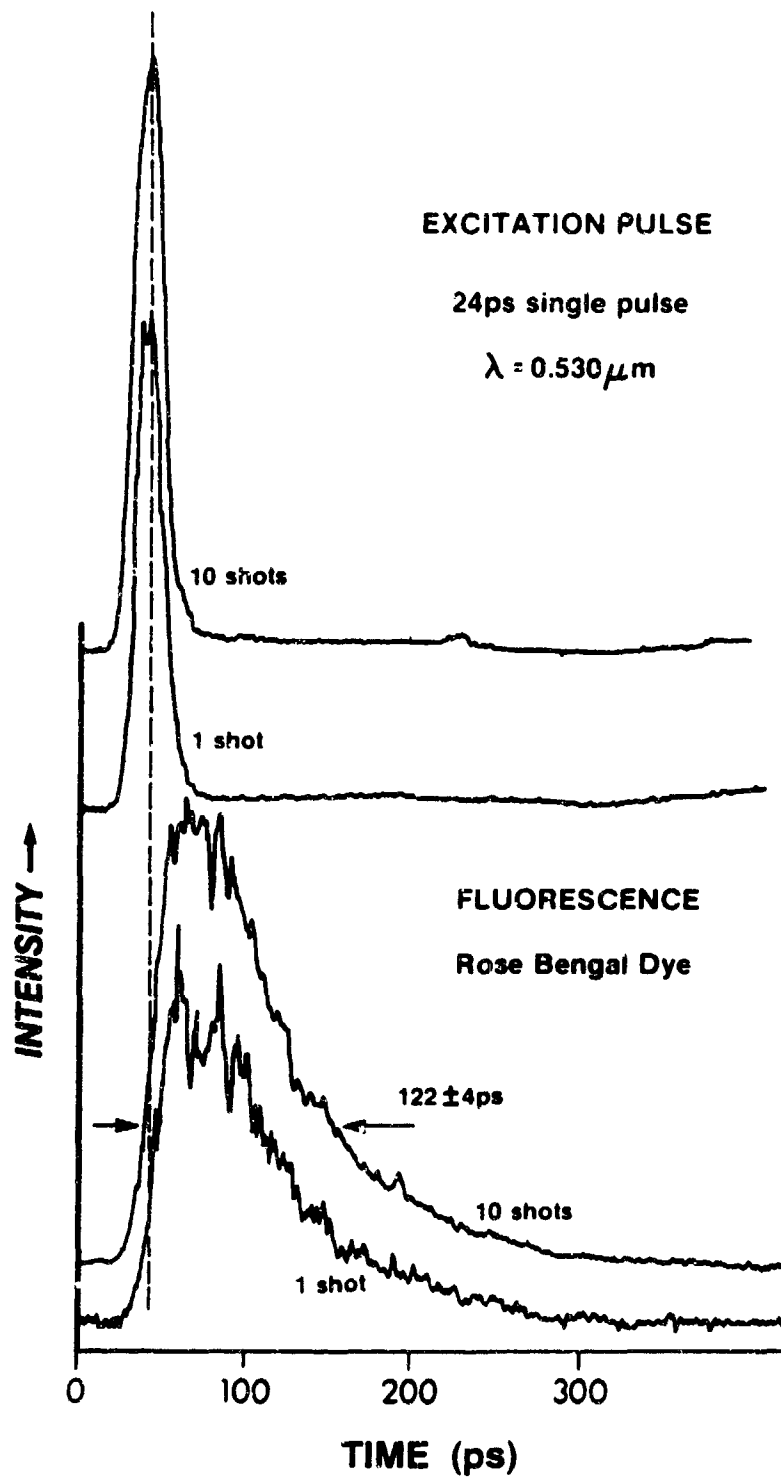
Figure 7.

SCHEMATIC OF JITTER-FREE STREAK CAMERA



E656

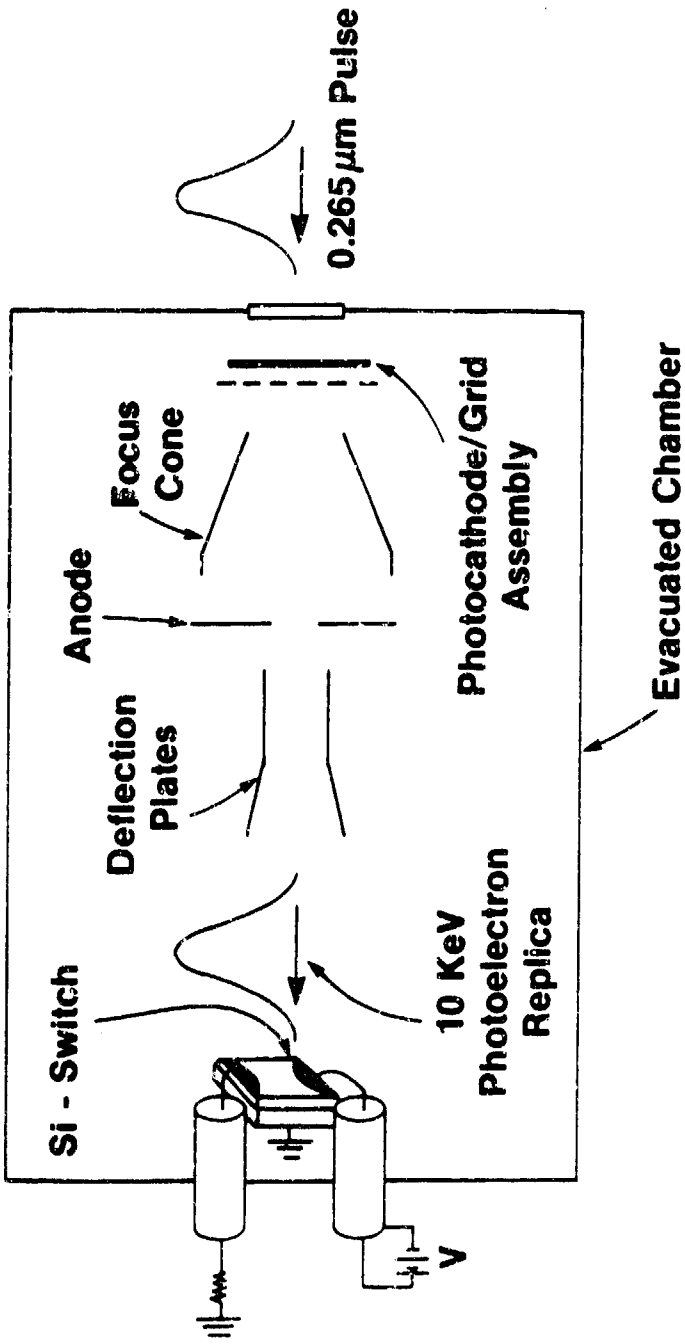




E522

PHOTOELECTRON SWITCHING LAYOUT

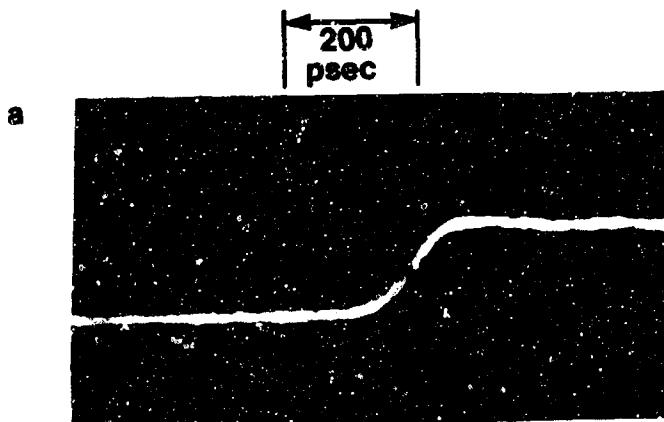
UR
LLE



E1370

Figure 11.

RISETIME MEASUREMENT OF PHOTOELECTRON SWITCHING



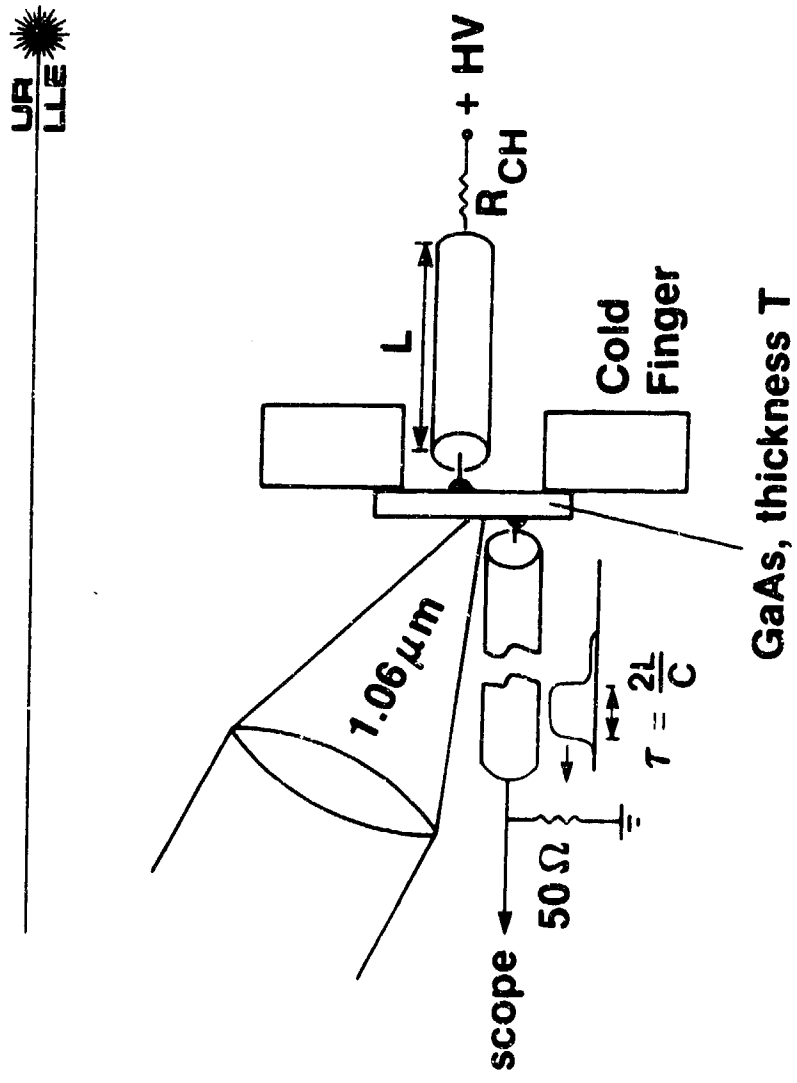
System Response - UV Incident on Si Switch
UV Pulse Width = 50 psec
Oscilloscope = 4GHz
Risetime ~ 100 psec



Photoelectron Switching
Risetime ~ 120 psec

E1369

**SETUP FOR LASER TRIGGERED
AVALANCHE SWITCHING**



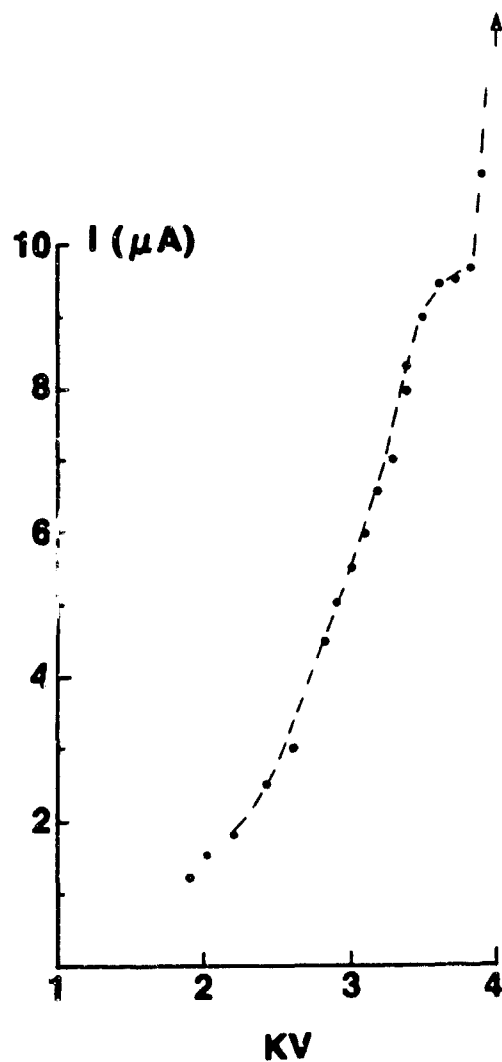
E1445

Figure 1j.

2006

I-V CURVE OF GaAs AT 77°K

UR
LLE

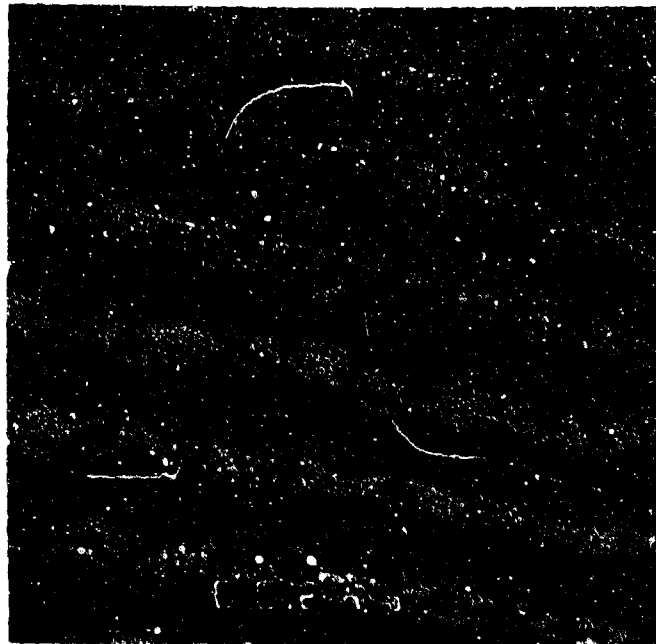


E1136

2006

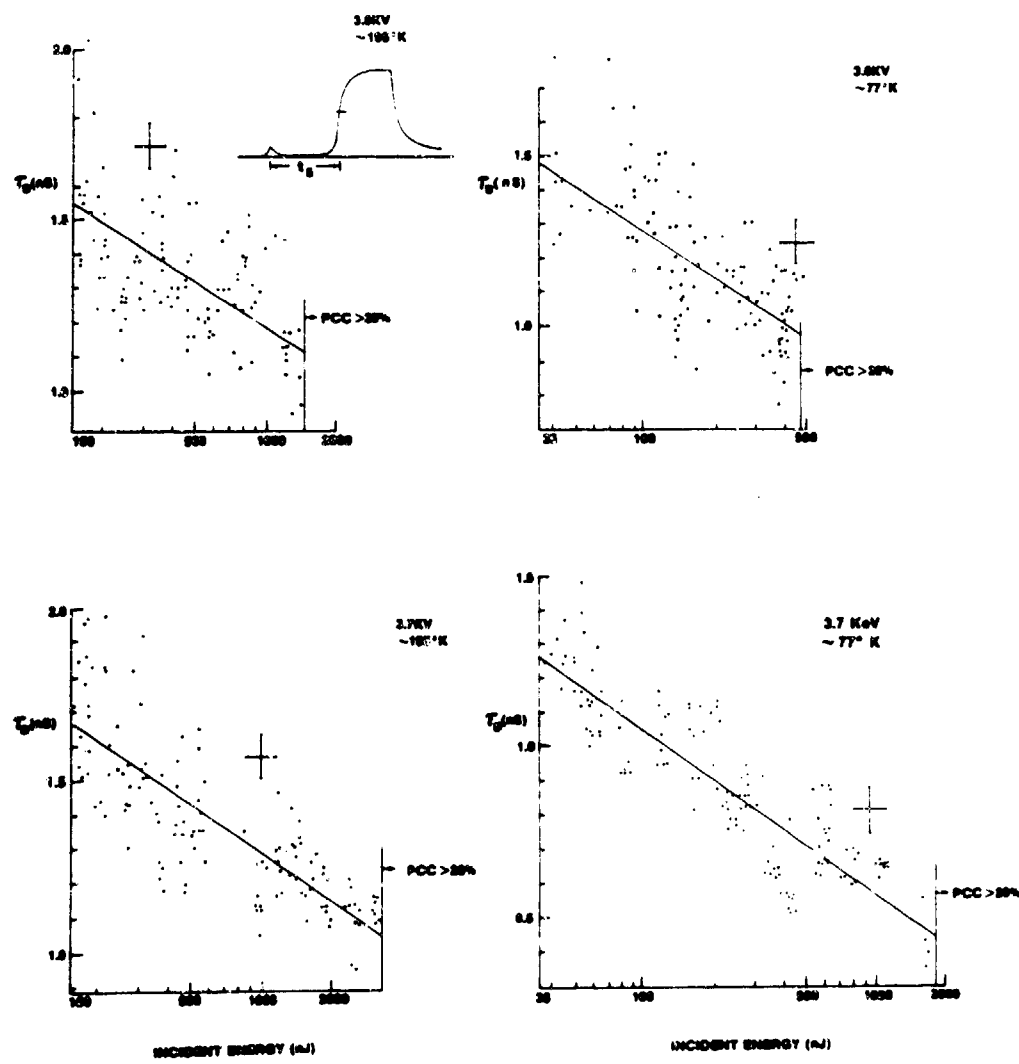
Laser Induced Avalanche Pulse

UR 
LLE

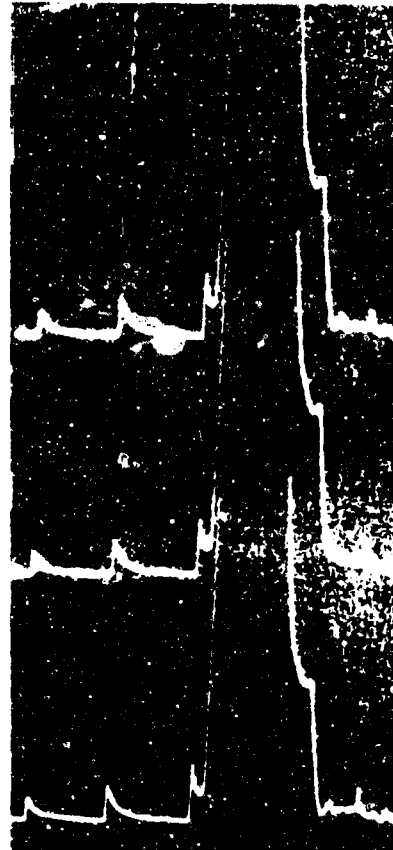


E1138

PULSE BUILDUP TIME, τ_B VERSUS INCIDENT ENERGY
FOR HV-AVALANCHE SWITCHING



Discrimination Capability of Avalanche Switch



E1137

139-1

PICOSECOND PHOTOCOCONDUCTIVITY AND ITS APPLICATIONS*

Chi H. Lee
Department of Electrical Engineering
University of Maryland

INTRODUCTION

A photoinduced plasma in a semiconductor can be used to control the transmission and propagation of an electromagnetic wave. By using a single picosecond laser pulse, it is possible to achieve a carrier density of the order of $10^{20}/\text{cm}^3$ ⁽¹⁾ in the photoinduced plasma. The use of picosecond laser pulses provides a method for the manipulation of plasma density, in addition to establishing near perfect isolation between the controlling and the controlled signals. We will discuss here the effect of a laser induced plasma in a semiconductor on the propagation of a low frequency (extending from DC to 100 GHz) electromagnetic signal. The effect of a laser induced plasma may be considered as either a change in dielectric or in the conductive properties of the semiconductor. In either mode, dielectric or conductive, it can be used effectively to control the propagating signal.

A single pulse in a mode-locked train has a peak power of the order of several hundred megawatts due to its ultra-short (few picoseconds) duration. Availability of such high powers has made it feasible to observe multiphoton effects which have not been

* Supported by the National Science Foundation, the Harry Diamond Laboratory, and the Minta Martin Aeronautical Research Fund.

observed with conventional light sources. Jayaraman and Lee⁽²⁾ investigated two-photon effects in GaAs by monitoring its photoconductivity and extended their investigations to study three-photon effects in CdS.⁽³⁾ During multiphoton excitation of photoconductivity, the absorption coefficient is rather small; consequently the carriers are generated quasi-uniformly in the bulk of the semiconductor and the role of diffusion and surface recombination is likely to be small.

Another important aspect of picosecond photoconductivity is that the time domain is shorter than the lifetime of the excited photocarriers in the semiconductor. From the fact that the temporal width of the exciting pulse is considerably smaller than the mean lifetime of the carriers, it is obvious that the steady-state is not achieved and that the observed phenomenon is transient, as was observed by Jayaraman and Lee⁽²⁾ in GaAs during excitation by picosecond pulses from a mode-locked Nd:glass laser. It was later shown by Mathur⁽⁴⁾ on the basis of theoretical considerations that it justified to replace the lifetime of free carriers in the expression for photoconductivity by the exciting pulse-width, as suggested by Jayaraman and Lee.⁽²⁾

One of the major applications of picosecond photoconductivity has been in ultrafast optoelectronic switching, which can be obtained with picosecond precision. Using a photoconductive switch, it was shown by Auston⁽⁵⁾ that switching and gating in a silicon transmission line structure can be achieved by picosecond optical pulses. This work was then extended by Johnson and Auston⁽⁶⁾ to switch and gate microwave signals by using the

conductive property of the plasma created in the bulk of the semiconductor. However, the use of Si as a material for a semiconductor switch has the disadvantage that the carrier recombination in Si is slow, being of the order of tens of microseconds, so that the repetition rate of the device is limited. It was pointed out by Lee⁽¹⁾ that a high repetition rate, of the order of 1 GHz, can be obtained by using Cr-doped GaAs, which has a free carrier life-time of 100 ps or less.⁽⁷⁾ In contrast with Si, this device turns off automatically due to the short lifetime of the carriers. Because of the high resistivity ($>10^8 \Omega \text{ cm}$) of GaAs, it can be DC biased up to 8 KV or more and a switching efficiency of 90-95% can be obtained.^(8,9) Another material which holds promise for high voltage optoelectronic switching is CdS_{0.5}Se_{0.5}.^(10,11) High resistivity specimens of CdS_{0.5}Se_{0.5} (10^7 to $10^8 \Omega \text{ cm}$) are available commercially. This switch can be turned on by a 0.53 μm pulse through single photon absorption and by a 106 μm pulse through two-photon absorption. We have also developed picosecond optoelectronic switching in a Blumlein pulse generator. This type of pulser possesses the potential of providing an output pulse amplitude equal to the charging voltage in an ideal case, contrary to the standard charged line pulser which can only switch out one-half the charging voltage even in the ideal case.⁽¹²⁾

It may be remarked here that the use of high resistivity material for optoelectronic switching does present some technological problems. One problem of great importance is the application of ohmic contacts with negligible contact resistance. It has

been observed by Mak et. al.⁽¹¹⁾ in $\text{CdS}_{0.5}\text{Se}_{0.5}$, and Leonberger and Moulton⁽¹³⁾ in InP, that the switchout voltage in charged line pulser configurations under low bias was much less than expected for a given energy of incident laser radiation. We believe that, in both cases, though the contacts were apparently ohmic under low intensity of excitation, the contact has some resistance. The irradiation may reduce the resistance of the bulk, but the contact resistance remains unaffected and therefore the switching efficiency is low. Mathur et. al.⁽¹⁴⁾ have used this technique to estimate the contact resistance under dynamic conditions. However, it has been observed by Chang et. al.⁽⁸⁾ that, at high DC bias, the efficiency of the switch increases, which suggests that residual resistance decreases with increase in bias.

Generally, it is believed that the build-up of free carrier concentration with laser irradiation is nearly instantaneous; therefore, the switching speed is essentially controlled by the temporal width of the exciting laser pulse, which is a few picoseconds. However, it has been pointed out by Mathur and Lee⁽¹⁵⁾ that, for thick samples, transit time effects are important if weakly absorbed radiation is used to generate the free carriers. The repetition rate of the switch is limited by the carrier recombination time. However, at a high intensity of excitation, causing a high concentration of carriers, the life-time of the carriers may be decreased due to Auger recombination or band-to-band stimulated radiative recombination.⁽¹⁰⁾

Effective use has been made of the electron-hole plasma generated in a semiconductor to control millimeter waves.⁽¹⁶⁾ The optical properties of the dielectric waveguides can be conveniently modified by the generation of the electron-hole plasma. The concentration and depth of the plasma can be easily controlled by a suitable choice of the power and wavelength of the laser pulse. Both amplitude and phase modulation can be achieved by this technique. In typical experiments, phase shifts as high as 1400°/cm of 94 GHz millimeter waves were observed,^(17,18) accompanied by less than 1 dB insertion loss. In one switching experiment, the generation of square millimeter wave signals at 94 GHz with variable pulse widths ranging from one to tens of nanoseconds has been reported.⁽¹⁹⁾

THEORY

The problem of picosecond optoelectronic switching relates, in essence, to the propagation of an electromagnetic wave of low frequency in a semiconductor containing a photoinduced electron-hole plasma. In the following analysis, we wish to show that the presence of an electron-hole plasma in the semiconductor results in the modification of the conductive as well as in the dielectric properties of the semiconductor. Starting from Maxwell's electromagnetic equation, we shall establish how the change in dielectric property can be interpreted in terms of a change in the conductive property.

Let us consider the propagation of an RF signal in a semiconductor containing an electron-hole plasma. The applied field, \vec{E} , will satisfy the Maxwell equation:

$$\nabla \times \vec{H} = \sigma \vec{E} + \frac{\partial \vec{D}}{\partial t} , \quad (1)$$

where σ is the dark conductivity and \vec{D} is the displacement vector. The effect of the electron-hole plasma is included in the term \vec{D} through the change in dielectric constant.

The displacement vector \vec{D} can be expressed in terms of the applied field,

$$\vec{D} = \epsilon_r \epsilon_0 \vec{E} , \quad (2)$$

where ϵ_r is the relative complex permittivity of the medium and ϵ_0 is the permittivity of vacuum. The complex permittivity can be expressed as

$$\epsilon_r = \epsilon' - j\epsilon'' . \quad (3)$$

Substituting for ϵ_r in equation (2), and inserting this value in the Maxwell equation, yields

$$\begin{aligned} \nabla \times \vec{H} = \sigma \vec{E} + j\omega \vec{D} &= \sigma \vec{E} + j\omega \epsilon_0 (\epsilon' - j\epsilon'') \vec{E} = \sigma \vec{E} \\ &+ \omega \epsilon'' \epsilon_0 \vec{E} + j\omega \epsilon' \epsilon_0 \vec{E} , \end{aligned} \quad (4)$$

where ω is the angular frequency of the applied field. In the presence of the electron-hole plasma, the complex permittivity is given by⁽¹⁶⁾

$$\epsilon_r = \epsilon_L - \frac{\omega_p^2}{\omega^2 + \nu^2} - j \frac{\nu}{\omega} \frac{\omega_p^2}{\omega^2 + \nu^2} \equiv \epsilon' - j\epsilon'' , \quad (5)$$

where ϵ_L is dielectric constant of the host lattice, including the contribution from the bound charges; ν is the collision frequency, and ω_p is the plasma frequency, which is given by

$$\omega_p = ne^2/\epsilon_0 m^* , \quad (6)$$

where n is the density of the photoinduced excess carriers.

Macroscopically, all the losses due to induced carriers are generally included in the term ϵ'' . We can define an effective conductivity, σ_{eff} , as follows:

$$\sigma_{\text{eff}} = \omega \epsilon_0 \epsilon'' . \quad (7)$$

Substituting for ϵ'' from equation (5), we obtain

$$\sigma_{\text{eff}} = \epsilon_0 \nu \frac{\omega_p^2}{\nu^2 + \nu} . \quad (8)$$

For a low frequency applied field ($\omega \ll \nu$),

$$\delta_{\text{eff}} = \frac{\epsilon_0 \omega_p^2}{\nu} = \frac{ne^2 \tau}{m} = \sigma \quad (9)$$

where σ is the mobility. Equation (9) is the usual expression for photoconductivity.

Moreover, considering that the complex refractive index of a material is given by

$$n^* = \sqrt{\epsilon_r} e^{-jk\kappa} , \quad (10)$$

it can be shown that the electromagnetic wave travelling in a semiconductor containing a plasma would be attenuated as well as phase-modulated. The attenuation depends on κ while the phase change is proportional to η . Both η and κ depend on the plasma density. A plasma state in a semiconductor, therefore, provides a flexible situation for switching of an electromagnetic signal in a conducting as well as in a dielectric mode. For frequencies up to 30 GHz, where microstrip transmission lines are used, a plasma state in the conductive mode can be used to control the

microwaves. However, for frequencies greater than 30 GHz, losses in the microstrip structures are high, and fabrication techniques become more difficult due to small strip width and substrate thickness. Therefore, dielectric waveguides are suitable alternatives for metallic waveguides. Under these conditions, it is appropriate to use the dielectric mode of the optically induced plasma in semiconductor to control the propagation of millimeter waves.

For frequencies up to 1 GHz, the wavelength of the propagating signal is much greater than the usual dimensions of the switch, which can be considered as a lumped circuit element. However, for millimeter waves, the wavelength of the propagating signal is comparable to the dimensions of the switch, and, therefore, for an accurate description, the switching element should be considered as a distributed circuit element. A phase change is produced when the signal is propagating through the switch. A detailed theoretical investigation has been presented by Lee and Mathur. (20)

APPLICATIONS

High speed optoelectronic switching

Fast optoelectronic switching is a potentially significant application of picosecond photoconductivity. To avoid thermal runaway, which is caused by leakage currents in Si, we have tried high resistivity crystals of semi-insulating Cr-doped GaAs and compensated $\text{CdS}_{0.5}\text{Se}_{0.5}$. It appears that high resistivity material will have low leakage current for small bias, but even at moderate electric fields, carriers may be injected in the

crystal from the metallic electrodes, thus setting up space charge limited currents. Under these conditions, the current builds up as the square of the applied voltage. Moreover, in the presence of traps, the current will increase with an exponent much greater than 2, with an increase in the applied voltage. It appears that the use of high resistivity materials as the switching element may not necessarily scale up the DC bias. Mourou⁽²¹⁾ has reported kilovolt switching with 2 KV bias across Au-doped Si at liquid nitrogen temperature. In our experiments,⁽²²⁾ it has been observed that a 2 KV DC bias can be applied to a CdS_{0.5}Se_{0.5} switch even at room temperature, and a switchout of 800 V can easily be observed. At low bias, the switching efficiency is limited by the contact resistance. This is corroborated by the fact that, at low bias, at very high intensities, the amplitude of the switchout signal tends to saturate. A switchout signal at a bias of 22.5 V as a function of laser intensity for GaAs in a charged line pulser configuration has been reported earlier.⁽¹⁴⁾

It is interesting, however, to note that this resistance at the contact is not a serious handicap at high bias. In fact, as has been mentioned above, the efficiency of switching increases at higher bias.⁽²⁰⁾ This suggests that, at least partially, the contact resistance may be due to a barrier at the metal-semiconductor surface. Therefore, in practice, even silver bearing epoxy contacts on etched surfaces have been found quite satisfactory for high voltage switching work. At high DC bias, the current in the crystal increases nonlinearly with applied voltage because of carrier injection, and considerable Joule heating may

take place in the semiconductor material. Then the resistance of the crystal decreases substantially and a significant fraction of the applied voltage appears across the charging resistor. This has been verified experimentally, so that pulsed biasing has been used at high voltages in our later experiments.

In order to overcome surface breakdown, we mounted the switches in a spark gap of 50Ω impedance, pressurized with 100 psi of nitrogen; 2mmx2mmx2mm cubic crystals of GaAs and $\text{CdS}_{0.5}\text{Se}_{0.5}$ were used as switch elements. A two-photon photoconductivity was excited by irradiating the switch with a 1.06 μm mode-locked laser. Bulk excitation of carriers increases the power handling capacity of the system. $\text{CdS}_{0.5}\text{Se}_{0.5}$ does not block a DC bias of more than 2300 volts. For higher biasing, we used a 10 to 30 nanosecond voltage pulse up to 7 KV.⁽²²⁾ The arrangement is shown in figure 1. A laser-triggered spark gap is used to produce a voltage pulse, which acts as a biasing pulse for the semiconductor switch. With a bias V_0 across the laser-triggered spark gap, it is possible to obtain a switchout of $V_0/2$. The use of a semiconductor switch in conjunction with the LTSG improves the jitter and the risetime is very fast. The electrical pulse switchout from this configuration is shown in figure 2.

In a modified form of the above configuration, the whole pulse train was used to trigger the laser spark gap. The voltage pulse thus generated was used to bias the Pockel cell as well as the semiconductor switch. In this configuration, the switchout single laser pulse is nearly synchronized with the biasing voltage pulse on the semiconductor switch. This arrangement is shown

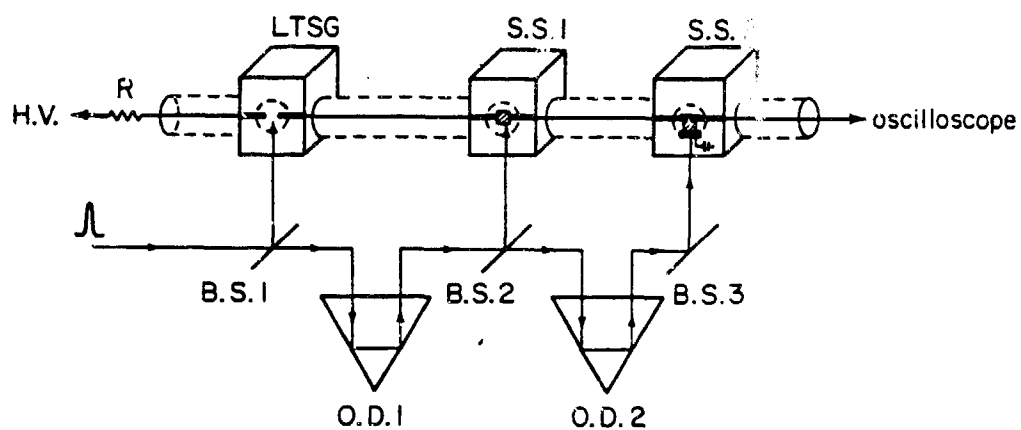


Figure 1. Diagram of multikilovolt switching system. The bias pulse is generated by the breakdown of a laser triggered spark gap (LTSG). Semiconductor switch 2(SS2) terminates the pulse after an appropriate optical delay (OD2) by shorting the center conductor of the transmission line to ground.

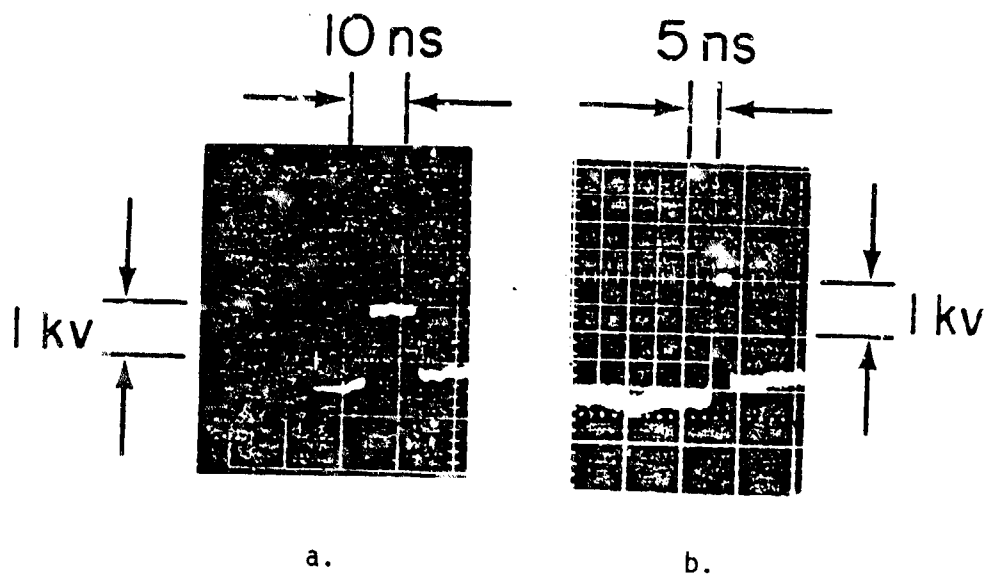


Figure 2. Switched out pulses from the configuration of figure 1: a) 8 ns wide; b) 3 ns wide.

in figure 3. The advantage of this configuration is that the constraint on the synchronization of the biasing voltage pulse and actuating optical pulse is very much relaxed. In this configuration, a single DC power supply can generate a pulse for both Pockel cell bias and semiconductor bias. However, this device configuration is useful only for switching out a fixed voltage which is good for actuating the Pockel cell. The switch-out from this configuration is shown in figure 4. The switching speed was estimated to be 55 ps. (22)

Ultrafast optoelectronic switching in a Blumlein pulse generator

Picosecond optoelectronic switching has been demonstrated in a charged line configuration. However, this configuration is constrained to switch out a pulse of amplitude $V_c/2$, V_c being the charging voltage, even in the ideal case. A Blumlein pulse generator, a modified charged transmission line, possesses the potential of providing a pulse amplitude which can be equal to the charging voltage in an ideal case. This is a decisive advantage when the pulse amplitude has to be scaled to the order of multikilovolts, because it relaxes the bias on a semiconductor switch to one-half the magnitude required in a charged line configuration. Bulk semiconductor optoelectronic switches have limited voltage blocking capability under multikilovolt DC bias due to carrier injection and thermal runaway. (9,14)

A Blumlein pulse generator consists of two transmission lines of characteristic impedance, Z_0 , connected in series with an output transmission line of impedance $2Z_0$, as shown in figure 5a. A pulse is generated by charging both transmission lines and

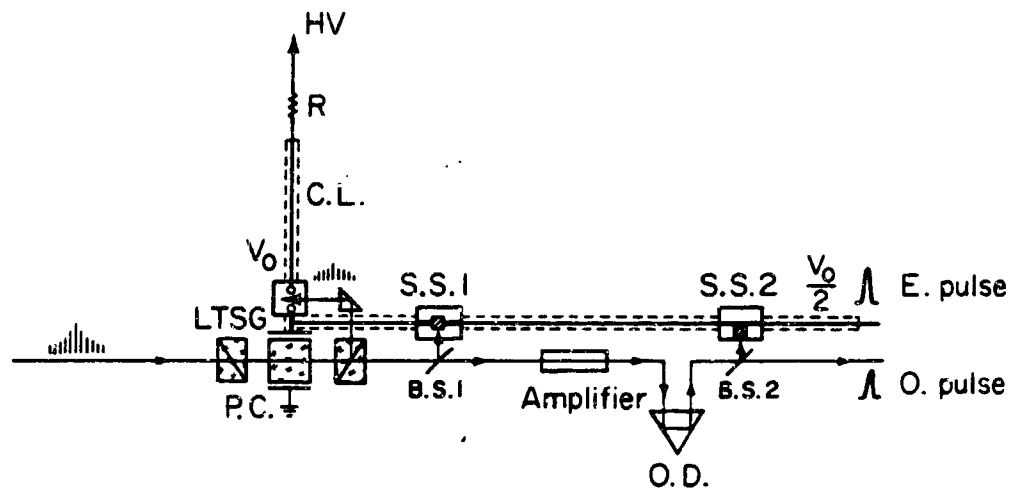


Figure 3. Diagram of a modified scheme of a charged line pulser. The LTSG is used to bias the Pockel cell as well as the semiconductor switch.

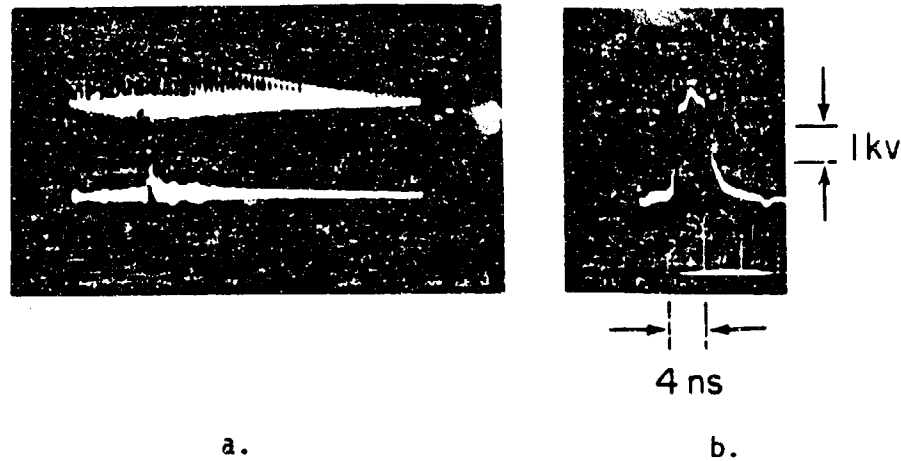


Figure 4. A switched out pulse from the configuration of figure 3: a) laser pulse; b) electrical pulse, using the laser pulse to switch on SS1 and SS2. The input impedance of the amplifier used to detect the single pulse was $1 \text{ M}\Omega$, to enhance the intensity of the trace.

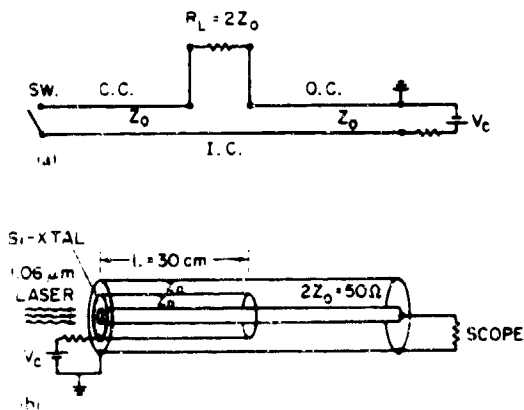


Figure 5. Blumlein pulse generator: a) schematic; b) coaxial geometry. (SW: switch; CC: center conductor; IC: intermediate conductor; OC: outer conductor.

closing one end of one of the transmission lines by a switch. It can be easily shown that the magnitude of the output pulse across a matched load, $R_L = 2Z_0$, is equal to the charging voltage, V_c , and that the pulse length equals the transit time across both the transmission lines. In case the switch has an internal resistance, R_S , the output voltage is reduced, and is given by

$$V_{out} = V_c Z_0 / (Z_0 + R_S) \quad (11)$$

where $R_S = R_b + R_c$; R_b is the bulk resistance of the semiconductor, which is a function of the incident laser intensity, and R_c is the contact resistance. V_{out} saturates at a value less than V_c when $R_b \ll R_c$.

In practice, the Blumlein pulse generator of coaxial geometry as shown in figure 5b is commonly used. It consists of a grounded outer conductor of I.D., 7.144 mm; an intermediate conductor (a thin cylinder) of diameter, 4.7625 mm, and a center conductor of diameter of O.D., 3.175 mm. A disk-shaped silicon optoelectronic switch of thickness 0.5 mm with annular electrodes is used to short the center and the intermediate conductors. The diameters are chosen to form a coaxial transmission line with characteristic impedance of 25Ω between the center and the intermediate, as well as between the intermediate and the outer, conductors. In this way, the impedance between the center and the outer conductor becomes 50Ω , which is then used for the transmission of the output pulse. A unique feature of this system is the fact that the disk-shaped switch conducts current radially in the distributed form as in an ideal boundary case, whereas other switches conduct current in a thin filamentary form

which is affected by internal inductance. This internal inductance, L , can result in a slow risetime of L/Z_0 of the output pulse.

The optoelectronic switch was fabricated from high resistivity ($\sim 10^5 \Omega \text{ cm}$) silicon. Annular aluminum electrodes were applied on one side by using a photolithographic technique. The switch was irradiated by a $1.06 \mu\text{m}$ laser from the opposite side of the electrodes. At this wavelength, the absorption coefficient of silicon is 10 cm^{-1} ; this radiation is therefore appropriate to create quasi-uniform electron-hole pairs throughout the bulk.

In the present experiment, a single picosecond pulse of duration 10 ps was selected from a mode-locked Nd:glass laser to actuate the Si switch. The intermediate conductor was biased up to 14 V with respect to the grounded outer conductor. Square pulses of amplitude 12 V could be generated by closing the optoelectronic switch by a $1.06 \mu\text{m}$ laser pulse, as shown in figure 6. A DC bias as high as 70 V could be applied and a switchout efficiency of 80% was obtained. On further increasing the DC bias, a breakdown was observed. The exact cause of the breakdown is not yet clear; however, we speculate that it may be due to the combined effects of surface breakdown and thermal runaway. (9,14) I-V characteristics suggests that the contacts are not truly ohmic. This is, however, not a handicap at high bias voltage, (7,8) but at low bias voltage this limits the switchout voltage.⁽⁸⁾ The radial geometry of the switch is used to elimin-

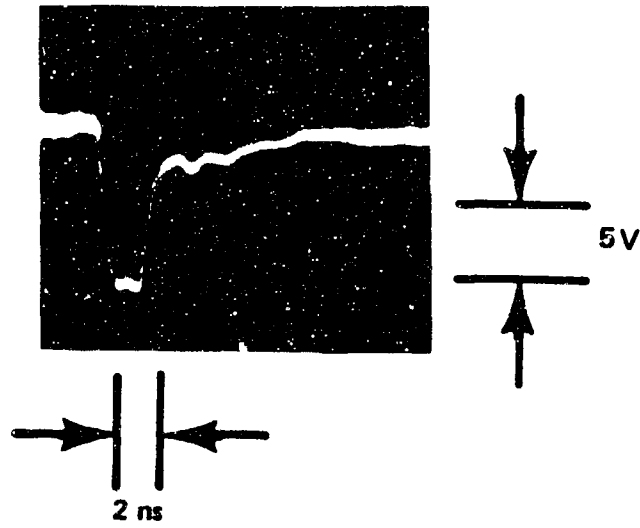


Figure 6. Oscilloscope trace of the switched out pulse. The sweep rate is 2 ns per division; the charging voltage is 14 V.

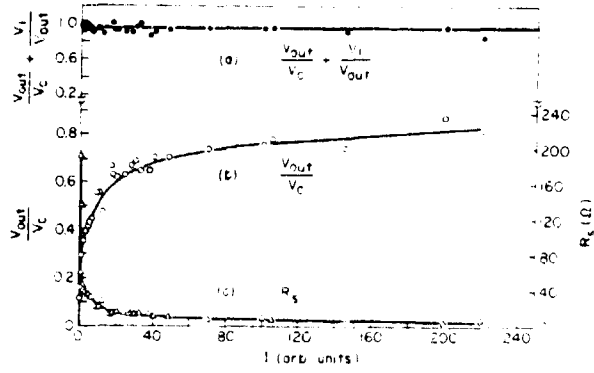


Figure 7. a) $V_{out}/V_c + V_1/V_{out}$; b) V_{out}/V_c ; and c) R_s , as functions of laser intensity. The solid lines are least square fits.

ate any inductive effect; however, the same may not be true if the laser spot does not have uniform energy distribution.

The post-pulse appearing at the trailing edge of the main pulse is due to the residual resistance of the switch. A simple calculation shows that the ratio between the post pulse amplitude V_1 , and main pulse amplitude, V_{out} , is given by

$$V_1/V_{out} = R_s/(Z_0 + R_s) . \quad (12)$$

Inserting equation (11) into equation (12), we obtain

$$V_{out}/V_c + V_1/V_{out} = 1 . \quad (13)$$

Equation (13) shows that the sum $V_{out}/V_c + V_1/V_{out}$ is independent of the resistance of the switch and also of the laser intensity. This is shown as in curve (a) in figure 7. The best fit is a straight line at 0.95. This deviation of 5% from the theoretical value is within the experimental error; however, the fact that most of the experimental points lie under the theoretical curve of equation (13) indicates a systematic error in the observations. We think that this is the result of underestimating the amplitude of the switched out pulse, possibly because of bandwidth limitations of the oscilloscope. The straight line plot justifies the Blumlein charged line model used here to explain the switchout and post-pulse amplitudes. According to our calculations, a post-pulse at the trailing edge of the main pulse is always expected for a resistive switch, in both a charged line pulser and a Blumlein pulser. The post-pulse is more pronounced in a Blumlein pulser because of the low impedance, 25Ω , of the transmission line as compared to 50Ω in the usual charged line.

To estimate the residual resistance of the switch, we plotted V_{out}/V_c as a function of laser intensity. V_{out}/V_c tends to saturate at higher laser intensity due to residual resistance,⁽⁸⁾ which has been estimated from figure 7b to be 4.8Ω at a switchout efficiency of 84%. This resistance is much higher than the bulk resistance, which can be calculated by measuring the incident energy of 0.75 mJ and from the knowledge of the absorption coefficient. The estimated bulk resistance of the switch is 0.3Ω , which is far less than the resistance computed from the switchout signal. We attribute this high value of residual resistance to the resistance at the contact, primarily because a barrier may be present when a contact is applied to a very high resistivity material. This conclusion is, however, tentative and needs to be investigated further.

Figure 7c depicts the laser intensity dependence of the switch resistance. At lower laser intensities, where the contact resistance is negligible compared with bulk resistance, the bulk conductance of the switch varies sublinearly with laser intensity. It may be a consequence of the presence of a continuous trap distribution in the silicon, as pointed out by Rose.⁽²³⁾

To summarize, we have demonstrated ultrafast optoelectronic switching in a Blumlein pulse generator, which has the potential of generating a pulse amplitude equal to the charging voltage. Attempts are underway to scale up the switchout voltage to the kilovolt region by using pulsed bias.

Millimeter wave control and switching

To control millimeter wave propagation optically, dielectric waveguides are more attractive. Lee *et. al.* (16) used a high resistivity silicon rectangular slice as a dielectric waveguide. The power of the unmodulated wave from the klystron was divided equally by directional couplers and fed into two arms of a bridge. One arm of the bridge was composed of a precision variable attenuator and a mechanical rotary vane phase shifter. The other arm of the bridge contained the silicon waveguide. The millimeter waves were recombined at the output end of the bridge, which was balanced initially. When a thin layer of electron-hole plasma is created near the illuminated surface of the silicon waveguide by the absorption of $0.53 \mu\text{m}$ radiation, a phase shift is introduced in the propagating wave. This upsets the balance of the bridge. By appropriate calibration, it is possible to determine the phase shift from the amplitude of the output signal. To measure the attenuation, the variable attenuation was set at the maximum and a pulse signal as a result of the laser induced plasma was obtained, which could be correlated with the attenuation of the propagating millimeter wave.

For gating of the millimeter wave signal, another silicon waveguide was inserted in the main transmission line downstream from the bridge. The bridge was balanced initially by adjusting the attenuator and the phase shifter. When the silicon waveguide in the bridge was illuminated by $1.06 \mu\text{m}$ radiation, the photo-induced plasma in the bulk of the semiconductor blocked the transmission of the millimeter wave through this arm. The bridge

then became unbalanced and a signal appeared at the output of the bridge. To switch off the millimeter wave signal, a second laser pulse with a proper delay relative to the first was used to illuminate the second waveguide in the main transmission line, downstream from the bridge. The photoinduced conductivity in the second silicon waveguide terminates the millimeter wave signal. In this way, millimeter-wave pulses as short as 1 ns and variable to tens of nanoseconds have been generated. (16)

Optical control of RF waves offers the following advantages: near perfect isolation between the controlling and the controlled devices; low static and dynamic insertion loss; possibility of fast response with picosecond precision; and high power handling capability. Our most recent study of these types of devices, using Cr-doped GaAs as the waveguiding medium, indicates that, due to rapid carrier recombination, only a single picosecond optical pulse is needed to produce an ultrashort millimeter wave pulse. This feature has been utilized to construct a high speed millimeter wave modulator with a repetition rate well in excess of 1 GHz. The experimental arrangement is depicted in figure 8. A millimeter-wave bridge similar to that used by Jacobs and Chrepta⁽²⁴⁾ was employed. The dielectric waveguide was a 25 mm long GaAs slab with a cross-section of $2.4 \times 1.0 \text{ mm}^2$, which was considered to be an oversized waveguide for the 94 GHz signals; this waveguide was inserted into one arm of the bridge. The ends of the slab were tapered for transitions with minimum reflection to the dielectric waveguide from a standard W-band waveguide operating in a TE_{10} mode. The dark resistivity of the

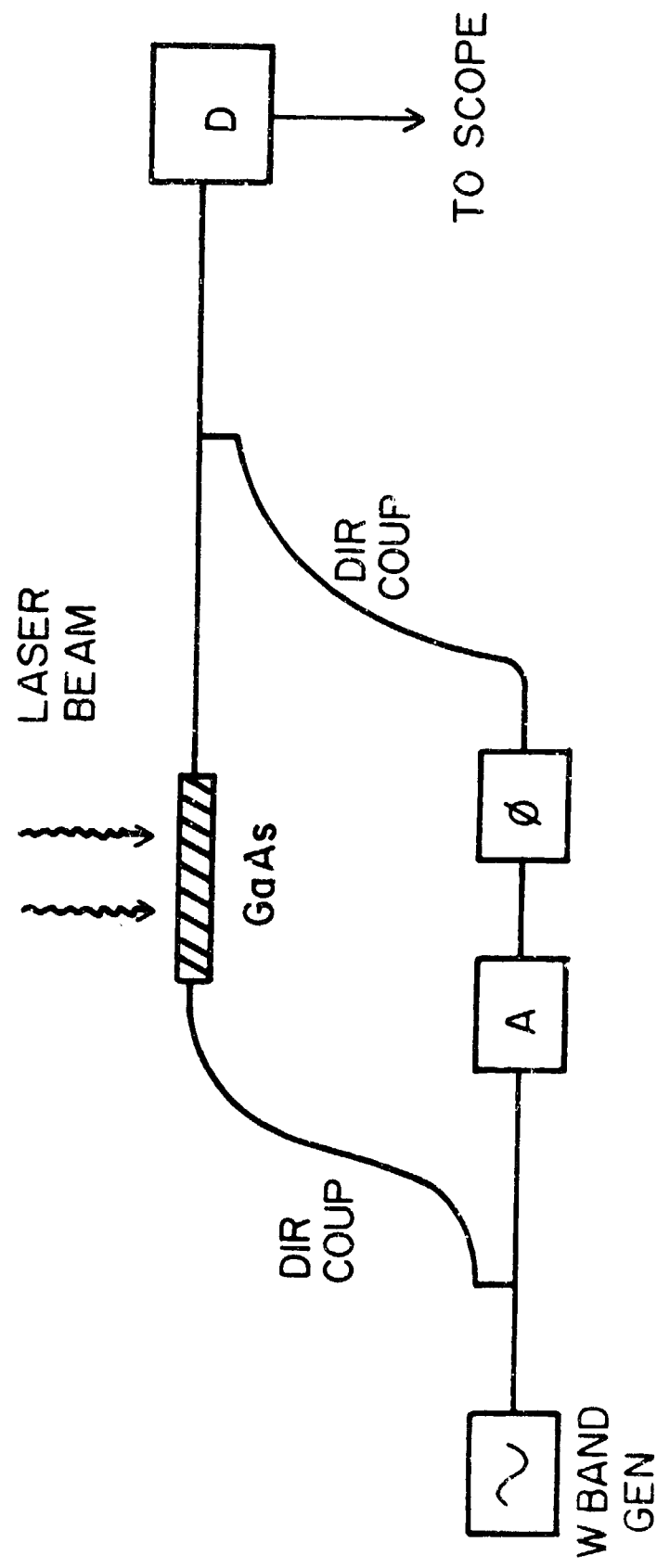


Figure 8. High speed millimeter wave modulator.

Cr-doped GaAs was $10^7 \Omega \text{ cm}$. Initially, without laser pulse illumination of the GaAs waveguide, the bridge was balanced by adjusting the variable attenuator, A, and mechanical phase shifter, ϕ , in the other arm so that there was no signal at the output. When a single $0.53 \mu\text{m}$ pulse, with about 20 nJ of energy around and 30 ps in duration, obtained from a frequency-doubled mode-locked Nd YAG laser, illuminated the GaAs waveguide, a high density electron-hole plasma was generated at the surface of the GaAs slab, causing a phase shift in the millimeter-wave signal as it propagated through the plasma covered region of the waveguide. The bridge became unbalanced and a signal appeared at the output of the bridge. This signal persisted until the excess carriers recombined. Inasmuch as the lifetime of the excess carrier is of the order of 100 picoseconds,⁽¹²⁾ we expect that the millimeter wave signals rise and decay rapidly. In fact, if an optical pulse train were to be used to illuminate the waveguide, a millimeter wave pulse train mimicking the optical pulse train should result. This indeed was the case, as shown in figure 8. The interpulse spacing of 7 ns in the millimeter wave pulse train is the same as that in the optical pulse train. Figure 9 also shows that a modulation bandwidth approaching 1 GHz is attainable. The pulse width of the individual pulse is not resolvable in this figure because the combined response time of the detecting and display systems is slower than the expected pulse width of about 200 picoseconds (estimated on the basis of carrier lifetime). We have devised a correlation technique to measure the pulse width of the coherent millimeter wave pulse.

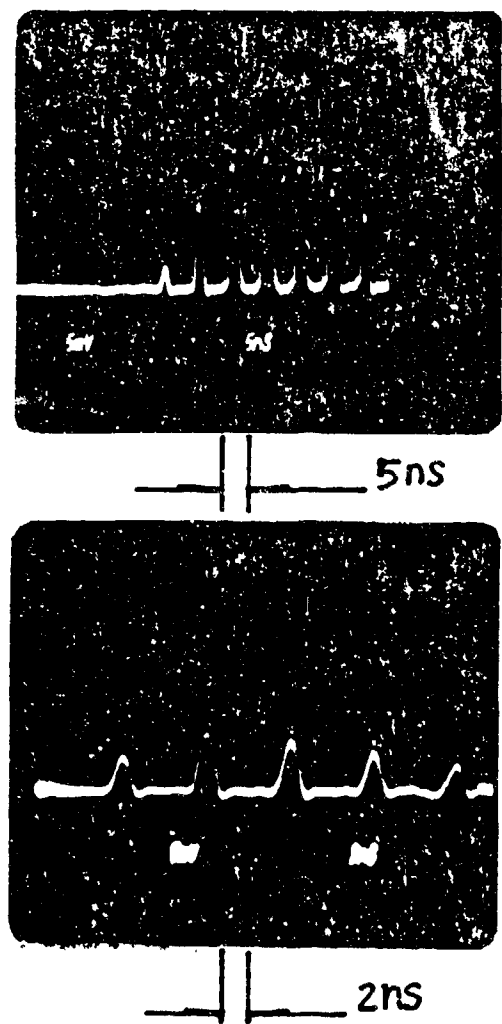


Figure 9. Optical pulse train (a) mimicked by millimeter wave train (b).

The measured pulse width is 600 ps, wider than the predicted pulse width by a factor of three. This discrepancy can be resolved by realizing that the millimeter wave pulse is generated by rapid phase modulation of the signal. As a result the pulse is actually "chirped," i.e., there is a large frequency sweep within the pulse. Group velocity dispersion will broaden the chirped millimeter wave pulse when it propagates in a positively dispersive guiding structure. Mismatches between the dielectric and metallic waveguides will also contribute to some broadening. Experiments, as well as a detailed theoretical calculation, are underway to provide more data for a quantitative analysis of the generation and propagation of the chirped millimeter wave pulse.

In conclusion, we have demonstrated the generation of a chirped millimeter wave pulse by optoelectronic methods. Using this technique, the modulation of millimeter wave signals at 94 GHz with a modulation bandwidth in excess of 1 GHz is readily achievable.

CONCLUSION

Fundamentally, photoconductivity under picosecond laser pulse excitation is not different than it is under ordinary light excitation. However, an attempt has been made to emphasize the way photoconductivity will manifest itself under picosecond laser excitation. In any analysis, the contribution of not only one-photon excitation, but also of multiphoton excitation, must be considered. The photoinduced plasma can be used both in a conductive as well as in a dielectric mode to perform the fundamental control operation. For example, for DC and microwave

control, the conductive properties of a photoinduced plasma are useful, whereas for millimeter wave control, the dielectric mode is used. The switching of voltage pulses using picosecond photoconductivity has engendered ultra-fast optoelectronics, where picosecond switching precision has been achieved. It appears, therefore, that the phenomenon of picosecond photoconductivity deserves more theoretical and experimental investigation.

REFERENCES

1. Chi H. Lee, *Appl. Phys. Lett.* 30, 84, (1977).
2. S. Jayaraman and Chi H. Lee, *Appl. Phys. Lett.* 20, 392, (1972).
3. S. Jayaraman and Chi H. Lee, *J. Appl. Phys.* 44, 5480, (1973).
4. V. K. Mathur, *J. Appl. Phys.* 49, 2845, (1978).
5. D. H. Auston, *Appl. Phys. Lett.* 26, 101, (1975).
6. A. M. Johnson and D. H. Auston, *J. Quantum Electronics QE-11*, 283, (1975).
7. V. K. Mathur and S. Rogers, *Appl. Phys. Lett.* 31, 765, (1977).
8. C. Chang, W. L. Cao, V. K. Mathur, Chi H. Lee (unpublished).
9. G. Mourou and W. Know, *Appl. Phys. Lett.* 35, 492, (1979).
10. V. K. Mathur, P. S. Mak, Chi H. Lee, *J. Appl. Phys.* 51, 4889, (1980).
11. P. S. Mak, V. K. Mathur and Chi H. Lee, *Optics. Commun.* 32, 485, (1980).
12. C. S. Chang, V. K. Mathur, M. J. Rhee and Chi H. Lee, *Appl. Phys. Letters*, in press.
13. F. J. Leonberger and P. F. Moulton, *Appl. Phys. Lett.* 35, 712, (1979).

14. V. K. Mathur, C. S. Chiang and Chi H. Lee, *Rev. Sci. Instr.*, 52, 616, (1981).
15. V. K. Mathur and Chi H. Lee, *J. Appl. Phys.* 51, 1634, (1980).
16. Chi H. Lee, Paul S. Mak and A. P. DeFonzo, *IEEE Journal of Quantum Electronics* QE-16, 277, (1980).
17. A. P. DeFonzo, Chi H. Lee, P. S. Mak, *Appl. Phys. Lett.* 35, 575, (1979).
18. M. G. Li, V. K. Mathur, W. L. Cao and Chi H. Lee, *Picosecond Phenomena III*, Springer-Verlag, in press.
19. Chi H. Lee, P. S. Mak, A. P. DeFonzo, *Electron. Lett.* 14, 733, (1978).
20. Chi H. Lee and Veerendra K. Mathur, *IEEE J. Quantum Electron.* QE-17, 2098, (1981).
21. M. Stavola, M. G. Sceats and G. Mourou, *Optics Commun.* 34, 409, (1980).
22. V. K. Mathur, W. L. Cao, C. S. Chang, M. J. Rhee and Chi H. Lee, *IEEE J. Quantum Electron.* QE-18, 205, (1982).
23. A. Rose, "Concepts in Photoconductivity and Allied Problems," Interscience, New York (1963).
24. H. Jacobs and M. M. Chrepta, *IEEE Trans. MTT-22*, 411 (1974).

WORKING GROUP REPORTS

SOLID STATE OPENING SWITCHES

M. Weiner, Chairman

SUMMARY

Various solid state opening switches are assessed for pulse power applications. Both junction (transistor, thyristor, etc.) and bulk devices (such as the optically activated switch) are considered. We find that until such devices are scaled up in voltage and current, large arrays of devices will be required, with concomitant problems in jitter, speed degradation, reliability, and cost. Research opportunities for the various switches are discussed.

INTRODUCTION

This report assesses present solid state opening switches for pulsed power applications. In order to bring the discussion into simpler focus, the applications are particularized to that of inductive energy storage. Further the discussion is given in terms of basic operating parameters for opening switches (such as turn-off time, maximum current density, etc.). As a result, other applications, such as series protective devices, may be analyzed using the present study. Crowbar devices, however, are arbitrarily excluded from this report since they are considered a form of closing switch (discussed elsewhere), used in a particular circuit configuration. Only current interruption switches are considered.

The approach used was to decide first on what characteristics are most important to the operation of an opening switch. Both recently developed as well as experimental solid state switches were tabulated in terms of these characteristics. The types of opening switches fell into two categories: junction and bulk devices. Generally speaking, the latter devices are still in the experimental stage, although much progress has been realized in the case of the optically activated switch. The junction devices, on the other hand, generally belong to a more mature technology. Here also, however, great progress has recently been realized, particularly for the GTO⁽¹⁾ and the gallium arsenide JFET.⁽²⁾

Once the switch parameters were tabulated, representative applications were chosen which the opening switches might impact. Rather than choosing specific applications, however, the applications were divided into various classes, each class representing a different range of turn-off time. This seemed to be a more manageable way for selection of the proper switch.

After deciding on the applications, the appropriate switches were selected, and the limitations and research problems identified. From this exercise, recommendations for further study were made.

DISCUSSION

a. Table of Opening Switches

Table 1 lists the various switches and the characteristics which are important for current interruption. Since the applications involve high energy systems, current density and hold-off

voltage are naturally relevant parameters. Voltage drop is very important since this affects strongly efficiency and heating. The turn-off time controls the risetime of the pulse delivered to the load in an inductive energy storage circuit. Thus, for example, a switch with a long opening time cannot be used to satisfy a short pulse requirement. Also listed is the type of control element and the current gain for each device.

The first five switches listed are of the junction type. The thyristor is at the slower end of the spectrum, although its power ratings are superior. A disadvantage is the fact that the current gain is less than one and high current counterpulse circuits must be employed to turn off the device. The MOSFETs and the gallium arsenide JFET have faster opening times but lower power ratings. To a large extent, the turn-off speed in these devices is limited by the ability of the gate current to discharge the device capacitance. For medium speed devices, the GTO represents a good compromise, having a good power rating and reasonably fast turn-off, on the order of a microsecond or so.

The last three devices, which are of the bulk type, are at present in the experimental stage. The optically activated switch⁽³⁻⁵⁾ is a promising device whose main advantages are extremely fast risetime, low turn-on jitter, and potential scalability. So far as the opening switch is concerned, scalability is most important, while jitter and risetime are of less concern. Possible problem areas of the optical switch should be identified. Large amounts of light energy will be required to obtain low voltage drop during the on-state. This is related to the

fact that the current gain is low, and that the production of light, suitable for carrier generation, is usually inefficient. Another problem that must be addressed is that of the opening time, which is controlled by the recombination time of the material. This important parameter may be varied by introducing impurities into the material, such as gold or chromium. This will reduce the recovery time of silicon from the microsecond range to the nanosecond range, and in the case of gallium arsenide, from the nanosecond range to the sub-nanosecond range. The introduction of impurities, however, has a deleterious effect on the on-state resistance; for a given amount of light excitation the resistivity increases, and this raises the voltage drop, one of the critical parameters of inductive energy storage. This can be overcome by supplying more light energy, which is an inefficient process caused by the low current gain. One possible technique for overcoming this deficiency, which requires further study, involves conversion of the light signal into an electron beam (using a photo-cathode), and then acceleration of the beam. The high voltage electrons produce numerous carriers, which provides the desired current gain.

The final two bulk devices considered were the Hall effect type⁽⁶⁾ and the deep impurity (DI)² type.⁽⁷⁾ Compared to the optically activated switch, these two bulk devices have received less attention and are in earlier stages of research. The Hall device depends on the introduction of a magnetic field to increase the resistivity of the semiconductor. Undoped material has been used for current interruption at $> 1 \text{ MW/cm}^2$, at frequ-

encies greater than 10 KHz. One of the problems found with this type device is that the off-state resistance is relatively low: the ratio of off-state to on-state resistance ranges from 100 to 1000. It is believed this ratio may be improved by introducing n-doping into the material.

The other bulk device is the deep impurity device, described by Sundberg and Henderson in this report. This device requires further study as to scalability, turn-off mechanisms, and the potential speed of turn-off.

b. Pulse Mode of Operation

The junction switches listed in Table 1 are rated for continuous (DC) operation. For many applications, inductive switching consists of steady (DC) current interrupted by short periods of lower current, so that DC current conditions dominate. On the other hand, it may be possible to operate these devices at considerably higher peak currents, for intervals a few microseconds long, without damage. This is done by providing greater drive to the gate. Certain disadvantages of this technique should be mentioned, however, and they include greater inefficiency, caused by the necessity for more drive energy, and a greater voltage drop. Nevertheless, the pulse mode may make it possible to operate at peak currents about 10X greater, compared to the DC mode. For inductive energy storage, the pulse mode is an attractive possibility since it is first possible to build up the charging current using a contactor (or any other switch able to absorb the energy dissipated during the charging time). When the proper current level is attained, the junction devices (operating

in the pulse mode) may be switched on while turning off the main switch. The on-time for the junction devices is therefore reduced, allowing the pulse mode to prevail without causing damage.

c. Applications

As mentioned previously, the various applications were, for the most part, grouped according to the turn-off time, as shown in Table 2. For pulse widths of 1 μ s or less, the turn-off time must be relatively fast, and this dictates the choice of element, in this case a MOSFET, JFET, bipolar, or bulk type. Since the voltage and current requirements are extremely large (25 KV to 50 MV and 2 KA to 10 KA), obviously a large array of junction devices will be required, numbering tens for the lower power applications, and thousands for the extreme cases. The bulk devices may play an important role here, if only because of their ease in scaling. In the second application, the pulse width is 1-100 μ s, which can be satisfied by a GTO or bulk device for the shorter turn-off times, and by a thyristor for the longer times. The peak currents are larger here, requiring more elements to do current sharing, but fewer elements for voltage sharing. The final application is to the large currents one may expect to find in a rail gun. The turn-off time of 1 ms or so is easily satisfied by a thyristor, but would require many devices in parallel. The bulk optical switch is also feasible, but would require large amounts of light energy to minimize conduction losses.

d. Arrays of Devices Using Junction Devices

The previous discussion makes it obvious that large numbers of elements, tens to thousands of junction devices, would be required for high voltage, high current opening switches. In the event these devices do not turn off simultaneously, because of jitter in the turn off prematurely, that element must block the entire voltage and is likely to fail. On the other hand, if a parallel element opens prematurely, additional current will be shifted to other elements, which also increases the chances for damage. Generally speaking, series elements present more serious problems to stacking of arrays. The turn-off jitter, which may be several microseconds long, will also lead to a degradation in the turn-off speed. The turn-off jitter is representative of an overall reliability problem which arises when considering arrays of devices which are not well matched. ⁽⁸⁾

If the jitter is caused by lack of device uniformity, then the jitter may be reduced by improving manufacturing techniques and quality control. Other sources of jitter arise from temperature variations within the device and lack of reproducibility of the drive signal.

CONCLUSIONS AND RECOMMENDATIONS

In opening switches, the junction and bulk devices are limited by the same thermal problems. The junction devices, if operated in the DC charging mode, will require tens to thousands of elements. In many cases, however, these devices can operate in a pulse mode, with lowered efficiency, but with possible 10X

improvement in peak current and reduction in the number of elements. For this reason the pulse mode warrants investigation in junction devices.

Traditionally, power junction devices have operated as relatively low voltage, high efficiency devices. There is apparently no inherent reason, however, why these devices cannot be operated with larger depletion widths, operating at higher voltages, but with larger voltage drop and lowered efficiency. Such devices would ordinarily be slow to turn on; however they can be light assisted during turn-on to speed up the process. Such "phototransistors" would therefore combine one of the best feature of the transistor-large gain-while retaining one of the best features of the optical switch-fast turn-on. So far as opening switches are concerned, the extra gain would improve performance. In regard to the turn-off of such a device, it would probably be longer than the ordinary transistor device, and other means, such as the addition of impurities, may be required to induce faster recovery. In any event, this type device is certainly worth exploring.

The bulk devices are extremely promising devices. When fully developed, these devices should be simpler to scale up in voltage because of the absence of any depletion region. As mentioned previously, compared to the optical switch, the (DI)² device and the Hall effect device will require further investigation fully to determine their potential. The following comments apply only to the optically activated switch.

In regard to the optically activated switch as a current interrupter, further work should be done to delineate carefully the trade-offs which exist between turn-off time and voltage drop, resulting from impurity doping. In order to improve hold-off, surface breakdown mechanisms should be studied and means found to minimize such effects. Another important research area involves matching the light source to the target. By this it is meant that the quantum efficiency for producing carriers should be as high as possible, while at the same time, the carrier profile should be distributed over the target in such a way so as to minimize thermal problems. In this regard, novel heat sinking techniques should be sought, such as materials which would allow the light signal to pass unattenuated and would provide heat sinking as well. Another area deserving attention is the use of a light source other than a laser. For opening switches the turn-on time is not critical, and a laser (which is usually capable of a fast risetime) is unnecessary. A light source such as a modulated flashlamp may be more than sufficient. The flashlamp should contain gas constituents, however, which cause the light intensity to drop quickly once the driver pulse is terminated. One should also consider techniques to improve gain, perhaps with an accelerated electron beam. Integration of the light source and the target into a single monolithic device is another potentially fruitful research area. For example, the device may consist of a gallium arsenide target and gallium arsenide laser diode. Finally, techniques should be studied to concentrate the light onto the target in the most efficient

manner, as for example, by use of a quartz fiber or by tailoring the material (situated between the laser and the target) in such a way as to focus the light onto the target.

Table 3 summarizes several of the research problems mentioned in this report, which deserve attention and are applicable to opening switches. The list is representative and does not include every issue discussed in the report.

REFERENCES

1. T. Nagano, T. Yatsuo, and M. Okamura, "Characteristics of a 3000V, 1000A gate turn-off thyristor," Record of Annual Meeting of the Industrial Applications Society, pg. 750, 1982.
2. B. Baliga, M. Adler, and D. Oliver, "Optimum semiconductor for power field effect transistors," IEEE Electron Device Lett. EDL-2, No. 7, July 1981.
3. G. Mourou, W. Knox, "High power switching with picosecond precision," Appl. Phys. Lett. 35, 492-495, (1979).
4. D. H. Auston, "Picosecond optoelectronic switching and gate in silicon," Appl. Phys. Lett. 25 101-103, (1975).
5. M. Weiner, J. Carter, R. Youmans, "Optically activated switch for nanosecond pulsers," Record of Fifteenth Modulator Symposium, pg. 164-167, June 1982.
6. P. Turchi, "Magnetoplasmodynamic and Hall Effect Switching for Repetitive Interruption of Inductive Circuits," Report of the Workshop on Opening Switches, January 1982.
7. T. Henderson, Report of the Workshop on Solid State Switches for Pulsed Power, January 1983.
8. J. O'Loughlin, Report of the Workshop on Solid State Switches for Pulsed Power, January 1983.

Table 1. Opening switches.

| Type | CONTROL ELEMENT, GAIN | CURRENT DENSITY (A/cm^2) | HOLD-OFF (V) | VOLTAGE DROP (V) | OPENING TIME (μs) | COMMENTS |
|----------------------------|-----------------------|------------------------------|--------------------|------------------|------------------------------------|--|
| Bipolar | Base, 5 | 10^5 | 100 500 1000 | 1-2 | 0.1-1 0.5-1 1-2 | Trade-off between voltage & current |
| MOSFET | Gate, 4-5 | 50 10 | 500 1000 | 2-3 | <0.1 | Turn-off limited by gate, depletion capacitance |
| GTO | Gate, 3-5 | 100 100 | 1000 2600 | 2-3 2-3 | 1-2 1-2 (85%) | Possible problem with voltage rate of rise during turn-off |
| Thyristor | Gate, 1 | 100-300 | 5000 | 1.5-2 | 100-200 | Mature technology, easy to parallel and series |
| GaAs JFET | Gate, 1 | 100 | 1000 | 2-3 | <0.1 | Under development |
| Optically activated switch | Light, electron beam | 1000 | 5000 | 100 | Si: 10 GaAs: 10 ns (undoped) | Low gain, scalable |
| Hall | Magnetic field | 3000 | 1000 | 8 | <1 | Low resistance ratio, 100-1000 |
| (DI) ² | Gate or light | 500 | 1000 | 3.5 | 1-10 | Under study to determine scalability |

Table 2. Opening switch applications.

| PULSE WIDTH (μ s) | VOLTAGE (kV) | CURRENT (kA) | APPLICATIONS | OPENING SWITCHES |
|---------------------------|-----------------|-----------------|-------------------------------|-----------------------------------|
| < 1 | 25-50,000 | 1-10 | CO ₂ FXR ATA | MOSFET JFET Bipolar Bulk |
| 1-100 | 350 | 10-1000 | Flashlamp Discharge PPT | GTO Thyristor Bulk |
| 1000 | 3 | 1000 | Rail | Thyristor Bulk |

Table 3. Basic research issues.

| BASIC RESEARCH PROBLEMS | RESEARCH APPROACH | SWITCH CONCEPT |
|--|--|----------------------------|
| 1. Surface breakdown mechanisms in semiconductor | Investigate various coatings for resistance to breakdown. | Bulk switcher. |
| 2. Development of new materials suitable for light activation. | Choose candidate materials and characterize mobility, quantum efficiency and recovery. | Optically activated switch |
| 3. Pulse mode behavior of semiconductor junctions. | Investigate junctions under various pulse mode conditions. | Transistor switches |
| 4. Interaction of light and semiconductor junctions. | Investigate various junction designs under light activation. | Photo-transistor switch |
| 5. New concepts in bulk switching. | Investigate new materials suitable for Hall effect and (DI)2 switching | Bulk type switch. |

HIGH POWER CLOSING SWITCHES

L. R. Lowry, Chairman

INTRODUCTION

There are many pulse power applications requiring very high power, high energy closing switches which are currently beyond the state-of-the-art in all but spark gaps. Spark gaps have many objectionable characteristics that may be eliminated by the use of semiconductor switches. The goal of this group was to determine, if any, those semiconductor concepts which are capable of showing potential for development to meet present requirements for high power closing switches.

APPROACH

The types of closing switches which were considered were limited to semiconductors, primarily Si and GaAs. A non-exhaustive set of switch parameters (blocking voltage, peak current, turn-on time, recovery time, forward voltage drop, jitter and material) was selected as a basis for evaluating the various types. This information is listed in Table 1.

Each of the semiconductor types listed in Table 1 was evaluated in terms of its potential for use in high pulse energy, high power closing switch applications in which spark gaps have traditionally been used. In order to assess the potential of various devices, values of peak voltage, peak current, pulse length, pulse risetime and PRF had to be specified. Switch parameters for four specific applications requiring high energy pulsed power currently under development were selected and are presented in

Table 2. A fifth set of switch parameters was chosen to correspond roughly to those of commercially available thyratrons which currently have very wide application (frequently because of the absence of a practical alternative). These are also presented in Table 2.

Each semiconductor switch concept was assessed in terms of its ability to satisfy the switch parameters listed in Table 2. Critical problem areas which must be addressed were identified and these are listed in Table 3. Areas in which research is required in order to determine whether a particular concept can really satisfy the switching requirements in Table 2 were identified and are listed in Table 4.

The conclusions identify semiconducting devices which we believe cannot achieve the switch parameters defined in Table 2, devices which appear to hold promise for achieving these requirements, and devices for which further characterization is required before a final assessment can be made.

SELECTED APPLICATIONS

The selected applications listed in Table 2 cover a broad spectrum of specifications for pulse power switching systems. The obvious features of the applications are the magnitude of the current and voltage requirements. Using conventional commercial devices, a large series-parallel array is obviously required to meet these specifications.

A common requirement in all specifications is a rate of current rise between 10^{11} and 10^{13} A/sec, with a majority of systems requiring 10^{12} A/sec. This is a major problem to be

addressed in using a single solid state switch or an array of devices. Another common requirement is the relatively short pulse lengths in these applications, on the order of 10^{-7} s, with a very low duty cycle, less than 10^{-3} . The requirements can be met in principle, using known device physics, applied in the context of the system requirement.

The device physics must be examined considering a trade-off between conventional operation, which stresses long pulse length, high duty cycle, and a moderate rate of current rise, and that required by the selected application. Also, the thermal demands of pulse power applications can be much different than those of relatively steady-state conventional applications. Thus, a large thermal transient cycle must be addressed in pulse power applications, based on much larger total power per device. The high rate of current rise requires determining and utilizing the physics of carriers generation during much shorter times than in conventional applications; the short pulse lengths do not require the analysis for long recombination times. Another change in solid state device design will be the acceptance of a forward dynamic conduction drop that is on the order of 1% of the system voltage; conventional solid state switching devices are made to drop less than 0.1 percent of the device blocking voltage. The low conduction drops occur in the long, high current pulses not required in pulse power applications. On the other hand, minimizing the conduction drop reduces switch dissipation and thus the required thermal energy removal.

The potential technology solutions to the problems of pulse power should have the following characteristics:

1. high voltage operation;
2. high current operation;
3. high rate of current rise;
4. accurate timing control;
5. large average power;
6. less than 1% conduction drop;
7. thermal management;
8. minimum and reasonable number of devices per system, for reliability;
9. repetition rate capability.

Application 5 is a special consideration for a general purpose switching device similar to the EG&G HY-5 thyratron. The specifications for this application are closer to conventional device parameters, but will require a device array and an increased rate of current rise. This application may be an ideal first step for solid state technology.

FUNDAMENTAL TECHNICAL PROBLEMS

The applications which attempt to utilize the candidate solid state semiconductor devices typically require voltages in excess of 40 KV, currents in excess of 20 KA, and pulse lengths less than 2 μ s. Pulse rates are from 10 Hz to 10 KHz. In all cases, a minimum di/dt of 10^{12} is required.

These requirements severely limit the possible choices of devices to switch the pulse into the load, if pulse formation is to occur in most directly. It is possible to construct a switch

incorporating many parallel discrete devices that are relatively slow to generate a primary pulse which could be compressed in time to arrive at the load with the desired pulse shape. This possibility was not addressed seriously, however, because it employs existing technology. It is recognized that some engineering will be required to apply semiconductor devices where spark gaps and other switches have been used exclusively. This is not a trivial task, but it is feasible.

The major parameters which were discussed are listed in Table 1, along with their desirable values. The most pressing problems are 1) blocking voltage, 2) forward voltage drop 3) peak current; 4) thermal limits; and 5) speed of current handling. Some devices can have very good current capacity but have excessively high forward voltage drop. Others might suffer from slow rise time, but have a very low forward drop.

Consider the blocking voltage problem. The voltage across the active device material must not exceed its safe intrinsic blocking voltage nor exceed the level that can be withstood between the terminals of the device when mounted in a system. For the machine voltages under consideration, pulse charging of the energy store is the only reasonable method considered. Assuming a field of 10^5 V/cm, the intrinsic maximum electric field in silicon, it appears possible to use a block of silicon as an active switch material, assuming turn-on could be achieved and surface flashover could be prevented. If, however, the length of the switch material has to be increased considerably in order to prevent surface flashover, the forward voltage drop

could cause excessive heating, or else it would not be possible to turn the device on uniformly.

Forward voltage drop per unit length is also an important consideration in selecting a device. There is a trade-off between the low forward drop obtained with doped material and the blocking voltage associated with high resistivity material. A device designed to obtain higher blocking voltage will likely have higher forward voltage drop, leading to higher dissipation and more complicated thermal management. Excessive voltage drops during the main body of the pulse, in conjunction with the required current flow, produce excessive device power dissipation. Devices such as the thyriscor tend to have the lowest forward drop, whereas the avalanche devices might drop as much as 5-10% of the blocking voltage. It is important to reduce this forward drop to less than 1%.

Current conduction through the switch can proceed along the surface of the active material or through the bulk of the material. It can also flow in a filamentary fashion in some devices. The triggering technique used to initiate conduction will, to some extent, determine the current flow process. Short wavelength photoconductive triggering will likely create surface conduction.

Another characteristic of current flow through the device is the speed with which full turn-on can be achieved. Current carriers must be generated or created, conducting areas formed, and adequate device material turned on at a rate faster than the material circuit response time, in order that instantaneous safe

temperatures are not exceeded. This factor is particularly noticeable in the conventional thyristor and was a major factor in ruling out the whole class of normally gated thyristors for fast pulse application. Also, pulse width and rise time can determine how much of the total device material is actively carrying current.

Thermal problems in semiconductors can cause failure through cracking, spot heating, device parameter shifts, gate burnout, etc. It is important that the allowable current density of the conducting portion of the device not be exceeded during any part of the pulse, and that the total pulse time be considered in analyzing the thermal design of a particular device. Transient or leading edge effects can be particularly troublesome because the voltage across the switch can be at a very high level as the current builds up, leading to high peak power dissipation. Additionally, all portions of the device might not be turned on simultaneously, which, together with the initial rise time transient heating, would promote burnout. Spot heating within the device can arise from (1) inadequate turn-on of the current carrying portions of the device; (2) skin effects arising from a high di/dt pulse, forcing current to flow in a thin layer on the surface of the device; (3) a tendency of the current to form filaments within the semiconductor body; (4) possible current pinching from magnetic effects; and (5) transitional area defects where two portions of the device meet.

High thermal stresses can lead to device failure during the main body of a pulse through mechanical failure or cracking of a

silicon wafer. For rep-rated devices, it is important that heat be removed from the active current carrying area as rapidly as possible, so that these mechanical stresses do not build up. Buildup of thermal energy within the device from pulse to pulse can vary the operating parameters over a wide range.

APPLICABLE SOLID STATE TECHNOLOGY

The candidate device technologies of Table 1 were each evaluated against the requirements of the applications of Table 2. The results are summarized in Table 3. A detailed discussion follows.

Gate Junction Devices

Included in this category are principally transistors and thyristors of conventional design. These devices employ geometries evolved over a number of years, making them eminently suitable for general industrial, utility, and commercial applications.

Although the ranges over which parameters vary are wide, these devices are not designed to carry very short, very high pulse currents of the kinds needed in the pulse power applications considered here. When attempts are made to utilize such devices in pulse power circuits, the devices will in general either not conduct the pulses desired, or if they do, they will quickly fail.

Conventional devices provide blocking voltages up to about 10 KV, which is well below that required for pulse power application. If they were to be used in pulse power circuits, many would have to be connected in series to achieve the overall

switch blocking voltage needed. When connected in series strings, conventional devices can often fail during turn-on because of differences in turn-on delay.

In summary, conventional transistors and thyristors cannot be satisfactorily utilized in pulse power circuits principally because their designs were optimized for different applications.

Avalanche Injection Gated Devices

Included in this category are devices which are only turned on by avalanche injection as well as those which conduct by avalanche injection. Specifically excluded from this category are devices which conduct by avalanche breakdown but are turned on by optical means.

An example of the class of devices which turn on by avalanche breakdown but are sustained in conduction by other means is the Reverse Blocking Diode Thyristor (RBDT). The structure of this device is like that of a thyristor (PNPN) but without a gate connection. The device is turned on by the application of an overvoltage pulse which causes avalanche breakdown to be initiated, causing internal carrier injection. These carriers give rise to currents which cause additional carrier injection at the two internal emitting junctions, which eventually provide sufficient internal feedback to sustain low voltage conduction as long as load current flows.

Because the avalanche breakdown process is very fast, these devices turn on more quickly than do conventional thyristors, but because they include the conventional thyristor structure, they

move from avalanche breakdown initiated conduction to emitter injected conduction exhibiting a low conducting drop. In addition, the RBDT devices can be series connected to form high voltage switches which do not exhibit the turn-on problems of conventional devices.

The other class of avalanche devices include those which conduct using the avalanche breakdown process coupled with feedback from at least one device junction. An example of such a device is an avalanche transistor which conducts when avalanche breakdown is initiated; carriers produced by this process constitute a current which flows through an emitting junction. The feedback of carrier injection from the emitting junction together with carriers produced by the avalanche breakdown process results in a relatively low conducting voltage drop.

Because the avalanche breakdown process is quite fast, such a device will turn on quickly, but the conducting drop is relatively high. Questions of series connection of devices to yield a high voltage switch and parallel connection of devices to form a high pulse current switch have yet to be resolved. Also, the possibilities of filamentary conduction within the device which could limit the peak current capability of the device must be addressed.

Light Fired Devices

Three types of light-initiated devices were considered: a) simple photoconductive devices; b) photoconductive devices which utilize avalanche current multiplication; and c) light-activated latching (LASS) devices. All of these devices offer the advan-

age of very low jitter triggering, without serious trigger circuit voltage isolation problems. Device types a and b appear to be directly scalable in terms of both voltage holdoff and current handling capability, whereas the presence of a blocking junction for devices of type c results in a fundamental limit in the device blocking voltage of about 10 KV. This is not a serious problem, however, because the excellent triggering characteristics of the device allow series stacking. The blocking voltages listed for types a and b are based on the breakdown field in silicon.

For all these types, the peak current density listed in Table 1 is based on values already achieved and is therefore conservative. For types a and c the turn-on time is determined by the rise time and pulse energy of the laser. The turn-on time for type b is a function of the laser rise time and energy and the avalanching time in the device. For all types, the recovery time is limited by the carrier recombination time, and possibly the carrier transit time for the device. For the avalanche device b, the recombination time must be at least comparable to the avalanching time, which sets the lower limit to the recovery time. Both types a and b could be fabricated from any semiconductor material available with high dark resistivity and good carrier mobility. The bipolar nature of the type c devices probably restricts the material to silicon.

For all light fired devices, the device-to-device jitter should be extremely low in a properly designed system, as Table 1 shows, since the turn-on characteristics are controlled entirely

by the light source. The initial forward voltage drop for these devices (particularly types a and c) is determined primarily by the light intensities used to turn them on. The values listed represent drops achieved, although considerable light intensity may be required.

For higher current applications, all three device types place different requirements on the light source. Charge gains of up to about 10^3 have been reported with an avalanche device, b, which reduces this problem. Both the avalanche and the LASS devices have the real advantage for longer pulse applications that they latch on, so that the laser need not remain on for the duration of the current pulse.

Electron beam gated devices were also considered. Although these devices appear very attractive for ultra-fast, low-to-moderate voltage applications, they did not seem appropriate for the high voltage (> 10 KV) applications we considered, due to difficulties in guiding the relatively low energy (~ 10 KeV) electrons to the semiconductor in the presence of the forward blocking field. Other parameters of the device should be similar to the photoconductive switch, except that the peak currents will be somewhat lower due to the short penetration depth of 10 KeV electrons.

Field Effect Transistors

Because field effect transistors (FETs) do not depend on minority carrier injection as a conduction mechanism, they switch from the off to the on state in a very short time compared with other devices. The majority carrier mobilities in GaAs is higher

than that of silicon, so that GaAs FETs appear to be the more promising of the two.

A limiting factor of the FET is the relationship between maximum blocking voltage and drain resistance. In order to maintain a reasonable switch series resistance, the maximum device blocking voltage must be limited to a relatively low value. For the GaAs FET, this value is approximately 1000 V, making it necessary to series connect a large number of devices to yield a switch with a blocking voltage sufficiently high to be useful in pulse power applications. Because so many devices must be series connected to obtain a useful switch, the FET does not appear to be as promising for use as a very high power closing switch as do some of the other candidate device types.

CONCLUSIONS

The switching concepts considered here involved semiconductor materials for use in very high pulse power closing switches. Using existing device structures, several types were considered to have possible application, with additional study of their switching behavior. Also, new types of semiconductor structures and switching techniques seemed promising, but extensive research is required to determine actual performance characteristics. The technologies considered fall into three broad categories.

Most Promising Technologies

Avalanche devices offer the possibility of high array densities because of the small amount of ancillary equipment required. To achieve high densities, several significant problems

in the physics of avalanche switching must be investigated and eventually solved. These problems include current filamentation, temperature of operation, and forward voltage drop. Basic information is required to determine the magnitude of these problems and to identify possible solutions.

Photoconductive devices have the possibility of meeting all of the basic switch performance requirements considered. However, information on these devices is preliminary, and extensive extrapolation is required. Much research and development is required to define the physical interactions which define the interrelations of the various device parameters (e.g., photon energy and quantity, blocking voltage, forward drop, turn-on time, etc.). The light source requirements need to be determined in view of device or material failure mechanisms.

Not Promising Technologies

Conventional junction devices are not suitable for the types of applications considered because of low di/dt and the general undesirable trade-offs between various parameters, plus the large number of devices required if acceptable individual devices are applied in arrays. E-beam initiated devices do not appear to be practical for high voltage applications because the beam voltage must be $\sim 10X$ the switch voltage in order to control beam placement, and because of the damage caused by the E-beam to the crystal. More basic information is required on E-beam switching. This may be available in the literature. FETs do not appear promising for the applications considered because of the large number of devices required.

Need Further Research to Evaluate

The (DI)² technology is promising but is just emerging and is too early to evaluate. The NASA support of this work should be continued and the pulse power community should monitor its progress.

RESEARCH RECOMMENDATIONS

All the devices considered for possible application in high power pulse systems exhibit present restrictions on their performance. To keep device array numbers reasonable, blocking voltage and current handling capabilities need improvement in a single device. For reasons of device degradation in turn-on time, parallel arrays are not desirable. Therefore, maximum current density limits in the devices need to be explored. Maximum blocking voltage in a single device is considered to be secondary in importance to current density problems. This is because switching is not anticipated to be as much of a problem for series as compared to parallel arrays.

Associated with high current densities is actual device performance at high currents and large current rise times (di/dt). Characterization in these operating regions is necessary. These regions of operation engender thermal problems in each device. Contact problems and packaging considerations should also be studied.

In the photoconductive devices, a possible improvement in performance may arise from research into photocconductance gain mechanisms. Also compact light sources, such as semiconductor lasers, are viewed as having a large priority in overall switch

technology development. However, the requirements of photoconductive switches should be determined in order to set the goals of solid state laser research.

A general need for improved switching times of high powered diodes has been identified. These devices certainly have many applications, one of which is switch protection. Research is needed also into types of failure mechanisms appropriate to pulse power application. These research recommendations are summarized in Table 4.

Table 1. Closing switch summary.

Categories:

1. Gated Junction Devices
2. Avalanche Injection Gated Devices
3. Photo Injection Gated Devices
 - a) Avalanche (30 μ J/cm²)
 - b) Photoconduction (30 mJ/cm²)
 - c) LASS
4. E-Beam Gated
5. FET (Majority carrier)
6. (DI)₂

| Projected Device Parameters | | | | | | |
|-----------------------------|---------------------|-------------------------------|------------------------|--------------|-----------------|---------------|
| Device | Structure Junctions | Blocking Voltage (V_{HO}) | Peak Current | Turn-on Time | Recovery Time | Material |
| 1 | ≥ 2 | 10 KV | 2 KA/cm ² | 2 μ s | 1 ms | Si |
| | ≥ 2 | 1 KV | 4 KA/cm ² | 0.25 μ s | 10 μ s | Si |
| 2 | ≥ 1 | 10 KV | 1 KA/cm ² | < 10 ns | ns to ms | Si, GaAs |
| | | | | | (Te) | Others |
| 3a | ≥ 0 | 10^5 V/cm | > 1 KA/cm | < 1 ns | 1 ns to " " | " |
| | | | | | 10 μ s (Te) | |
| 3b | ≥ 0 | 10^5 V/cm | > 4 KA/cm | < 1 ps | 1 ps to " | " |
| | | | | | 10 μ s (Te) | |
| 3c | ≥ 3 | 10 KV | > 10KA/cm ² | < 1 ps | 10 μ s | Si |
| | | Same as 3a and 3b | | | | Large bandgap |
| 4 | | | | | | |
| 5 | 2 | 1000 V | 10 KA/cm ² | < 1 ns | 5 ns | GaAs |
| 6 | - | 10 KV* | 10 A* | - | - | Si, GaAs |

*Goals of present NASA contract.

Table 2. Applications of solid state switches.

| | I | II | III | IV | V |
|------------------|------------------------|------------------------|--------------------------|------------------------|------------------------------------|
| | <u>ATA</u> | <u>E-Beam Laser</u> | <u>E-Discharge Laser</u> | <u>PBFA</u> | <u>HY-5</u> |
| Blocking voltage | 250 KV | 500 KV | 50 KV | 1 mV | 50 KV |
| Peak current | 20 KA | 100 KA | 50 KA | 1 MA | 5-10 KA |
| Pulse width | 50 ns | 2 μ s | 100 ns | 50 ns | 1-10 s |
| Repetition rate | 10 KHz | 100 Hz | 1 KHz | 10 KHz | 1-10 KHz ² ₉ |
| Rise time | 10 ns | 100 ns | 10 ns | 10 ns | --- |
| di/dt | 2×10^{12} A/s | 2×10^{12} A/s | 5×10^{12} A/s | 5×10^{13} A/s | 1×10^{11} A/s |

Table 3. Comparison of devices and requirements of the application.

| Device | Applications | | | | |
|--|---|--------------------------------|---|--|------------------------------------|
| | I | II | III | IV | V |
| 1 di/dt limited; array inductance; large no. devices | | | | | di/dt, triggering user problems |
| 2 Possible; 15 devices in stack; heat removal | Possible; 20 device stack; (Engineer) | Possible; similar to AIA | Paralleling problem; filamentation (Research) | 5 devices in series; di/dt problem; possibly needs res. and engr. | 220 |
| 3a One device possible; cryogenic temperature; laser problems; thermal problems; possible V_F problem | | | (Research) | Possible solid state laser | |
| 3b One device possible; laser problems; thermal problems | Long pulse problem (no latch); laser problem | Possible | (Research; fabrication) | Needs large laser | |
| 3c Stack of 35 devices; laser problems | 50 devices; laser problems | | (Research) | 5 devices in series; needs research; in pack- aging and laser | |
| 4 Not practical - needs E-beam 10X blocking voltage | | | | | |
| 5 Too many devices required in stack | | | | | |
| 6 Not adequately characterized | | | | | |

Table 4. Recommended research areas.

| | | |
|---|-------------------------|--|
| Maximum current density (device physics) | Contracts/Grants | Avalanche (filamentation), photoconductive avalanche, photoconductive |
| Large current ohmic contacts (device physics) | Contracts/Grants | All photoconductive devices |
| Photoconductive gain mechanisms (device physics) | Contracts/Grants | |
| Characterize scalable devices dI/dt, I, V | Contracts/Grants | All |
| Thermal characteristics of device system | Contracts | All |
| Dynamic conductive voltage drop (device physics) | Contracts/Grants | Avalanche devices |
| Failure mechanisms in pulse power mode of operation (device physics) | Contracts/Grants | All |
| fast switching rectifiers | Contracts/Grants | All |

EXTREMELY FAST RISETIME SWITCHES

Robert B. Hammond, Chairman

OBJECTIVE

The objective of this group was to consider solid state devices which have demonstrated or show potential (in a single device) for sub-10 nanosecond risetime and megawatt or greater power handling; to consider these devices for both closing and opening switch applications and as protective devices; to identify devices which show promise for pulsed power applications; and to identify research priorities and objectives for a three to five year term.

APPROACH

After some discussion, the group decided on a four segment approach. These were

- 1) to choose device types to consider;
- 2) to define and prioritize important device parameters;
- 3) to evaluate, from fundamental limits, the potential of device types for pulsed power applications; and
- 4) to recommend research objectives and priorities.

The following device types were considered:

- 1) photoconductors;
- 2) avalanche photoconductors;
- 3) avalanche transistors;
- 4) field effect transistors;
- 5) PIN deep-level devices; and
- 6) varistors.

The following important switch parameters were defined:

- 1) rise time;
- 2) fall time;
- 3) blocking voltage;
- 4) current density;
- 5) efficiency; and
- 6) scalability in a single device.

The following switch parameters were considered to be of secondary importance:

- 1) energy density;
- 2) I^2t product;
- 3) delay;
- 4) jitter;
- 5) recovery time;
- 6) waveform distortion;
- 7) voltage gain;
- 8) current gain;
- 9) weight/volume ratio; and
- 10) reliability.

Near the outset of the discussions, it was determined that sub-10 nanosecond rise time was not needed for the specific applications which were the focus of the Workshop as a whole. Because of this, the group concentrated on the properties of single devices, emphasizing the parameters listed above and considering fundamental limits in the scaling of single devices in terms of speed, voltage, and current. System cost was not specifically addressed.

Besides the six device types listed above, which were discussed in detail, other switches we also considered: a) Josephson junctions, b) ovonic switches, c) bipolar transistors, and d) thyristors. These devices were not considered in detail because switch a requires 4 K temperature and has extremely low voltage hold-off, switch b is unreliable due to material nonuniformity and filamentary current, switch c did not look as promising as field effect transistors, and switch d does not have a sub-10 nanosecond risetime. Also, optically triggered thyristors were not considered because there was no one in the group familiar with these devices.

The body of this summary contains six sections. Each section discusses the conclusions of the group about a particular device type. Before continuing, a general comment is in order. All the devices considered must be judged in terms of thermal limits. Thermal management, particularly for high average power applications, is an important focus for research in all solid state switches considered for pulse power applications. Heating affects the different device types in different ways and these effects need to be assessed. Also scaling, light access, and device geometry each pose different constraints for cooling the various device types.

PHOTOCONDUCTORS

Background

Photoconductors are bulk devices, not junction devices. They have been used mostly as closing switches for extremely fast rise time applications; however, application as opening switches is

possible. Their principle advantages as power switches are their extremely fast rise time capability (sub-picosecond closing, few picosecond opening), very low voltage drop (arbitrarily small, in principle), very low jitter (light source limited), and their almost arbitrary scalability in voltage and current in a single device. Greater than 100 KV at several KA has been switched in a small device without approaching any fundamental limits. Their primary limitation is the burden placed on the excitation source for the switch, which may be a light source or an electron beam. At least a microjoule of excitation energy is required per megawatt of switched power.

Physical Principles

The principles of operation of photoconductor switches may be summarized simply (see figure 1)): a) electrical (ohmic, low resistance) contacts are placed on the surface of a photoconductive material, b) the off-state resistance and thus current leakage is determined by the resistivity of the photoconductive material, c) to close the switch, the region between the contacts is excited with a light or electron pulse which is absorbed in the photoconductive material, producing free carriers (electrons and holes), d) thus, a highly conductive path is produced between the electrodes (turn-on is determined primarily by the length of the excitation pulse and turn-off is determined by the recombination of the carriers or carrier sweep-out).

The on-state resistance of the photoconductive switch may be calculated from the properties of the switch material and the excitation pulse:

METHOD OF OPERATION

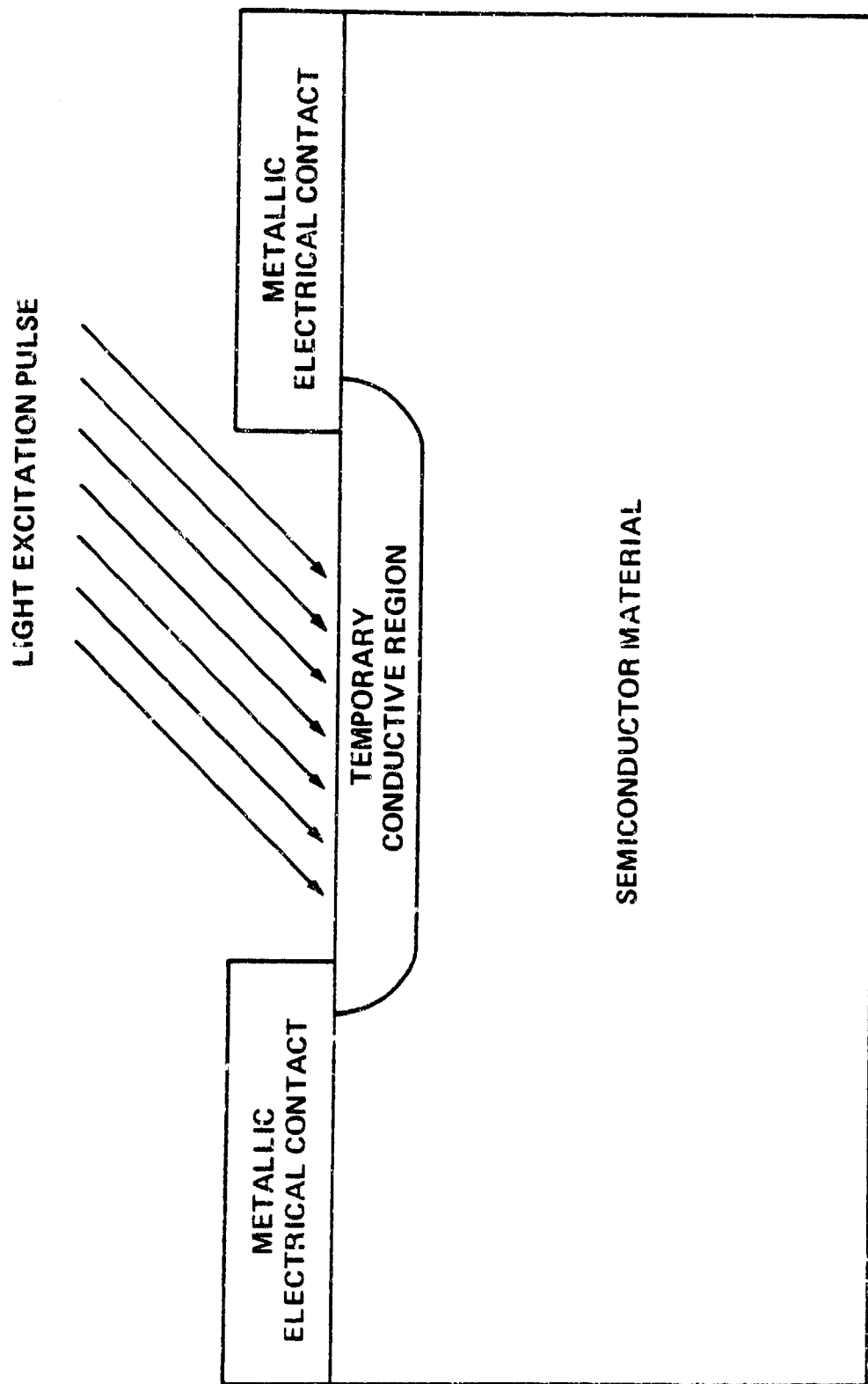


Figure 1. Operation of a photoconductive switch.

$$R_{on} = (\ell^2 E_p) / (q\mu E) \quad (1)$$

where ℓ is the spacing between the contacts, E_p is the energy consumed in making each electron-hole pair, q is the electronic charge, μ is the sum of the electron and hole mobilities, and E is the total energy in the excitation pulse. (This equation ignores light reflection losses and contact resistance; both of which can be negligible, in principle.) Using equation (1), the energy required in exciting the photoconductor in order to deliver power to a load can be calculated. This is the excitation energy required for a closing switch application. (Here, we assume a zero source impedance.)

$$P/E = (X E_f^2 q \mu) / E_p \quad (2)$$

where P is the electrical power delivered to the load, X is V_{drop}/V_{bias} , and E_f is the electric field in the off-state (10^5 V/cm). This equation determines the switching efficiency. Note that the risetime of the switch is basically only limited by the length of the exciting light or electron beam pulse. Thus, equation (2) shows how much energy must be delivered to the photoconductive switch within the required rise time in order to deliver a certain power to the load.

Material Requirements

Material requirements for photoconductive switching are high resistivity (low leakage), and high carrier mobility (high switch efficiency). It is also desirable to be able to make low resistance, injecting, ohmic contacts to the material (low contact resistance, and low loss from carrier sweep-out). The voltage blocking capability is determined by the dielectric strength of

the material. This is about 10^5 V/cm for most materials. Pulsed bias may be required to achieve this limit due to heating from leakage current. (The materials used for these switches are intrinsic semiconductors whose conductivity increases exponentially with temperature, so thermal runaway of leakage current must be avoided.) Current density can be extremely high (10^7 A/cm² is possible) but thermal limits and switch efficiency dictate current densities much lower.

Desirable materials for these applications are:

Silicon

Sum of electron and hole mobilities (300 K): $1925 \text{ cm}^2/\text{V s}$

Carrier lifetime: $1 \text{ ns} - 1 \text{ ms}$

Intrinsic resistivity at 300 K: $2.3 \times 10^5 \text{ ohm cm}$

Dark current heating (10^5 V/cm, 300 K): 2000 W/cm^3

Absorption length (1.06 micron light): 1000 microns

Absorption length (0.85 micron light): 15 microns

GaAs

Sum of electron and hole mobilities (300 K): $9300 \text{ cm}^2/\text{V s}$

Carrier lifetime: few ns

Intrinsic resistivity at 300/K: 10^9 ohm cm

Dark current heating (10^5 V/cm,300/K): 0.2 W/cm^3

Absorption length (1.06 micron light): 1000 microns

Absorption length (0.85 micron light): 2.0 microns

Generally, mobilities in semiconductor materials are quoted for low electric fields and low carrier and impurity concentrations. The intrinsic materials useful for photoconductive switching have low impurity concentrations and will have low

electric fields in the on-state; however, excited carrier concentrations should be high to achieve high current densities. At high carrier concentrations, carrier-carrier scattering limits the mobilities of electrons and holes. These effects are fairly complex but are well studied in silicon. Figure 2 shows calculated sums of the electron and hole mobilities in Si as a function of excited carrier density and temperature. Going to higher concentrations of excited carriers decreases carrier mobility and therefore switch efficiency. Thus, the on-state current density can be increased by producing higher carrier concentrations, but only at the expense of switch efficiency. It is likely that it is not desirable to exceed carrier concentrations of 10^{17} cm^{-3} because of this. Another important observation from figure 2 is that, at carrier concentrations of 10^{18} cm^{-3} and higher, mobility increases with increasing temperature. This region must be avoided to avoid thermal instability.

Conclusions

Using figure 2 and assuming a carrier concentration of 10^{17} cm^{-3} , a temperature of 300 K, and a 1% voltage drop, a number of parameters can be calculated for photoconductive switching with Si:

| | |
|------------------------------|--|
| Switching efficiency: | 20 microjoules/megawatt |
| Current density (on state): | $1.35 \times 10^4 \text{ A/cm}^2$ |
| Joule heating (on state): | $1.35 \times 10^7 \text{ W/cm}^3$ |
| Temperature rise (on state): | 8 K/microsecond |
| Current (1.06 micron light): | $1.35 \times 10^3 \text{ A/cm}$ of contact |
| Current (0.85 micron light): | 20 A/cm of contact |

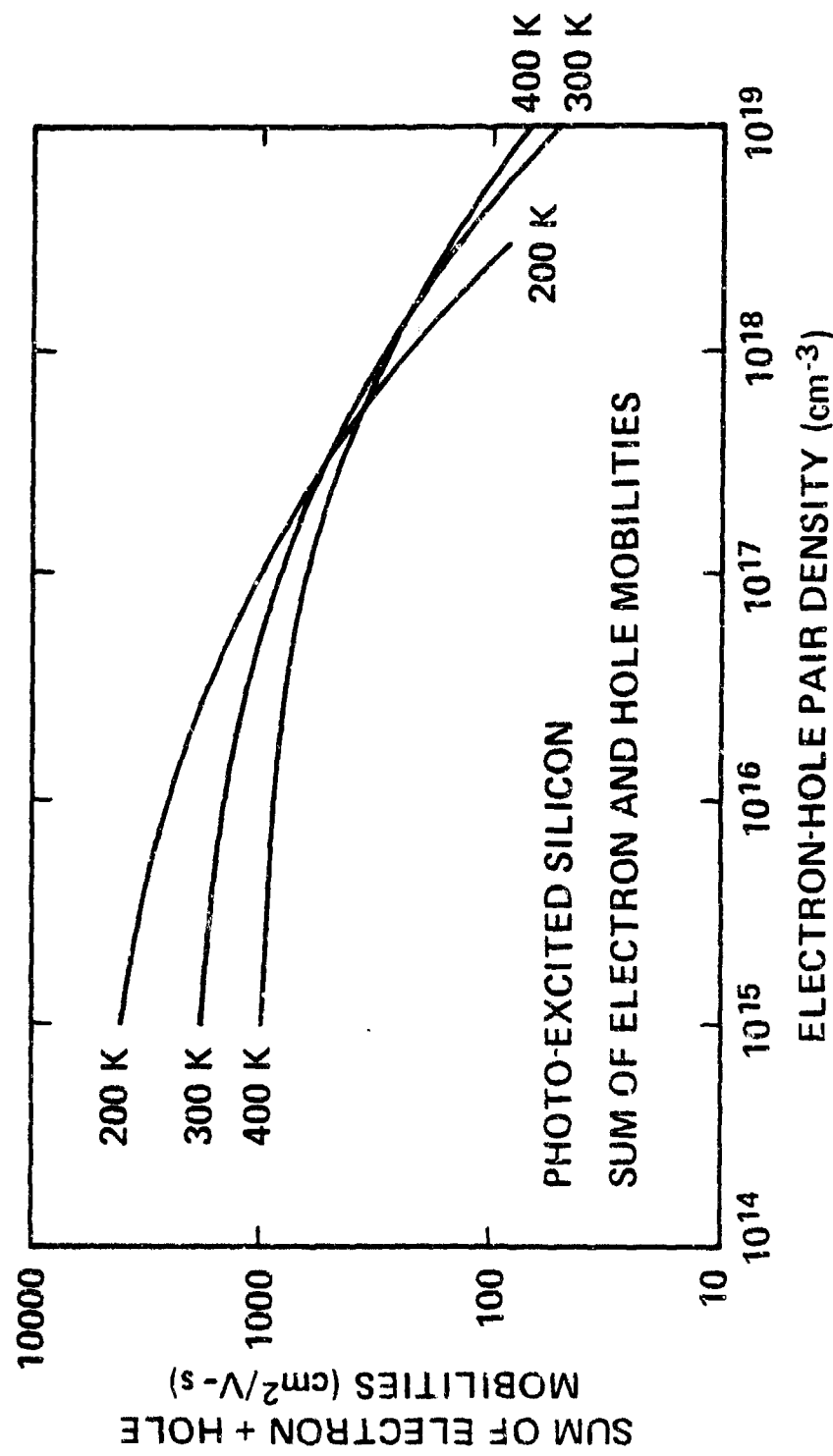


Figure 2. Dependence of the sum of the carrier mobilities in silicon on excited carrier density and temperature.

The approximate factor of five improvement in mobility in GaAs yields the following values for this material, using the same switching parameters. (Carrier-carrier scattering has not been studied as extensively in GaAs as in Si but similar effects may be expected.)

| | |
|------------------------------|-------------------------------------|
| Switching efficiency: | 4 microjoules/megawatt |
| Current density (on state): | 5.4×10^4 A/cm ² |
| Joule heating (on state): | 5.4×10^7 W/cm ³ |
| Temperature rise (on state): | 1.5 K/microsecond |
| Current (1.06 micron light): | 5.4×10^3 A/cm of contact |
| Current (0.85 micron light): | 11 A/cm of contact |

GaAs is attractive for its improved efficiency, improved power handling, and lower heating; however, it does not have the flexibility in control of carrier lifetime which Si has, nor is it as inexpensive. Also, although this has not been investigated for photoconductive switching, it is expected that Si will have lower contact resistance. Both materials have increased mobilities at low temperatures and thus cooling will improve efficiency, power handling, and heating.

Only two wavelengths of excitation light have been considered for the photoconductive switch, 1.06 microns and 0.85 microns. The first was chosen because of the number of experiments which have been performed using this wavelength and because of its attractiveness due to long absorption length; the second, because of the availability of compact, efficient, reliable solid-state light sources at this wavelength: semiconductor laser diodes and light-emitting diodes. These sources have overall efficiencies

of conversion from electrical to optical power between 10% and 30%, and have sub-nanosecond speed.

Because of the wide latitude in absorption length, high conversion efficiency, and low damage induced in semiconductors, it would be valuable to consider electron beam excitation sources for photoconductive switches. Sub-micron to millimeter absorption lengths can be obtained with electron energies below the threshold for lattice damage in Si (250 KeV) and GaAs (600 KeV). Using electron beam excitation would require careful system configuration due to the acceleration of electrons in the electrical field of the switch.

Research Recommendations

In order of priority:

1. Excitation sources

a. Light sources

i. Evaluate efficient and reliable light sources at about one micron wavelength.

ii. Evaluate system requirements for photoconductive switching using semiconductor light sources.

b. Electron beams.

i. Evaluate damage effects in photoconductive switches.

ii. Determine limits on system configuration for high-voltage photoconductive switching.

2. Contacts

a. Evaluate limits to R_{on} from contact resistance.

b. Develop high injection efficiency contacts.

3. Surface breakdown.
 - a. Determine mechanisms and limits of surface breakdown.
 - b. Evaluate surface passivation schemes to prevent surface breakdown.
4. Thermal management
 - a. Evaluate limits on system performance due to dark current heating, high duty cycle, light access.
5. Scaling
 - a. Evaluate limits to scaling imposed by space charge limited current.
 - b. Evaluate limits to scaling from switch inductance.
6. Opening photoconductive switch.
 - a. Evaluate switch efficiency, power handling, and thermal management requirements for opening switch applications.

AVALANCHE PHOTOCONDUCTORS

Background

Avalanche photoconductors may be bulk-effect devices. They are light-activated, similar to photoconductors, but have shown a considerably lower energy requirement for switching. Only one set of experiments is known to have been reported in the literature on avalanche photoconductive switching. These experiments were performed on Cr-doped, semi-insulating GaAs, at 77 K and 196 K. Silver paint contacts were made to the material, which was biased very near the observed breakdown field of 78 KV/cm. Switching was initiated by a deeply penetrating, 1.06 micron light pulse. The GaAs switch replaced the center conductor in a 50 ohm transmission line which also served as a charge line.

Thus, both the load and source impedances were 50 ohms. Results of the experiments can be summarized as follows.

Contact spacing on GaAs switch:.....0.5 mm

Maximum bias voltage:.....3.7 KV

Maximum power switched to load:.....59 KW (both temps)

Minimum optical energy for switching:....35 nJ (77 K)

....150 nJ (196 K)

Sustaining voltage:.....7.4% of V_{bias}
(both temps)

Rise time:.....500 - 700 ps

Delay:.....1.0 - 1.5 ns

Jitter:.....150 ps

Device conditioning:.....50 - 100 shots
(slight changes in minimum optical
energy and rise time.)

These results can be converted to the case of zero source impedance to determine the optical energy required for switching.

These are 0.15 microjoule/MW at 77 K, and 0.64 microjoule/MW at 196 K.

If this type of switching is caused by bulk avalanche of photoinjected carriers, it is inherently scalable. However, if the carrier multiplication is by avalanche injection at a contact, it may not be scalable. Avalanche injection is a likely mechanism in the above-mentioned experiment because of near certain existence of surface potential barriers at the contacts to the GaAs.

Physical Principles

There are two modes of operation of photoconductive devices: a) the photoconductive mode; and b) the avalanche mode. The avalanche mode has not been specifically addressed theoretically; a preliminary analysis is presented here. For both avalanche and photoconductive cases, an external agent (either photon or electron beam) controls the current through the device. The space-time evolution of the (electron or hole) carrier density in a photoconductive device is given by the continuity equation:

$$\partial_t n_j + \nabla \cdot (n_j \bar{v}_j) = S_{ext} + v_i n_j - \beta n_j n_k - \eta n_j, \quad (3)$$

($k, j = 1, 2$; $k, j = 1$ for electrons, $k, j = 2$ for holes)

where \bar{v} = mean carrier velocity at (\vec{r}, t) ;

S_{ext} = external source uniformly or non-uniformly producing carriers at (\vec{r}, t) ;

v_i = ionization rate (sec^{-1}) (for the photoconductive mode, $v_i = 0$; for the avalanche mode, $v_i \neq 0$);

β = recombination coefficient ($\text{cm}^6 \text{ sec}^{-1}$); and

η = trapping coefficient (sec^{-1}).

Assuming one-dimensional carrier flow (figure 3), and integrating equation 3 over the volume of the device (shaded),

$$\int_V \partial_t n_j dV + \int_V \nabla \cdot (n_j \bar{v}_j) dV = \int S_{ext} dV + v_i \int n_j dV - \beta \int n_j n_k dV - \beta \int n_j dV \quad (4)$$

Letting N = total number of carriers in shaded volume, V , and n = constant,

$$\int_V n_j dV = nV = N.$$

and

$$\int_V n_j n_k dV = n^2 V.$$

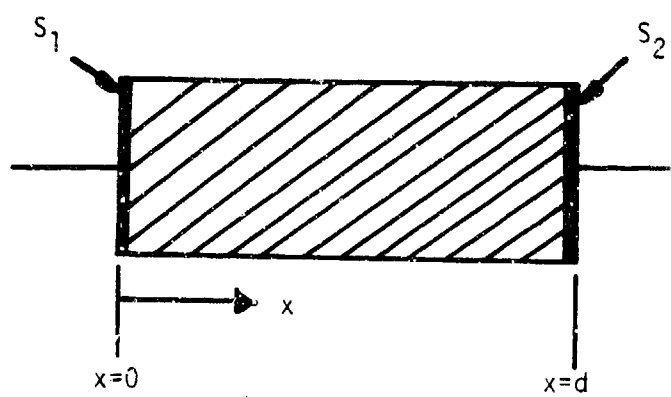


Figure 3. Model for avalanche photoconduction calculation.

Then

$$\frac{dN}{dt} + \int_S \bar{n} \bar{v} \cdot dA = S_{ext} + v_i N - \beta' N^2 - \eta N, \quad (5)$$

where $\beta' = \beta/v$.

$$\text{Also, } \int_S \bar{n} \bar{v} \cdot dA = \int_{S_1} \bar{n} \bar{v} \cdot dA + \int_{S_2} \bar{n} \bar{v} \cdot dA; \quad (6)$$

on S_1 , $\bar{J} \cdot dA > 0$ and on S_2 , $\bar{J} \cdot dA < 0$, so that

$$\int_{S_1} \bar{n} \bar{v} \cdot dA = j_1(t, 0) \frac{A_1}{e}, \quad (7)$$

$$\text{and } \int_{S_2} \bar{n} \bar{v} \cdot dA = j_2(t, d) \frac{A_2}{e}, \quad (8)$$

where A_1 is the area of S_1 , A_2 is area of S_2 , and $j = n\bar{v}$.

The densities of both electrons and holes must be found in order to determine growth and steady-state conditions, using appropriate boundary conditions. (Although there is initially a dark current, $S_{ext} = 0$ (no laser); in this case, the multiplication due to electron impact ionization is less than the loss mechanisms β and η .) When the laser is turned on,

$$S_{ext} + v_i N > \beta' N^2 + \eta N, \quad (9)$$

causing current growth to a possible steady-state which needs to be described.

Conclusions

In order to take advantage of the much reduced energy requirement of avalanche photoconductive switching (compared to simple photoconductive switching), minimum sustaining voltage, and minimum rise times, delay, jitter, and the necessity for cooling are introduced. The limits to these quantities already observed in the first set of experiments, however, show that this

class of devices may have considerable promise for pulsed power applications.

The lowest voltage drop will be achieved with the laser on, providing a constant source of electron-hole pairs. This mode of operation has not been investigated at all and may provide an opening switch. The overall efficiency may also be better for the closing switch.

Research Recommendations

1. Fundamental mechanisms

What is the fundamental avalanche multiplication mechanism? Is it bulk or contact related? Is there a steady state after the laser is turned off? (Note that the initial conditions for this state are different than the original conditions). What is the potential for opening switch applications.

2. Voltage drop

What are the steady-state voltage drops? (Voltage drop depends on whether the excitation stays on or not, and needs to be determined by solving the above equations and by experimental verification.)

3. Material parameters

What are the important material parameters determining the minimum optical energy for turn-on, voltage drop, etc. Also, what materials are available which might have desirable properties?

4. Device conditioning

Device conditioning, i.e., performance as a function of number of shots must be examined. This normally degrades to an equilibrium value after a certain number of shots, and is the

result of changes in the scattering processes leading to lower ionization rates and higher on-state voltage.

AVALANCHE TRANSISTORS

Background

The avalanche transistor is a bipolar, electrically triggerable, closing switch. Its present range of characteristics is

Voltage 200 - 1000 V

Current 10 - 30 A ($1-3 \times 10^3$ A/cm² average, but filamentary)

Rise time 1 - 5 ns.

The range of its characteristics which will be feasible in two to three years is

Voltage ~ 10 KV

Current >1000 A

Rise time 0.1 - 1 ns

10 KV was a limit believed by the group to be a practical maximum number for silicon junction devices, based on considerations of leakage current, thermal runaway, etc., and is subject to question. Current conduction is filamentary and the specification assumes that some multifilament technique for current conduction is developed. In fact, if internal paralleling of device elements is developed in this way, orders of magnitude improvement in current handling are possible.

Physical Principles

The principle of operation is believed to be second breakdown, that is, injected current modifies internal electric field, causing avalanche multiplication and creation of an electron-hole

plasma which in turn collapses the field (voltage) across the device. Once current flow begins, it appears to constrict to a narrow channel.

The avalanche transistor is a bipolar, double-diffused, epitaxial device. Its blocking voltage is approximately proportional to the thickness of the n-region (~ 20 V/ μ m). A lightly doped epitaxial layer appears to be the key to reliable triggering into second breakdown. The sustaining voltage is ~ 10 -20% of the blocking voltage. Its rise time is determined by the velocity of the ionization wave, which can be fast (100 ps) or slow ($>$ ns).

Conclusions

The avalanche transistor is promising as a fast, closing switch. It has desirable electrical triggering and a desirable fast rise time. However, its filamentary current flow and high sustaining voltage are undesirable.

Certain features of its operation are not well-understood: rise time, involving plasma formation dynamics and ionization wave velocity; delay time; and jitter. Thermal management is a critical issue in all power applications, and more information is required about thermal coefficients and cooling; power dissipation (duty cycle); slow thermal degradation over time; and leakage currents relative to blocking voltage, relative to thermal runaway.

Research Recommendations

If this device is to be useful for pulsed power, techniques for scaling up to higher current must be developed. Further research should be concentrated in the following areas.

1. Physics of the final state (highest priority)
 - a. Filament formation
 - b. Filament expansion and contraction dynamics
 - c. Densities and instabilities of plasma
 - d. Forcing multichanneling by ballasting
 - i. Ballasting techniques resistor materials, base or emitter or both.
 - ii. Uniformity of materials
 - iii. Uniformity of current distribution possible among the various device elements.
 - iv. Multichanneling effects on rise time and jitter
2. On-state, sustaining voltage (lower priority)
 - a. Relation of sustaining voltage to plasma maintenance
 - b. Can altering device geometry or structure help?
 - c. Relationship to processing parameters (doping, thickness, defect densities) and carrier lifetime.

FIELD EFFECT TRANSISTORSBackground

Field effect transistors (FETs) are three-terminal solid state devices in which current flow through the device occurs by the field directed drift of majority carriers. Majority carrier current flowing from the source to the drain is controlled by a voltage applied to a gate electrode which electrically influences

carrier concentration and electric potential in the region between the source and the drain. FETs made with a vertical structure are the most likely candidates for high power switching applications since they are capable of high current densities, blocking voltages approaching that of bulk material, and high power densities (particularly in common drain configurations).

Recently, a new class of devices, the vertical junction FET (VJFET), has begun to attract attention because of its exceptional performance. Non-saturating triode-like I-V characteristics have been observed in short-channel silicon VJFETs called static induction transistors, or SITs, and in GaAs VJFETs. These devices are very fast, capable of switching from an open switch condition to a closed switch condition with low on-resistance ($< 1 \Omega$) in less than 1 ns. Therefore, these devices can offer significant power switching capabilities for pulsed power applications. The present state-of-the-art performance achievable with VJFETs is presented below. (These data are based on devices available from Tohoku Metal Inc. and Mitsubishi Inc.)

| <u>Device</u> | <u>V_B</u> | <u>t_{switch}</u> | <u>R_{ON} / area</u> | <u>J_{peak}</u> | <u>I_{peak}</u> |
|--------------------------|-------------------------|--------------------------------|--|------------------------------|------------------------------|
| 25K183 (Tohoku Metal) | 800 V | 250 ns | .4 Ω/cm^2 | 30 A/ cm^2 | 60 A |
| MF 175 (Mitsubishi) | 80 V | 0.4 ns | .4 Ω/cm^2 | 60 A/ cm^2 | 8 A |

Physical Principles

On resistance.

A high voltage FET is a majority carrier device in which the conduction properties are determined by the doping and thickness

of the substrate needed to support the blocking voltage required, and by the mobility of the majority carrier. The on-resistance is given by

$$R = \frac{W}{q\mu N}, \quad (10)$$

where q is the electronic charge, μ is the carrier mobility, N is the background carrier concentration, and W is the thickness of the active portion of the drain region where the voltage is supported. In terms of the breakdown voltage, V_B , W and N can be expressed as

$$W = \frac{2V_B}{\epsilon E_C} \quad (11)$$

and

$$N = \frac{\epsilon E_C^2}{2qV_B} \quad (12)$$

where E_C is the electric field at breakdown. Combining equation 10, 11 and 12, the on resistance can be expressed as

$$R = \frac{4V_B^2}{\epsilon \mu E_C^3} \quad . \quad (13)$$

For a given material, where to first order E_C , ϵ , and μ are constants, the on resistance goes up as the square of the breakdown voltage, indicating that high voltage FETs will be increasingly at a disadvantage compared to SCRs, which scale as the square root of the breakdown voltage. However, this equation

also indicates that materials which have a high mobility and breakdown field offer the potential of having a low on resistance.

Control.

Field effect transistors are controlled either by a junction gate (JFETs), a metal Schottky gate (MESFETs), or insulating gates (MISFETs). Both the JFETs and MESFETs are normally on devices which require a voltage to turn the device off (by reverse biasing the gate relative to the source and depleting the channel of carriers). The MISFET is generally a normally off device in which current flow is prevented by the presence of a region of conductivity type opposite to the substrate, between the source and drain. The device is turned on by creating a conducting channel across this region using charge attracted to the surface by an electric field established by a gate-to-source voltage of appropriate polarity. All three device types are controlled by charging and discharging a gate capacitance; once the device is on, no additional gate current is required.

All FET devices are inherently opening as well as closing switches and equally fast in either regime. They are also inherently very fast, because no charge need be injected into or removed from the bulk of the device to turn it on or off; this is in contrast to bipolar devices. The ultimate speed of the device is determined by the resistance in the gate circuit and the size of the gate-to-source capacitance (this capacitance limits the speed with which the channel can be depleted in the case of the JFET or MESFET, or the rate with which the charge in the surface

channel can be added or removed for a MISFET). Speeds as fast as 500 psec should be possible, particularly in GaAs.

Choice of Materials

The two most attractive materials for a high voltage FET are silicon and gallium arsenide. Silicon FETs can be JFETs, MESFETs, or MISFETs, and are most commonly MISFETs. In GaAs, only JFETs and MESFETs are at present possible. The major advantage silicon has at this time is the advanced state of its processing technology relative to GaAs; high voltage devices up to 1000 V and 5 A (continuous) have been built.

However, GaAs offers several significant potential advantages relative to silicon. The first is that electron mobility in GaAs is a factor of six higher than in silicon, and the second is that the GaAs bandgap is 30% wider than the gap in silicon. The significance of the latter is that the peak field at breakdown scales with the bandgap, with the result that the on resistance of GaAs at a given blocking voltage can be expected to be a factor of two smaller than of silicon on the basis of this factor alone (inasmuch as the on resistance scales as the cube of the peak breakdown field). When this effect is added to the factor of six improvement in mobility, the on resistance of GaAs can be expected to be a factor of twelve lower than of silicon at room temperature. The factor increases to 16 at higher temperatures (150 °C). Also, because of the large band gap, GaAs will have a higher temperature capability, easily 300 °C, whereas silicon will be difficult to operate over 200 °C.

Also, GaAs will offer substantially higher speed possibilities compared to Si, since the parasitic gate resistance will be reduced the same factor of twelve. For devices of the same on resistance, the capacitance of GaAs will be an order of magnitude smaller because it will be a factor of twelve smaller in size.

Expected Performance in Pulse Applications

The performance of GaAs and silicon FETs may be compared in terms of current density:

| <u>1 KV blocking and 40 V forward drop</u> | | <u>10 KV blocking and 40 V forward drop</u> | |
|--|--------------------------|---|------------------------|
| GaAs | 10^3 A/cm ² | | 10 A/cm ² |
| Si | 10^2 A/cm ² | | 1 A/cm ² |

The gate control currents for switching in both devices will be 0.1 A/cm²s, where the actual current will depend on the switching speed. For example, at 1 ns switching speed, the gate currents are 100 A/cm², for which a 1 KV GaAs has a gain of 10 and a 1 KV silicon FET has a gain of unity.

Scalability and Present Performance

It is possible at this time to fabricate silicon FETs, as large as 7.5 mm X 7.5 mm, which will block 1 kV. Recent work has shown that high voltage (150 V) GaAs FETs can also be fabricated. In the near term, it is expected that GaAs devices with 1000 V capability and the same areas as those in silicon will be possible. In both cases, it is expected that devices as large as 1 cm² will be possible within five years. In the longer term, it

is likely that JFET devices with areas of 10 cm^2 will be possible in either silicon or GaAs. It is not known, however, whether insulated gate devices of either material will be possible with this area because of the problems of making defect free insulating gate capacitors.

Devices with voltages higher than 10 KV are not likely because of limitations in both materials (low switching gains and high on resistance). In all cases, the advanced nature of silicon processing will make it easier to fabricate larger area devices, but it is expected that, because of the rapid progress being made in GaAs technology, similar area devices in this material will be available within several years.

Research Recommendations

Due to the extremely high speed, electrically gated switching possible with VJFET devices, and the possibility of providing fast opening and closing operation, it is recommended that research be directed toward the better understanding and development of these devices, and that programs be established to investigate both silicon and GaAs as materials for pulse power applications. Specifically, programs aimed at fabricating 1000 V, 20 A, FETs, with 1 nsec switching speed, should be considered. At these currents and voltages, it is likely that the devices will be useful in pulse radar applications, and will serve as basic units for feasibility studies of their high power applicability.

PIN (OR [DI]²) DIODEBackground

The term PIN diode refers to a device with hole injection (P) from one electrode and electron injection (N) from another into a channel region, which is essentially intrinsic (I) in resistivity. These particular PIN devices (not yet commercially available) also contain deep impurities which provide the basis of operation. Hence, they are referred to as (DI)², that is, double injection, deep impurity. Recently, such devices have been built using conventional planar silicon technology, with a variety of practical gating schemes. These gating schemes result in a family of semiconductor switches, transducers, and detectors.

These devices employ bulk, and not junction effects. The electrodes play no fundamental role, so long as they provide an unlimited supply of charge. The P⁺ and N⁺ regions are degenerately doped merely to make good ohmic contact. Operation begins with high level injection, primarily of electrons, because negatively charged deep traps provide a recombination barrier for holes. The off state is governed by the simple ohmic resistance of the material (2.5×10^5 ohm cm in Si) and ultimately by the electron space charge, as in a vacuum tube. Switching occurs when the injected holes sufficiently depopulate (neutralize) the negative traps and allow rapid transit of holes across the material and a neutralization of the negative space charge. This leads to S-type switching.

Gating schemes include light gating (light neutralizes the traps), injection gating (injected holes neutralize traps), and voltage gating through MOS gates (which alters the trapped charge and the space charge). By manipulating a combination of gate characteristics, the blocking voltage can be increased or decreased, yielding current or voltage amplification. Also, the holding voltage can be electrically controlled by MOS or injection gating to obtain active turn-off. At cryogenic temperatures (LN_2) in silicon, photo-induced turn-on and turn-off are possible. Turn-on can be extended to room temperature, but turn-off requires a higher bandgap material at room temperature.

Gates can control the turn-on delay or dwell time. The switching time (closing) will remain relatively constant. The shortest rise times and fall times in present devices are in the range of 100 ns. Most recent work has concentrated on gold as the deep level in silicon. Other deep impurities which introduce deep traps have been shown to provide S-type switching, and GaAs devices using Chromium and Oxygen as the active deep impurities are possible.

Physical Principles

In the gateless (DI)² diode, switching occurs when the applied voltage exceeds a threshold voltage, V_T . This happens when the hole transit time equals the off state hole lifetime. A very short hole lifetime, τ_h , results in a high value of V_T and also a short transit time at the switching point.

For gated switching, the switching time can be slightly shorter than the hole lifetime ($< 10^{-8}$ s). Here the gate can be

biased initially near the switching point. The ultimate switching speed is probably limited to near the minimum hole lifetime, which depends upon the type and nature of the deep impurity. The delay time in turn-on after gating is depends on the hole trap fill time. The gating can be any combination of optical, current (injection) or voltage (MOS) gating. Once the device is in the high injection on state, the hole lifetime changes from the short τ_h off state value to a longer $\tau_h = \tau_e = \tau$, which is just the steady-state lifetime.

The speed of the fall time is inherently more limited than the rise time. Fall time is controlled by trap equilibration; it can, in principle, be extremely fast. A great variety of deep impurities is available for study, with a various of trapping cross-sections and locations within the gap. The shortest fall time would probably be obtained with a direct bandgap material, such as GaAs.

Voltage Scaling

The blocking voltage, V_T , is dependent upon the square of the channel length, L , between the anode and cathode:

$$V_T = CL^2, \quad (14)$$

where C is a constant for a given material, depending upon trapping cross-section, thermal velocity, trap concentration, and hole mobility. This dependence has been experimentally verified up to a kilovolt (at a channel length of about 10 to 15 mils). Higher voltages (up to 50 KV) are being investigated at the present time. The limiting value of V_T is determined by bulk avalanche. The multiplicative constant in equation 14 can be

scaled by the trap concentration, etc., to increase V_T until this fundamental limit is reached. 50 to 100 KV is probably the practical upper limit, however, for Si and GaAs in a single device.

The question of jitter needs to be addressed. It would likely be limited only by heating effects, assuming that time is available between switching for full trap equilibration.

Current Scaling

In the on state, conduction is by way of filamentary plasma (essentially neutral). The current density in this plasma has been estimated to be as high as 10^6 to 10^7 A/cm². Average current densities in small devices with a channel length of about 0.1 mm, however, are in the range of 3×10^2 to 3×10^3 A/cm².

In principle, current scaling can be achieved by widening the electrodes. However, the on state holding voltage, V_H , of the plasma is dependent upon the channel length. The plasma will initially be struck at the point where the microscopic interelectrode spacing is a minimum or where the field concentration is highest (as with sharp cornered electrodes). Slight protrusions (which can be shaped for field control) within the electrode can provide preferential locations for plasma breakdown to occur. This would spread out the filaments in a predictable manner, preventing hot spots and generally increasing the current handling capability. Of course, if the interelectrode spacings of these "bumps" on the electrodes are not precisely equal, there will be slight discontinuities in the vertical plasma region of the on state. Current scaling in avalanche transistors may require similar techniques.

Gating

The number of gating schemes for (DI)² devices exceeds the possibilities now available in other devices. However, only optical gating will be considered here. Optical gating usually involves the creation of hole-electron pairs by photons with energy equal to or greater than the bandgap energy. In the (DI)² device, optical gating is obtained by extrinsic ionization (or deionization) of the active impurity level. Past work has emphasized electrically gated devices; in fast, high voltage switching, however, optical triggering may be preferred.

The time response of optical gating is determined by the product of the optical capture cross-section and the photon flux. Multiple internal reflection techniques can improve this. Optical gating may require low light levels to unlatch the onset of the plasma, which results from injection, not the optically created charge. Photon capture is a maximum at an energy in the range of 1.5 to 1.7 times the separation of the deep level from the appropriate band edge. This light is deeply penetrating and especially suitable for large, high power devices. From the standpoint of fast switching it would be desirable to illuminate the channel completely in order to affect all the charge states most rapidly.

These devices can also perform as extrinsic photoconductors. An infrared photon can excite a trapped electron from deep levels into the conduction band, or ionize a neutral deep level hole into the valence band. The free carriers thus produced can provide conduction simultaneously throughout the device volume.

Conclusions

(DI)² devices are very versatile and offer a potential for pulsed power switching. They can provide either S-type or N-type switching and can be gated by a third terminal or with sub-bandgap light. However, research is necessary to determine whether these devices can be scaled to high power and to high speed. Rise times as short as 100 nanoseconds have been achieved, but fundamental limits to rise time need to be investigated. Delay can be gate controlled, but its change with scaling needs to be determined. Jitter has not been specifically addressed in past work and needs study.

Current is filamentary, which is a disadvantage, in general, for power switching. Control of current flow needs to be investigated. Finally, the fundamentally different switching mechanisms under a variety of gating schemes should be studied for possible applications.

Research Recommendations

1. Devices should be scaled to multi-KV, KA range to determine scaling effects on speed, voltage, current density, and delay.
2. Switching efficiency for light gating should be assessed and compared to photoconductors and avalanche photoconductors.

ZnO VARISTORSBackground

A varistor is a two terminal, nonlinear, voltage controlled device exhibiting a high resistance standby state (on the order of 10^9 Ω), that can be quickly switched to a very low resistance

on-state (on the order of several ohms), with an I-V characteristic similar to back-to-back Zener diodes. Although the transition time involved is dependent upon the rise time of the voltage waveform, experiments have demonstrated that varistor rise times are less than or equal to 50 ps. Parasitics associated with package design can increase this rise time to ns. The fast rise time is attributable to tunneling, which is the primary conduction mechanism of ZnO varistors.

The power handling capabilities of ZnO varistors is quite well-known. Commercial varistors are already available for use in simultaneous megavolt and kiloampere applications. For example, many power utilities incorporate varistors for use in lightning protection for long lines. The ability of ZnO varistors to channel energy makes them very suitable protection devices for sensitive equipment that could experience severe electrical overstresses.

The only limitation identified in varistor usage is heat dissipation. Like other devices, continued operation (for seconds at a time) may result in heat buildup and degradation in its power handling capabilities. At elevated ambient temperatures (100 °C and above), a varistor will continue to operate, but only at the expense of advanced aging effects. These effects are exhibited as an increase in leakage current (tens of μ A to hundreds of μ A) and a decrease in the maximum number of overstresses the device can safely handle.

In pulse power switching applications, varistors do not have an externally controllable switching capability, and their use as

switches for pulsed power is doubtful. They can be employed as photoconductors triggered by X-ray or UV illumination, but this is not an optimum use of the material. Because of their very high speed, high voltage scalability, and high current scalability, they are attractive as protective devices for solid state switches.

Conclusions

ZnO varistors do not possess a third terminal control, nor do they have a switching current-voltage characteristic. However, they possess very fast rise times (<1 ns). They can handle low to extremely high power, with no scaling problems. ZnO varistors provide excellent protection from electrical over-stresses.

REFERENCES

Photoconductors

1. J. M. Dorkel and Ph. Leturcq, "Carrier mobilities in silicon semi-empirically related to temperature, doping, and injection level," Solid State Electronics 24, 821 (1981).
2. D. H. Auston and P. R. Smith, "Picosecond optical electronics for high-speed instrumentation," Laser Focus April, 1982, page 89 (and references therein).
3. G. Mourou, W. Knox, and S. Williamson, "Picosecond high-power switching and applications," Laser Focus April, 1982, page 97 (and references therein).
4. R. B. Hammond, Editor, Proceedings of the Workshop on Picosecond Photoconductors and Applications Los Alamos National Laboratory, August, 1982.
5. W. C. Nunnally and R. B. Hammond, "Optoelectronic Switches for Pulsed Power Applications," in Picosecond Optoelectronic Switches edited by C. H. Lee, to be published by Academic Press, 1983.

Avalanche Photoconductors

1. S. Williamson, G. F. Albrecht, and G. Mourou, "Laser triggered Cr:GaAs HV sparkgap with high trigger sensitivity," *Review of Scientific Instruments* 53, 867 (1982).

Avalanche Transistors

1. R. L. Davies, F. E. Gentry, "Control of electric field at the surface of p-n junctions," *IEEE Trans. El. Dev.*, 31 3 (1964).
2. L. E. Gavrilov, "The application of avalanche triodes in nuclear electronics circuits (review), *Pribory i Tekhnika Eksperimenta*, No. 6, pp. 5-17 (Nov.-Dec. 1973).
3. V. A. K. Temple, M. S. Adler, "Calculations of the diffusion curvature related avalanche breakdown in high voltage planar p-n junctions, *IEEE Trans. El. Dev.* ED-22, 910, (1975).
4. T. Matsushita *et al.*, "Highly reliable high-voltage transistors by use of the SIPOS process, *IEEE Trans. El. Dev.* ED-23, 826 (1976)
5. Keiichi Kcyanagi, Kunio Hane, Tokio Suzuki, "Boundary conditions between current mode and thermal mode second breakdown in epitaxial planar transistor," *IEEE Trans. El. Dev.* ED-24, 672 (June 1977).
6. J. E. Carroll and P. J. Probert, "Current/voltage characteristics of transistors operating in current mode second breakdown," *IEE Journal of Solid State and Electron Devices*, 3, 41 (1979).
7. I. V. Grekhov, A. F. Kardo-Sysoev, L. S. Kostina, "Breakdown Delay and Excitation of Ionization Waves in p-n Junctions," *Sov. Tech. Planar Letters*, 5, No. 8, pp. 394-400 (Aug. 1979).
8. I. V. Grekhov, A. F. Kardo-Sysoev, L. S. Kostina, S. V. Shenderey, "High-Power Subnanosecond Switch," *Electronics Letters*, 17, 422 (1981).
9. F. A. Selim, "High-voltage, large-area planar devices," *IEEE Electron Devices Letters*, EDL-2, 219 (1981).
10. J. C. Koo, M. D. Pocha, "Physical Modeling of Avalanche Transistor Switching," UCRL-53303, Lawrence Livermore Laboratory, August 12, 1982.

Field Effect Transistors

1. J-I. Nishizawa, T. Terasakim and J. Shibata, "Field-effect transistor *versus* analog transistor (static induction transistor)," *IEEE Transactions on Electron Devices* ED-22, 185 (1975).

2. B. J. Baliga, M. S. Adler, and D. W. Oliver, "Optimum semiconductors for power field-effect transistors," *IEEE Electron Device Letters* EDL-2, 162 (1981).
3. B. J. Baliga, "Power Semiconductors," *IEEE Spectrum*, December, 1981.
4. R. P. Love, P. V. Gray, and M. S. Adler, "A large area power MOSFET designed for low conduction losses," *Technical Digest of the International Electron Devices Meeting*, p. 481, 1981.
5. M. S. Adler and S. R. Westbrook, "Power semiconductor switching devices: a comparison based on inductive switching," *IEEE Trans. El. Dev.* ED-29, 947 (1982).
6. P. M. Campbell, R. S. Ehle, P. V. Gray, and B. J. Baliga, "150 volt vertical channel GaAs FET," *Technical Digest of the International Electron Devices Meeting*, p. 258, 1982.

(DI)² Diodes

1. H. T. Henderson and K. L. Ashley, *Physical Review* 186, 811 (1969).
2. H. T. Henderson and K. L. Ashley, *Proc. IEEE* 57, 1677 (1969).
3. Murray A. Lampert and Peter Mark, *Current Injection in Solids*, Academic Press (1970).
4. H. T. Henderson, K. L. Ashley, and M. K. L. Shen, *Physical Review* B6, 4079 (1972).
5. H. T. Henderson, J. Asbrock, and A. Kapour, *Technical Digest of the International Electron Devices Meeting*, p. 680 (1979).
6. V. Mantha and H. T. Henderson, *Solid State Elec.* 23, 275 (1980).
7. S-B. Ko and H. T. Henderson, *IEEE Trans. on El. Dev.* ED-27, 62 (1980).
8. A. Kapour and H. T. Henderson, *IEEE Trans. on Elec. Devices* ED-27, 1268 (1980), ED-28, 275 (1981), ED-28, 557 (1981).

ZnO Varistors

1. M. Smith, et al., *General Electric Transient Voltage Suppression Manual*, Third Edition, 1982.

STATE TRANSITION SWITCHES

Ihor M. Vitkovitsky, Chairman

INTRODUCTION

A variety of materials is available for the development of solid state switching for pulsed power applications. This group has considered materials which changes conductivity as a result of phase transitions or other changes of state. Change-of-state-materials have a wider range of applications and broader scope of mechanisms available than other types, such as semiconductors. It is the construction of the group that these materials provide a highly promising avenue for developing reusable opening switches (for inductive storage) and closing switches with specialized characteristics, such as extremely fast rise time.

The best example of the state change switching is the exploding fuse,⁽¹⁾ using metals such as aluminum. As a result of ohmic heating, the metal undergoes melting and vaporization, producing a conductivity change of about a factor of 100. Figure 1 illustrates, as an example of the relevant quantities associated with fuse operation, the dependence on deposited energy of the conductivity, σ , of aluminum. While this type of phase transition has been used for many years as a method of current interruption and current commutation, there are a number of factors that limit the use of fuses in pulsed power systems. Some of the more important constraints are small change in resistivity (i.e., by about two orders of magnitude); high dissipation of energy (and problems resulting from the explosive pres-

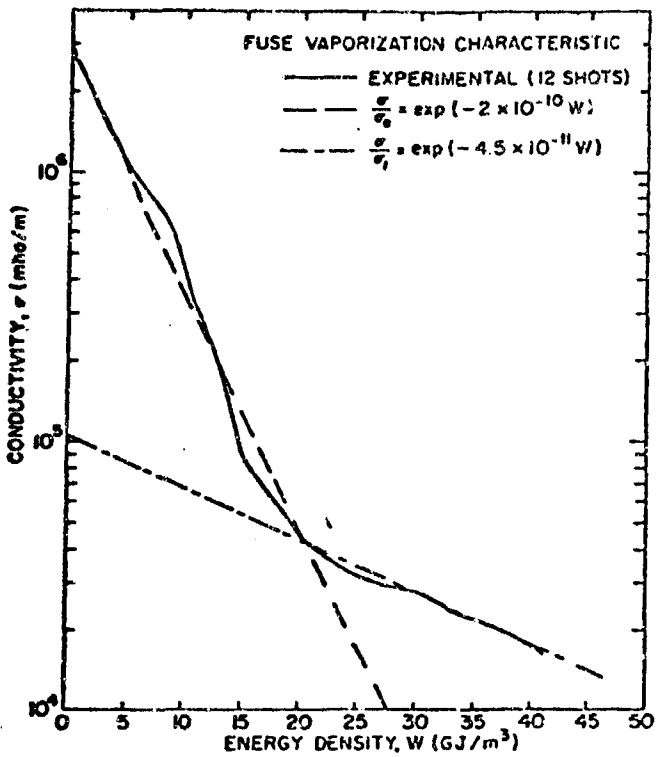


Figure 1. Dependence of the conductivity of the aluminum fuse on the energy dissipated in the fuse (reference 1).

sures affecting neighboring structures); limited rise-time; and the need to replace a fuse after each discharge.

Materials which change conductivity at lower (non-vaporizing) temperatures, following laser irradiation, or as a result of other controlling factors (e.g., externally applied magnetic fields), have recently become available on a commercial or limited laboratory scale. Their properties have been studied and they have been used in applications associated with circuit control (including large current surge arrestors). They have not been used in pulsed power applications to any significant degree.

There are some applications that can evolve with medium term research and development. Long term research is likely to lead to solutions that would eliminate all of the constraints associated with fuses as well as lead to advances in closing switch technology.

The major reasons for concluding that promising results will be realized as a consequence of an aggressive research program are the characteristics of some of the candidate materials already available commercially, and the possibility of the development of new materials with properties specifically engineered for pulsed power applications. These materials are characterized by having bulk conductivity or a multiplicity of conductive zones, and an attendant change in σ at low (non-melting) temperatures. Because their properties are often those of a metallic phase, very high power densities can be handled. Typically, the change in σ is several orders of magnitude (in contrast to a factor of 100 for fuses) as indicated for two materials in

figure 2. The materials may offer load sharing. These factors suggest that scaling is very flexible in terms of the variety of applications, and, to first order, the scaling is unlimited.

Potential concerns related to the application of the phase-transition materials in high power pulsers are such factors as mechanical integrity during and after switching, fabrication uniformity (e.g., affecting electric field distributions) and possible difficulties in connecting to the electrodes. Additionally, it is recognized that the technical base is weak and much less is known about the characteristics of these materials than of metallic fuses and semiconductor switches.

The main objectives of this group were to categorize the materials with the potential for pulsed power applications, provide (where known) their most important characteristics, and focus on the issues related to the development of viable switching devices.

BACKGROUND INFORMATION

Tables 1 and 2 provide an overview of the materials of interest to switching, and their properties. One category, ferromagnetics, is used for pulse shaping rather than switching. For that reason and because it is currently utilized in pulse power systems, it is not discussed below.

DISCUSSION

Allotropic Phase Transitions

Several oxides are known to undergo phase transitions at given critical temperatures. These transitions are characterized by a change from a non-conductive state to a highly conductive

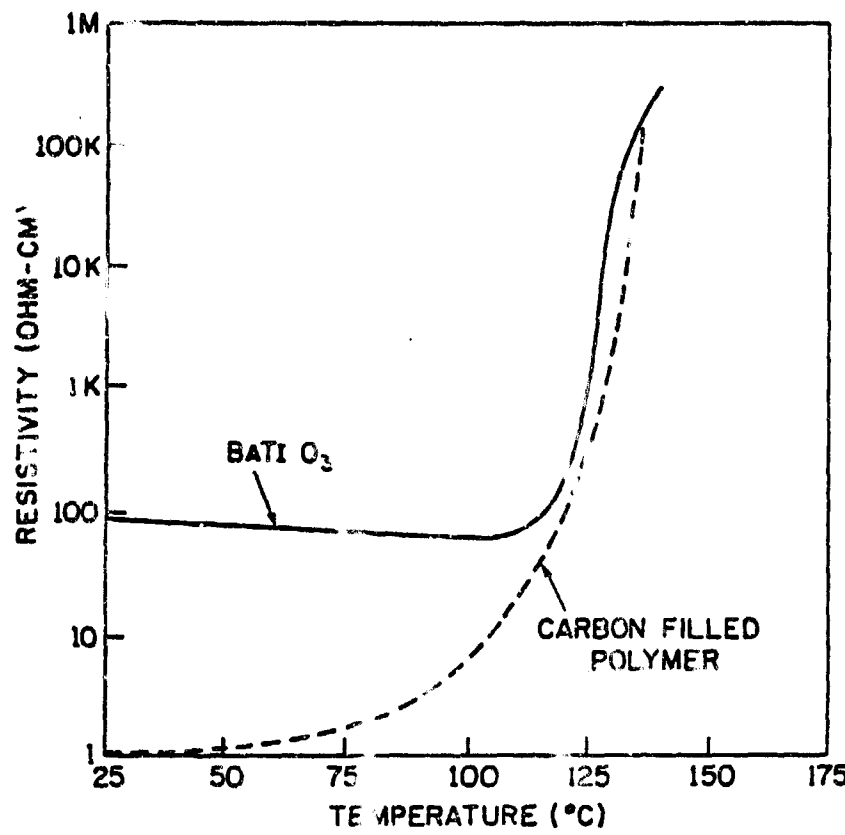


Figure 2. Dependence of the resistivity of BaTiO₃ and CFP on temperature (references 2 and 3).

Table 1. Categories of possible switching materials.

1. Metal-Insulator Transitions (e.g., V_2O_3).
 - a. Mechanically (pressure) driven.
 - b. Thermally driven.
2. Change of State Materials
 - a. Crystalline-to-amorphous transitions.
(e.g. carbon filled polyethylene material)
 - b. Crystalline-to-crystalline transitions
(e.g. $BaTiO_3$)
3. Polycrystalline Electron Tunneling Materials (e.g., varistors
(for closure)).
4. Magnetic Field Saturation of Ferromagnets
5. Materials with Superconducting to Normal Transitions.

Table 2. Candidate materials for solid state switches.

| Material | ρ for off-state | ρ/ρ_0 | Blocking Field | Trigger* Energy | Switching Time Limit | Type of trigger | Comments |
|---|----------------------------|------------------|-------------------------|----------------------|--|---|---|
| 1. Metal-insulator | $10^{-4} \Omega \text{cm}$ | $10^3 - 10^8$ | 10^6 V/cm | small | a) $1^2 R \mu\text{s}$ range b) Acoustic c) Laser pulse | a) $1^2 R$ heating b) Pressure c) Laser | Opening Small samples tested |
| a. Metal transition | | | | | | | OK in parallel Series requires load sharing |
| 2. Charge-off-state | | | | | | | Opening Potentially large number of materials are available has negative temp. coeff. |
| a. Carbon filled polyethylene | $1 \Omega \text{cm}$ | 10^4 | 20 KV/cm | $< 10\%$ | $10 \mu\text{s}$ | $1^2 R$ | |
| b. Ferroelectrics (e.g. BaTiO ₃) | $1-100 \Omega \text{cm}$ | 10^5 | $> 10 \text{ KV/cm}$ | small | $< 1 \text{ ns}$ | $1^2 R$ | |
| c. Solid-liquid | $10^{-5} \Omega \text{cm}$ | 10^{10} | 200 KV/cm | 100 J/cm^3 | ps | Laser | Closing |
| 3. Varistor | $0.1 \Omega \text{cm}$ | $10^6 - 10^{12}$ | $1-10 \text{ KV/cm}$ | a) Small b) Small | < 1 ns < 1 ns | a) Voltage b) Light | Closing Bulk scalable |
| 4. Magnetic | - | dt/dt | Configuration sensitive | Small | 10 ns | Saturation | Pulse shaping |
| 5. Superconducting | 0 | - | Same | - | 1 ns | Thermal pulse | Opening |

* Related to energy transferred by the switch.

state. Well-known examples are VO_2 and V_2O_3 , which have an insulator-to-semimetal transition. By varying chromium doping, the transition temperature can be varied from around room temperature to a few hundred degrees centigrade. VO_2 has a transition temperature typically at 65° C . Most work has been done with single crystals, which have an off-to-on resistivity ratio greater than 10^5 . The oxide, VO_2 , has a sharp transition which occurs in a few millidegrees. It undergoes a thermal transition whose speed depends on the excitation technique; ⁽⁴⁾ if electrically induced, the transition speed is faster than $1 \mu\text{s}$. The conductor-to-nonconductor transition, which would be used for operating switches, may also be induced by pressure, presumably in times of the order of $1 \mu\text{s}$.

One issue associated with exploitation of allotropic phase materials is that of making a large size polycrystalline body while preserving the high quality switching behavior of single crystal. The initial (cold) resistivity listed in Table 2 for a metal-insulator transition (M-I) material is that for single crystal V_2O_3 . However, it can be expected that processing into polycrystalline bulk material would not increase this value by large factors. The low resistivity and extremely narrow temperature range over which the transition occurs suggests that V_2O_3 is one of the more interesting materials to be developed for switching. Proper processing of polycrystalline bulk material may also preserve the high blocking voltages shown in Table 2 for single crystal oxides.

It should be noted that basic fabrication procedures, at least of single crystals, have been established, and the thermal transition in V_2O_3 has been already used in several applications. One sophisticated application of the high current density in the on state is to light modulation. An interdigitated structure of parallel conducting and non-conducting paths was fabricated and successfully tested.⁽⁵⁾ Rise time in this application is less than 1 μ s and current density in the conducting path is greater than 10^5 A/cm². Rise time can be considerably improved by laser switching, and because the transition involves a few millidegrees, recovery time is expected to be short.

Crystalline-Amorphous Polyethylene-Carbon Composites

The Naval Research Laboratory has shown⁽⁶⁾ that commercially available carbon-polyethylene composites have potential as turn-off switches. Although thermally triggered, these have demonstrated potentially useful responses (Table 2). The composites consist of conducting chains of carbon particles which are broken by the volume expansion (~2%) of the polyethylene matrix, due to a thermally induced crystalline-amorphous phase change. For this device to be useful, physical scalability, adequate tolerances for series load sharing, sufficiently long fatigue life, and overstress ability must be assured. It must also be established whether such composites can be improved by changing the form, type, and spatial distribution of the carbon (and hence also of the polyethylene). Other important issues are the possible use of other materials for either or both phases, and whether there are analogous systems that might be switched by different, e.g.,

electrical or magnetic, means. This switch is essentially a system of many microswitches, operated by limited expansions in the matrix. Thus, a basic question is whether composites consisting of conducting particles in non-conducting electrostrictive or magnetostrictive matrices could be made for high power electrical or magnetic switching.

Crystal-Crystal Phase Change

Reference 6 identifies commercially available PTC BaTiO₃ as a potential opening switch. Both thermally (I^2R derived) and electrically triggered switching appear practical; the latter possibly allowing useful repetition rates. Substantial work is needed to determine the suitability of this material for pulsed power uses. This includes reducing the on resistivity and demonstrating scalability, inasmuch as the commercial materials have been developed for very different ranges and types of applications than of interest here. Substantial composition processing studies are needed, with potentially important inputs from studies of grain boundary effects on conductivity and switching. There is also the importance of analogous systems, in addition to further development of BaTiO₃.

Laser-Induced Solid-Liquid Phase Transitions

Laser-induced solid-liquid transitions can be used for extremely rapid (relative to the mechanisms discussed above) opening switches. Annealing of a semiconductor by a laser induces a transition to a highly conducting liquid phase.⁽⁷⁾ This transition can be induced in less than 1 s with an appropriate short optical pulse.⁽⁸⁾ The resistivity of the material changes by a

factor of more than 10^{10} . After thermal excitation, the material cools down to the amorphous, polycrystalline or crystalline state in a few hundred ns. The threshold energy density required to produce the transition is about 0.2 J/cm^2 .

Varistors

Varistor polycrystalline materials have similar characteristics to those of back-to-back Zener diodes, but much greater current ($>10^5 \text{ A}$) and energy ($\sim 100 \text{ KJ}$) handling capability. They are used for pulse sharpening or clipping because of their very fast response ($<1 \text{ ns}$) and extreme nonlinearity. Varistors have the potential for switching using either light induced or electric field induced triggering. However, this application needs further development. Varistors are clearly useful as transient over-voltage protective devices, used in conjunction with other switching devices.

A new and potentially exciting development would be the incorporation of varistor granules internal to spark gaps. The varistor material serves to control and initiate the discharge by field grading and electron emission. This approach has a potential use for high voltage and high current switching with more control and reliability than that of a conventional spark gap.

Superconducting to Non-Superconducting Transitions

Switches based on transitions from a superconducting to a non-superconducting state have already been demonstrated. However, a key issue for their use for pulse power has been their very low off resistivity. Unless major increases can be obtained, this otherwise very attractive switch does not appear

practical for the needs of interest here. However, mechanically induced superconductivity, and especially granular superconductors, may offer orders of magnitude increases in off resistivity, and hence deserve further consideration.

CONCLUSIONS

A research program which would lead to development of materials with state transitions providing a means of switching high power pulses requires first, and foremost, determination of the basic physical limits of such materials. Maximum hold-off electrical fields and maximum current densities are not known for most of the candidate materials. While it is not unequivocally clear whether significant improvements can be made in those materials, they deserve considerable study because of their very high potential. The extent of the research required to demonstrate the feasibility of specific systems, such as V_2O_3 , or $BaTiO_3$, can vary widely, depending on the application and the status of the material. The broader issues of mechanisms of conduction and switching, processing science and technology, and the development of new and better materials should be addressed aggressively, while at the same time, work should be continued on known materials.

RESEARCH RECOMMENDATIONS

1. The relationship of resistivity in single crystals to that in polycrystalline structures should be determined. (Only small crystals of V_2O_3 have been studied.) The properties, relative to pulsed power use, of materials other than V_2O_3 should be studied. Polycrystalline ceramic materials in bulk

quantities should be developed. Uniformity and mechanical integrity should be examined.

2. What is the relationship between resistivity, and carbon type in carbon-filled polyethylene materials? Can other fillings, such as metal powders, be used? Scalability to thicker sheets should be examined. Degradation problems should be identified.
3. The on resistivity of BaTiO_3 should be lowered, and the possibility of increased hold-off field examined. Thermal-mechanical fatigue and fracture should be studied. Deeper penetration of laser light into the bulk is required.
4. Switching kinetics of varistors should be studied (optical and other triggers should be developed).
5. Higher power density magnetic materials, more uniform for improved jitter, are required.
6. New superconducting systems, such as granular superconductors, should be explored to determine whether suitably high off resistivities can be obtained.

REFERENCES

1. There is an extensive literature dealing with exploding wires as fuses. A typical reference, describing recent work, is by J. Salge *et al.*, "Circuit Breaking by Exploding Wires in Magnetic Energy Storage Systems," Proc. of the International Conference on Energy Storage, Compression and Switching, Torino, Italy, Plenum Press, N.Y. 1976.
2. The data dealing with the temperature dependence of ceramics (BaTiO_3) are from work by M. Kahn, "Effect of Heat Treatment on the PTCR Anomaly in Semiconducting Barium Titanate," Ceramic Bulletin, 676 (1971).
3. Carbon-filled polymer data describing the electrical performance are obtained from work by F. A. Doljak, "Polyswitch PTC devices - a new low resistance conductive polymers-based PTC

device for overcurrent protection," IEEE Transactions on Components, Hybrids and Manufacturing Technology CHMT-4, Dec., 1981.

4. J. B. McChesney and H. T. Guggenheim, J. Phys. Chem. of Solids 30, 225 (1969).
5. J. Fair, H. Fetterman, S. Bachaner, P. Zavrotsky, C. Parker, Appl. Phys. Lett. 31, 11 (1977).
6. R. Ford and I. M. Vitkovitsky, this report.
7. T. E. Farber, Theory of Liquid Metals, Cambridge Univ. Press, Cambridge, U.K. (1972).
8. B. L. Lew, et al., Appl. Phys. Lett. 34, 864 (1979).

APPLICATIONS RELATED ISSUES

James P. O'Loughlin, Chairman

INTRODUCTION

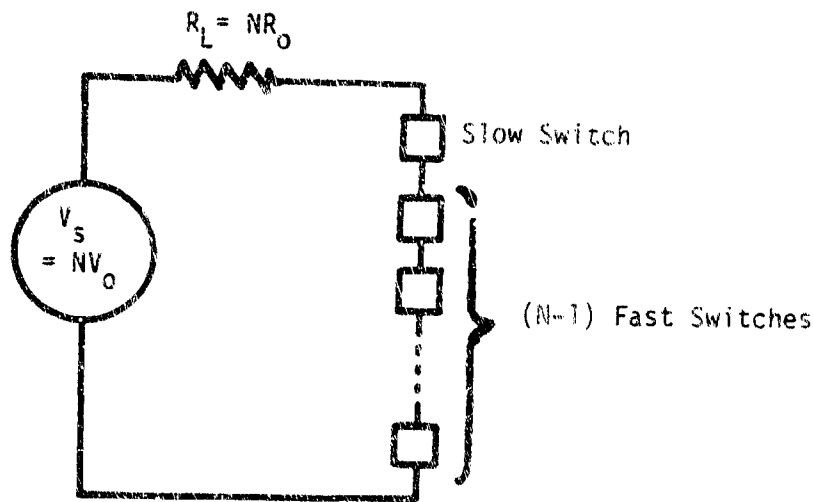
The objective of this group was to study and report upon application oriented problems of solid state switches and, in particular, the influence of device characteristics on the performance of switch arrays. Additional objectives were the identification of specific problem areas, and recommendation for the solutions of problems related to solid state switching applications. Because of the limited time available it was necessary to restrict the attention of the committee to a particular problem in the application of solid state switches. After a brief survey of possible applications, the topic of switch arrays was selected.

Existing devices have limited individual ratings and must be assembled in arrays to meet the required switching functions in medium and high power applications. Since medium and high power applications are of the greatest general interest, the problems associated with arrays have a wide range of practical application and relate to all types of devices. At the present time, the most impressive application employing arrays is the power inverter used in the electric power industry for DC power transmission and for interconnecting asynchronous AC grids. These inverters use SCRs, and the array problems have been well-addressed in this low frequency case. The SCR was therefore adopted as a typical device for the discussion of array problems associated

with faster high power pulse applications. However, bulk optically controlled photoconductive devices were also considered.

The most important considerations related to arrays are uniform voltage and current distributions, degradation of switching speed and efficiency due to compensating networks, triggering methods, minimum total element count, reliability, and fault tolerance. In the ideal situation, all elements of an array would be identical and their characteristics would track exactly at all times. If this were the case, voltage and current sharing would be assured and, just as important, the speed of the array would be the same as the speed of the individual elements. The fact that real elements are not identical requires the use of compensating circuits to equalize the differences, or as usually implemented, to degrade the characteristics of the elements to the extent that their individual differences are made negligible, the net result being an acceptably uniform array but with degraded switching time. (One obvious procedure for improving switch performance would be to improve discrete device reproducibility in manufacturing, or by better part selection.)

Solid state devices are extremely intolerant to overvoltage stress; this is the most difficult problem with series arrays. A simplified model of a series stack is shown in figure 1, where a string of N elements are all identical except for one which has a slower switching speed and longer delay. The overvoltage stress on the slow element is shown in figure 2 as a function of the speed mismatch and the total number of elements. It is important to note that mismatched characteristics in the order of 10% have



Slow Switch: $R_s(t) = R_x \exp[-\alpha_s(t-\delta/\alpha_f)]$;

Fast Switch: $R_f(t) = R_x \exp(-\alpha_f t)$;

Array Switching Time: $t_A = (1/\alpha_f) \ln \left[\frac{R_0/R_x}{e-1} \right]$;

The voltage (normalized) across the Slow Switch is:

$$N \exp(-\alpha_s t + \eta \delta)$$

$$V_{sn} = \frac{N(R_0/R_x) + \exp(-\alpha_s t + \eta \delta) + (N-1) \exp(-\alpha_f t)}{N(R_0/R_x) + \exp(-\alpha_s t + \eta \delta) + (N-1) \exp(-\alpha_f t)}$$

This voltage is a maximum when:

$$t_m = (1/\alpha_f) \ln \left[\frac{(1-\eta)(N-1)}{\eta N(R_0/R_x)} \right]$$

Where η = mismatch in switching speeds = α_s/α_f

δ = fractional delay mismatch = $\alpha_f \Delta t$.

Figure 1. Simplified model of a series array.

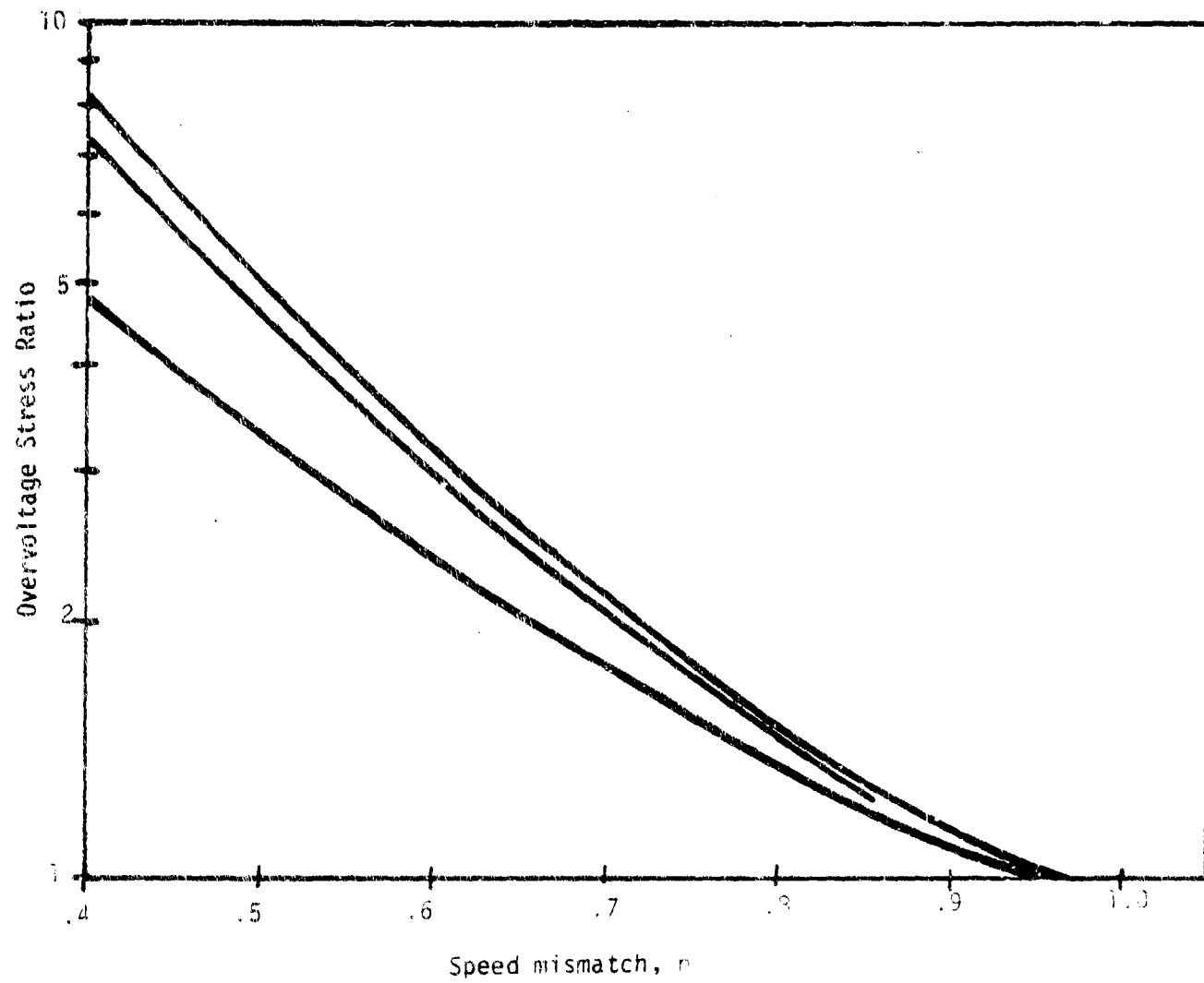
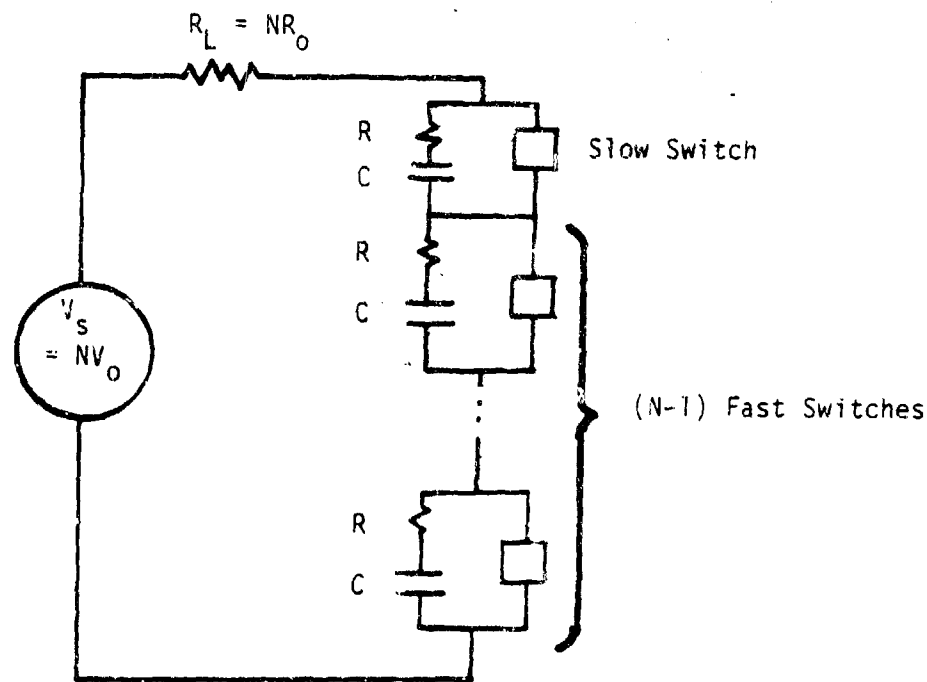


Figure 2. Overvoltage stress dependence on mismatch in speed and number of elements in the array.

significant penalties and typically uncompensated device uniformity is in the order of 50%. Consequently, arrays must be generously compensated and speed must suffer associated degradation. The simplest compensation circuit is an R-C network as shown in figure 3. The effect of this compensation, adjusted for a ten-to-one stress reduction, on the array switching time, is shown in figure 4 for element mismatches of 0.7 and 0.85. (These calculations assume that surface area and heat sinking in high average power applications do not force compromises relating to switching speed.)

In the case of power inverter arrays, the overall result is acceptable because of the relatively low switching speed requirement. In applications requiring array speeds which are close to the device speed, the nonuniformity of the device characteristics, coupled with the compensation penalty, can exclude the use of solid state arrays. The non-uniformity problem is further aggravated by the drift of characteristics with temperature and with age. The age drift is particularly important when considering long term reliability. Parallel operation of semiconductor devices in arrays is usually not a problem with respect to achieving balanced current distribution. The forward characteristics are generally very uniform, and at pulse current levels, the coefficient of resistance is positive, which acts as a self-stabilizing influence.

It is desirable to have the minimum number of components in any array, principally for economic and space reasons. The reliability of an array does not change with the number of elements,



The stress will be reduced by a factor K if

$$R = R_0/2X,$$

$$C = (2X/\eta_f R_0) \ln \left[\frac{(1-\eta)(N-1)}{\eta(R_0/R_X)} \right]$$

Figure 3. Simple compensation network.

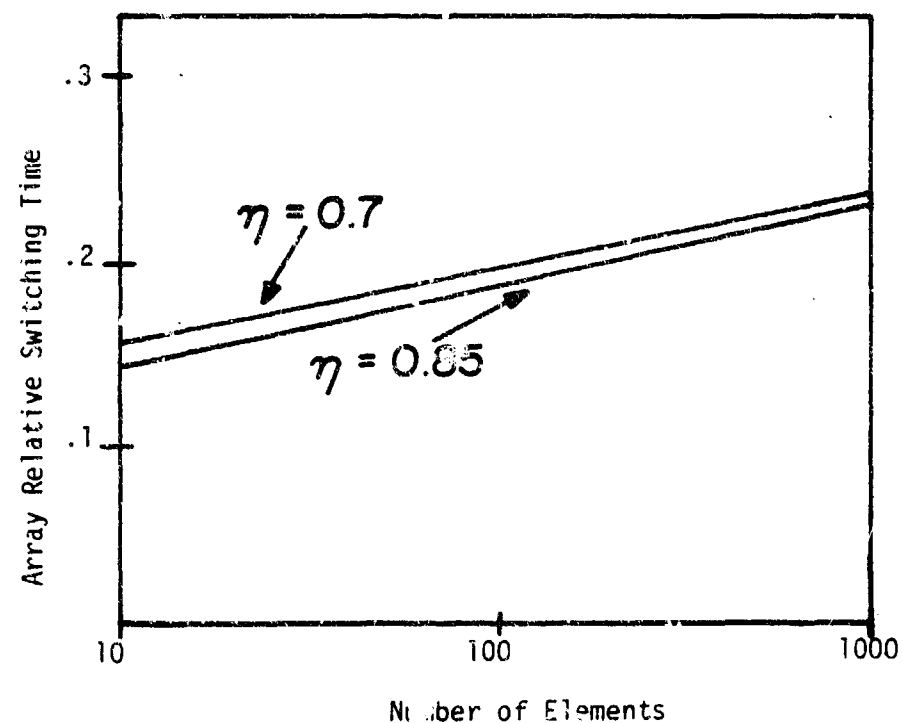


Figure 4. Relative switching time of an array vs. the number of elements in the access.

provided the same overdesign safety factor (redundancy) is used and the elements all have the same MTBF. Some cases involving small array numbers have a quantizing effect which prevents realization of a specific overdesign because fractions of an element cannot be used. This results in apparent discrepancies, when comparing arrays, not caused by the array size, per se, because the overdesign, and thus the reliabilities, differ. One reliability factor that should be considered is the MTBF of the element itself; that is, a higher voltage rated element will produce fewer elements in the array, but the MTBF of the higher voltage element may be less than that for a lower voltage element. In this case, the lower voltage element array will be more reliable, but may have other disadvantages because of the greater number of elements.

The photoconductive bulk semiconductor switch appears to offer the possibility of making switch elements of very high voltage, greatly reducing the array number for high voltage applications. It is interesting to estimate the voltage scaling properties of this device, assuming that the switch is modeled as a coaxial device (figure 5). The semiconductor switch material is the central cylinder. The analysis assumes that the semiconductor photoconductive process is not a limitation; the purpose of the analysis is to evaluate the limits imposed by other factors. The fundamental relations are

$$l = V/E_1, \quad (1)$$

$$V = R_1 E_2 \ln R_2/R_1, \quad (2)$$

$$j = I/2\pi\delta R_1, \quad (3)$$

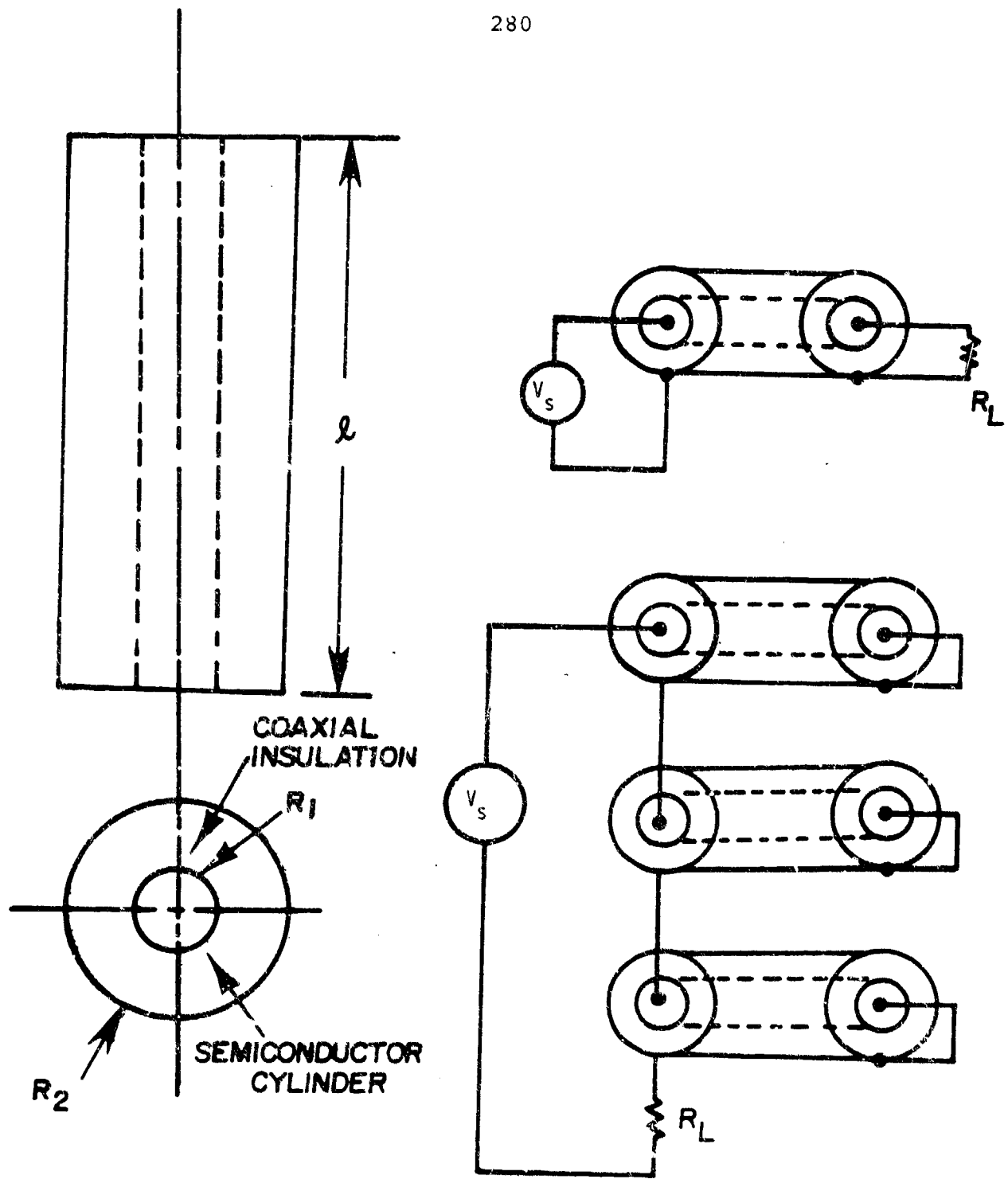


Figure 5. Coaxial configuration for a bulk semiconductor photodiode switch.

$$I = V/R_L, \quad (4)$$

$$L = 2 \cdot \ln R_2/R_1 \times 10^{-9}, \quad (5)$$

and

$$U = \pi R_2^2 \ell, \quad (6)$$

where

V = operating voltage (V),

E_1 = dielectric strength of the bulk semiconductor (V/cm),

ℓ = length of the semiconductor (cm),

E_2 = dielectric strength of the coaxial insulation (V/cm),

R_1 = radius of the semiconductor (cm)

R_2 = outer radius of the coaxial insulation (cm), determined by equation (2)

j = current density (A/cm^2),

δ = current skin depth, $\sim 6.61 \sqrt{\rho \tau_s}$ (cm),

L = switch inductance (H),

U = volume of switch (cm^3),

R_L = load resistance (ohms),

τ_s = switching speed (sec),

ρ = resistivity relative to copper.

Combining equations (1), (2), (3), (4), and (6), the volume becomes

$$U = \frac{V^3}{4\pi E_1 (R_L \delta j)^2} \exp \left[\frac{4\pi (R_L \delta j)}{E_2} \right]. \quad (7)$$

This expression indicates that size scales as the voltage cubed and also that the term $(R_L \delta j)$ plays a major role in the size scaling. Letting

$$\xi = R_L \delta j \quad (8)$$

and optimizing the volume with respect to ξ by setting

$$\frac{dV(\xi)}{d\xi} = 0 ,$$

$$\xi_{\text{opt}} = \frac{C_2}{2\pi} = R_L \delta j \quad (9)$$

and

$$V_{\text{opt}} = \frac{\pi V^3}{E_1 E_2^2} e^2 . \quad (10)$$

Equation (10) is a very interesting result. It shows that the optimum (minimum) volume scales directly as the voltage cubed and inversely as the dielectric strength of the semiconductor; most surprising, it scales inversely as the square of the coaxial insulation dielectric strength. Equation (10) is plotted in figure 6, with $E_1 = 2 \times 10^5$ V/cm and $E_2 = 4 \times 10^5$ V/cm, which represent the best practical values. Although this estimate excludes terminals, photon sources, and does not consider the basic semiconductor physics, it does indicate that a rather reasonable size is possible, to megavolt; however, because of voltage scaling, a multimegavolt unit would become awkward. On the basis of voltage and size, array structuring would begin no higher than about one MV.

The switching speed limitation can also be approximated from this model (figure 5), if it is assumed that the inductance of the switch, and not the inherent semiconductor characteristics, is the limiting factor. In this case,

$$\tau_s = L/R_L ; \quad (11)$$

combining equation (11) with equations (1) through (5),

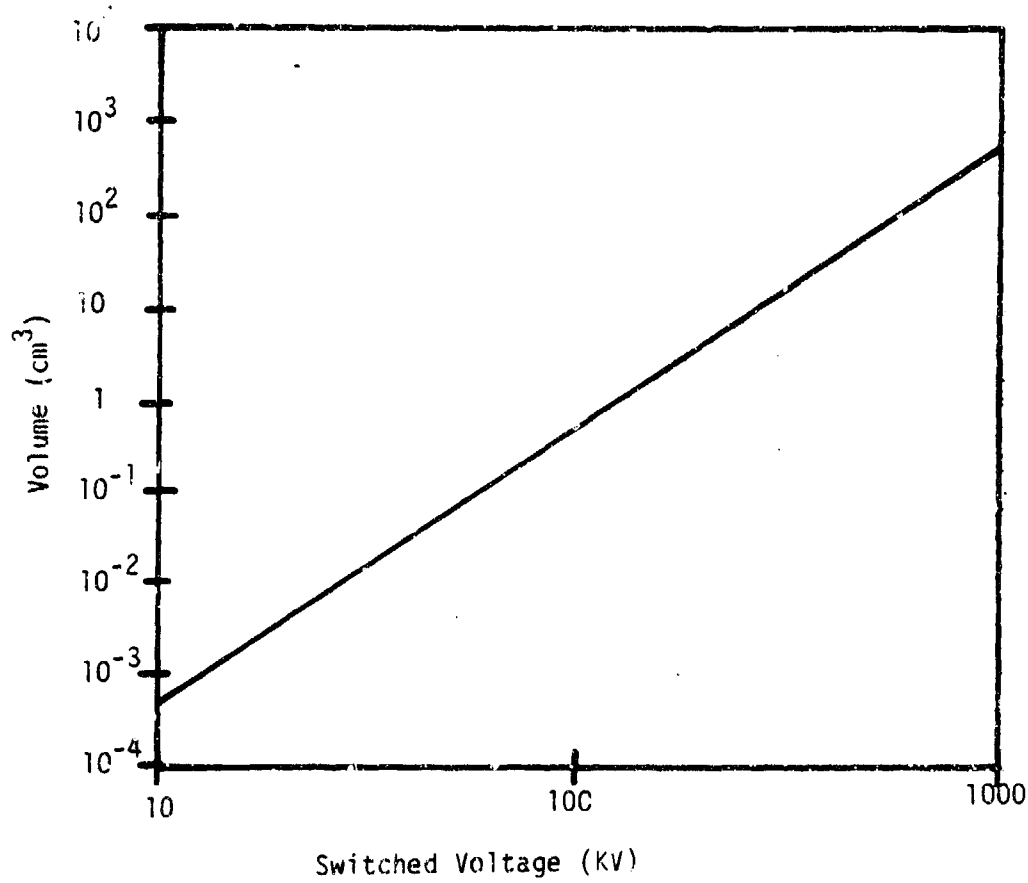


Figure 6. Optimum volume of coaxial switch as a function of switched voltage.

$$\tau_s = 6.9 \times 10^{-15} \frac{\rho j V^2}{E_1 E_2}. \quad (12)$$

Equation (12) indicates that switching time scales as the square of the voltage. As an estimate of the limitations of inductance, equation (12) is plotted in figure 7 as $1000 \tau_s / \rho$ vs V for various values of j. The resistivity, ρ , was normalized to 1000 times that of copper, and E_1 and E_2 were chosen to be 2×10^5 and 4×10^5 V/cm, respectively. Although this analysis is simplified, it appears that switching speeds imposed by the coaxial switch inductance are quite minimal, and will not be the limiting factor in most applications.

CONCLUSIONS

It was concluded that arrays with the least number of elements are generally preferred. In terms of the characteristics of the elements, it is desirable to improve both their rating and their uniformity. The improvements in rating relate to two basic types of switch applications, each with different criteria. First there is the switch which directly determines output pulse characteristics, and therefore has the requirements of peak voltage, peak current and rise time which are identical to the load pulse. The second type of switch is used in conjunction with a pulse compression or similar type of circuit where the switch characteristics are related to the load waveform in terms of energy. In both cases uniformity is desirable because it decreases the compensation required in arrays, and therefore diminishes the degradation of switching speed, efficiency, cost and size.

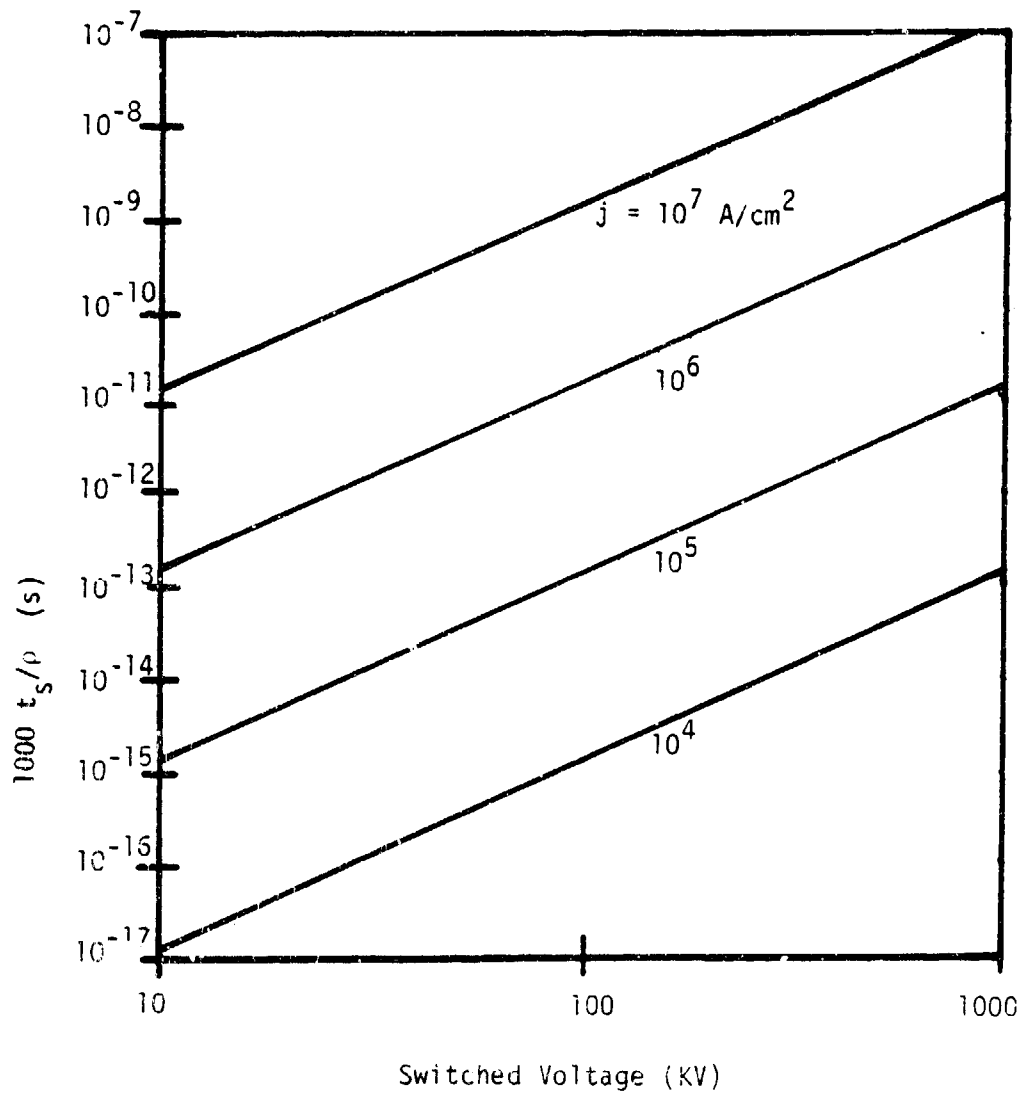


Figure 7. Inductance limited switching speed of a coaxial switch.

For arrays with ratings of less than 50 KV to 100 KV and speeds greater than about one microsecond, triggering by transformers is satisfactory. For higher voltages and faster speeds, optical triggering is superior. Optically driven bulk semiconductor photoconductive switches have the potential of handling hundreds of kilovolts and hundreds of kiloamperes per element. At this time, the limitations have not been established and depend upon many factors other than the fundamental physics of the photoconductive process. Some of these factors are insulation, current distribution, contact resistance, geometry, electromechanical forces and thermal limitations. In general, a surface layer of a conductor exposed to a pulsed magnetic field is heated to a thermal energy density which corresponds to about that of the applied field; this heating mode could be the dominant limitation.

RESEARCH RECOMMENDATIONS

The group recommends the following research activities:

1. Analysis of the consequences of varying the critical solid state switch characteristics upon the performance of arrays. This includes assessment of the potential methods and cost of implementation as a function of increased reproducibility, and improved thermal drift and aging.
2. Development of better compensating circuits to reduce the effects of component mismatch, minimizing degradation of array performance, lowering cost, and improving reliability.
3. More efficient utilization of optically triggered devices by way of a better match between the optical source wave-

length and the device bandgap. This includes the possibility of combining the light emitting source with the device as an integral unit.

4. The problem of contact resistance between the semiconductor and the circuit connection must be solved. The fundamental limitations imposed not only by the semiconductor physics, but also by other factors, such as electromechanical forces, the strength of the material, and geometry constraints, must be addressed. Surface voltage creep, current distribution, and optical source management should be considered.

5. Study of the thermal constraints imposed by average power dissipation in fast rep-rated or single pulse circuits. These should be considered for discrete devices and arrays, with associated compromises in circuit performance.

APPENDICES

APPENDIX A
DEEP IMPURITY TRAPPING CONCEPTS
FOR POWER SEMICONDUCTOR DEVICES

Gale R. Sundberg
NASA Lewis Research Center

and

H. Thurman Henderson
University of Cincinnati

ABSTRACT

High voltage semiconductor switches using deep impurity-doped silicon now appear feasible for high voltage (1-100 KV), high power (> 10 KW) switching and protection functions. Recent discoveries have demonstrated several practical ways of gating deep impurity doped silicon devices in planar configurations and of electrically controlling their characteristics, leading to a vast array of possible circuit applications. A new family of semiconductor switching devices and transducers are possible based on this technology. New deep impurity devices could be simpler than conventional p-n junction devices and yet use the same basic materials and processing techniques. In addition, multiple functions may be possible on a single device, as well as increased ratings.

INTRODUCTION

The device physics, the range of potential applications, and the benefits of this technology in terms of expanded power ranges, lower size, weight and cost, and integrated circuit compatibility, are examined below. This paper describes a unique

material study representing a departure from conventional junction semiconductor effects, employing a phenomenon caused by deep impurities in the band gap normally avoided in junction devices. Table 1 lists a family (because of the large number of devices emerging from the study) of devices which are consequences of the phenomenon.

In understanding how deep impurity devices work, bulk effects in silicon (or some other semiconductor material) rather than typical p-n junction characteristics must be examined. Events in silicon doped, with a deep impurity, such as gold, between charge injecting electrodes are of particular interest. (By deep energy levels are meant one or more energy levels at or very near the center of the energy band, obtained by adding appropriate impurities. The center in silicon lies at 0.55 ev from both the conduction and valence bands.) Shallow impurities are used to compensate the material (that is, to adjust the Fermi level), but not to form conventional p-n junction. Three types of gating are possible and have been explored. Switching can be accomplished by light gating, injection gating (the addition of an injection type gate in the space between anode and cathode) or MOS voltage gating (a metal-oxide-semiconductor gate).

Table 2 contains five major applications that are of considerable interest for further development. Most of the effort to date has been expended on switching devices and transducers. The primary interest at this time is in switching devices with gate controlled threshold voltages (limited only by the breakdown voltage of silicon), controllable holding voltage with very low

Table 1. A new semiconductor family.

DEVICE PHYSICS

- ° BULK EFFECTS
- ° DEEP ENERGY TRAPS
- ° VERSATILE, EFFICIENT GATING

POTENTIAL APPLICATIONS

- ° GATE CONTROLLED SWITCHING DEVICES
- ° VOLTAGE CONTROLLED OSCILLATORS
- ° SENSITIVE, MINIATURE TRANSDUCERS
- ° PULSE WIDTH MODULATORS
- ° MEMORY DEVICES IMMUNE TO RADIATION

BENEFITS

- ° INEXPENSIVE HOMOGENEOUS MATERIALS
- ° SIMPLE FABRICATION PROCESSES
- ° EXPANDED POWER RANGES
- ° INTEGRATED CIRCUIT COMPATIBILITY

Table 2. Potential applications.

| | | |
|---|---|---|
| <u>GATE CONTROLLED SWITCHING DEVICES</u> | <ul style="list-style-type: none"> ◦ THYRISTOR-LIKE SWITCHING ◦ ZERO VOLTAGE DROP DIODES ◦ LOGIC FUNCTIONS | <ul style="list-style-type: none"> ◦ PWM CONTROLLERS ◦ DISCRIMINATORS ◦ OPTICAL SWITCHES |
| <u>VOLTAGE CONTROLLED OSCILLATORS</u> | <ul style="list-style-type: none"> ◦ VOLTAGE-10-FREQUENCY CONVERTER ◦ AM AND FM OSCILLATOR/DETECTORS | <ul style="list-style-type: none"> ◦ TEMPERATURE-10-FREQUENCY THERMOMETER |
| <u>SENSITIVE, MINIATURE TRANSDUCERS</u> | <ul style="list-style-type: none"> ◦ GAS FLOW METERS ◦ MAGNETIC FIELD - HALL TYPE PROBE | <ul style="list-style-type: none"> ◦ INFRARED DETECTORS |
| <u>PULSE WIDTH MODULATOR</u> | <ul style="list-style-type: none"> ◦ VOLTAGE CONTROLLED DELAY LINE ◦ VOLTAGE CONTROLLED PULSE WIDTH | |
| <u>MEMORY DEVICES IMMUNE TO RADIATION</u> | <ul style="list-style-type: none"> ◦ CHARGE STORAGE IN DEEP LEVELS ◦ SMALL SIZE, VERTICALLY INTEGRABLE | |

forward voltage drop, and thyristor-like switching with both turn-on and turn-off capability. Very sensitive, miniature transducers have been of less interest. The gas flow meter is a hot wire anemometer type, 0.2 mm on a side, with response times around one second and with much greater sensitivity than a p-n junction device. The multiple internal reflection extrinsic infrared detectors have demonstrated quantum efficiencies greater than 34%, a flat detectivity curve out to 160 K and multiple frequency ranges using silicon-germanium alloys. The behavior of voltage controlled oscillators and detectors, voltage controlled pulse width modulators and delay lines, and temperature-to-frequency thermometers is based on pre- and post-breakdown oscillations in devices with certain doping characteristics. Because of the possibility of charge storage in deep levels, very small, vertically integratable memory devices, having an excellent immunity to radiation, have been predicted.

The primary benefits listed in Table 3 are the possibilities of very high switching voltages in the tens of kilovolts and of high power switching at megawatt levels. The feasibility of very low or zero forward voltage drop with very low on state power requirements could give extremely good efficiency for high power switching. IC compatibility of the devices using conventional materials, planar topologies and conventional semiconductor processing technologies provides the very real possibility of low cost and straightforward transfer of the technology from a university laboratory to industry.

Table 3. Benefits.

INEXPENSIVE HOMOGENEOUS MATERIALS

- SILICON, GERMANIUM, GALLIUM ARSENIDE
- CONVENTIONAL DOPANTS
- ALUMINUM OR OTHER METALLIZATIONS

SIMPLE FABRICATION PROCESSES

- CONVENTIONAL SEMICONDUCTOR TECHNOLOGY
- PLANAR SURFACE TOPOLOGIES

EXPANDED POWER RANGES

- UP TO 50 KILOVOLTS
- POSSIBLE MEGAWATT POWER SWITCHING

INTEGRATED CIRCUIT COMPATIBILITY

- PLANAR TOPOLOGY
- MICROCIRCUIT SIZE
- USES LSI, VLSI TYPE PROCESSES

THEORY

The left portion of figure 1 illustrates the band gap of intrinsic silicon, where E_C represents the conduction band edge, E_V is the valence band edge, and the dotted line is the Fermi level. Four typical shallow donors (for n-doping) are shown E_C ; several shallow acceptors (p-doping) are shown near E_V . Shown near midgap are deep impurity acceptors due to gold and zinc, which have been studied most extensively at this Laboratory. The first laboratory demonstration of the traps-filled-limit behavior at liquid nitrogen was made using a neutron induced 'A' center at 0.7 ev below E_C ; thallium at 0.26 ev above E_V was also examined as a possible candidate. The two energy level diagrams to the right show the effect of double doping, that is, adding an n-type impurity or a p-type impurity to move the Fermi level to one of the deep trap levels. This compensates the trap in such a manner that it will accept and hold an electron or a hole and empty only when gated, that is, by the effect of high induced fields, rather than thermally.

The upper part of figure 2 shows a cross-section of a double injection, deep impurity device. The bulk material is gold-doped silicon, compensated by a shallow donor such as phosphorus. The energy level diagram is shown below. The gold acceptor level at 0.54 ev is activated and dominates the device behavior. Also shown in the upper portion are the anode and cathode formed by diffusing p^+ - and n^+ -regions into the bulk material. These regions provide efficient ohmic contacts and the appropriate band bending at the surface to promote high level injection of holes

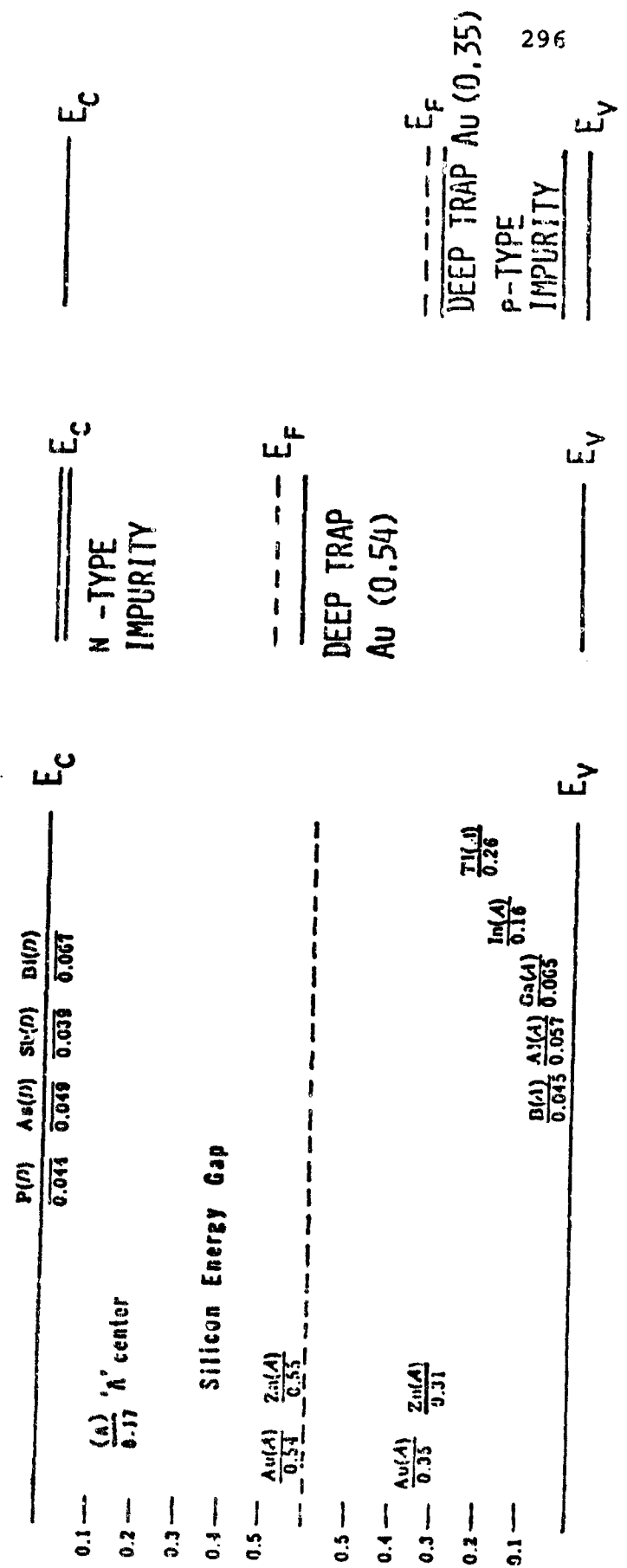
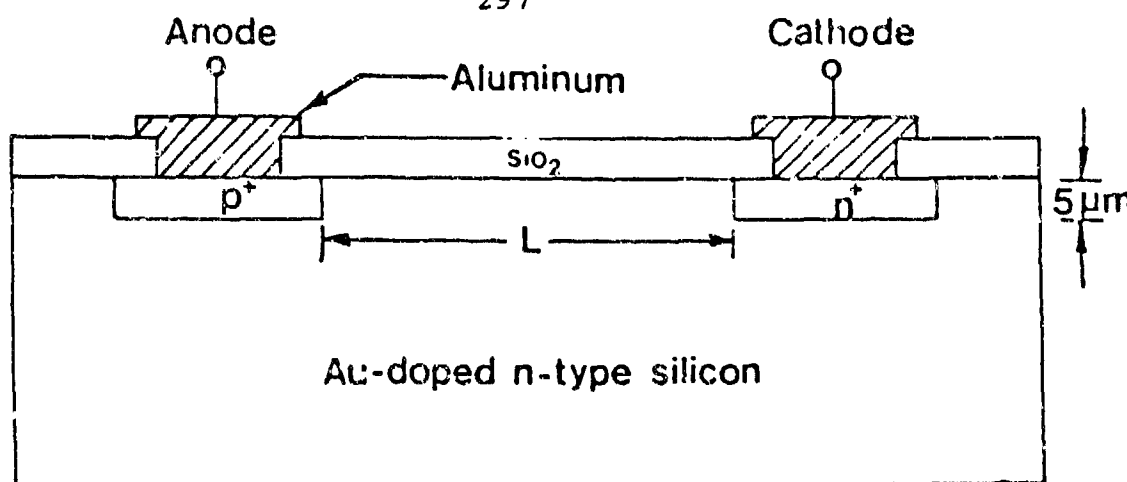
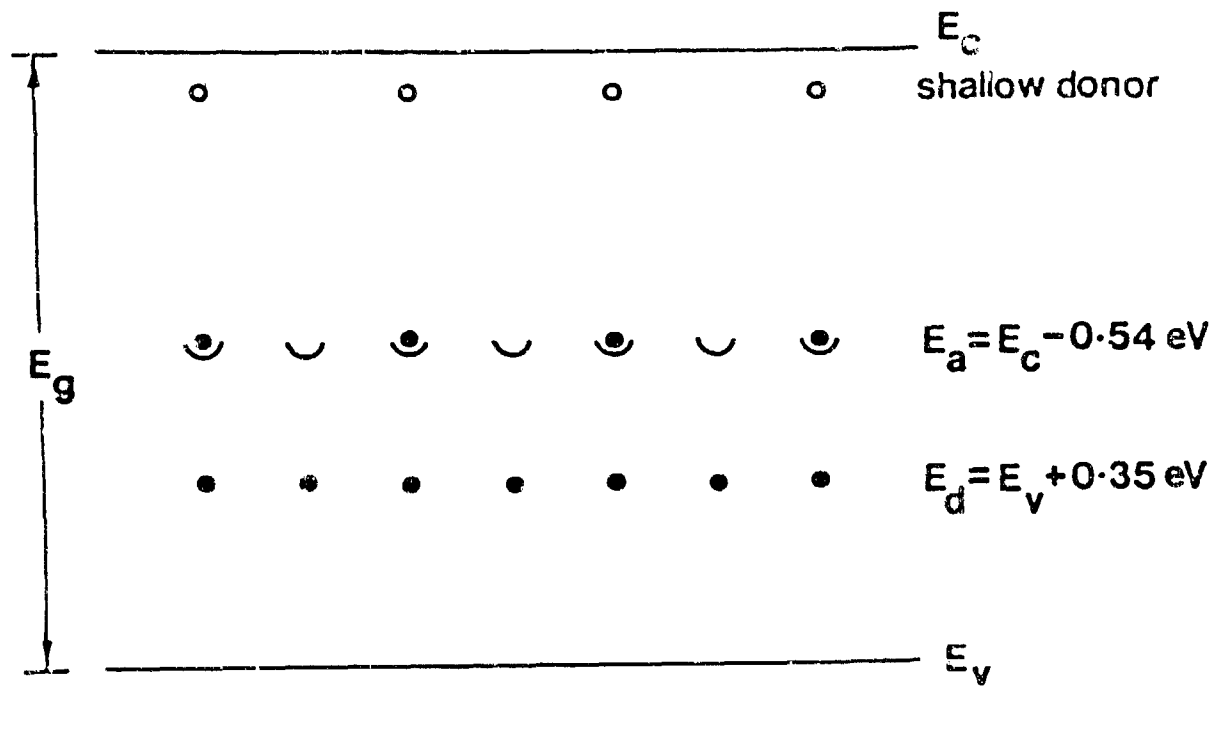


Figure 1. a) Impurity levels in silicon; b) shift in Fermi level in silicon containing deep traps.



a.



b.

Figure 2. a) Double injection device; b) energy level diagram for the device in (a).

and electrons, that is, double injection. If only an n^+ -region were produced, the device would exhibit single injection behavior (figure 3).

The left side of figure 3 illustrates a log-log plot of a neutron irradiated silicon diode with a single injecting electrode. As voltage increases across the diode, current increases, following an Ohm's law dependence out to about 100 volts, where it suddenly increases four to five orders of magnitude up to point b, after which it follows a typical square law behavior. The sudden increase is called the traps-filled-limit; the voltage at this point is V_{TFL} . A typical oscilloscope trace of the breakdown is shown to the right. The characteristics of this device appear similar to those of a zener diode with a very sharp knee.

Figure 4 shows the switching characteristics of a double injection diode made from gold-doped n-type silicon. The log-log plot of current vs. voltage to the left shows typical switching characteristics, the S-type curve characteristic of a thyristor. The various regions of the curve are labeled. V_0 is the transition voltage, where the diode moves from Ohm's law to a space-charge-limited square law behavior until it reaches a threshold voltage, V_{TH} , where it breaks into a high current conduction region. V_M is the holding voltage, sometimes referred to as the forward voltage drop. In many of the early devices, V_M was of the order of 10% of V_{TH} . However, improvements are being made in this ratio. The right-hand plot is the double injection switching curve as it would appear on an oscilloscope.

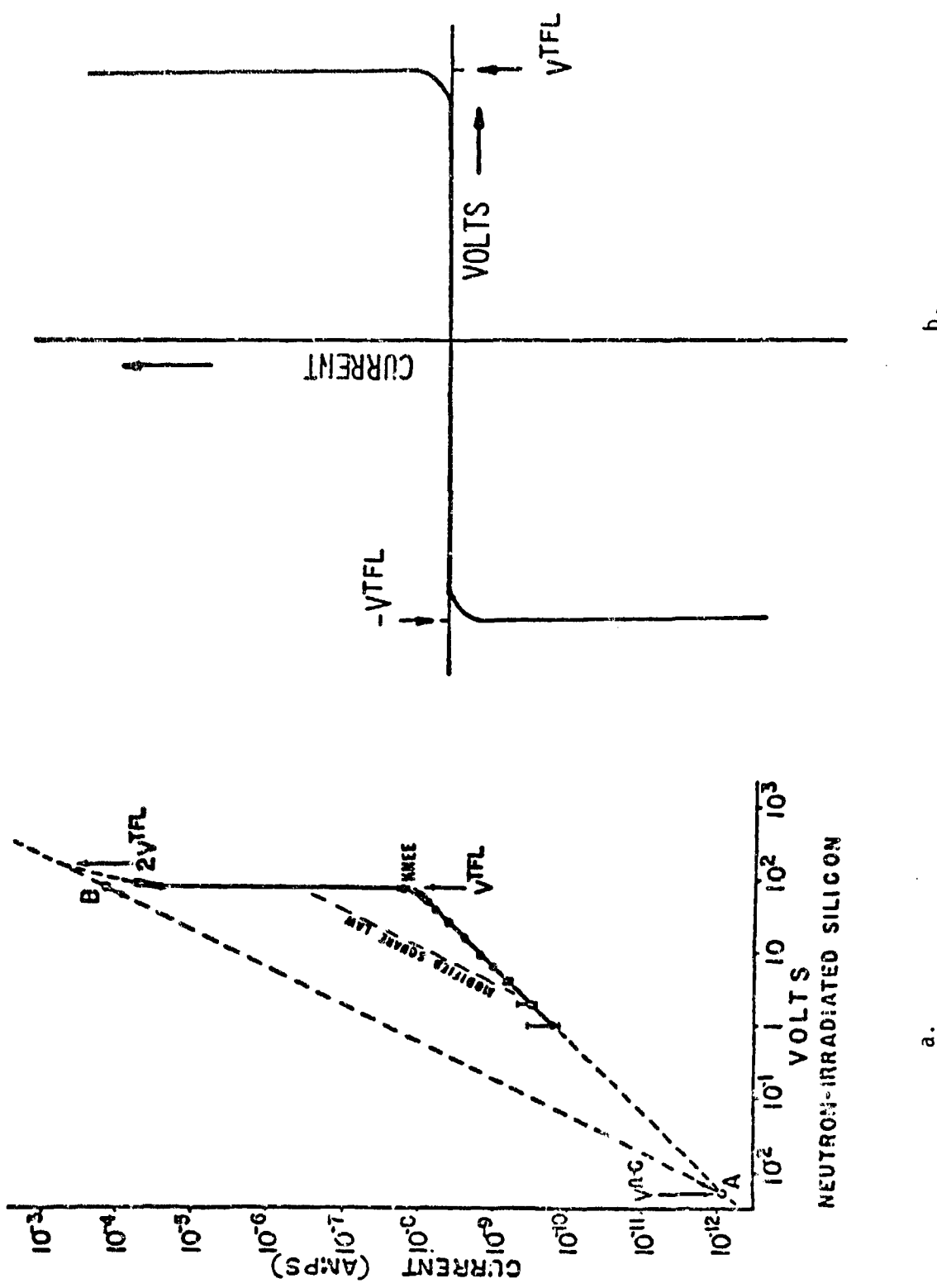


Figure 3. a) Switching characteristics for a diode with a single injecting electrode; b) oscilloscope trace for the diode in (a).

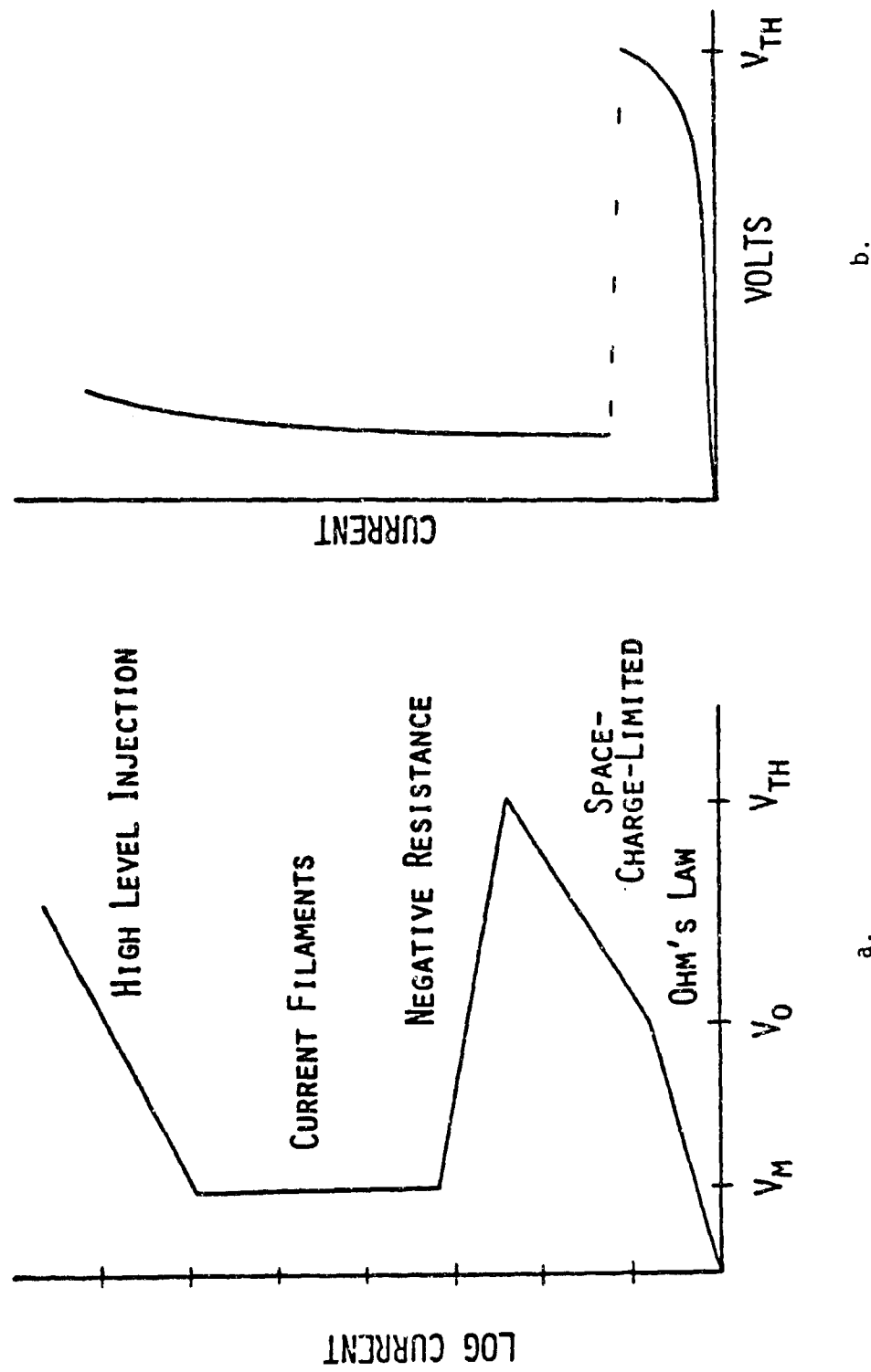
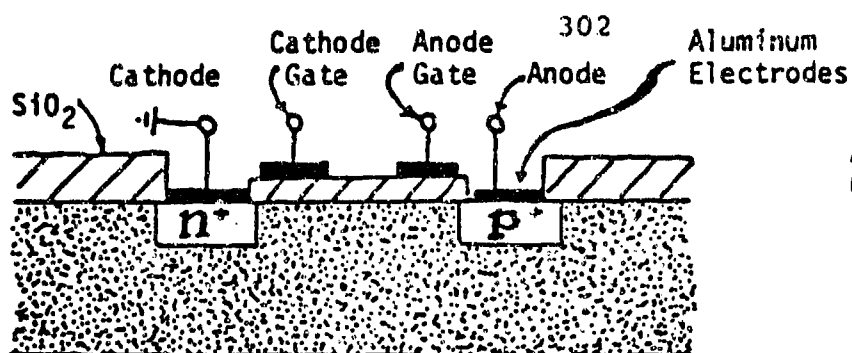


Figure 4. Switching characteristics of a double injection diode:
a) log current vs. log voltage; b) current vs. voltage.

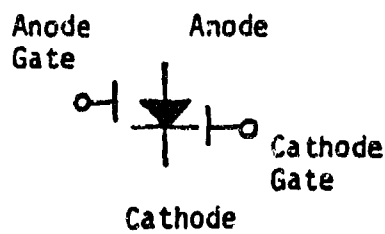
The upper portion of figure 5 depicts a double injection, gold-doped, n-type silicon diode with two gates added; these are called MOS (metal-oxide-semiconductor) voltage gates. Applying a positive voltage to the cathode gate (or negative to the anode gate) will decrease the threshold voltage from V_{TH} to V_{TH}'' , or turn the diode off from a conducting state. It has been found that the cathode gate is more effective in controlling the switching behavior. Therefore, in practice, both gates have been replaced by one gate located near the center of the channel, but closer to the cathode. As the gate voltage is increased positively, V_{TH} decreases, and vice versa. The holding voltage is not much affected by the gate voltages.

Figure 6 shows a top view and a cross-section of a gold doped, compensated silicon device with an injection gate located in the channel between anode and cathode. This drawing shows a p^+ injection gate, which has been used for most of the experimental work to date. However, similar effects have been obtained recently with an n^+ injection gate. With the p^+ gate, a positive gate-to-cathode voltage usually provides an n-type breakdown curve, leading to oscillatory behavior; however, a negative gate-to-cathode voltage will decrease the holding voltage.

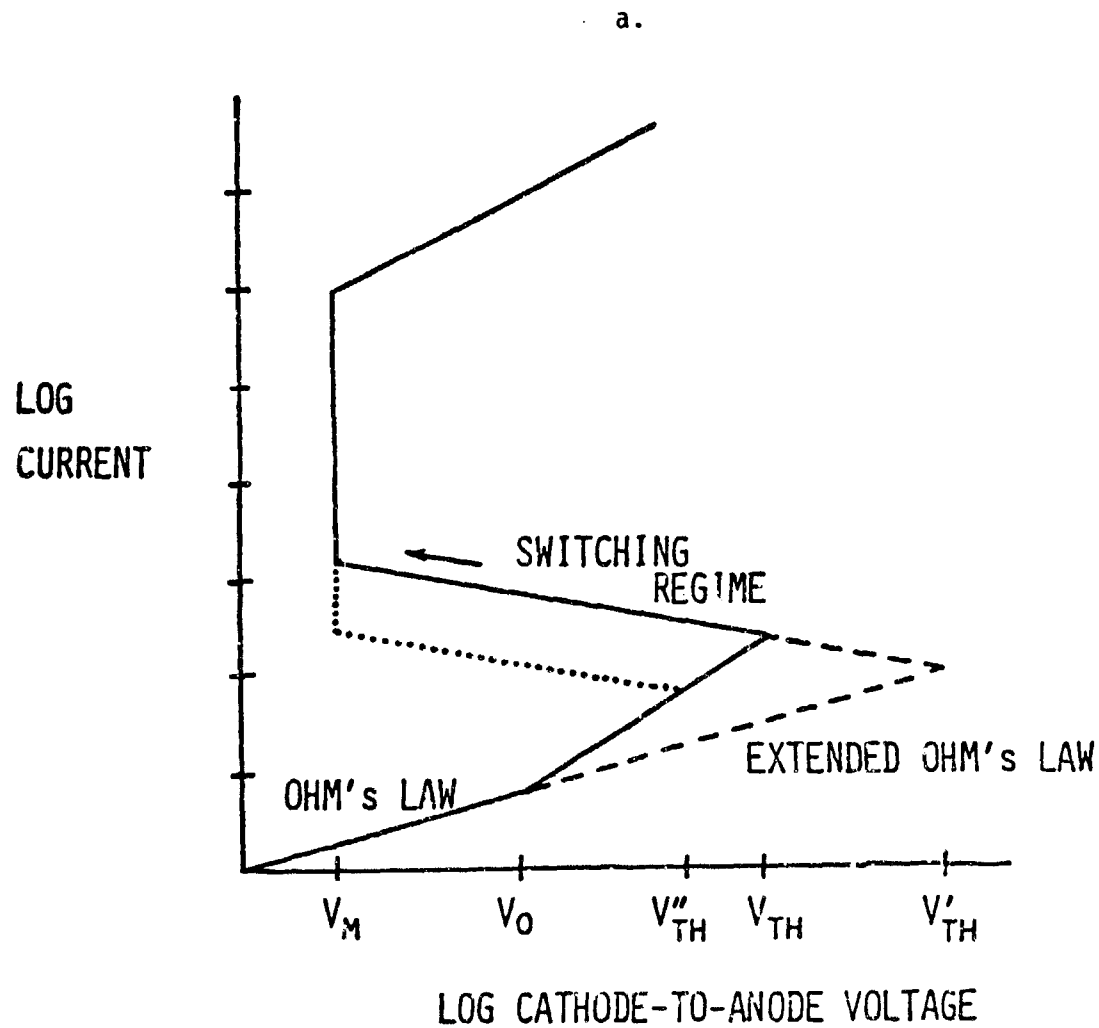
Figure 7 contains photographs of two oscilloscope traces of the switching characteristics of the injection gated device. Both pictures show current on a scale of 10 mA per division vs. voltage at 20 V per division. The top picture shows a threshold voltage of about 155 volts and a holding voltage of 16 to 20 volts, depending on the current level. The gate voltage is zero



N -TYPE, GOLD-DOPED SILICON SUBSTRATE

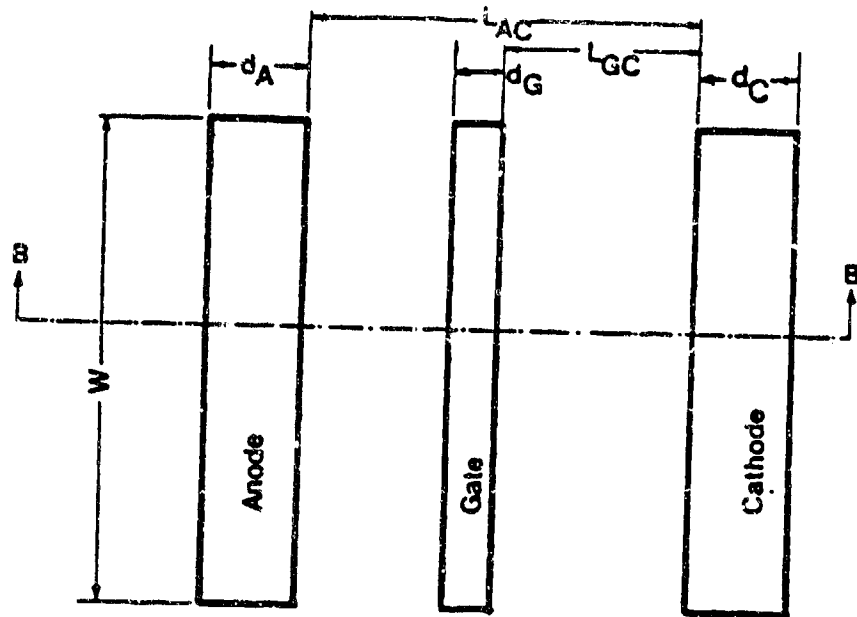


PROPOSED DEVICE SYMBOL

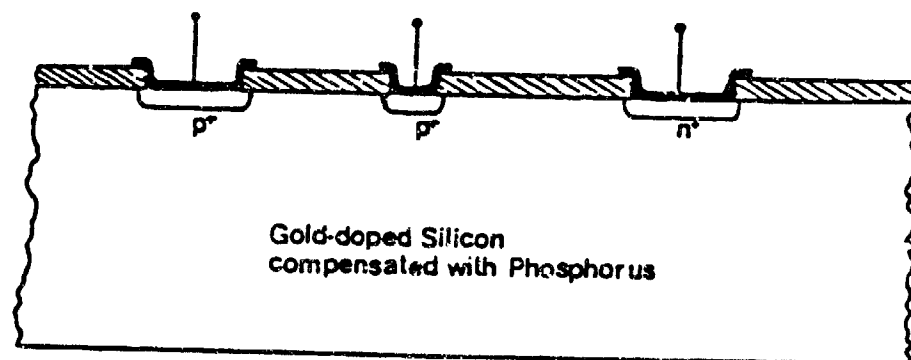


b.

Figure 5. a) Two gate double injection diode; b) Switching characteristics, illustrating voltage gating, for the diode in a).



a.



Section B-B

b.

Figure 6. Top view (a) and cross-section (b) of an injection gated device.

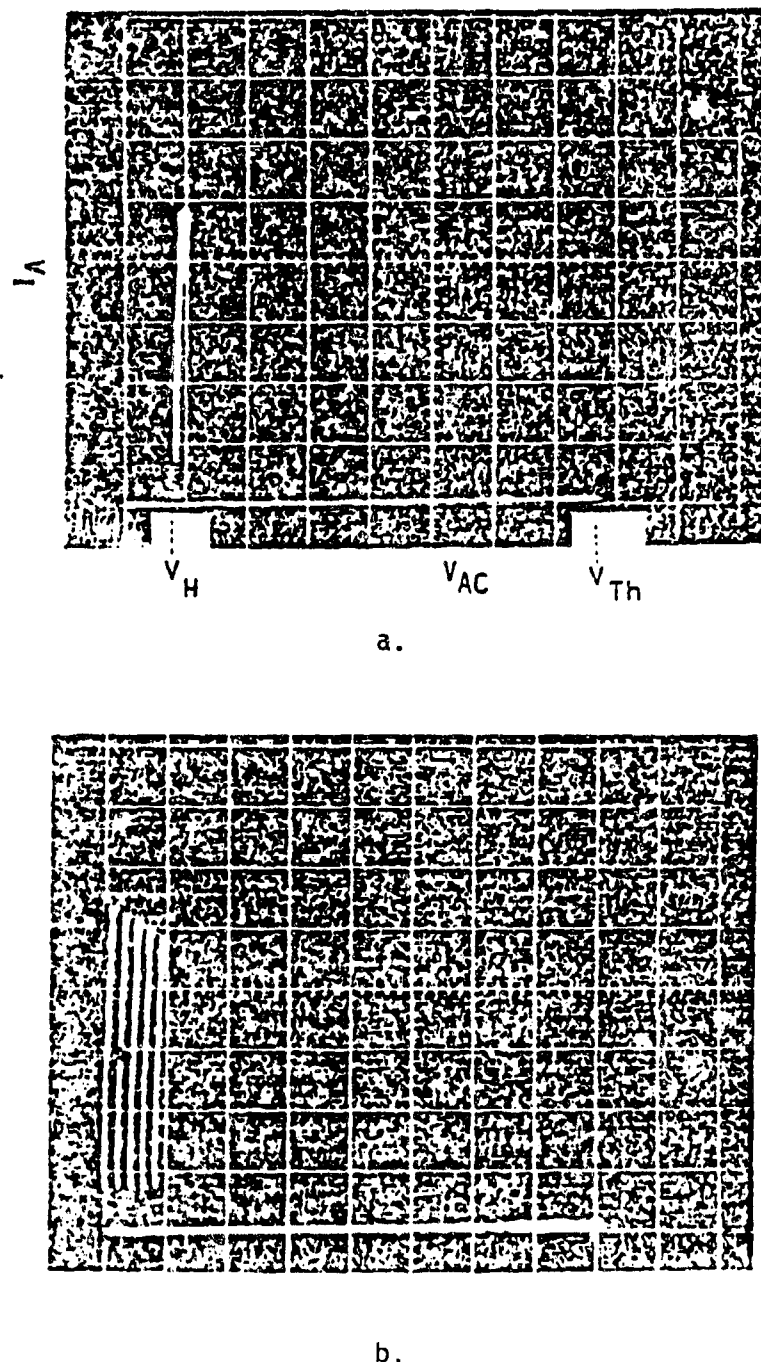


Figure 7. Switching characteristics of an injection gated device. Current: 10 mA per division; voltage: 20 V per division. Trace a) single switching event; trace b) superposition of several switching events.

for this photograph. The remarkable result of an injection gate is shown in the superposition of several traces in the lower picture. As the gate-to-cathode voltage is made more negative (in 10^{-4} volt increments), the holding voltage is decreased. In fact, with $V_{GC} = -16$ volts, the holding voltage is at or near zero. This presents the very exciting possibility of a device with zero forward voltage drop, leading to a very energy efficient switch. Obviously, there is some power loss in the gate, but experimental data has shown these losses to be less than 10% of the primary conduction losses. Improved processing of the bulk silicon has reduced V_H by a factor of 4 or 5, also.

Keeping in mind the physics of the deep impurity device and its switching capabilities, that is, the possibility of varying both the threshold and holding voltages, it is worth while to consider the voltage limitations in silicon. Threshold voltage as a function of length in or across a slab of silicon is plotted in figure 8. The breakdown limit is shown as a function of length in bulk silicon. The calculated curve for p-n junction devices is quite conservative, inasmuch as it is based on the breakdown limit across the depletion region assuming one side of the junction to be very lightly doped. This provides an upper limit in the region of around 10 kilovolts. Deep impurity devices also have a square law breakdown threshold, but a smaller coefficient. The calculated curve for the deep impurity material lies to the right of the p-n junction curve and shows a factor of ten or more higher breakdown limit. Neglecting surface effects and material defects, there appears to be a very real possibility

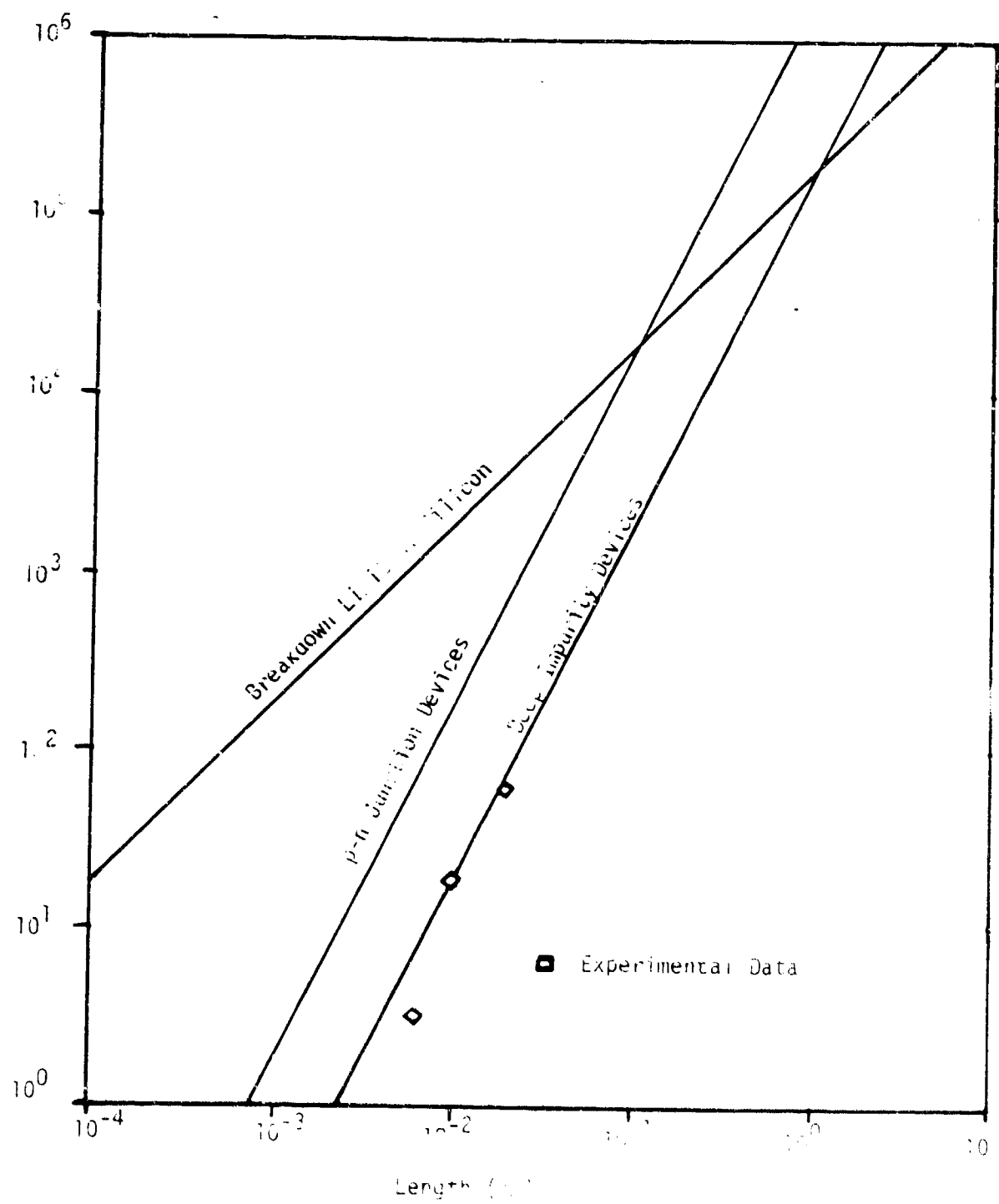


Figure 8. Threshold voltage as a function of junction length.

of devices with threshold voltages in the 10 to 100 kilovolt range. Recent experimental data confirms the curve up to 800 volts. With the possibility of threshold voltages extending beyond 10 kilovolts, and current capability directly proportional to electrode area, a multitude of new applications are possible for semiconductor devices. With controllable threshold voltages, zero forward voltage drop, and low standby power, deep impurity devices become very attractive switching candidates for future high energy space and aeronautical power systems. Circuit breakers, switching and protection devices, and inverters for the prime power system are some potential applications. Power switching and circuit protection switches for high power traveling wave tubes, beam weapons and radars also appear feasible. These applications are summarized in Table 4.

In power controller or circuit breaker applications, a deep impurity switch could combine the advantages of conventional solid state switching with zero voltage drop, low standby power, small size and high voltage limits. The primary limitation at this time is the lack of technology development.

In summary, a new family of deep impurity semiconductors has been described which has outstanding potential for high energy applications, where small size, high voltage and low forward voltage drops would be primary advantages. With these new semiconductors, switching applications appear possible at voltage and power levels impossible with conventional semiconductors. These devices have additional applications as detectors, transducers, and oscillators.

Table 4. Switching applications of deep impurity devices.

SPACE

- ° REMOTE POWER CONTROLLERS AND CIRCUIT BREAKERS
- ° TRAVELING WAVE TUBES
- ° HIGH INTENSITY LASERS, BEAM WEAPONS
- ° HIGH VOLTAGE INVERTERS

AERONAUTICS

- ° REMOTE POWER CONTROLLERS AND CIRCUIT BREAKERS
- ° CROSS-STRAPPING OF GENERATORS
- ° RADAR

APPENDIX B

NONLINEAR RESISTIVE SWITCHES

R. D. Ford and I. M. Vitkovitsky
Naval Research Laboratory

INTRODUCTION

Varieties of opening switch functions associated with high power inductive storage⁽¹⁾ are, at present, performed by such devices as explosively driven circuit breakers,⁽²⁾ fuses⁽³⁾ and combinations (staging) of these.⁽⁴⁾ Explosively driven switches are used in applications including inductive storage systems powered by rotating machinery, where long conduction time and fast interruption are essential. Fuses provide substantially faster opening times than explosive switches and are often used in inductive systems where capacitor banks provide the source of current. Fuse vaporization energy, derived from the current source, reduces the efficiency of the energy transfer from the inductor to the load. Other types of opening switches, needed in repetitive operation or with very fast opening time, depend on the use of diffuse discharges. Such switches include plasma erosion switches⁽⁵⁾ and electron-beam controlled ionized gas switches.⁽⁶⁾

The use of solid material with non-linear resistivity, where the resistance value of the material changes dramatically at some point related to its thermodynamic phase change, provides another approach to an opening switch. Switches based on the use of such

materials have the desirable characteristic of volume discharge, in contrast to arc discharges, which allows current interruption and voltage hold-off to occur simultaneously. The phase change produces a transition from high to low conductivity. The recent development of such thermally controlled solid materials has stimulated consideration of their potential application as opening switches, including their use as possible replacements for explosively driven switches and exploding wire fuses in large inductive storage systems, with power output $>10^9$ W. The most important advantage in employing these materials for switches is their reusability (unlike single-shot explosively driven and fuse switches). By adjusting the current density in such switches, the conduction time (i.e. the on time) can be adjusted to long (seconds) conduction periods.

Figure 1 shows the nonlinear resistivity of two materials, BaTiO₃ ceramic and carbon-filled polymer (CFP) (their properties and switching mechanisms are described in references 7 and 8, respectively). These materials exhibit positive temperature coefficients (PTC) above temperatures of about 100°C, associated with the Curie temperature of the BaTiO₃, and with the phase transition from the crystalline form of the CFP polymer to its amorphous state. The dramatic change of several orders of magnitude in the resistivity makes these materials suitable for true opening switches, i.e., for circuit elements which change from conductors to non-conductors, without requiring recovery time for voltage blocking.

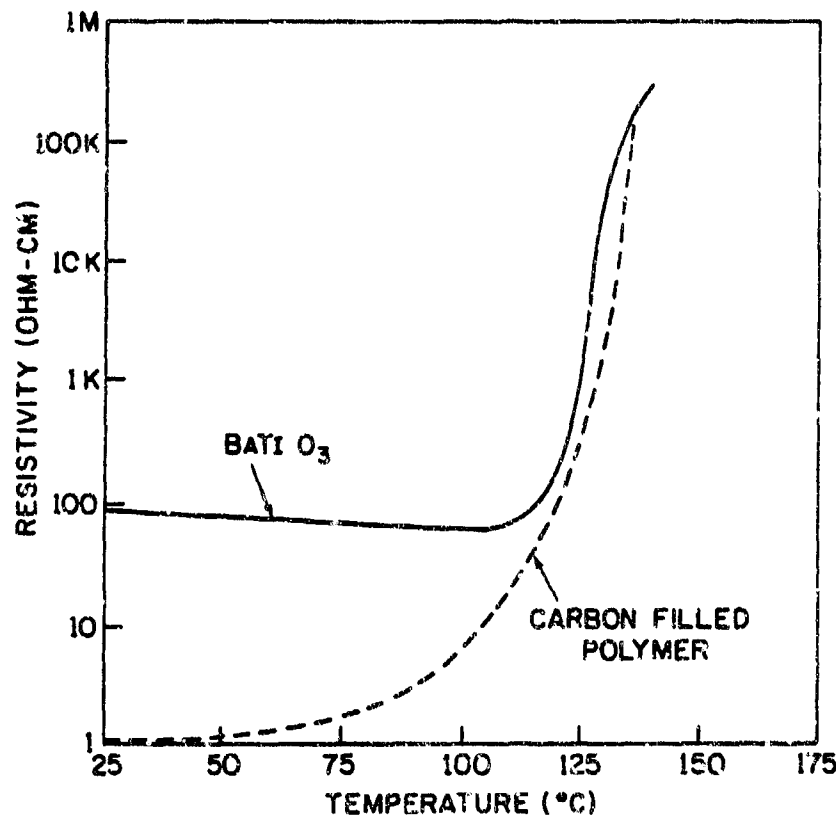


Figure 1. Resistance characteristics for commercially available FTC switching materials. The curve for BaTiO₃ (reference 7) exhibits a small negative temperature coefficient at lower temperatures. The curve for CFP (reference 8) is characterized by a weak resistance increase at lower temperatures.

APPLICATION IN INDUCTIVE STORAGE CIRCUITS

Differences in the BaTiO₃ and CFP resistivity curves and in value of the on state resistivity suggest that they are adaptable to different inductive storage circuits.

Semiconducting Polycrystalline PTC Materials

As figure 1 indicates, BaTiO₃ has a switching characteristic associated with very narrow temperature range, ΔT , of about 20°C. This makes it adaptable to triggerable circuits, i.e. to circuits with the switching element appropriately triggered to induce the conductivity change. The small temperature range allows the material to return to its initial conducting state with only a small amount of heat removal. In contrast, because of its substantial increase of resistance at a temperature well below its transition temperature, CFP must be cooled almost to room temperature to recover its initial resistivity. Thus, BaTiO₃ can, potentially, be used in burst output pulsers, with minimum pulse-to-pulse separation dictated by the heat removal configuration. (Pulsers providing a train of several closely spaced high power (10^{10} W) output pulses have been constructed, by using one opening switch per pulse within the train.) Because BaTiO₃ starts at substantially higher resistivity (~100 Ω cm) than CFP, its applications may be limited by the physical size to currents of about 10 KA. Reference 7 indicates that practical BaTiO₃ ceramic systems, with resistivities less than 1 Ω cm, might become available.)

To relate current density and switching time, a simplifying assumption of no loss of heat (generated by the ohmic heating)

leads to a simple scaling relation between those quantities.⁽⁹⁾ The conducting material increases in temperature, T , at a rate proportional to the electric power density input (given in terms of current density, j),

$$\frac{dT}{dt} = \frac{\rho j^2}{C_v} , \quad (1)$$

where C_v is heat capacity per unit volume, and ρ is the resistivity, of the material. Representing the resistance characteristic shown in figure 1 by an exponential, $\rho(T) = \rho_0 e^{\alpha T}$, the solution of equation (1) is

$$e^{\alpha T} = 1 - \frac{\alpha \rho_0 j^2 t}{C_v} , \quad (2)$$

If the initial resistance increases by γ , such that $\rho = \gamma \rho_0$, then

$$\frac{1}{\gamma} = 1 - \frac{\alpha \rho_0 j^2 t}{C_v} , \quad (3)$$

and $t \approx C_v / \alpha \rho_0 j^2 , \quad \text{for } \gamma \gg 1 . \quad (4)$

Equation (4) can be written in terms of the applied field, $E = \gamma j \rho$,

$$t = C_v \rho_0 \gamma^2 / \alpha E^2 . \quad (5)$$

Recognizing that the maximum value of j that can be passed by the non-linear material is determined by the maximum electric field, E_m (i.e., $j = E_m / \gamma \rho$), the scaling for minimum opening time, t_{min} , is obtained,

$$t_{\min} = C_v \rho_0 \gamma^2 / \alpha E^2 . \quad (6)$$

The last relationship indicates the importance of the blocking (breakdown) field of the non-linear materials in their ability to switch rapidly. Experimental confirmation of the scaling relation (5) is given below.

Because of the very narrow temperature range, ΔT , over which switching occurs, low energy trigger pulses can be used to control large energy systems. Figure 2 shows a circuit using a trigger, resulting in such performance. Figure 2a shows current switching that reflects the model associated with equations (4) and (5), i.e., the transition to high resistance results from ohmic heating by the source current. It is possible also to control the time and rate of switching the transition by an external high current, short duration, pulse. At a critical value of E_{trigger} (figure 2b), switching controlled by trigger power is obtained.

The value of the maximum field that could be supported across a 0.127 cm thick sample was measured by applying an increasingly large driving potential to the sample. Thus, at 400 volts, a breakdown occurred at the surface of the sample, suggesting that $E_m = 3.1 \text{ KV/cm}$. Using a lower power supply potential of 20 V (i.e. an applied field of 157 V/cm), measured switching time was compared with that predicted by the scaling equation (5). Taking $C_v \approx 1.5 \text{ J/cm}^3 \text{ }^\circ\text{C}$, and noting from figure 2a that the 100 Ω cm samples produced $\gamma \approx 10$ with $E_m = 157 \text{ V/cm}$, the switching time from equation (5) is ~ 2.5 for $\alpha = 0.23$, where α has been determined from the resistivity vs. temperature curves

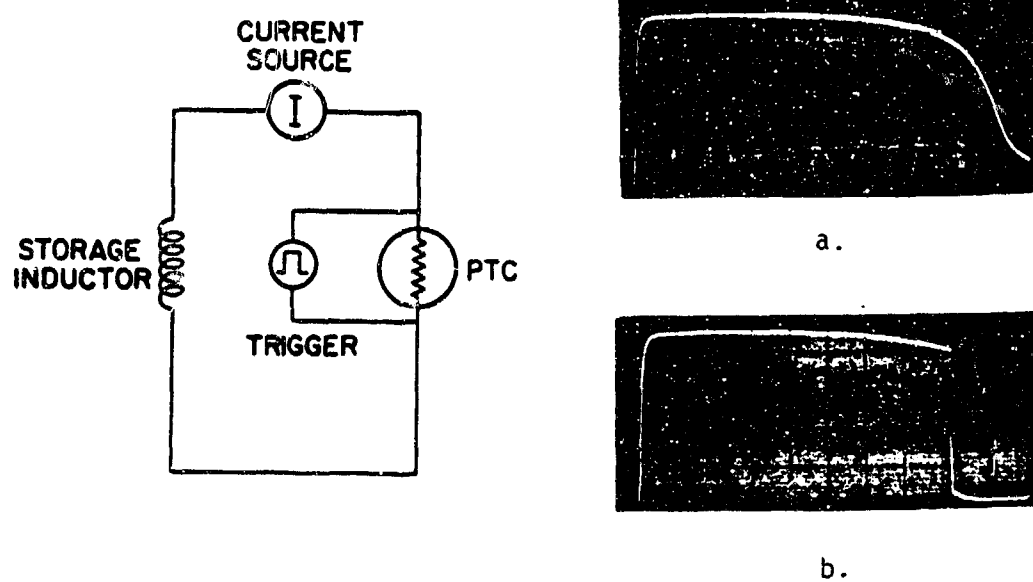


Figure 2. Effect of trigger amplitude on the switching characteristics of BaTiO_3 . The circuit to the left illustrates the experimental arrangement. Trace (a) shows the effect of ohmic heating by the source current; trace (b) illustrates switching controlled by trigger power.

given in reference 8. The measured switching time is close to 1.5 s, observed in Fig. 2a.

Polycrystalline Carbon-Filled Conductor (CFP)

Figure 1 shows that the resistivity of cold CFP is about two orders of magnitude lower than that of the ceramic BaTiO_3 . The high conductivity allows the CFP material to be used in a manner similar to the exploding fuses used in inductive storage circuits. This can be seen from the scaling derived below. Denoting quantities referring to fuses by the symbol F, and those to CFP by the symbol C, relations for the energy deposited into the switch at the time that switching occurs can be defined

$$w_F = \int_{T_0}^{T_F} M_F C_F \, dT + w_F, \quad (7)$$

and

$$w_C = \int_{T_0}^{T_C} M_C C_C \, dT + w_C, \quad (8)$$

where T_0 is room temperature, T_F is vaporization temperature of copper, and T_C is the transition temperature (~ 120 °C) of the polymer from its polycrystalline to its amorphous state, with the attendant strong resistivity change of the carbon chains. M represents the masses of the switches; C , their specific heat capacities; and w , the energies associated with latent heats of transition. For purposes of comparison of the cost in switching energy of the two materials, assume that they have the same resistance during conduction (i.e., cold resistance), so that $R_F = R_C$. Also assume that the final inductive voltage to appear across the switching elements is V . Thus, for respective switch

lengths L_F and L_C , the voltage is limited by the breakdown field of the material, E , so that $V = L_F E_F = L_C E_C$. The ratio of the two switching energies is (from equation 1),

$$\frac{W_C}{W_F} = \frac{M_C \int_{T_D}^{T_C} C_C dT}{M_F \int_{T_F}^{T_C} C_F dT} = \frac{M_C}{M_F} Y, \quad (9)$$

where $W_w \approx W$ and Y is the ratio of the integrals. Denoting densities of the materials by δ_F and δ_C , and cross-sectional areas by A_F and A_C , equation (9) becomes

$$\frac{W_C}{W_F} = \frac{\delta_C A_C L_C}{\delta_F A_F L_F} Y = \left(\frac{\delta_C}{\delta_F} \right) \left(\frac{A_C}{A_F} \right) \left(\frac{E_F}{E_C} \right) Y. \quad (10)$$

Introducing the respective resistivities, ρ_F and ρ_C , the requirement of initial switch resistance, $\rho_F L_F / A_F = \rho_C L_C / A_C$, yields

$$\frac{W_C}{W_F} = \frac{\delta_C \rho_C L_C E_F}{\delta_F \rho_F L_F E_C} Y = \left(\frac{\delta_C}{\delta_F} \right) \left(\frac{\rho_C}{\rho_F} \right) \left(\frac{E_F}{E_C} \right)^2 Y. \quad (11)$$

For copper fuses, $\delta_C / \delta_F = 0.1$ and, if $\rho_C = 1 \Omega \text{ cm}$, $\rho_C / \rho_F \approx 3 \times 10^5$. As is shown later in the discussion of the experiments, $E_F / E_C \approx 0.1$, so that $W_C / W_F \approx 300 Y$. To obtain the approximate value of Y , consider that the conduction in CFP is by graphite only, so that the integral of C changes linearly with temperature between room temperature and the transition temperature of $\approx 120^\circ\text{C}$. The integral of C for Cu (for temperatures ranging from room to

vapcrization values) is about 30 times larger. Thus, $W_C/W_F \approx 10$, and approaches unity for $E_C \approx 30$ KV/cm. Actually, for very long conduction times, E_F is lower yet, so that the ratio W_C/W_F is more in favor of solid CFP.

The small amount of energy that must be deposited in CFP material to produce a drastic increase in resistivity allows it to be used in a manner similar to a fuse. The low switching temperature leads to reproducible behaviour, suitable for repetitive use (unlike one-shot operation of the fuse), provided sufficient cooling time is available.

Reference 8 indicates the nature of the mechanism responsible for the strong change in resistivity with temperature. The carbon particles distributed in the polycrystalline matrix are sufficiently dense (forming about 50% of the composite) to link into chains that lead to low resistivity at ambient temperature. As conduction of the current heats the carbon and the surrounding polymer, a phase change in the polymer occurs at the transition temperature, accompanied by a volume change of about 2%. This breaks the conducting carbon chains and increases the resistance. Upon cooling, gradual re-linking of chains occurs. The PFC material recovers to approximately 90% of its initial conductivity within a few minutes, with essentially full recovery over a 24 hour period. As ohmic heating rate is increased, permanent damage occurs, i.e., the material becomes substantially more resistive at ambient temperature.

EXPERIMENTAL RESULTSBaTiO₃ Ceramic

Small samples, 1.4 cm in diameter and 0.12 cm thick, produced by Keystone Carbon Co (Piece Part Number.: RL5405-3.0-120-20-PTO) were pulse tested using the circuit shown in figure 2. The current sources were either a DC supply or a 21.6 mF capacitor, charged to 200 V, and storing 440 J. The nominal resistance of the samples was 2.5 Ω and deviated by $\pm 0.5 \Omega$. The samples were rated for steady-state blocking of 20 V. Using the DC power supply to provide currents up to 20 A, switching occurred at about 8 s, converting electrical energy into ohmic heat, and depositing about 2.0 KJ/cm³ into the ceramic. Without triggering, the current trace in figure 2a shows the opening time to be around 1.5 s. Using a 1200 μ F capacitor charged up to 400 V (providing a trigger pulse energy of up to 100 J, representing about 5% of energy required for switching), the switching time was reduced to a minimum value of about 1 ms, seen, for example, in figure 2b. In a different experiment, designed to determine the breakdown fields, currents up to 100 A were switched. The results of the test indicated that BaTiO₃, with a resistivity in the 300 Ω cm range, can be used for voltage blocking at hold-off field values greater than 3 KV/cm, for current densities that depend on conduction time (e.g., 10 A/cm² for 4 s), and to provide 1 ms opening times, without need of any recovery period.

To determine the power and energy handling capabilities of BaTiO₃ under pulsed conditions, a 20 mF 200 V, capacitor was used

as a 40 A current source, providing 80 msec conduction through the switch before opening. A 3.6 mF, 140 V, capacitor triggered the switch; the opening time was between 1 and 10 ms, a result similar to that in the experiment in which the conduction time was 4 sec (figure 2). The relative energies expended in the switch were 320 J over the first 80 ms, and 35 J associated with the trigger. The power density associated with the BaTiO₃ is $> 4 \times 10^4$ W/cm³, and the switching efficiency is ~ 90%. As the power is increased beyond this level in the test samples, voltage breakdown occurs. It appears to be a surface cracking, independent of the medium (such as air or oil) which surrounds the sample.

To determine how data obtained with small samples scales to large switches, additional testing, employing parallel devices, was performed. The results indicated that no problems arise by increasing the switch current. In a two-unit parallel arrays, the switching time corresponded to that of the element which switched faster. Series combinations without load sharing (i.e., without using resistive grading, such as that used with a CFP stack of two units) are not suitable for increasing switch blocking voltage. The deviations of the resistances of individual units unbalances the electric fields and leads to the breakdown of the weaker unit.

Carbon-Filled Polycrystalline Material

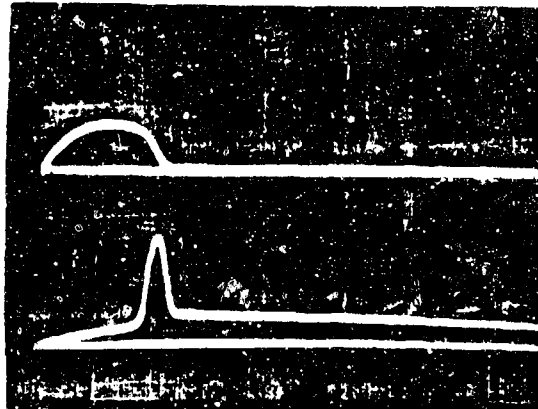
Carbon-filled polycrystalline material has a resistivity substantially lower⁽⁸⁾ than that of BaTiO₃. It is available-commercially as a current limiter device with the trade-name,

Polyswitch. Its resistivity is in the Ω cm range. Units made by Raychem, having a steady-state current rating of 9 A, were tested with pulsed currents between 100 s and 500 s long, up to 10 KA, and provided circuit interruption similar to that achieved with fuses.

Figure 3 shows the current and voltage waveforms across the CFP switch and across the exploding wire fuse. Raychem production part PSR 20528 was used in these tests. Reference 8 indicates that $R/R_0 \approx 10^5$ (where R is the maximum switch resistance at 125 °C, and R_0 is the resistance at room temperature). Table 1 summarizes the characteristics of the circuit and switch performance shown in figure 3. The switch performance is compared to that of fuses used in a similar function.

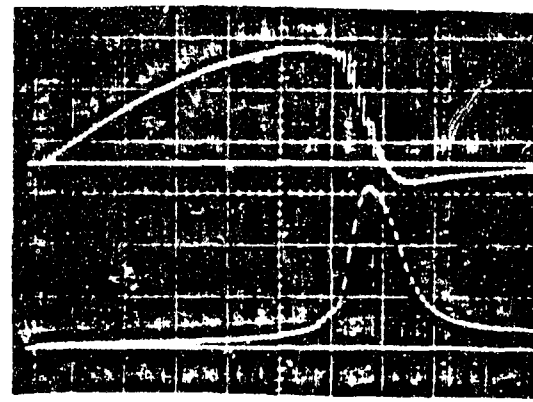
For the circuit shown in figure 4, the ratio of I_{load}/I_{switch} indicates a switch resistance change factor of 100 (i.e., to a switch resistance seven times higher than the load resistance). It was further noted in the tests that the initial switch resistance, R_0 , degrades from 9 m Ω to 12 m Ω after the first opening, if insufficient time for re-linking of carbon chains is not available. No further degradation occurs with a larger number of shots.

Although the CFP switch is capable of resistance changes of 10^5 , actual resistance values are established by circuit parameters. For example, the 0.125 load resistance of figure 4 limits peak voltage (and therefore thermal energy to the CFP) to 75 V. For these tests, the CFP initial resistance, R_0 , was 9 m Ω , as noted above; curve 1 in figure 4 shows a peak switched current



PTC POLYMER SWITCH

a.



COPPER WIRE FUSE IN AIR

b.

Figure 3. Comparison of the current and voltage waveforms associated with conduction and opening of the CFP (a) and the copper (b) fuse. The sweep rate for trace (a) is 200 μ s per division; for trace (b), 100 μ s per division.

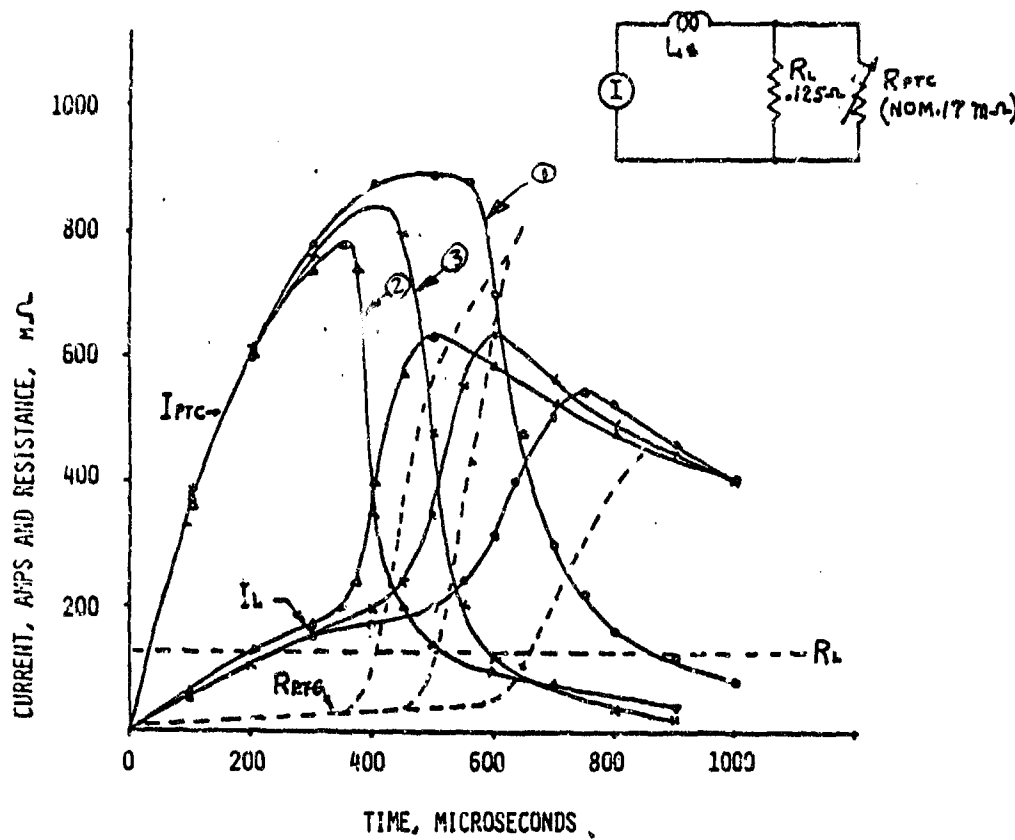


Figure 4. Behavior of the CFP fuse as a function of the number of switching events. The circular data points represent the first discharge; the triangular data points represent subsequent, highly reproducible, discharges. The effect of mechanical compression of the switch with a large number of discharges is indicated by the data points represented by crosses.

of 1 KA at approximately 550 μ s. After this test, the initial switch resistance degraded to 12 m Ω , producing the operating conditions of curve 2. No further degradation occurred when the switch was operated repeatedly at approximately 2 minute intervals.

Curve 3, which falls between curves 1 and 2, resulted from applying mechanical pressure across the PTC switch to reestablish conductive carbon bonds. This result, decreased initial resistivity affected by pressure, provides a good picture of how the device controls the resistivity, and suggests a relatively simply technique for using mechanical pressure to select switch operating parameters, such as commutation time for a given current level.

The performance of CFP can be characterized by considering it as a resettable fuse. Table 1, comparing the characteristics of the Polyswitch with those of the copper fuse exploded in air, provides the key points for assessing Polyswitch performance and scaling to higher power applications. Because of the factors controlling the scaling (equation (11)), the switch efficiency obtained in inductive storage applications can potentially be better than with existing fuses.

CONCLUSIONS

The results of the experiments performed on commercially available small samples of BaTiO₃ and CFP provide scaling relations that indicate possible future uses of such materials in opening switch development. As an example of potential uses, CFP material has been considered for use in a multi-MJ inductive

storage system to replace non-reusable fuses. Another feature demonstrated in the experiments, accurate triggering time of switching, can be designed into a large scale switch.

The reusability of the switch can be also employed in generating high frequency repetitive pulse bursts, such as those obtained with explosive switches and fuse combinations. In such an application, one opening switch per pulse (in a given pulse train) is required; a series of reusable switches could be employed here.

REFERENCES

1. R. D. Ford, D. Jenkin, W. H. Lupton, and I. M. Vitkovitsky, *Rev. Sci. Instr.* 52, 694 (1981).
2. R. D. Ford and I. M. Vitkovitsky, *Rev. Sci. Instr.* 53, 1098 (1982).
3. V. A. Burtsev, et al., *Nuc. Fusion* 17, 887 (1977).
4. Yu. D. Bakulin, V. F. Kuropatenko, and A. V. Luchiuskii, *Sov. Phys. Tech. Phys.* 21, 1144 (1976).
5. R. A. Meger, R. J. Commissio, G. Cooperstein, and S. Goldstein, *Appl. Phys. Lett.* (to be published).
6. R. J. Commissio, R. F. Fernsler, V. E. Scherrer, and I. M. Vitkovitsky, (unpublished), Naval Research Laboratory Report 4975 (1982).
7. M. Kahn, "Effect of Heat-Treatment on the PTCR Anomaly in Semiconducting Barium Titanate," presented at the 72nd Annual Mtg. of American Ceramic Society, Philadelphia, Pa., May 5, 1970 (Electronics Division No. 16-E-70).
8. A. F. Doljak, *IEEE Trans. on Components, Hybrids, and Manufacturing Technology* CHMT-4, 372 (1981).
9. A. E. Rubson, private communication.

TABLE 1. Opening switch characteristics.

| <u>Circuit Parameters</u> | | |
|-------------------------------|--|-----------------------|
| Energy stored | 1000 J (with the capacitor bank at 400 V) | |
| Peak current | 2 KA (resistance limited) | |
| Charging time | 500 μ sec | |
| Load resistance | 0.125 Ω (with a maximum voltage drop of 150 V) | |
| <u>Switch Characteristics</u> | | |
| | <u>EFP</u> | <u>Copper Fuse</u> |
| Area | 8 cm ² | 0.115 mm ² |
| ρ_0 | 1 Ω cm | 3 $\mu\Omega$ cm |
| R/R ₀ | > 10 ⁵ | > 10 ² |
| Generated field | 2 KV/cm | ~ 1 KV/cm |
| Opening time | 40 μ s | ~ 25 s |
| Efficiency | ~ 90% | ~ 90% |
| Use | Resettable | One shot |

APPENDIX C

PHOTOCONDUCTIVE POWER SWITCHES*

W. C. Nunnally
Los Alamos National Laboratory

INTRODUCTIONBackground

Photoconductivity has been used for many years to change the current flow in a circuit by changing the conductivity of a circuit element with photons. In a photoconductive material, usually a semiconductor, an incident photon creates an electron hole pair which is separated and swept out of the device by an applied electric field, illustrated by the basic arrangement in figure 1. This effect is commonly used to detect light; more recently at Los Alamos and elsewhere, together with high speed lasers, the effect has been used to switch moderate voltages with very fast rise times (10 ps), to drive deflection systems in streak cameras and laser Pockel and Kerr cell systems, and to provide extremely fast sampling for high speed devices. The low to moderate voltage devices that use photons to control the conductivity between two electrodes have been designated photoconductive circuit elements (PCE). When the resistance of the device can be changed many orders of magnitude in a short period of time, the device can be designated a photoconductive switch. The switch will be efficient if the final resistance is much less than the external circuit resistance. The basic components and

* This material has appeared in a Los Alamos report.

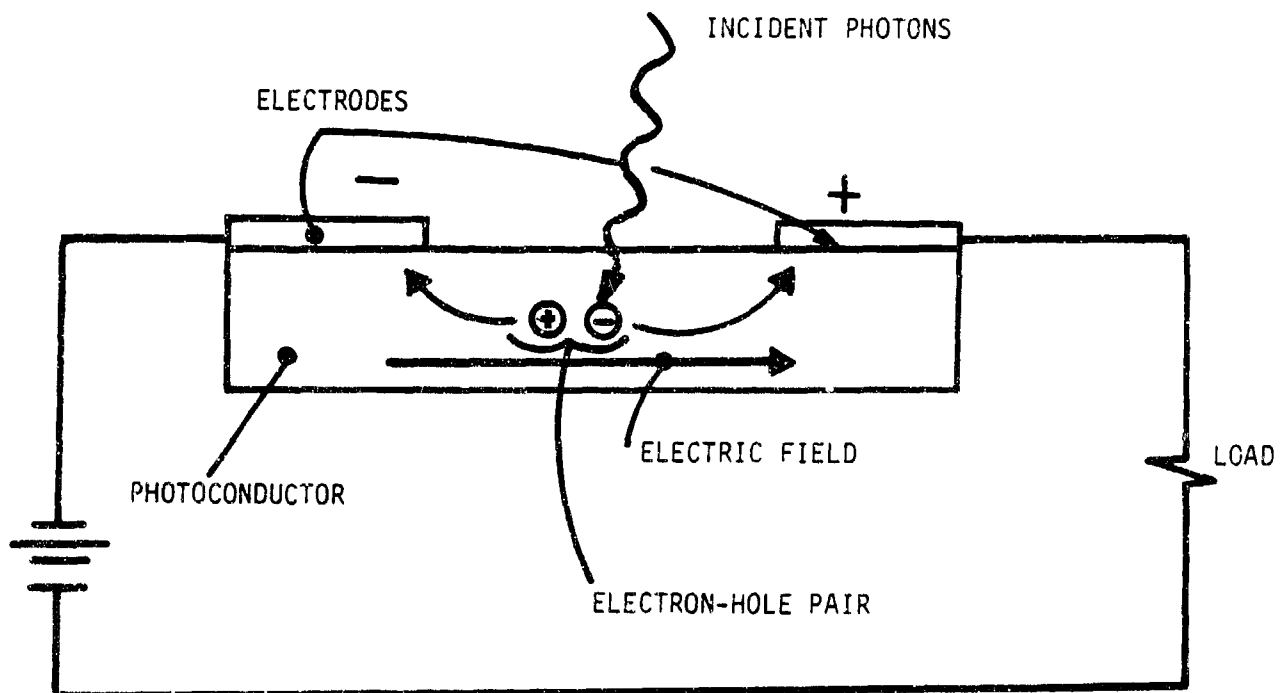


Figure 1. Basic photoconductive circuit.

geometry of a photoconductive switch are illustrated in figure 2. This technology is currently under development at Los Alamos for high speed detectors and switches. Its extrapolation to high voltage or high current regimes, or both simultaneously, suggests major advantages when compared to the conventional solid state switching devices used in AC power systems, and even to the super high power gas and water spark gaps used in weapons simulation and defense related systems.

Applications

AC Power Systems

The general applications of high power switches in AC power systems include the megawatt power level AC-DC and DC-AC converters that interface with very high voltage AC and DC power transmission lines and line fault interrupters that protect these transmission lines, as well as massive motor controllers for large industries. Millions of AC induction motors in the US are regulated with motor controllers which adjust the power flowing to the motor, depending on that required by the load. The DC power supply industry currently uses switching circuits to change the DC voltage level provided by the AC power line to a different, desired voltage in a light-weight, efficient manner. Switching DC power supplies are used in nearly all computer and aerospace applications because of their cost-effectiveness. All of these switching activities at present use solid state devices, such as thyristors and power MOSFETs, assembled in large parallel and series arrays to operate at high voltages and currents.

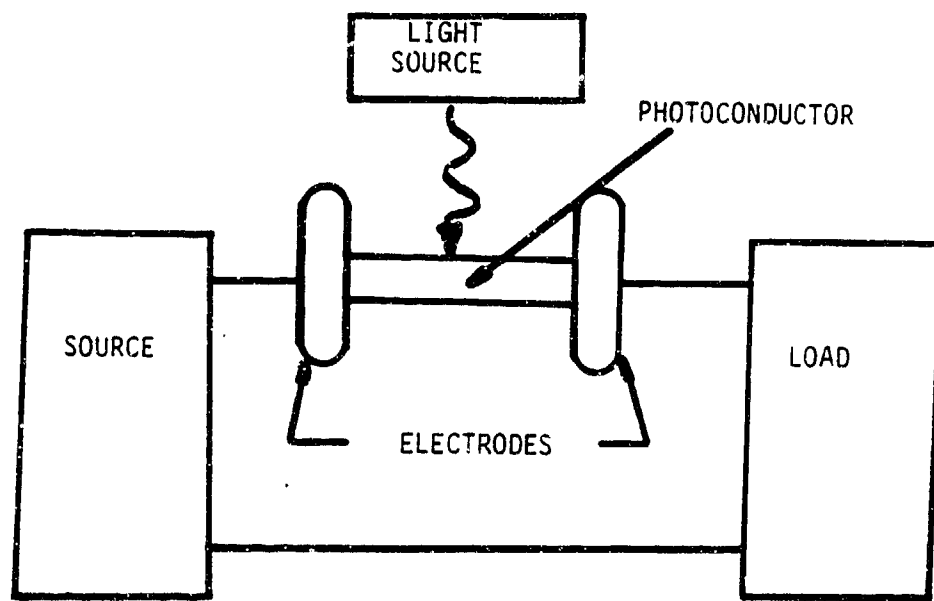


Figure 2. Simple photoconductive switch.

Pulse Power Systems

The other area of power switch application is pulsed power, in which short pulses of energy are conditioned and delivered to various loads at peak power levels up to several tens of terawatts. At the present time, these activities are associated with nuclear weapons simulation systems, inertial confinement fusion research projects, (both laser and particle beam), electric discharge laser driver systems for isotope separation development, and most recently, directed energy weapon power supplies (both laser and particle beam). Multiple, parallel and series high pressure gas or water spark gaps are now used to generate and deliver terawatt peak power, low repetition rate pulses. Megawatt peak powers at moderate to high repetition rates are formed using low pressure gas thyratrons, while gigawatt peak powers at moderate to high repetition rates require a combination of thyratrons and multistage magnetic pulse compression systems.

ADVANTAGES OF PHOTOCOCONDUCTIVE POWER SWITCHES

The major advantage of the Photoconductive Power Switch (PCPS) is simplicity. Simplicity of fabrication results in a rugged, cheap system which can be scaled to any application. Simplicity of operation through optical control results in performance that has the potential to surpass nearly all of the conventional switch technologies in their present applications. The general high power PCPS shown in figure 3 consists of a cylinder of photoconductive material with electrodes on each end, and a cylindrical light source in the center. The potential of

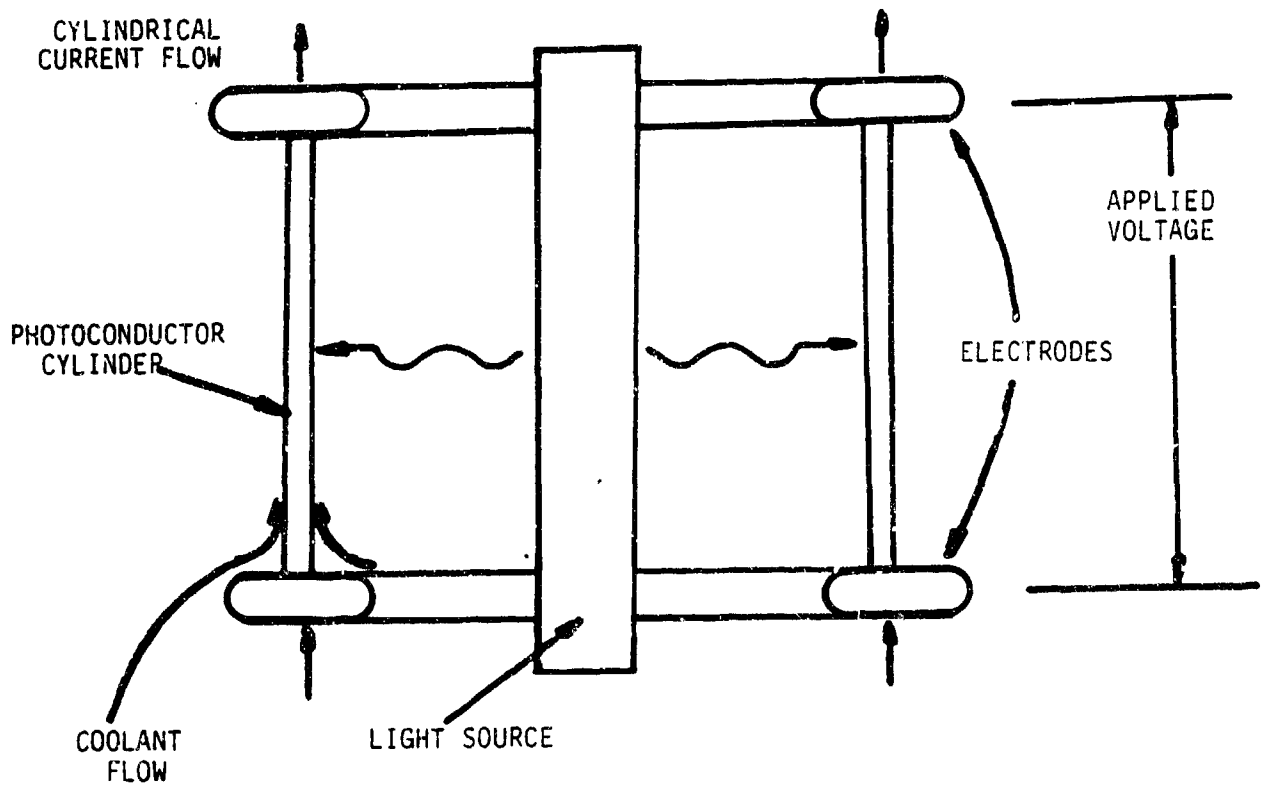


Figure 3. Cylindrical photoconductive switch.

this technology and its advantages are listed and discussed briefly below.

Linear Voltage Stress

The maximum operating voltage of a photoconductive switch is determined by the length of the device. This property permits scaling the device length between the electrodes (shown in figure 3) to operate at the desired voltage. Since the electric field strength of semiconductor photoconductive materials is large, a high voltage device can be very compact, i.e., a megavolt switch can be 10 cm long. In addition, the operation of the device is independent of the applied voltage, if less than the maximum design voltage, since turn-on is determined by the optical energy incident on the surface. The linear voltage stress of the PCPS material results in a system that is easily graded, so that each length segment of the switch is stressed equally by transients. This implies that the PCPS system does not require transient suppressors, as do arrays of conventional devices.

Linear Current Capability

The maximum current conduction capability of a photoconductive switch is determined by the width of the device. This property permits scaling the device width to accommodate application current requirements. Current is carried by the entire circumference of the cylindrical switch, shown in figure 3.

Large Current Surge Capability

The maximum current per unit width of the switch illustrated in figure 3 is dependent on the thermal properties of the photoconductive material and the surface available for heat transfer.

Note that both sides of the conducting cylinder in figure 3 are available for heat transfer, so that the distance heat must be transferred to the coolant is small; the thermal resistance of a PCPS is extremely low. The thermal properties of photoconductive semiconductor materials are excellent, while the damage temperature of the switch is much higher than for conventional devices because no junctions are involved. In addition, the conduction resistance of a PCPS is independent of device width for a constant optical turn-on energy, which permits the resistive energy dissipation in the switch to be distributed over a large volume. Simultaneously, increasing the width of the device also increases the area available for heat transfer, so that a single PCPS can be designed to handle any power level. In addition, the switch resistance can be decreased by increasing the incident optical energy, so that conduction losses can be controlled for any application and the conduction voltage drop can be reduced even below the standard junction drop of conventional devices.

Optical Turn-On Control

The rate of turn-on is controlled by the time rate of increase in light intensity incident on the surface of the device. Thus, the switching action is independent of the circuit conditions and the control system is isolated from the circuit. The advent of high power, fast pulse lasers permit turning PCPS devices on in nanoseconds instead of the hundreds of nanoseconds required for MOSFETs, and the microseconds required for thyristors. The fast turn-on reduces switching losses and also permits high frequency operation, in switching power supplies, for

example. The low jitter of the high power lasers permits precise timing of the turn-on process so that sub-nanosecond time resolution of high power switches is possible. The other benefit of optical control is the possibility of multiplexing and redundancy. Several switches spanning the same electrode gap can be used, and the activating light pulse switched remotely between devices or switched to a standby device. The uniform space and time irradiation of a PCPS device causes the entire switch to turn on simultaneously, so that accumulation transients, which overvoltage portions of conventional switches used in arrays, do not exist.

Circuit Parameter Control

As mentioned previously, the conduction resistance of PCPS devices is independent of the device width for a constant optical energy. The circuit inductance, however, decreases as the current path width is increased, so that a very low inductance device can be fabricated. This property is very important in very high speed devices, independent of the operating power level. Inductance is a large problem at high powers because of the large conductor separations required for megavolt operation. The switch of figure 3 can be very low inductance if it is the center conductor of a large diameter coaxial transmission line, in which the coaxial conductor spacing is determined by the maximum voltage requirements, and the circumference or conductor width is determined by the inductance required.

Material Limited Turn-Off Control

The carrier recombination rate is dependent on the trap doping level of the semiconductor used as the photoconductive material. This property allows the turn-off time of a PCPS device to be selected. This characteristic will permit, in principle, the use of PCPS devices as high power repetitive pulse switches, because the characteristic recombination times are much shorter than those of thyratrons currently used in repetitive applications. In addition, circuit breaker or opening switch applications may be possible using materials with large trap densities to produce very fast recombination times.

Solid State Reliability and Lifetime

All of the above advantages of PCPS devices should be available with the standard solid state reliability and lifetime. The flexibility based on the above properties permits the design for a specific application to be conservative and thus reliable.

Liquid Nitrogen Operation

Photoconductive switches can be operated at liquid nitrogen temperatures with several very important advantages. First, the photoconductive dark current resulting from thermal carrier generation can be reduced to the point where thermal runaway is not a problem. In this case, the applied electric field or voltage can be increased to a level at which avalanche switching after optical initiation is possible. The process has been shown to decrease the optical energy required for triggering up to three orders of magnitude. In addition, liquid nitrogen operation

could make enhanced cooling possible, and thus a more compact switch.

RESEARCH AND DEVELOPMENT REQUIRED FOR PCPS APPLICATION

Several areas of research and development are required to make PCPS applicable to all of the areas discussed. These areas can be divided into three major categories; switch material evaluation, fabrication technology, and light source development. Basic details of these are briefly discussed below.

Photoconductive Materials Evaluation

Practical electrical field stress.

The maximum electric field stress of photoconductive materials, and the optimum electrode geometries for the combination of the semiconductor, the metal electrodes, and the medium between the light source and the switch, must be determined experimentally and correlated with analytical results. Small scale experiments at Los Alamos have used a 3 cm long, 0.5 cm square silicon bar to switch a peak voltage of 100 KV and a peak current of 4.5 KA in a 200 n pulse.

Current conduction capability.

The current surge capability of the photoconductive material, as well as that of the electrodes and the contacts, must be determined experimentally. In conventional solid state devices, the I^2t product is measured for comparison of switch and diode devices. The I^2t product is a measure of the maximum energy the device can absorb without damage, and implies that the device can carry a large current for a short time or a smaller current for a longer time. Calculations indicate that photocon-

ductive switches have a much larger I^2t product than conventional devices, but experimental verification is required. The large values of the I^2t product and the wide range of currents and times over which the devices are to be used requires a large investment in experimental facilities. Los Alamos experiments are investigating the several hundred nanosecond regime at very high currents.

Fabrication technology.

The fabrication of contacts and the physical environment of large photoconductive devices requires research into the surface states of the photoconductive material and the physical conditions at the interface of the material and its environment. In addition, a thorough knowledge of the physical processes and the electromagnetic fields at the semiconductor-metal interface is required to develop reliable switches for the many applications discussed. Los Alamos is currently evaluating several electrical contact and high voltage grading techniques for high power PCPS devices.

Thermal runaway characteristics.

The characteristics of the switch system that minimize thermal runaway problems must be determined. The removal of heat from the switch material is the major switch problem to be addressed because of the large thermal response times for these systems. The removal of heat is limited by the heat transfer coefficient at the switch coolant boundary. Adiabatic switches can be used for burst mode and single pulse applications, but the power level of repetitive pulse switches and continuously oper-

ating AC power switches will be limited by the removal of heat.

Light Source Development

Light sources for the many possible applications of PCPS will require additional development. The rapid development of high power lasers, as well as efficient solid state light sources, have made the practical application of PCPS feasible. For the single, large power, short pulse power applications, such as weapons simulation and inertial confinement fusion research, the light sources are well developed. Several glass laser systems have been developed to deliver kilojoules of one micron photons in less than a nanosecond, which is ideal for the switching of a large single multiple megajoule electrical pulse of several hundreds of nanoseconds duration.

The light sources for switching short electrical pulses at medium to high repetition rates (10-100 KHz) require the most development. The glass type lasers currently used to deliver the one micron wavelength photons that are ideal for silicon photo-conductive switching cannot, at present, be operated in the repetitive high optical power mode because the excess heat cannot be removed from the lasing solid state material in the time between pulses. Solid state light sources operate in the proper wavelength region with a much larger efficiency than flashlamp pumped glass type lasers, but the peak power required has not been demonstrated in a single system. Thus, a solid state light source using array techniques that are added using distribution tactics or fiber optic light guides are a possibility. Another

possibility is the use of solid state light array pumped glass or YAG lasers whose cross-section is distributed to enhance the removal of heat. The conventional flashlamp pump sequence is very inefficient because a majority of the pump energy is not in the correct wavelength or time aperture for pump, whereas a distributed solid state array can be wavelength tuned and well controlled in time and space to increase the overall system pump efficiency.

The development of light source systems for AC power applications require the largest scaling of the current light sources technologies. The duration of the 60 Hz power cycle requires a long pulse light pulse to maintain the carrier density throughout the long electrical pulse. In addition, the reduction of switching losses requires a very high power optical pulse for fast turn-on. However, a short pulse, high power, laser can be used for turn-on, and a solid state light source for carrier maintenance during the long current pulse. The requirement involves the application of the solid state light source system in continuous operation mode and the operation of the laser or high power light source with a repetition rate of 60-240 Hz, continuously. Again, solid state pumped glass or YAG lasers are a candidate for further development in this area.

The other application in the AC power arena is that of switching power supplies, which operate switches at a 50 percent duty level continuously, to generate square wave outputs up to 100 KHz. Higher frequencies of operation, and thus more efficient and lightweight systems, are possible with photocconductive

switches, if light sources can be developed for this frequency of operation. This is another area of light source development that remains unexplored at this time. A photoconductive material with a short recombination time or turn-off time must be used in this application. Thus, the light source pulse duration must be equal to the electrical pulse duration. This is probably the most demanding light source problem yet discussed, and requires the largest extrapolation of current technology.

ANALYSIS OF PHOTOCODUCTIVE POWER SWITCHES

Resistance of Photoconductive Switches

The resistance of the photoconductive volume shown in figure 4 is determined by the standard resistance equation,

$$R = \ell/\sigma A, \quad (1)$$

where σ is the material conductivity, ℓ is the electrical path length, and A is the cross-section through which current flows. The area for the photoconductive volume of figure 4 is given by

$$A = d_e w, \quad (2)$$

where w is the width of the photoconductive volume, and d_e is the effective depth of penetration of the activating light source, that is, the effective absorption length. The conductivity of the material

$$\sigma = n e \mu_n + p e \mu_p, \quad (3)$$

where n and p are the electron and the hole density densities, respectively, e is the electron and the hole charge, and μ_n and μ_p are the electron and the hole mobilities, respectively. The incident photons create hole-electron pairs of equal density much

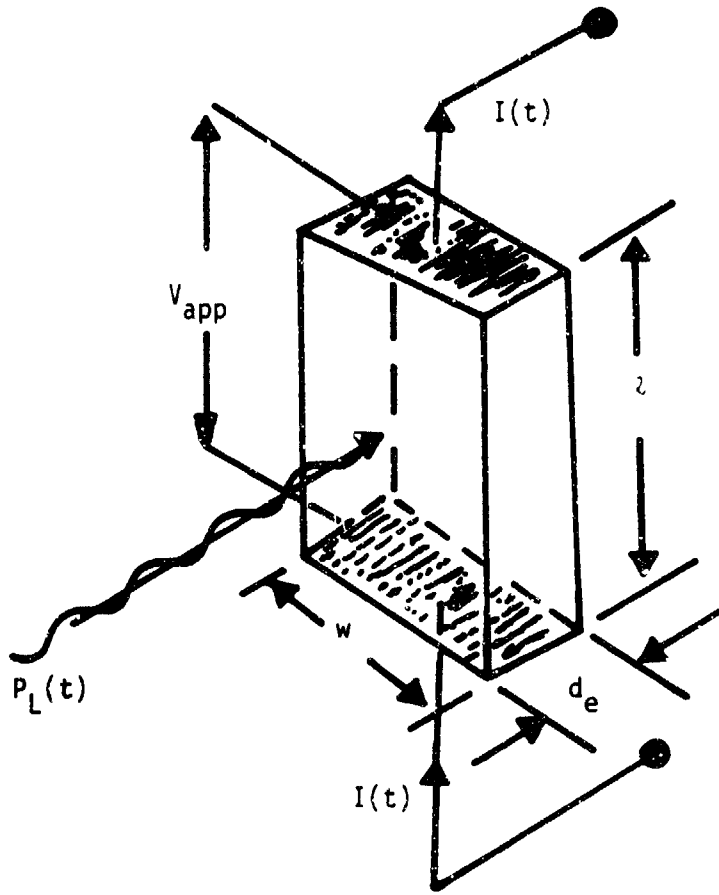


Figure 4. Model for the calculation of the resistance of a photoconductive switch.

greater than the background density, so that, if the electron mobility is assumed to be significantly greater than the hole mobility, the conductivity becomes

$$\sigma = ne\mu_n. \quad (4)$$

The time rate of change of the carrier density is given by the equation

$$\frac{dn}{dt} = P_L(t)(1-r)/(E_\lambda w\ell d_e) - n/\tau_r - (1-\eta_i)n/\tau_t \quad (5)$$

where $P_L(t)$ is the time varying incident light power in watts, r is the material reflectivity at the light wavelength, $w\ell d_e$ is the volume of the photoconductor irradiated by the light, E_λ is the photon energy, τ_r is the material recombination time, η_i is the contact injection efficiency, and $\tau_t = \ell/v_d$ is the transit time of the system where v_d is the carrier drift velocity and ℓ is the length of the carrier path. The first term in equation (5) describes the rate of electron hole production, the second term describes the rate of electron and hole attrition due to recombination, with a characteristic e-folding time of τ_r and assuming an infinite number of recombination centers, and the third term describes the rate of carrier loss due to the contact injection inefficiency, $(1-\eta_i)$. If the last two terms are grouped with coefficient β , defined by

$$\beta = 1/\tau_r + (1 - \eta_i)/\tau_r, \quad (6)$$

the solution to the equation for the carrier density becomes

$$n(t) = e^{-\beta t} \int_0^t e^{\beta t} (P_L(t)(1-r)/(E_\lambda w\ell d_e)) dt. \quad (7)$$

If the light power, $P_{(0,t)}$, is assumed to be constant, P_0 , for a period of time, t_L , then the carrier density becomes

$$n(t) = P_0(1-r)(1-e^{-\beta t})/(E_\lambda w\ell d_e \beta) \quad (8)$$

for time such that $0 < t < t_L$. If the light source is turned off instantaneously at $t = t_L$, the carrier density decreases in time as

$$n(t) = n_0 e^{-\beta t}, \quad (9)$$

for time such that $t_L < t$. n_0 is the value of $N(t)$ at $t = t_L$. If the injection efficiency is assumed to be unity, and the recombination time, τ_r , is much longer than the optical pulse length, t_L , then the term $(1-e^{-\beta t})$ can be approximated as βt , so that the carrier density at $t = t_L$ becomes

$$n(t) = P_0(1-r)t_L/(E_\lambda w d_e). \quad (10)$$

The total energy in the light pulse is given by

$$E_L = t_L P_0, \quad (11)$$

so that the resistance from equation (1) for an injection efficiency of unity and $t_L \ll \tau_r$ becomes

$$R = \ell^2 E_\lambda / (e \mu_n E_L (1-r)), \quad (12)$$

which is independent of the pulse width for a constant optical energy deposited in the photoconductive volume.

The steady-state resistance can be determined by setting $dn(t)/dt = 0$ in equation (5) and solving for $n(t)$. Then the steady-state resistance of the switch is

$$r_{ss} = \ell^2 E_\lambda (1/\tau_r + (1-n_i)/\tau_t) / (P_L(t)(1-r)e \mu_n) \quad (13)$$

Previously, the injection efficiency of the material contacts had been assumed to be unity for simplicity. The transit time, τ_t , for most devices is very small, so that the $1/\tau_r$ term corresponding to the material recombination time can be neglected in some materials unless the contact injection efficiency is very near unity. For example, a switch made of silicon with a length of 3

cm must have a contact injection efficiency on the order of 0.99 for the two terms contained in α to be comparable. For the second term to be negligible, the contact injection efficiency in the silicon switch must be of the order of 0.999. It is interesting to note that the steady state resistance of the switch varies with applied voltage if the recombination time is neglected in equation (13).

The contact injection efficiency is a crucial part of a photoconductive switch. Note that reducing the effective recombination time, β , with a non-unity contact injection efficiency, increases the amount of optical power required to maintain a constant carrier density, and thus reduces all of the gain parameters. The contact injection efficiency can be made unity in small scale devices and corresponds to a perfect ohmic contact.

I^2t PRODUCT FOR PHOTOCODUCTIVE SWITCHES

Commercial semiconductor switches and diodes are characterized by their measured I^2t product, which determines the damage level of energy deposited in the device. Devices usually have a single pulse 60 Hz AC surge rating and a continuous 60 Hz AC rating. The length of the device current pulse can be increased if the current is reduced, or the pulse length can be shortened and the current increased, so that the I^2t product is constant over a relatively broad range.

Energy is deposited in the resistance of the device and raises the temperature of the material to the damage temperature. The junction device damage temperature is about 180 °C, whereas the melting temperature of silicon is about 1400 °C. The energy,

Q , deposited in a resistance, R ,, by a current $I(t)$ in time t is given by

$$Q = \int_0^t [I(t)]^2 R dt . \quad (14)$$

In the adiabatic case, all of the energy is absorbed in the switch volume, i.e., none of the energy is removed by thermal diffusion during the current pulse. In this case, the total temperature change is determined by the specific heat of the material and the mass of the switch volume, that is,

$$Q = mc_p (T_{final} - T_{initial}) = mc_p \Delta T , \quad (15)$$

where m is the mass of the switch conducting volume, $lwd_e \rho$, and ρ is the material density. Using equations (14) and (15), the calculated $I^2 t$ product for the adiabatic photoconductive switch, with the resistance defined in equation (12), is

$$(I^2 t)_c = \rho w d_e c_p \Delta T e \mu_n (1-r) E_L / (E_\lambda l) . \quad (16)$$

Equation (16) assumes that the carrier density created by the light energy, E_L , remains constant, and thus the resistance remains constant for all time t , which is not the case if the current pulse length is comparable to the recombination time of the material, or if the contact injection efficiency is less than unity. Additional optical energy must be added to maintain the carrier density lost to recombination and contact injection efficiency in the long pulse case.

In order to compare the measured value of $I^2 t$ for commercial devices and that calculated using the previous assumptions, the value of $I^2 t$ for a unit cross-section and unit current path length is determined in the following manner. The single pulse surge capability of a large 4000 V diode (80 mm diameter and an

approximate thickness of 1 mm), in a cylindrical compression package, is around $1 \times 10^6 \text{ A}^2 \text{ s}$. The electric field stress, E_{\max} , in the bulk of the semiconductor is around 40 KV per cm.

The length of the current path can be defined as

$$l = V_{\text{app}}/E_{\max} \quad (17)$$

If the measured value is defined as $(I^2 t)_m$, the comparison value of $I^2 t$ per unit area for the conventional device is given by

$$(I^2 t)_m^* = (I^2 t)_m/A_d = 2 \times 10^8 \text{ amp}^2 \text{ sec/m}^2, \quad (18)$$

where A_d is the area of the diode wafer through which current flows. The same type of modification to the calculated adiabatic value of $I^2 t$, $(I^2 t)_c$, for the photoconductive switch, yields

$$(I^2 t)_c^* = \rho c_p \Delta T \epsilon \mu_n (1-r) E_L / (E_\lambda l), \quad (19)$$

where the calculated value of $(I^2 t)_c$ has been divided by the area, $w d_e$, and where l is defined by equation (17). If the calculated comparison value and the measured comparison value are equated to determine the optical energy required on the photoconductor to equal the best conventional device, the following relation for the surface optical energy density is obtained:

$$E_L / (lw) = 2 \times 10^8 E_\lambda / (w \rho c_p \Delta T \epsilon \mu_n (1-r)), \quad (20)$$

which scales inversely as the width of the device. This is to be expected, inasmuch as the resistance of the photoconductive switch is independent of its width and increasing the width only reduces the power dissipated per unit volume.

Choosing $w = 0.1 \text{ m}$, $T = 1000^\circ \text{C}$, $R = 0.3$, and using $c_p = .07 \times 10^3 \text{ J/Kg}^\circ \text{C}$, $\rho = 2.33 \times 10^3 \text{ Kg/m}^3$, $\mu_n = 0.13 \text{ m}^2/\text{sec}$, and $E_\lambda = 1.2 \times 20^{-19} \text{ joules}$ for a 1.06 micron wavelength, the

surface density of optical energy is calculated to be 10 joules/m² or 1.0 mJ/cm². Note that this value is easily obtained with solid state light devices, and that the result scales inversely with width. Choosing a larger w would decrease the optical energy density, but the total energy density for a constant length l is independent of the width, w . The important point is the potential of this technology in terms of current conduction capability, inasmuch as an increase in surface energy density increases the adiabatic current conduction capability by reducing the device resistance; thus the resistively deposited energy is reduced for a given current and time. It is easy to imagine increasing the I^2t product for photoconductive switches several orders of magnitude over conventional devices. In addition, the fast turn on time of photoconductive switches will permit operating at very short pulse lengths and thus at very high currents for short periods of time.

The single pulse surge capabilities of the photoconductive switch are very large. For example, if $E_L = 10$ J, $w = 1$ m, and $\mu = 0.1$ m, using the same assumptions as the previous example, the value for the I^2t product of equation (15) is found to be 1.5×10^7 A²s. Thus this switch will conduct 10 MA for an electrical pulse 150 ns long, with an optical trigger energy of 10 J.

RATIO OF TURN-ON TO SUSTAINING OPTICAL POWER

The previous calculations assumed that the carrier density during the surge currents and the repetitive pulse currents were constant, or that the recombination time was infinite. In a

realistic switch, the carriers will recombine and the density will have to be maintained with additional optical energy. If the desired carrier density in time is given by

$$n(t) = n_0 (1 - e^{-t/t_r}) , \quad (21)$$

where t_r is the e-folding rise time of the carrier density, and thus the e-folding time of the resistance decrease or the switching time, and n_0 is the steady-state density desired. The time rate of carrier density change in equation (15) can be solved for the laser power required to generate a time varying density $n(t)$:

$$P_L(t) = E_\lambda w d_e (dn(t)/dt + \beta n(t)) ; \quad (22)$$

substituting from equation (21) for $n(t)$, equation (22) becomes

$$P_L(t) = n_0 E_\lambda w d_e (e^{-t/t_r} (1/t_r - \beta) + \beta) . \quad (23)$$

The first term in equation (23) is the power required to turn on the switch in time t_r ; the second term is the power required to maintain the carrier density n_0 in steady-state operation. At $t = 0$, the maximum optical power required for turn-on is

$$P_{L\max} = n_0 E_\lambda w d_e / t_r , \quad (24)$$

and for $t \gg t_r$, the sustaining power is

$$P_{L\text{sus}} = n_0 E_\lambda w d_e \beta , \quad (25)$$

so that the ratio of the maximum power to the sustaining power is

$$P_{L\max}/P_{L\text{sus}} = 1/(\beta t_r) . \quad (26)$$

If the injection efficiency is unity, then from equation (6), β is equal to $1/t_r$, and the ratio becomes

$$P_{L\max}/P_{L\text{sus}} = t_r/t_2 . \quad (27)$$

For example, if $t_r = 20$ nanoseconds and $\tau_r = 20$ microseconds (as in silicon), the maximum power is 1000 times as large as the sustaining power. Two light sources could be used to provide the optical power time sequence required.

The energy required to maintain the carrier density, n_0 , for one recombination time, is given by the product of the sustaining light power and the recombination time, τ_r ,

$$E_{Lsus} = P_{Lsus} \tau_r = N_0 E_\lambda \lambda d_e \tau_r / t_r . \quad (28)$$

The total energy delivered to the switch during the pulse is the integral of the light power over the electrical pulse, or

$$E_{LT} = \int_0^{t_{ep}} P_L(t) dt , \quad (29)$$

where t_{ep} is the electrical pulse length. The energy required to turn on the switch is the integral of the light power for three rise time constants, or

$$E_{turn-on} = n_0 E_\lambda \lambda d_e (1 + 2\beta t_r) , \quad (30)$$

where β is defined by equation (6). If the contact injection efficiency is unity, then β is equal to $1/\tau_r$, so that the last term of equation (30) is negligible if τ_r is much greater than t_r .

SWITCHED ENERGY GAIN

The gain of a photoconductive switch is best described using the ratio of the energy transferred to the load, to the laser energy incident on the surface. If a matched system is considered (figure 5), in which the source impedance is equal to the load impedance, and the switch resistance is much lower than the load impedance, then the energy delivered to the load, assuming the

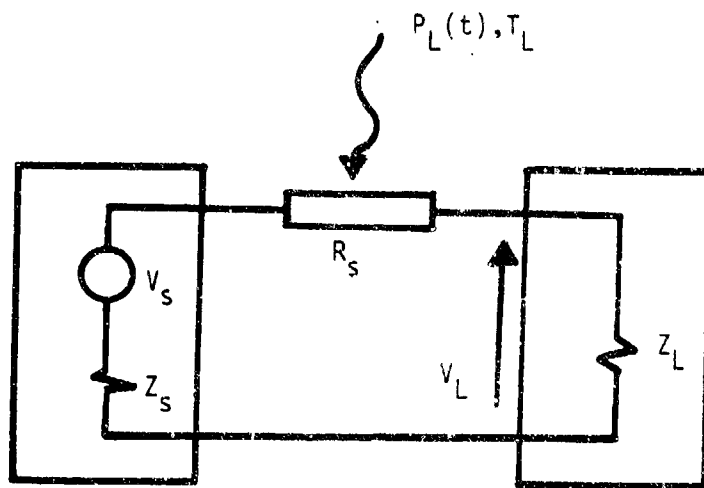


Figure 5. Circuit for calculation of switched energy gain.

electrical pulse rise time is much less than the pulse length, is given by

$$E_{load} = (V_s/2)^2 / Z_L t_{ep} \quad (31)$$

where V_s is the source voltage, Z_L is the load impedance, and t_{ep} is the electrical pulse length. If the maximum electrical pulse length is determined by the heat capacity of the switch volume, then

$$t_{ep} = Q / (I^2 R_s) = \rho d_e w l c_p \Delta T / (R_s I^2), \quad (32)$$

where Q is the heat delivered to the switch, and I is the load current,

$$I = V_s / (2Z_L) . \quad (33)$$

The switched energy gain becomes

$$E_{load}/E_{light} = \rho d_e w l E_{max} c_p \Delta T \mu_n (1-4) / (V_s E_{\lambda} Z_L), \quad (34)$$

where the switch length has been chosen from equation (16).

Using $\rho = 2.33 \times 10^3 \text{ Kg/m}^3$, $E_{max} = 1 \times 10^7 \text{ V/m}$, $c_p = 0.7 \times 10^3 \text{ J/Kg} \cdot ^\circ\text{C}$, $e = 1.6 \times 10^{-19} \text{ coul}$, $\mu_n = 0.13 \text{ m}^2/\text{s}$, $E = 1.2 \times 10^{-19} \text{ J}$, and $r = 0.3$, and choosing $Z_L = 1 \Omega$, $V_s = 1 \times 10^6 \text{ V}$, and $d_e = 200 \times 10^{-5} \text{ m}$ for a width of 1 m, the switched energy gain is about 4×10^5 ; this is a very large value. This simple calculation assumes that the carrier density is constant after turn-on, or an infinite recombination time. In addition, the electric field during conduction is assumed low so that the mobility is not saturated. However, the extremely large potential of this technology is indicated by this first order calculation of the possible switched energy gain.

STEADY-STATE POWER GAIN

Another important parameter (applicable only if the switch is in steady-state operation) is the power gain. This is the ratio of the power flowing through the switch into the load, to the sustaining light power maintaining the carrier density. If the rate of energy dissipation per unit volume in the switch is defined as Q' , then the steady-state temperature distribution across the light absorption distance is given by

$$T(x) = Q'x^2/(2K) + \{2(T_{\text{edge}} - T_{\text{center}})/d_e - Q'd_e/(4K)\}x + T_{\text{edge}} , \quad (35)$$

where K is the thermal conductivity, T_{edge} and T_{center} are the temperature of the edge and the center of the conducting volume, respectively, and the surface of the conduction region is defined as $x = 0$. The rate of heat flow per unit area from the switch material must equal the rate of heat flow per unit area into the coolant at the boundary, so that

$$KdT/dx = h(T_{\text{edge}} - T_{\text{fluid}}) , \quad (36)$$

where h is the heat conduction coefficient and T_{fluid} is the average coolant temperature. Evaluating the derivative in equation (35) at $x = 0$, the switch surface, and using equation (17), the maximum rate of heat removal, and thus the maximum rate of heat deposition, per unit volume in steady-state is

$$Q' = 4h(T_{\text{fluid}} - T_{\text{edge}})/d_e + 8K(T_{\text{center}} - T_{\text{edge}})/d_e^2 , \quad (37)$$

where the first term describes the heat flow from the switch material to the coolant, and the second term describes the heat flow from the center of the conducting switch region to the sur-

face of the switch. The thermal resistance from the center of the conducting switch region to the coolant fluid per unit area is given by

$$R_T = d_e / (2K) + 1/h . \quad (38)$$

The first term in equation (38) is the thermal resistance of the photoconductor, and the second term is the thermal resistance of the switch-fluid interface and region. The first term is much smaller than the second for any semiconductor material, especially with the small effective depth of optical penetration, that is, the thin conduction region. Thus, the heat flow of the system is dominated by the conduction from the solid to the coolant. Then the temperature distribution in the photoconductive material is uniform, and T_{center} is approximately equal to T_{edge} , so that the heat removal rate is approximately

$$Q' = 4h(T_{edge} - T_{fluid})/d_e . \quad (39)$$

The average power dissipated in the switch volume must then be less than or equal to the heat removed, or the product of Q' and the conducting volume,

$$I^2 R_c = Q' w l d_e , \quad (40)$$

where I is the average current through the switch and load, R_c is the steady state on resistance, defined by

$$R_c = \lambda / (N_0 \mu n_c w d_e) , \quad (41)$$

and n_c is the steady-state carrier density. The power gain is determined by the ratio of the load power to the sustaining optical power. This ratio is

$$P_{gain} = I^2 Z_L / (N_0 E_\lambda w l d_e \beta) , \quad (42)$$

which can be expressed, using equation (41) for n_0 , as

$$P_{\text{gain}} = I^2 R_o Z_L \mu_n e / (\epsilon_\lambda \ell^2 \beta) . \quad (43)$$

Replacing $I^2 R_o$ using (equation (40)), and using equation (17), the power gain becomes

$$P_{\text{gain}} = 4hwZ_L \mu_n e E_{\text{max}} (T_{\text{edge}} - T_{\text{fluid}}) / (\epsilon_\lambda \beta V) . \quad (44)$$

Note that the quantity $2Z_L/V = 1/I$ for a matched system, so that the power gain can also be written as

$$P_{\text{gain}} = 2hw\mu_n e E_{\text{max}} (T_{\text{edge}} - T_{\text{fluid}}) / (\epsilon_\lambda \beta I) , \quad (45)$$

which is inversely proportional to the load current or the total number of carriers.

Again, choosing $h = 500 \text{ J/sm}^2 \text{ }^\circ\text{C}$, $Z_L = 1 \Omega$, $V = 1 \times 10^6 \text{ V}$, $w = 1 \text{ m}$, $e = 1.6 \times 10^{-19} \text{ coul}$, $\beta = 5 \times 10^4 \text{ s}^{-1}$, $\mu_n = 0.13 \text{ m}^2/\text{s}$, $\epsilon_\lambda = 1.2 \times 10^{-19} \text{ J}$, $T_{\text{fluid}} = 30^\circ\text{C}$, $T_{\text{edge}} = 1000^\circ\text{C}$, and $E_{\text{max}} = 1 \times 10^7 \text{ V/m}$, the power gain for this example is about 30 for the 1 meter width. Note that increasing the switch width will increase the power gain, so that a 10 m wide switch would have a power gain of 300. If the amount of heat being deposited in the material is too large, the sustaining laser power can be increased to reduce the switch resistance, but the steady-state power gain will be reduced.

REPETITIVE PULSE POWER GAIN

In the quasi-steady state mode of operation, an equilibrium is reached between the steady-state removal of heat and the repetitive deposition of energy in the switch material by short, high power pulses at a pulse repetition rate, PRR. In this case, the electrical pulse length and the rise time of the light control pulse are both much less than the material recombination time, so that a sustaining light source is not required. Then the average light power is

$$P_{\text{Lave}} = E_{\text{turn on}} \cdot \text{PRR} = n_0 E_{\lambda} \omega d_e \cdot \text{PRR} \quad (46)$$

from equation (30). The ratio of the average power deposited in the load to the average light power is the repetitive pulse power gain, or

$$RP_{\text{gain}} = I^2 Z_L t_{\text{ep}} / (n_0 E_{\lambda} \omega d_e), \quad (47)$$

where the PRR in the numerator and the denominator cancel. The requirements on the heat transfer and the energy deposition in the switch are identical to those in the steady-state case, so the repetitive pulse power gain is

$$RP_{\text{gain}} = I^2 Z_L t_{\text{ep}} R_o \mu_n e / (E_{\lambda} \omega^2). \quad (48)$$

In the repetitive pulse case, the average rate of energy dissipation in the switch is equal to that removed (equation (40)), or

$$Q' = I^2 R_o t_{\text{ep}} \cdot \text{PRR} = 4 \hbar \omega (T_{\text{edge}} - T_{\text{fluid}}). \quad (49)$$

Then the repetitive pulse power gain is equal to

$$RP_{\text{gain}} = 4 Z_L E_{\text{max}} \hbar \mu_n e (T_{\text{edge}} - T_{\text{fluid}}) / (E_{\lambda} V_s \cdot \text{PRR}), \quad (50)$$

which is related to the steady-state power gain by

$$RP_{\text{gain}} = P_{\text{gain}} \beta / \text{PRR}, \quad (51)$$

implying that, for silicon with a recombination time of 20×10^{-6} s, or $\beta = 5 \times 10^4$, the repetitive pulse gain is greater than the steady-state power gain for $PRR < 5 \times 10^4$. A more appropriate set of parameters for repetitive operation are $V = 3 \times 10^5$ V, $Z_L = 12 \Omega$, and $PRR = 1 \times 10^4$, providing a repetitive power gain of about 1.5×10^4 for the other conditions listed below equation (45).

THERMAL RUNAWAY AND THERMAL RECOVERY TIME

The problem of thermal runaway has been neglected in the previous discussion. In the case of the I^2t product, the rating is a measure of the single pulse surge capability of the device. For single pulse applications, thermal runaway is not a problem unless fast switch turn-off is desired because, after the pulse, the switch system has a very long time in which to return to its original temperature.

Conventional devices are also rated for 60 Hz applications with a separate I^2t product for continuous operation, usually much lower than the single pulse surge rating. Thus, in the case of repetitive pulses or in 60 Hz continuous AC applications using photoconductive switches, the problem of thermal runaway must be addressed. Thermal runaway occurs in semiconductor materials when the temperature increases, resulting in higher carrier concentrations and higher dark currents, causing additional power dissipation, which in turn causes additional carrier generation and a regenerative runaway. To prevent thermal runaway from causing premature conduction when the source voltage is applied, the thermal energy deposited in the switch during conduction must

be removed prior to voltage application to the switch for the next pulse. Thus the switch temperature must recover to a value that is compatible with the operating conditions of the system. The differential equation for the time rate of energy change in the switch volume is given by

$$mc_p \frac{dT}{dt} = I^2 R_o - hwl(T - T_{fluid}). \quad (52)$$

The temperature distribution in the switch is assumed uniform because the thermal resistance in the switch material is much less than that of the solid to coolant interface, so that the temperature of the surface is also the temperature of the entire switch volume. Then the differential equation for the switch temperature can be written as

$$\frac{dT}{dt} + \alpha T = I^2 R_o / (mc_p) + \alpha T_{fluid}, \quad (53)$$

where the coefficient α is equal to the inverse of the thermal response e-folding time of the system, and is defined by

$$\alpha = hwp / (mc_p) = h / (pc_p d_e). \quad (54)$$

If the maximum change of temperature is defined as

$$T_{max} - T_{fluid} = \Delta T_{max}, \text{ where}$$

$$\Delta T_{max} = I^2 R_o / (mc_p \alpha) = I^2 R_o / (hwl), \quad (55)$$

then the solution to equation (53) during the electrical pulse is

$$T(t) = T_{fluid} + \Delta T_{max} (1 - e^{-\alpha t}), \quad (56)$$

and the maximum temperature of the switch at the end of the electrical pulse, $t = t_{ep}$, is

$$T_{max} = T(t_{ep}) = T_{fluid} + \Delta T_{max} (1 - e^{-\alpha t_{ep}}). \quad (57)$$

At the end of the electrical pulse, the driving term in equation (53) is removed and the solution to the thermal differential equation with a shift in time, t' , such that $t' = t - t_{ep}$, is

$$T(t') = T_{fluid} + (T_{max} - T_{fluid})e^{-\alpha t'}. \quad (58)$$

The thermal recovery time, t_{rec} , is defined as the time required for the switch surface, and thus the entire switch volume, to return to some minimum temperature, T_{min} , which is greater than T_{fluid} . If equation (57) is substituted in equation (58) and $(1 - e^{-\alpha t_{ep}})$ is approximated by αt_{ep} when $T(t_{rec}) = T_{min}$, then the thermal recovery time can be expressed as

$$t_{rec} = (1/\alpha) \ln(\Delta T_{max} \alpha t_{ep} / (T_{min} - T_{fluid})). \quad (59)$$

For limited T_{max} , the value of t_{rec} will be approximately equal to three thermal response times, or $3/\alpha$.

If $h = 500 \text{ J/m}^2 \text{ s}^{-1} \text{ }^\circ\text{C}$, $c_p = 0.7 \times 10^3 \text{ J/kg }^\circ\text{C}$, $\rho = 2.3 \times 10^3 \text{ Kg/m}^3$, $d_e = 2 \times 10^{-4} \text{ m}$, $t_{ep} = 1 \times 10^{-7} \text{ s}$, $I = 5 \times 10^4 \text{ A}$, $R_o = 0.01 \Omega$, $w = 0.5 \text{ m}$, and $l = .1 \text{ m}$, then $\alpha = 1.5 \text{ s}^{-1}$ and $\Delta T_{max} = 1 \times 10^6 \text{ }^\circ\text{C}$. If $T_{min} = 20 \text{ }^\circ\text{C}$ and $T_{fluid} = 10 \text{ }^\circ\text{C}$, $T_{max} = 160 \text{ }^\circ\text{C}$, and the thermal recovery time $t_{rec} = 1.9 \text{ s}$. Note that this calculation is for heat removal from one side of the switch volume and uses only the volume of the conducting region. The calculated thermal recovery time is the interval between output pulses, during which the source voltage must not be applied to the switch. If voltage is applied to the switch prior

to this minimum time after the previous pulse, the switch will conduct due to thermal runaway.

This very slow thermal recovery time will dramatically affect the operation of photoconductive switches in the repetitive pulse and the continuous 60 Hz AC mode of operation. The maximum switch temperature will probably be restricted, so that liquid nitrogen operation should be investigated. The optical power on the device may be increased to decrease the switch resistance, and thus the thermal energy deposited in the switch.

APPENDIX D

HIGH POWER SUPERCONDUCTING SWITCHES

Donald U. Gubser
Naval Research Laboratory

The important parameter for switches is the product $J_c \rho$, where ρ is the normal state resistivity and J_c is the critical current density. Superconductors possess very large J_c ($\sim 10^7$ A/cm²) but ρ is generally low. Using standard equations, it can be shown theoretically that the upper limit for the product $J_c^2 \rho$ is given by

$$J_c^2 \rho = 18.7 \frac{k}{h} \frac{H_c^2}{8\pi} T_c ,$$

where k is Boltzman's constant, $\hbar = \frac{h}{2\pi}$, is where h is Planck's constant, H_c is the thermodynamic critical magnetic field, and T_c is the superconducting transition temperature. The following table lists H_c , T_c , calculated $J_c^2 \rho$ values, and the $J_c \rho$ product (for $\rho = 300$ μ ohm cm) for three candidates switch materials.

| | T_c (K) | H_c (Gauss) | $J_c^2 \rho$ (watts/cm ³) | $J_c \rho$ (amp ohm cm) |
|------|--------------|------------------|--|----------------------------|
| Nb | 9 | 2000 | 3.5×10^{11} | 3.2×10^3 |
| NbN | 16 | 2000 | 6.2×10^{11} | 1.4×10^4 |
| V3Ga | 16 | 6000 | 5.6×10^{12} | 3.9×10^4 |

From the above table, it is seen that the two high T_c compound superconductors are preferable to elemental Nb for forming switches.

The theoretical limit of $J_c^2\rho$ has only been approached for NbN as a consequence of its naturally occurring "granular" micro-structure. This value ($J_c = 3 \times 10^7$ amp/cm², $\rho = 300$ ohm-cm) was achieved by S. Wolf at the Naval Research Laboratory on a very narrow microbridge. Other work has been done at Argonne National Laboratory on larger geometry NbN switches, but the values obtained there were a factor of thirty smaller ($J_c^2\rho(\text{NRL}) = 0.9 \times 10^4$, $J_c^2\rho(\text{ANL}) = 0.03 \times 10^4$). A further improvement might be expected by using $V_3\text{Ga}$; however, since the microstructure is not naturally granular, some means must be devised to alter its microstructure without affecting its superconducting properties.

For fast response switches, thin film ($\leq 1\mu\text{m}$) superconducting switches would be best. The small cross-section geometry leads to large resistance while the thinness result in a small heat capacity per unit length, and the ability to activate the switch by non-thermal means (such as by using a microwave pulse). Results for a particular rectangular strip, using NRL's experimental values for NbN (close to the theoretical limit), are tabulated below.

| I (A) | t (cm) | w (cm) | L (cm) | R (ohms) |
|----------|-----------|-----------|-----------|-------------|
| 300 | 10^{-4} | .1 | 100 | 3000 |
| 3000 | 10^{-4} | 1 | 100 | 300 |

APPENDIX E

List of Participants

| | |
|--|---|
| Michael S. Adler General Electrical Company Building 37, Room 2077 Corporate Research and Development Center Schenectady, NY 12345 (518)385-8175 | Arthur H. Guenther AFWL/CA Kirtland AFB, NM 87117 (505)844-9856 |
| Barry L. Ballard FTD/TQTD Wright-Patterson AFB Dayton, Ohio 45433 (513)257-3158 | Robert B. Hammond MS D-429 Los Alamos National Laboratory Los Alamos, NM 87545 (505)667-1813 |
| David L. Blackburn National Bureau of Standards Building 225, Room B-310 Washington, D.C. 20234 (301)921-3541 | Paul Haugsjaa GTE Laboratories, Inc. 40 Sylvan Road Waltham, MA 02154 (617)890-8460 Ext. 2512 |
| David W. Forst International Rectifier 233 Kansas Street El Segundo, CA 90245 (213)772-2000 | H. Thurman Henderson Dept. of Electrical Engineering University of Cincinnati Cincinnati, OH 45221 (513)475-4461 |
| Jerome B. Brewster Westinghouse Electric Corp. Research and Development Center 1310 Beulah Road Pittsburgh, PA 15235 (412)256-3590 or 3625 | Emanuel Honig E11, MS 429 Los Alamos National Laboratory Los Alamos, NM 87545 (505)667-1688 |
| Tommy R. Burkes T. R. Burkes, Inc. P.O. Box 16577 Lubbock, TX 79490 (806)885-4887 | Jerry L. Hudgins Dept. of Electrical Engineering Texas Tech University Lubbock, TX 79409 (806)742-3504 |
| Richard D. Ford Code 4770 Naval Research Laboratory Washington, D.C. 20375 (202)767-2468 | Yu Kao Westinghouse Electric Corp. Research and Development Center 1310 Beulah Road Pittsburgh, PA 15235 (412)256-7593 |
| Bobby Gray RADC/OCTP Griffiss AFB, NY 13441 (315)730-4381 | M. Kristiansen Dept. of Electrical Engineering Texas Tech University Lubbock, TX 79409 (806)742-2224 |

Erich E. Kunhardt
 Dept. of Electrical Engineering
 Texas Tech University
 Lubbock, TX 79409
 806/742-3545

Bogoljub Lalevic
 Rutgers University
 Dept. of Electrical Engr.
 Piscataway, NJ 08854
 (201)932-3871

Chi H. Lee
 University of Maryland
 Dept. of Electrical Engineering
 College Park, MD 20742
 (301)454-2442

Lionel M. Levinson
 General Electric Co.
 Room KW-B322
 Corporate Research and
 Development Center
 Schenectady, NY 12301
 (518)385-8562

L. R. Lowry
 Westinghouse Electric Corp.
 Research and Development Center
 1310 Beulah Road
 Pittsburgh, PA 15235
 (412)256-3339 or 3319

Michael Mando
 U.S. Army MERADCOM
 Electric Power Laboratory
 DRDME-EA
 Fort Belvoir, VA 22060
 (703)664-5081

Gerard Mourou
 Laboratory for Laser Energetics
 University of Rochester
 250 E. River Road
 Rochester, NY 14623
 (716)275-2092

William C. Nunnally
 E11, MS429
 Los Alamos National Laboratory
 Los Alamos, NM 87544
 (505)667-1360

James P. O'Loughlin
 AFWL/AREP
 Kirtland AFB, NM 87117
 (505)844-1786

Paul F. Pittman
 Westinghouse Electric Corp.
 P.O. Box 10864
 Pittsburgh, PA 15236
 (412)892-5600, Ext. 5383

Michael D. Pocha
 MS L-156
 Lawrence Livermore National Lab.
 P.O. Box 5504
 Livermore, CA 94550
 (415)422-8664

William M. Portnoy
 Dept. of Electrical Engineering
 Texas Tech University
 Lubbock, TX 79409
 (806)742-3533

Duard L. Pruitt
 MS 108-205
 RCA
 Moorestown, NJ 08057
 (609)778-2153

Richard W. Rice
 Code 6360
 Naval Research Lab.
 Washington, D.C. 20375
 (202)767-2131

Karlheinz Schoenbach
 Dept. of Electrical Engineering
 Texas Tech University
 Lubbock, TX 79409
 (806)742-3595

Mark E. Snyder
 AFWL/NTAI
 Kirtland AFB, NM 87117
 (505)844-0327

Gale P. Sundberg
 MS 7104
 NASA Lewis Research Center
 21000 Brookpark Road
 Cleveland, OH 44135
 (216)433-4006,
 Ext. 5221

Victor A. K. Temple
General Electric Co.
Building 37, Room 278
Corporate Research
and Development Center
Schenectady, NY 12345
(518)385-8755

Peter J. Turchi
R and D Associates
1401 Wilson Blvd.
Arlington, VA 22209
(703)522-5400

Larry R. Turner
Foreign Science and
Technology Center
220 7th Street, NE
Charlottesville, VA 22901
(804)296-5171
Ext. 591 or 671

Ihor M. Vitkovitsky
Code 4770
Naval Research Laboratory
Washington, D.C. 20375
(202)767-2468

Maurice Weiner
U.S. Army ERADCOM
Electronics Technology
and Devices Laboratory
DELET/PL
Fort Monmouth, NJ 07703
(201)544-5406

P. Frazier Williams
Dept. of Electrical Engineering
Texas Tech University
Lubbock, Texas 79409
(806)742-1399

Duane Wolley
General Electric Company
Building 7, Box 2
Electronics Park
Syracuse, NY 13201
(312)456-2738

Horst R. Wittman
U.S. Army Research Office
P.O. Box 12211
Research Triangle Park,
NC 27709
(919)549-0641

Donald C. Wunsch
The BDM Corporation
1801 Randolph Road, S.E.
Albuquerque, NM 87106
(505)848-5000



TAMARRON
JANUARY
1983
WORKSHOP
ON

SOLID STATE PULSED POWER SWITCHING



